

**“Model-based Control of Plate Vibrations using  
Active Constrained Layer Damping.”**

**by**

**Chak CHANTALAKHANA**



**Department of Mechanical Engineering  
University of Sheffield  
Supervisor: Dr. Roger Stanway  
January 2000**

**Thesis submitted in partial fulfilment of the requirements for the Ph.D. degree**

## SUMMARY

In this thesis, the author presents a numerical and experimental study of the application of active constrained layer damping to a clamped-clamped plate. Piezoelectric actuators with modal controllers are used to improve the performance of vibration suppression from the passive constrained layer damping treatment.

Surface damping treatments are often effective at suppressing higher frequency vibrations in thin-walled structures such as beams, plates and shells. However, the effective suppression of lower frequency modes usually requires the additional of an active vibration control scheme to augment the passive treatment. Advances in the technologies associated with so-called smart materials are dramatically reducing the cost, weight and complexity of active structural control and make it feasible to consider active schemes in an increasing number of applications. Specifically, a passive constrained layer damping treatment is enhanced with an active scheme employing a piezoceramic (PZT) patch as the actuator. Starting with an established finite element formulation it is shown how model updating and model reduction are required to produce a low-order state-space model which can be used as the basis for active control. The effectiveness of the formulation is then demonstrated in a numerical study.

Finally, in the description of the experimental study it is shown how modes in the frequency range from 0 to 600 Hz are effectively suppressed: the two lowest modes (bending and torsional) through active control, the higher modes (around ten in number) by the passive constrained damping layer. The study's original contribution lies in the experimental demonstration that given a sufficiently accurate model of the plate and passive constrained damping layer, together with a suitable active feedback control algorithm, spillover effects are not significant even when using a single sensor and single actuator. The experimental traces show, in some instances, minor effects due to spillover. However, it can be concluded that the presence of the passive layer introduces sufficient damping into the residual modes to avoid any major problems when using only the minimum amount of active control hardware.

## **ACKNOWLEDGEMENTS**

Firstly, I would like to thank my supervisor, Dr Roger Stanway, for his invaluable help, advice and guidance throughout this research study and my three-year period in the UK. Working with him has been an invaluable experience in my research training. I also would like to thank Professor J. R. Wright and Dr A. R. Johnson, my examiners, for their constructive comments.

I am indebted to many members of the Applied Dynamic Group in the Department of Mechanical Engineering at the University of Sheffield. Discussions with them were of great help to me, I want to mention particularly Mr J. Rongong, Mr A. Kyprianou, Mr S. Patsias, Dr W. Staszewski, Dr K. Worden and our technicians, Mr J. Clarke and Mr D. Webster.

I also would like to express my gratitude to my family and my former teachers who educated me. I am appreciative of many friends who I have met in UK for comforting my life here. Many thanks to Ms Nattinee Attiratanasoonthorn for partial help to prepare this manuscript.

Finally, I wish to acknowledge my indebtedness to Thai Government for supporting my study and to the European Research Office of the US Army for partial funding of the control equipment under contract number N68171-98-M-5388.

# CONTENTS

	<i>Page</i>
<b>Summary</b>	i
<b>Acknowledgments</b>	ii
<b>List of illustrations</b>	vii
<b>List of tables</b>	xi
<b>Notation</b>	xii
<b>Abbreviations</b>	xv
<b><u>Chapter 1: Introduction</u></b>	
1.1 Vibration control of mechanical structures	1
1.2 Passive vibration control	1
1.3 Active vibration control	5
1.4 Outline of contents	9
<b><u>Chapter 2: Active constrained layer damping treatments: review of the literature and statement of problem</u></b>	
2.1 Historical development from active control to hybrid schemes	11
2.2 Design of a passive constrained damping layer for use in hybrid schemes	13
2.3 Modelling of flexible structures with an active constrained damping layer	17
2.4 Active control strategies	20
2.5 Problem under review	24
2.5.1 <i>Purpose of the study</i>	25
2.5.2 <i>Strategy</i>	26
2.6 Summary of Chapter 2	27

	<i>Page</i>
<b><u>Chapter 3: Theory</u></b>	
3.1 Objectives	29
3.2 Finite element modelling	30
3.2.1 <i>The plate model</i>	30
3.2.2 <i>Verification of plate model</i>	33
3.2.3 <i>Summary of finite element modelling</i>	36
3.3 System identification	38
3.3.1 <i>Modal data extraction</i>	38
3.3.2 <i>Updating the finite element model</i>	41
3.3.3 <i>Summary of system identification</i>	43
3.4 Modal control	44
3.4.1 <i>Pole placement</i>	45
3.4.2 <i>Spillover effects</i>	46
3.4.3 <i>Summary of modal control</i>	48
3.5 Summary of Chapter 3	48
<b><u>Chapter 4: Design of passive control and refined plate model</u></b>	
4.1 Objectives	49
4.2 A frequency survey of test plates	49
4.3 Design of a constrained damping layer for a clamped-clamped plate	54
4.4 Model updating	57
4.4.1 <i>A tentative model</i>	58
4.4.2 <i>Identification of natural frequencies and damping factors from the test plate</i>	61
4.4.3 <i>Model updating, iteration and the refined model</i>	62



	<i>Page</i>
A1.3 <i>Equations of motion</i>	105
A2 Verification using Warburton's method	107
<b><u>Appendix B: System identification</u></b>	
B1 Peak picking method	109
B2 Model updating	110
B3 Transformation of structural damping matrix to viscous damping matrix	113
B4 Guyan reduction	115
<b><u>Appendix C: Modal control</u></b>	
C1 Modal control	117
C1.1 <i>Pole placement</i>	117
C1.2 <i>State estimator</i>	118
C2 The effects of truncated models with state estimator	119
<b><u>Appendix D: Copy of a paper submitted to Journal of Sound and Vibration</u></b>	121
<b><u>Appendix E: Copy of a paper submitted to Smart Materials and Structures</u></b>	160
<b><u>References</u></b>	200

## LIST OF ILLUSTRATIONS

	<i>Page</i>
<u>Figure 2.1.</u> Surface damping configurations	14
a) passive constrained damping layer	
b) active constrained damping layer followed Azvine (1994;1995)	
c) active constrained damping layer followed Baz and Ro (1993;1996)	
d) active constrained damping layer followed Lam et al (1997)	
<u>Figure 2.2.</u> Strategies for active vibration control of flexible systems	28
<u>Figure 3.1.</u> A rectangular element of the three-layer plate	31
a) co-ordinate system and nodes of the elements	
b) displacement of the elements at $x$ - $z$ plane	
<u>Figure 3.2</u> Drawing of simplified plate	34
<u>Figure 3.3.</u> Deviation of first ten natural frequencies predicted by the finite element model from Warburton's solution.	35
<u>Figure 3.4.</u> Schematic of a mass-spring-damper system	39
<u>Figure 3.5.</u> Flow chart showing procedures to obtain an updated model of the plate(iterative loops are not included see Figure B.2 in Appendix B, section B2)	44
<u>Figure 3.6.</u> A diagram showing the effect of residual modes on a closed-loop control system (Balas, 1978)	47
<u>Figure 4.1.</u> Experimental arrangement for the basic clamped-clamped plate	50
<u>Figure 4.2.</u> Measurement points (number in bold) and selected nodes for model reduction of the panel plate	50
<u>Plate 1.</u> Photograph of three-layer plate showing PZT1 and PZT2 used in Experiments and measurement points corresponding to Figure 4.2	51
<u>Figure 4.3.</u> Measured FRFs of two identical panel plates	52
, — plate no.1 and - - - - - plate no.2	
(a) point mobility forced and measured at point 7 (FRF7_7)	
(b) transfer mobility forced at point 7 and measured at point 23(FRF7_23)	



	<i>Page</i>
<u>Figure 5.5.</u> Arrangement of the clamped-clamped plate with a square PZT element used as actuator and 2 accelerometers for sensing	76
<u>Figure 5.6.</u> Arrangement of the closed-loop clamped-clamped plate with electronic equipment for digital control implementation	77
<u>Figure 5.7.</u> Measured FRFs (FRF7_23) of three-layer plate with and without active control using PZT1 and ACC1 (Figure 5.5)	78
<u>Figure 5.8.</u> Measured FRFs (FRF7_23) of three-layer plate with and without active control using PZT1 and ACC1 and 2 (Figure 5.5) a) gain as designed b) with an amplified gain factor = 1.6	80
<u>Figure 5.9.</u> FRF7_7: a comparison of passive and active schemes in relation to untreated plate	81
<u>Figure 5.10.</u> FRF7_23: a comparison of passive and active schemes in relation to untreated plate	81
<u>Figure 5.11.</u> FRF7_17: a comparison of passive and active schemes in relation to untreated plate	82
<u>Figure 5.12.</u> FRF7_13: a comparison of passive and active schemes in relation to untreated plate	82
<u>Figure 5.13.</u> FRF7_5: a comparison of passive and active schemes in relation to untreated plate	83
<u>Figure 5.14.</u> Configuration of PZT actuator a) for operation in $x$ and $y$ directions b) for operation in $x$ direction only	84
<u>Figure 5.15.</u> Arrangement of the clamped-clamped plate with 4-strip PZT elements used as actuator and a single accelerometer for sensing	84
<u>Figure 5.16.</u> Simulation results: predicted FRFs (FRF7_23) of three-layer plate with and without active control for PZT actuator operating in $x$ direction only (Figure 5.15)	85
<u>Figure 5.17.</u> Simulation results: applied voltage for PZT actuator a) operating in both $x$ and $y$ directions b) operating in $x$ direction only	85

	<i>Page</i>
<u>Figure 5.18.</u> Measured FRFs (FRF7_23) of three-layer plate with and without active control using 4-strip PZT2 and ACC1 (Figure 5.15)	86
<u>Figure 5.19.</u> Measured FRFs (FRF7_23) of three-layer plate with and without active control using 4-strip PZT2 and ACC1 (Figure 5.15) with an amplified gain factor = 2.4	86
<u>Figure 5.20.</u> Arrangement of the clamped-clamped plate with 2 PZT actuators (one square element and one 4-strip elements) and 2 accelerometers for sensing	87
<u>Figure 5.21.</u> Measured FRFs (FRF7_23) of three-layer plate with and without active control using PZT1 and 2 with a single-channel amplifier and ACC1 (Figure 5.20) a) gain as designed b) with an amplified gain factor = 1.4	88
<u>Figure 5.22.</u> Measured FRFs (FRF7_23) of three-layer plate with and without control using PZT1 and 2 with a 2-channel amplifier and ACC1 (Figure 5.20) a) gain as designed b) with an amplified gain factor = 1.4	90
<u>Figure 5.23.</u> Simulation results: FRFs (FRF7_23) of three-layer plate with and without active control using PZT1 and 2 with a 2-channel amplifier and ACC1 (Figure 5.20)	91
<u>Figure 5.24.</u> Simulation results: FRFs (FRF7_23) of three-layer plate with and without active control using PZT1 and 2 with a 2-channel amplifier and ACC2 (Figure 5.20)	92
<u>Figure 5.25.</u> Simulation results: FRFs (FRF7_23) of three-layer plate with and without active control using PZT1 and 2 with a 2-channel amplifier and ACC1 and 2 (Figure 5.20)	92
<u>Figure 5.26.</u> Measured FRFs (FRF7_23) of three-layer plate with and without active control using PZT1 and 2 with a 2-channel amplifier and ACC2 (Figure 5.20) a) gain as designed b) with an amplified gain factor = 2.0	93
<u>Figure 5.27.</u> Measured FRFs (FRF7_23) of three-layer plate with and without active control using PZT1 and 2 with a 2-channel amplifier and ACC1 and 2 (Figure 5.20) a) gain as designed b) with an amplified gain factor = 1.6	94

	<i>Page</i>
<u>Figure 5.28.</u> FRF7_23: A comparison of passive and active schemes in relation to untreated plate: the best case of using 2 PZTs with a 2-channel amplifier and 2 ACCs	95
<u>Figure A.1.</u> Displacement of a rectangular element of the three-layer plate in $x$ - $z$ plane	102
<u>Figure A.2.</u> The first ten mode shapes of $9 \times 6$ mesh size panel plate corresponding to their natural frequencies	108
<u>Figure B.1.</u> Illustration of peak picking method a) location of natural frequencies b) definition of half-power points	110
<u>Figure B.2.</u> Flow chart of procedures in the model updating algorithm	113

## LIST OF TABLES

<u>Table3.1:</u> A comparison of the first ten natural frequencies of panel plate from the finite element program and from Warburton's approximate solutions	35
<u>Table 3.2:</u> A comparison of the first five natural frequencies from the finite element program, the analytical solutions and NASTRAN/MSE	37
<u>Table 3.3:</u> A comparison of the first five modal loss factors from the finite element program, the analytical solutions and NASTRAN/MSE	37
<u>Table 4.1</u> Material properties of the three-layer plate	55
<u>Table 4.2</u> Measured and predicted first six natural frequencies and damping factors of the three-layer plate	62
<u>Table 5.1</u> Controllability and observability indices	68
<u>Table 5.2</u> Poles and corresponding gains of controller and estimator	73
<u>Table 5.3</u> Re-designed estimator gains	91

## NOTATION

$\alpha_{1,2}$	weighting constants for obtaining control gains
$A_a$	cross-sectional area of the PZT actuator ( $\text{m}^2$ )
$\mathbf{b}$	input vector ( $2r \times 1$ )
$b_a$	width of the PZT actuator (m)
$\mathbf{B}$	input matrix ( $2n \times n$ )
$\mathbf{B}_0$	input matrix ( $n \times n$ )
$\mathbf{C}$	measurement matrix ( $2m \times 2n$ )
$d_{31}$	piezoelectric constant ( $\text{mV}^{-1}$ )
$e_{13}$	ratio of the modulus of elasticity between the constraining layer and the base plate
$\mathbf{e}$	estimation error vector ( $c \times 1$ )
$E_{1,3}$	modulus of elasticity of the constraining layer and the base plate respectively ( $\text{N}/\text{m}^2$ )
$E_a$	modulus of elasticity of the PZT actuator ( $\text{N}/\text{m}^2$ )
$f(t)$	force as a function of time (N)
$\mathbf{f}$	input vector ( $n \times 1$ )
$G$	modulus of rigidity ( $\text{N}/\text{m}^2$ )
$\mathbf{G}$	gain matrix ( $n \times 2m$ )
$h_{1,2,3}$	thickness of the constraining layer, viscoelastic layer and base plate respectively (m)
$h_{23}, h_{13}$	ratios between the thicknesses of viscoelastic layer and the base plate, and the constraining layer and the base plate, respectively
$\mathbf{H}$	modal measurement matrix ( $l \times 2n$ )
$\mathbf{I}$	identity matrix ( $n \times n$ )
$j, k, l, m, n, r$	integers
$\mathbf{J}$	cost function
$\mathbf{k}_c$	gain vector ( $c \times 1$ )
$\mathbf{L}$	physical measurement matrix ( $l \times 2n$ )
$\underline{m}, \underline{k}, \underline{c}$	single mass, stiffness and damping coefficients, respectively (kg, N/m, N.s/m)

$\mathbf{D}^R$	reduced-order viscous damping matrix (transformation of $\mathbf{Z}^R$ ) ( $r \times r$ )
$\mathbf{M}_j, \bar{\mathbf{K}}_j$	mass and complex stiffness matrices for the $j$ th element ( $\text{kg}, \text{N/m}^2$ )
$\mathbf{M}, \mathbf{D}, \mathbf{K}$	global mass, damping and stiffness matrices ( $n \times n$ )
$\mathbf{M}^R, \bar{\mathbf{K}}^R$	reduced-order mass and complex stiffness matrices ( $r \times r$ )
$\mathbf{Q}, \mathbf{R}$	weighting matrices for obtaining optimal control gains
$\mathbf{q}$	eigenvector
$s$	Laplace number
$t$	time
$t_a$	thickness of the PZT actuator (m)
$T_s$	sampling time
$u_{1k,3k}$	longitudinal displacement in $x$ axis at node $k$ of the rectangular element of the constraining layer and the base plate, respectively (m)
$\mathbf{u}$	input vector ( $n \times 1$ )
$\mathbf{U}$	eigenvector matrix ( $2r \times 2r$ )
$v_{1k,3k}$	longitudinal displacement in $y$ axis at node $k$ of the rectangular element of the constraining layer and the base plate, respectively (m)
$V(t)$	applied voltage across the PZT actuator (V)
$\mathbf{w}$	mode-controllability vector
$w_k$	transverse displacement along the $z$ axis at node $k$ of the rectangular element (m)
$\frac{\partial w}{\partial y_k}, \frac{\partial w}{\partial x_k}$	rotational displacement about the $x$ axis and $y$ axis respectively (rad)
$x(t)$	linear displacement as a function of time (m)
$\mathbf{Y}$	state vector ( $2n \times 1$ )
$\mathbf{z}$	output vector ( $l \times 1$ )
$\mathbf{Z}^R, \mathbf{K}^R$	reduced-order imaginary term and real term, respectively, of the complex stiffness matrices ( $r \times r$ )
$\eta$	loss factor of viscoelastic layer
$\nu_1, \nu_2, \nu_3$	Poisson's ratio of constraining layer, viscoelastic layer and base plate, respectively
$\rho_1, \rho_2, \rho_3$	density of constraining layer, viscoelastic layer and base plate, respectively ( $\text{kg/m}^3$ )
$\rho_k$	assigned eigenvalue

$\omega$	angular frequency (rad/s)
$\lambda$	eigenvalue
$\zeta$	damping factor
$\sigma_a$	stress developed in the PZT actuator (N/m <sup>2</sup> )
$\xi$	modal co-ordinate vector ( $2n \times 1$ )
$\mathfrak{G}$	mode-observability vector
$\Phi$	weighting matrix (vector for the single input/single output system) ( $2n \times 1$ )
$\Lambda$	eigenvalue matrix ( $2n \times 2n$ )
$\Delta_j$	displacement vector of the rectangular element $j$ ( $28 \times 1$ )
$\Delta\mathbf{A}_{1,2}$	mass-normalised correction matrices for damping and stiffness matrices, respectively ( $n \times n$ )
$\Delta\mathbf{D}, \Delta\mathbf{K}$	correction matrices for the damping and stiffness matrices, respectively
$e^{(\cdot)}$	exponential operator
$i$	complex operator, $\sqrt{-1}$
$[ ]^d$	denotes discrete-time formulation
$[ ]^T$	denotes matrix transpose
$[ ]^{-1}$	denotes matrix inverse
$[ ]^*$	denotes complex conjugate matrix transpose
$[ ]_c$	subscript for controlled terms
$[ ]_r$	subscript for residual terms
$[ ]_{new}$	subscript for updated matrix
$[ ]_{sym}$	subscript for symmetrical matrix
$[\dot{x}]$	denotes differentiation of $x$ variable with respect to time
$[\ddot{x}]$	denotes double differentiation of $x$ variable with respect to time
$[\hat{\xi}]$	denotes estimate of $\xi$

## **ABBREVIATIONS**

<b>ER</b>	<b>Electro-rheological</b>
<b>FRF</b>	<b>Frequency response function</b>
<b>GHM</b>	<b>Golla-Hughes-McTavish</b>
<b>IMSC</b>	<b>Independent modal space control</b>
<b>LQG</b>	<b>Linear quadratic gaussian</b>
<b>LQR</b>	<b>Linear quadratic regulator</b>
<b>MR</b>	<b>Magneto-rheological</b>
<b>MSE</b>	<b>Modal strain energy</b>
<b>PPF</b>	<b>Positive position feedback</b>
<b>PVF<sub>2</sub></b>	<b>Polyvinylidene fluoride</b>
<b>PZT</b>	<b>Plumbum (lead) zirconate titanate</b>
<b>SMA</b>	<b>Shape-memory alloy</b>

# **CHAPTER 1**

## **INTRODUCTION**

### **1.1 Vibration control of mechanical structures**

In the early days of vibration control, attempts were focused on the development of structural design and damping mechanisms to suppress vibrations in mechanical structures. Typical techniques involved designing the structural stiffness to avoid exciting resonant frequencies and the use of vibration isolators and absorbers to protect structures from external excitation (Den Hartog, 1934). These types of vibration control techniques are usually classed as passive where the term passive means that the devices operate by dissipating or storing energy with no need for an external energy supply. Since the development of control theory and the arrival of new technology relating to sensors, actuators and digital signal processors, active vibration control has been available to tackle vibration problems. A major benefit of active control is that a controlled structure can adapt to a changing environment, for example, to temperature variations. Also active control can generally offer more effective suppression of undesirable vibrations, but at a cost in terms of additional cost, weight and complexity.

### **1.2 Passive vibration control**

In a lightly damped structure, even the smallest excitation force acting at or near a resonant frequency can result in significant and undesirable vibration levels in the structure. There are a number of techniques to avoid or reduce these vibrations. In general, the structure should be designed such that its natural frequencies do not correspond to

excitation frequencies in order to avoid the excitation of resonances. Natural frequencies of a lightly damped structure depend on the mass and stiffness characteristics of the structure. In principle, control of the natural frequencies is simpler for a structure subjected to a single excitation frequency where one solution is to change the mass and stiffness properties of the structure (Crede, 1965). It is difficult to generalise on whether mass or stiffness should be modified. However it is often more realistic to change stiffness since this might be effected simply by changing the material used for the structural components. Another alternative is the use of a vibration absorber which was introduced by Ormondroyd and Den Hartog (1928). The absorber operates through changing the number of degrees of freedom of the structure to separate natural frequencies away from an excitation frequency. The simplest form of the absorber is a single mass-spring system. The absorber is placed at the point where excitation occurs and the natural frequency of absorber is tuned to the excitation frequency. Practical vibration absorbers will generally also include a damping element (Reed, 1995).

The above techniques are used mainly to avoid exciting resonances in lightly damped structures exposed to a single excitation frequency. In general, there are many mechanical systems excited by a broad band of frequencies, for example, automotive suspensions, aircraft interiors and civil engineering structures. It is extremely difficult to avoid exciting resonances in such systems. The introduction of damping is often an effective way to reduce levels of vibration at resonance. Damping technology for vibration control has been developed since the late 1930s and the early years of the 1940s (Jones, 1979). Progress in the development damping materials and mechanisms since the 1960s has been immensely effective in suppressing undesirable vibrations, especially in aerospace applications. These

advances in damping technology will be discussed later. In industrial machinery the addition of suitable damping to the components of a machine is often difficult owing to the complexity of the machine structure. Vibrations generated by the operation of such machines is clearly undesirable and some form of vibration isolator is commonly used to reduce the transmission of forces from a machine to its foundations. The vibration isolator usually consists of a material with suitable stiffness and damping properties. Vibration isolation is now widely used for machine installations owing to the availability of commercial devices and practical guidelines for implementation (Recca, 1995).

Damping in a mechanical structure can originate from a variety of sources. Typical sources include internal damping mechanisms in the form of viscoelastic materials and elastomers and external damping mechanisms such as viscous devices, surface damping treatments and shunted piezoelectric devices. For structural design, external damping mechanisms are usually essential in order to provide adequate suppression of vibrations. For thin-walled structures such as beams, plates and shells, surface damping and shunted piezoelectric damping treatments promise an effective solution to vibration control over a broad band of excitation frequencies. These passive damping techniques exploit the concept of absorbing strain energy from modes of vibration and then dissipating the energy in another form - usually heat or electrical energy through various mechanisms (Johnson, 1995). Surface damping treatments involve the addition of damping to beam and plate structures which are subject to surface strains. Materials with a high loss factor such as viscoelastic materials are added as an additional layer on the top of the host structure. Extensional strains resulting from structural vibration are damped by internal friction of the added layer. However, to achieve higher damping, a thicker layer of damping material is required.

Shear damping in the viscoelastic layer can provide higher damping than extensional damping for an equal weight of materials used (Ross et al, 1959). The viscoelastic layer is constrained at the free surface by adding a stiff metal sheet. As a result of this additional sheet, the viscoelastic layer is placed in shear. This technique can be applied to the skin parts of structures subjected to fluctuating excitation. The treatment is known as constrained layer damping and the use of this treatment will form a substantial part of this thesis.

The use of a piezoelectric material as a passive damping mechanism was first introduced by Forward (1979). The benefit of using a piezoelectric material arises from the reciprocal ability to convert mechanical strain to electrical charge and *vice versa*. The piezoelectric patch is shunted with an electrical resistance or impedance so as to dissipate the mechanical energy as electrical energy. Hagood and von Flotow (1991) presented two types of electrical impedance network: resistive and resonant circuit shunting. The first circuit involves a resistor placed in parallel with the capacitive piezoelectric patch. This passive piezoelectric device provides a high loss factor and high stiffness and has similar material behaviour to that of viscoelastic materials. Resonant circuit shunting involves a series of an inductor and a resistor in parallel with the piezoelectric patch. The operating principle is similar to that of a tuned damper in a mechanical vibration isolator or absorber. However, note that for tuning to low frequency resonances an abnormally large inductor may be required.

Piezoelectric materials also have the ability to act as sensors or actuators in active vibration control, a point which will be emphasised in the next section. Passive vibration

control is still very popular for many applications. However, there are performance limitations inherent in the use of purely passive vibration control techniques. An alternative approach to controlling structural vibrations is to use active control configurations in place of, or in addition to, passive devices.

### **1.3 Active vibration control**

Active control of vibrating structures generally exploits the concept of feedback control. A feedback control system consists essentially of sensors, actuators and control elements. The actuator is usually provided with power from an external source and thus, unlike passive devices, is able to provide an active energy input to the system. In a feedback system, an output signal is measured and compared with a reference signal. The difference, or error, between the measured and reference signals is fed to a controller which determines the input to the actuator such that the controlled output is driven towards a desired value.

Control theory is usually divided into classical and modern categories. In classical control, design of the control system takes the plant transfer function as the starting point. Graphical methods such as the Nyquist diagram, Bode plot and root-locus technique are used in classical control system design. These methods were developed before the advent of modern digital computers and all avoid the need to solve the differential equations governing the plant, sensors, actuators and controller. The major drawback of classical control theory is that, in its basic form, its application is limited to linear, time-invariant systems with a single input and single output. The availability of rapid digital computers in the 1960s opened the way for an alternative approach: time domain analysis using so-

called state space techniques. State space techniques operate directly on the governing differential equations and can readily accommodate plants with multiple inputs and multiple outputs. State-space methods form the basis of modern control theory and can deal with non-linearities and time-varying behaviour more readily than classical methods. There are many well-established algorithms for designing feedback control systems using state-space methods. However, when applying such techniques to lightly damped vibrating structures there are special problems which have to be overcome.

The key problem of vibration control in flexible systems containing beam- or plate-like elements is that when structural damping is small and the stiffness is low then natural frequencies are liable to occur at low frequencies. Resonances which result, are difficult to suppress by passive means because of the long wavelengths involved (Hansen and Snyder, 1997). Here, active vibration control offers an alternative method for reducing levels of structural vibration. Most control algorithms are based upon feedback control but feedforward techniques have also been applied (Hansen and Snyder, 1997). Noise control is perhaps the most frequent application of feedforward control because of the availability of a measurement of the disturbance source. Modal control theory (Simon and Mitter, 1968; Porter and Crossley, 1972) is the basis of most algorithms for vibration control (Meirovitch and Baruh, 1985). Pioneering work on the implementation of modal control theory for vibration control of lightly damped structures was presented by Balas (1978). Although, in principle, a vibrating structure has an infinite number of modes, in practice a finite-order model is required to enable efficient implementation using a digital controller. When using a finite-order model, uncontrolled modes may be excited and a lightly damped structure can easily be de-stabilised. Since Balas's original paper, researchers have tried to

develop modal control algorithms which overcome these drawbacks. Typical examples of such methods are Independent Modal Space Control (IMSC) (Meirovitch and Baruh, 1982) and Positive Position Feedback (PPF) control (Fanson and Caughey, 1990). Robust and optimal control has also been tried, primarily to provide greater reliability and to reduce energy consumption. For example,  $H$ -infinity and Linear Quadratic Gaussian (LQG) optimal control have been used for vibration suppression (Burl, 1999). Rapid advances have been made in the past fifteen years in applications of modal control to lightly damped structures. There is no doubt that this progress is largely due to developments in computers and also in smart materials from which sensors and actuators can be manufactured.

Smart materials have inherent properties to convert one form of energy to another, for example, changing mechanical motion to an electrical signal when used as sensing devices or *vice versa* for actuators. Bailey and Hubbard (1985) presented a study of the active vibration control of a cantilever beam using a piezoelectric polymer (polyvinylidene fluoride) or  $PVF_2$  as a distributed-parameter actuator. The  $PVF_2$  layer was placed at the top of the cantilever beam and the control voltage was proportional to the negative velocity at the tip of the beam, so as to provide a bending moment in the  $PVF_2$  layer for suppressing vibration. Piezoelectric, shape-memory alloy (SMA), electro-rheological (ER) fluids and magneto-rheological (MR) fluids have also been used as actuators for flexible systems (Culshaw, 1996). Using piezoelectric materials, SMAs and ER and MR fluids as embedded sensors and actuators in flexible structures is an advantageous way of reducing control device weight and including their dynamic characteristics in mathematical models of the structures. For example, Crawley and Luis (1987) described uses of piezoelectric

materials as actuators in distributed structures. The formulation of the static and dynamic behaviour of beams with piezoelectric actuators was described in this study. The ability of the models to account for observed behaviour was also demonstrated. Baz et al (1990) presented a preliminary study on using a shape-memory alloy as actuators to control beam vibration. A distinct advantage of shape-memory alloys is that they have low power requirements. SMAs have already been used widely in robot technology where the actuators are embedded in the structures. There are also many potential applications for ER and MR fluids in structural control. These smart fluids can be used in various modes of operation as described in a survey paper (Stanway et al, 1996). Applications and development of smart materials are still an intensive topic of research (see, for example, *Journal of Smart Materials and Structures Special Issue on Passive and Active Damping Technologies* (Guest Editors: N. M. Wereley and G. R. Tomlinson), Volume 5, No.5, pp.509-722, 1996 and *IMechE Journal of Systems and Control Engineering Special Issue on Smart Materials and Systems* (Guest Editor: R. Stanway), Volume 212, No.13, pp.149-238, 1998).

In this thesis, attention will be focused on the control of plate vibrations. As mentioned above, active schemes are, in principle, capable of suppressing the low frequency modes which arise in lightweight structures. In practice the use of an active feedback scheme can degrade and even de-stabilise the structure owing to the influence of the higher frequency modes. It was suggested in an earlier study of vibrations in rotating machinery (Firoozian and Stanway, 1988) that the addition of passive damping could prevent de-stabilisation. In what follows here passive damping is added to the plate in the form of a constrained damping layer. The combination of passive and active damping will then be studied. This

combination of passive and active damping will be referred to as “active damping control” (Azvine et al, 1995).

#### **1.4 Outline of contents**

The present study is concerned with a clamped-clamped aluminium plate which was first investigated by Azvine and his colleagues (1994). This plate is a simplified version of an instrument-box cover found in a military aircraft. Azvine’s brief was to investigate active constrained layer damping treatments as a means of suppressing bending and torsional vibrations which were causing the instrument box to malfunction in service. Active constrained layer damping was developed from a shear damping mechanism using a constrained damping layer. Piezoelectric actuators were placed on the metallic constraining layer of the mechanism and used to increase the induced shear strain in a viscoelastic layer, thus increasing the overall damping. Negative velocity feedback was used along with non-collocated sensors and actuators in an attempt to control the first two modes of vibration. Using two actuators, the benefits of the constraining layer were clearly demonstrated: higher feedback gains could be used to give lower resonant peaks without causing instability. However, this study indicated the need for better models of the host plate, the passive constraining layer and the piezoelectric actuators together with a more effective control algorithm based upon this model. At the same time, it was essential for the eventual application that the amount of hardware be minimised.

In this thesis, the authors describe a novel approach to controlling both the bending and torsional vibrations of the clamped-clamped plate. Initially, the technique of Baz and Ro (1996) is extended to produce a finite element model of the plate together with the passive

constraining layer. Using system identification techniques, the model is validated using data from the test facility. Model reduction and model updating are then applied to produce a compact model which is capable of accounting for observed behaviour. Following a comprehensive numerical study, an active constrained layer damping treatment is implemented experimentally and a comprehensive set of test results is presented.

In the following chapters, a survey of uses of this active damping concept is presented (Chapter 2) and justification of schemes to use with the present study is addressed at the end of Chapter 2. Relevant theories on finite element modelling, system identification and modal control are described in Chapter 3. The more detailed mathematics is placed in appendices. The design of a constrained damping layer and establishment of a refined finite element model of the plate are presented in Chapter 4. Numerical simulations of active control strategies are verified with experimental results in Chapter 5. Finally, conclusions and recommendations for future work are provided in Chapter 6.

## **CHAPTER 2**

### **ACTIVE CONSTRAINED LAYER DAMPING TREATMENTS : REVIEW OF THE LITERATURE AND STATEMENT OF PROBLEM**

#### **2.1 Historical development from active control to hybrid schemes**

The application of active control techniques to suppress vibrations in flexible structures poses some special problems. These problems arise primarily from the distributed nature of such structures and the resulting large number of degrees of freedom which are required in a mathematical model to account for observed behaviour. If a lumped parameter model is derived then this generally needs to be reduced in order prior to controller design. Balas (1978) investigated the so-called spillover effects which result from ignoring higher order modes when implementing active feedback control. It was shown that spillover effects are liable to degrade or even de-stabilise the response of the closed-loop system. Various techniques for reducing the influence of spillover effects have been proposed. One effective technique in which modal transformations were employed so as to control each mode independently was described by Meirovitch and his colleagues (1983). It was shown that no spillover occurs if the number of actuators is equal to the order of the lumped parameter model and the number of sensors is capable of identifying all of the controlled modes. Furthermore the performance of so-called independent modal-space control (IMSC) was shown to be superior in almost every respect to techniques which seek to exploit the coupling in a flexible structure in order to minimise the number of actuators and sensors. Unfortunately the hardware requirements for the independent control of modes can be daunting and alternative techniques have been investigated with the aim of reducing spillover effects whilst reducing the number of actuators and sensors.

Early attempts at achieving these aims almost invariably involved experiments using various cantilevered beams with piezoelectric elements to implement the control. Bailey and Hubbard (1985) overcame spillover effects by employing a distributed parameter control algorithm. A drawback with this method concerned the need to provide a measurement of the angular velocity of the beam's tip. Since such a measurement was not available the experiments were limited to control of the fundamental mode. An alternative approach was proposed by Fanson and Caughey (1990). These authors described experiments to control the first six bending modes of a cantilevered beam using so-called positive position feedback (PPF). It was shown that using PPF the effect of spillover is to stabilise rather than de-stabilise the closed-loop system. In a further example involving a cantilevered beam, Baz and his colleagues (1992) showed how the attributes of IMSC and PPF could be combined to provide effective real-time control of structural vibrations using a smaller number of actuators.

In the early 1990s, reports began to appear of an alternative approach to controlling structural vibrations: using active techniques to augment the damping provided by a passive constrained layer added to the host structure. It had long been recognised that passive constrained layer damping is most effective at suppressing vibrations of the higher frequency modes. Using a hybrid approach, it appeared feasible to use active control to suppress the lower modes while the passive layer would reduce spillover from the higher frequency modes. Baz and Ro (1993) demonstrated the feasibility of this concept using the ubiquitous cantilevered beam but soon progressed to more complex structures such as plates and shells.

In what follows here, a survey of applications of active constrained layer damping treatments is given. The survey, which focuses on beam and plate-type structures, is divided into three parts. The first part is concerned with the choice of parameters in the passive design of an added damping layer where the passive mechanism is ultimately intended to complement the active control performance. In the second part, modelling techniques for flexible structures, such as beams and plates, treated with an active constrained damping layer, are reviewed. This review includes model updating strategies for matching the various models with the observed behaviour of the structures. Active control schemes are finally addressed with emphasis on control algorithms and sensing and actuating devices. Finally, this chapter introduces the plate vibration problem which will be investigated in this thesis and the purpose of study and strategy are also described.

## **2.2 Design of a passive constrained damping layer for use in hybrid schemes**

The main function of an active constrained layer damping treatment is to increase the shear strain in the viscoelastic layer by using an actuator placed on top of the passive damping mechanism. In addition, the actuator can generate bending moments to control directly plate vibration, as in the case of fully active control. An important aspect of the passive constrained damping layer when used with active schemes is that control authority through the bending moments can be degraded by unsuitable properties of the viscoelastic material (Liao and Wang, 1997). Selection and detailed design of the passive damping layer must be considered carefully in order to provide the best performance of both passive and active control functions.

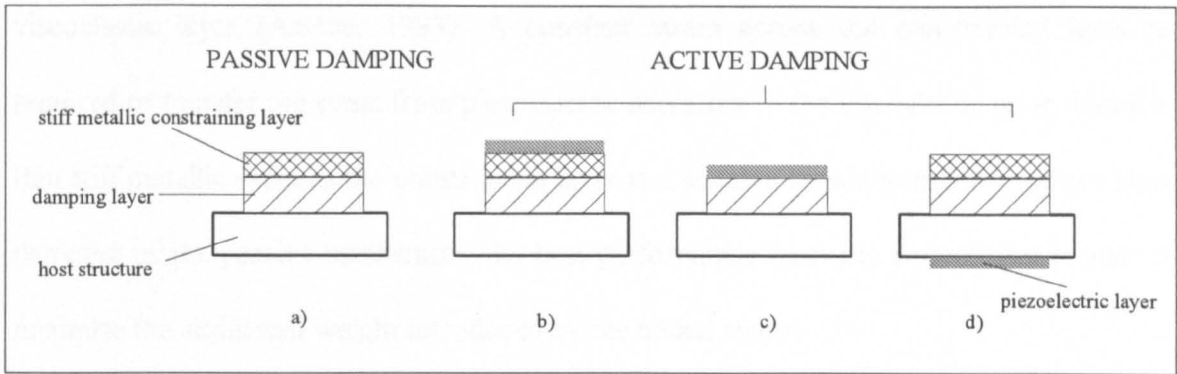


**Figure 2.1.** Surface damping configurations

- a) passive constrained damping layer
- b) active constrained damping layer followed Azvine (1994;1995)
- c) active constrained damping layer followed Baz and Ro (1993;1996)
- d) active constrained damping layer followed Lam et al (1997)

In a traditional passive constrained layer damping treatment, two distinct layers are added to the host structure, see Figure 2.1(a). The first layer usually consists of a viscoelastic material whose purpose is to introduce damping. The second layer usually consists of relatively stiff metallic material whose purpose is to constrain the motion of the damping layer and thus enhance the available damping forces. There are two alternative ways in which this arrangement can be augmented so as to introduce active control and thus increase the induced shear strain in the viscoelastic layer. Piezoelectric material can be added to operate as an actuator to increase the extensional strain of the metallic constraining layer (Azvine et al, 1995), see Figure 2.1(b) or alternatively a piezoelectric material can be used as the constraining layer itself (Baz and Ro, 1996), see Figure 2.1(c). However, the stiffness of a piezoelectric material is usually less than that of a host structure made of aluminium or steel. In general, increasing the stiffness and thickness of the constraining layer also increases passive damping (Ross et al, 1959; Huang et al, 1996). In the case of a metallic constraining layer with an add-on piezoelectric actuator, a thick constraining layer does reduce the effect of transfer strain from the actuator to the

viscoelastic layer (Azvine, 1993). A constant strain across the constraining layer is required to transfer the strain from piezoelectric actuators to the viscoelastic layer. Using a thin stiff metallic sheet as the constraining layer is a suitable choice in order to obtain high damping of the passive mechanism, the best performance from the active scheme and to minimise the additional weight introduced by the added layers.

In designing the viscoelastic layer, a high loss factor is generally a desirable property to provide effective energy dissipation. However, this property varies with temperature and frequency. Consequently the designer needs to consider viscoelastic materials which can operate within the temperature and frequency range of interest. Nashif et al (1985) provided data on commercially available viscoelastic materials which could be used as the damping layer. Shear damping can be augmented by increasing the damping layer thickness or increasing the space between the constraining layer and the host structure such that a high shear strain in the damping layer can be achieved. In practice, it is difficult to find a thick damping layer possessing the required shear stiffness and the high loss factor (Ross et al, 1959). In addition, a thick damping layer can degrade the transmissibility of bending moment generated by a piezoelectric actuator to a host structure. Theoretically, as the ratio of damping layer thickness to the thickness of the host structure approaches zero, the ratio of modal loss factor to material loss factor approaches a finite value (Jones, 1995). The practical result of this theoretical observation is that thin damping tapes are often used.

There are a number of configurations of the constrained layer damping treatment which can be used in order to introduce significant damping into a structure. Examples include

the use of a spacer to increase the gap between the constraining layer and the host structure and the use of multiple constrained damping layers (Ross et al, 1959). The use of multiple constrained damping layers provides more stiffness in the first constraining layer. However, the overall loss factor does not improve significantly. Nevertheless, the main advantage of using the multiple layers incorporating multiple damping materials for the damping mechanism is the resulting improvement in performance over a broader temperature range. Two constrained damping layers with two different damping materials, which provide a high loss factor at different temperatures, are placed either in sequence on top or placed on either side of the host structure so as to produce a high loss factor over a greater temperature range (Nashif et al, 1985). Partial coverage of the constrained damping layer also has been investigated (Plunkett and Lee, 1970; Nashif et al, 1985). These investigations show that damping can be maximised by placing the damping patch edges over areas of maximum curvature in the structure to be controlled. Damping depends on the length of the constraining layer in relation to the bending wavelength of the structure. For a long constraining layer, the shear strain induced some distance from the maximum curvature of the bending modes may not be significant and the strain of the damping layer is exerted as an extensional motion along with the constraining layer. However, a constraining layer length which is effective at a specific lower frequency mode of bending vibration may cause deterioration of damping of the higher modes involving short wavelengths (Nashif et al, 1985; Lesieutre and Lee, 1996). To operate effectively over a broad frequency range, generally the damping treatment should be placed so as to completely cover the flexible structure.

### **2.3 Modelling of flexible structures with an active constrained damping layer**

Models of beams and plates treated with an active constrained damping layer are required in order to examine the likely performance of active control schemes before the implementation stage. To obtain suitable models, there are three possible analytical formulation techniques: derivation of the governing differential equations, Rayleigh-Ritz approaches (Rongong et al, 1997) and finite element analysis. Compared to a finite element model, the governing differential equation and Rayleigh-Ritz approach models have the advantage that the influence of physical parameter variations can readily be studied. The performance of the controlled structures can be studied through changes in parameters such as material properties and the choice of control scheme (Shen, 1994). However in practice, finite element modelling is probably a more effective technique for dealing with distributed systems. The finite element model can be formulated to match a point of interest in a structure and also the boundary conditions can be modified more easily. Khatua and Cheung (1973) presented a finite element formulation of multi-layered constrained layer damping beams and plates. The constraining layer and the host structure were treated as thin stiff beams and plates. The viscoelastic layer was exposed to shear strain related to relative displacement of both stiff layers. This work was extended to include the addition of active damping by Baz and Ro (1996). Here the piezoelectric layer was used as the stiff constraining layer. The system equations were established specifically to perform active control using collocated sensors and actuators. It will be shown in the present thesis that using state space methods, along with modern control theory, the present author's approach does not require this assumption of collocated sensors and actuators. Baz and Ro (1996) assumed that the loss factor property of damping layer is constant. In general, a loss factor of viscoelastic materials, used as the damping layer, is

frequency dependent. Several methods have been developed to model constrained layer damping with frequency-dependent characteristics. Johnson and Kienholz (1982) and Veley and Rao (1996) used the modal strain energy method for describing a modal loss factor of the damping layer. An advantage of the method is the saving in the time and effort needed to model the constrained layer damping treatment. Development of a mathematical equation of the loss factor has been investigated, for example, fractional derivatives (Bagley and Torvik, 1983) and the Golla-Hughes-McTavish (GHM) method (Golla and Hughes, 1985). An alternative approach to obtain an accurate model of the constrained layer damping with frequency-dependent properties is the use of model updating techniques to match a mathematical model with the observed behaviour of a host structure.

Model updating has been used extensively in the field of structural mechanics. Modern structures are increasingly more complex and accurate structural models are essential for use with modern control algorithms. Traditionally, dynamicists have used direct experimental modelling techniques to identify system models (for example, Ibrahim and Saafan, 1987). This latter method is concerned essentially with physical parameter identification. Difficulties in applying the technique arise due to incompleteness of the model and the requirement for large amounts of measurement data. Usually the number of system modes to be identified is less than the number of measurement points, in which case it causes the system matrices to be ill conditioned and non-unique (Mottershead and Friswell, 1993). The modern trend in structural modelling is to use experimental data to update existing analytical models.

Inman and Minas (1990) presented several model updating techniques using modal data (identified natural frequencies, damping factors and mode shapes) from experiments to match the finite element models to observed behaviour. For damped structures, there are two key updating techniques: model correction by eigenstructure assignment or alternatively pole placement. Eigenstructure assignment requires knowledge of the eigenvalues (natural frequencies and damping factors) and also the eigenvectors (mode shapes) from experiments in order to implement the algorithm. A certain amount of computational effort is needed to perform the iterations required by this method and it is often difficult to obtain reliable measurements of mode shapes. The pole placement technique for updating the analytical model uses measured natural frequencies and damping factors to modify stiffness and damping matrices so as to match desired responses. Disadvantages associated with updating via pole placement are in deciding which parameters are updated and also that the responses from predicted models are not exactly reproduced due to lack of measured eigenvector information (Friswell and Mottershead, 1995). Other model updating techniques and a philosophy for general applications have been reviewed by Mottershead and Friswell (1993).

The common problem of structural modelling is that the size of mass, damping and stiffness matrices generated by finite element modelling is very large. This causes difficulties in computations for control system design. Model reduction techniques are generally used to reduce the size of the matrices by eliminating unnecessary variables. Guyan reduction (Guyan, 1965) is a common method to eliminate unwanted co-ordinates from the model. However, reduction techniques do affect the accuracy of the predicted

responses. Great care must be taken when using a reduced-order model for control system design where spillover effects may occur.

## **2.4 Active control strategies**

Control algorithms and experimental configurations using active constrained layer damping treatments have been presented by many investigators. For complex modern control algorithms, effective and accurate structural models are needed to produce robust control systems. Robustness of controlled systems implies that a controller has the ability to tackle uncertainties such as time varying behaviour, perturbations due to noise and the use of truncated models (Burl, 1999). In what follows here, the development of control schemes for active constrained layer damping treatments is reviewed.

Baz and Ro (1993) demonstrated the use of the piezoelectric films as combined sensors and actuators in an application of the active constrained layer damping treatment in which the sensor layer was placed between the viscoelastic layer and the host cantilever beam. Also, an actuator layer was placed on the top of the viscoelastic layer. With this configuration, the output piezo-sensor voltage generated from induced strain, which is proportional to the beam curvature, was manipulated by a proportional and derivative controller to provide a command signal to the piezoelectric actuator. The active scheme was designed to control an infinite number of modes of the beam vibration and to study the effects of varying controller gains. Shen (1994) studied the controllability, observability and stability of a beam with active constrained layer damping using piezoelectric materials as both the sensor and actuator layers. Azvine et al (1995) applied negative velocity feedback to augment the shear damping in a constrained damping layer bonded to a

cantilever beam. Unlike the above configurations, PZT actuators, placed on the top of a metallic constraining layer, see Figure 2.1(b), were used to induce extensional strain in the constraining layer and then shear strain in the damping layer. However, non-located sensors and actuators were used in this work to control the first two modes of beam vibration. This contrasted with the suggestion by Balas (1979) who proposed the use of collocated sensors and actuators with direct velocity feedback. This collocation ensures that the mode shapes of controlled modes must displace in the same direction at the points of measurement and actuation. Other configurations of the active constrained layer damping treatment have been studied to improve vibration suppression. Liao and Wang (1996) proposed a new configuration of the active treatment in which connectors are used to join the free end of the piezoelectric constraining layer and the host structure. The transmissibility of the active action can be enhanced in this way due to the fact that direct control authority of the piezoelectric layer to the host structures is reduced through the soft viscoelastic layer. Lam et al (1997) also used a metallic sheet as the constraining layer for the active constrained layer damping treatment to control the vibration of a cantilever beam. Unlike the configuration described by Azvine et al (1995), the piezoelectric patch was placed directly on the host structure to perform hybrid control using purely passive and fully active mechanisms, see Figure 2.1(d). Lam and her colleagues found that placing the piezoelectric actuator on the opposite side to the passive layer can reduce the control effort significantly more than that required for fully active control and the active constrained layer damping treatment. Baz and Ro (1995) utilised linear quadratic optimal control to obtain optimised proportional-plus derivative control gains and to minimise the displacement responses of the active constrained layer damping beam. To avoid instability problems caused by sensor and actuator dynamics, it is generally necessary to select small

control gains when using the proportional-plus-derivative controller (Baz, 1997a). Instability of the active constrained layer treatment is likely when using higher control gains, as indicated by Baz (1997b), and the passive treatment becomes dominated by the active scheme when the gains approach infinity. This implies that the gain and phase margins of the controlled structures are decreased which is critical since acceptable robustness is often characterised by specifying minimum gain and phase margins. Baz (1997a,b) developed boundary control of the cantilever beam with an active constrained layer damping treatment to ensure global stability of all the modes of vibration. It was found that the total energy of the controlled beam does not increase with time if a negative longitudinal velocity feedback of the signal from the piezoelectric constraining layer is used. This longitudinal velocity signal can be obtained from relationships between the longitudinal displacements of the host beam (the sensor layer) and the constraining layer (Baz, 1997a,b). Boundary control was developed for cantilever beams but Baz noted that it has the capability of being extended to treat plates and rotating beams.

The above control strategies were developed to suppress bending vibrations of beam structures. For a two-dimension vibration mode (concurrent bending and torsional), Shen (1995) suggested that control algorithms more advanced than the simple proportional-plus-derivative control might be needed to control simultaneously the bending and twisting vibration modes of cantilever beams using the active constrained layer damping treatment. This implies that, using full coverage of the active constrained damping layer together with the proportional-plus-derivative controller, it may not be possible to obtain effective control in two dimensions where there is concurrent bending and torsional motion. In such a case, segmented sensors and actuators might provide better performance. For example,

to attenuate levels of coupled bending and twisting in a cantilever beam, Aldraiham and Wetherhold (1997) used a piezoelectric composite actuator where PZT bars are placed in an epoxy matrix. The coupled bending and twisting vibration of the beam was reduced effectively by using the actuator with suitable orientation in relation to the PZT bars alignment.

Investigations have progressed to more complex structures, notably plates. Using a cantilevered plate, partially treated with an active constrained damping layer, Baz and Ro (1996) showed how the bending mode could be controlled effectively using a simple proportional control arrangement. A comparison of active, passive and hybrid (i.e. active constrained layer damping treatments) appeared in the study by Veley and Rao (1996). A cantilevered beam and also a plate clamped on all four sides were used as host structures to examine and compare active, passive and hybrid control strategies. The design objectives were to minimise the weight of the structures and also to achieve high levels of damping. The results showed that the hybrid approach is superior to the active control of an untreated plate in that a given damping ratio can be achieved using less than half the mass. Azvine et al (1994) presented an application of active constrained damping treatments to the plate clamped along two opposite ends. This plate is also used in the present study. The plate is a simplified version of an instrument box cover found in a military aircraft. Azvine investigated active constrained layer damping treatments as a means of suppressing bending and torsional vibrations which were causing the instrument box to malfunction in service. Negative velocity feedback was used along with non-collocated sensors and actuators in an attempt to control the first two modes of vibration. Using two actuators, the benefits of the constraining layer were clearly demonstrated:

higher feedback gains could be used to give lower resonant peaks without causing instability. However, this study indicated the need for better models of the host plate, the passive constraining layer and the piezoelectric actuators together with a more effective control algorithm based upon this model. At the same time, it was essential for the eventual application that the amount of hardware be minimised.

## **2.5 Problem under review**

The plate vibration problem used in the present study originates from work by Azvine et al (1994). The plate dimensions are approximately 400 mm × 190 mm and the plate is fixed along the shorter opposite edges. This plate structure is the foundation of a control box inside an aircraft fuselage where severe vibrations occur. Excessive levels of vibration applied to the foundation can result in electrical connector failures and subsequent malfunctions of the control equipment. To study strategies for vibration suppression, Azvine et al (1994) simplified this structure to a panel plate which clamped along its shorter sides.

In the work by Azvine and his colleagues, initial attempts at active control aimed to suppress simultaneously the first two modes, bending and torsional, of plate vibration. The plate was treated partially with passive constrained damping layers to perform vibration suppression, especially of the high frequency modes. A PZT ceramic was used as an actuator to provide the active control function. The control algorithm employed negative velocity feedback. To implement the algorithm, the best actuator locations had to be found so that they corresponded to the maximum curvatures of the vibration modes to be controlled. However, it was noted that the best location for controlling one mode could

have detrimental effects on another controlled mode (Azvine, et al 1994). The controller gains were chosen arbitrarily to obtain adequate vibration suppression. For more complex structures with multiple controlled modes, this control technique would be difficult to apply when attempting to ensure that the number of sensors and actuators is minimised and energy supplied to the active elements is minimised.

Modal control, formulated in state-space co-ordinates (Balas, 1978) is an alternative form of control algorithm in which the stability of the controlled system can be studied numerically before implementation. Optimal selection of control gains also can be achieved using this technique. To design the modal controller, an analytical, finite- element model of a panel plate formulated in state-space co-ordinates is required. The analytical model predictions need to be matched with the observed behaviour of the plate using experimental identification techniques. The present study provides an example of active vibration control that is applicable to many other flexible structures.

### *2.5.1 Purpose of the study*

In the present study, a clamped-clamped plate is used as the host structure to investigate strategies for vibration suppression. The traditional passive damping treatments described in the previous chapter will be augmented using active control schemes. The plate will be fully covered with the viscoelastic layer and a further metallic constraining layer which together comprise the passive damping mechanism. Plumbum (lead) Zirconate Titanate (PZT) material is used as the actuator to enhance the constraining layer strains. As a result the induced shear strain (and damping) in the viscoelastic layer is increased.

Whereas the application of a damping treatment to a structural component is a relatively straightforward operation, caution must be exercised before proceeding to consider the addition of active control. There are two reasons why circumspection is required. First, active control requires the provision of sensors, actuators and computing elements which can add considerably to cost, weight and complexity. Second, there are the spillover problems arising from the active vibration control of the distributed structure.

### *2.5.2 Strategy*

A model-based approach is developed to investigate active constrained layer damping of a clamped-clamped plate. Finite element modelling is used to formulate the equations of motion of the plate and its passive damping treatment. Major advantages occurring from the use of the finite element method are that the model can be modified conveniently to suit any changes in the system and the model is physically meaningful because it is formulated using the material properties and dimensions of the system. Active control is more conveniently formulated in state-space notation which requires transformation of the finite element model (Firoozian and Stanway, 1988). This transformation is straightforward in principle but difficulties can arise in practice. The choice of model order is crucial if observed behaviour is to be accounted for without requiring excessive matrix dimensions. To obtain an acceptable compromise, formal model reduction techniques (Avitabile et al, 1989) will be used here. Also, it has been found necessary to use model updating algorithms (Mottershead and Friswell, 1993) in order to obtain sufficiently close correspondence between model predictions and observed behaviour. Modal control theory (Balas, 1978) associated with coupling of the control force is used. An advantage of coupling the force is to control a number of modes

simultaneously using the minimum number of actuators. Figure 2.2 summarises the strategies used in the present study.

## **2.6 Summary of Chapter 2**

A survey of uses of the active constrained layer damping treatment to beam- and plate-type structures has been presented. Passive design of the constrained damping layer, modelling of the structures with the active treatment and the active control strategies (control algorithms and the active treatment configurations) have been discussed in detail in separate sections. To avoid confusion, some fundamental theory, for example the placement of sensors and actuators and the robustness of reduced-order models for controllers will be treated in detail in the relevant chapters.

Finally, A statement of the problem of controlling plate vibrations used in the present study has been addressed. Justification of strategies also has been made to use as procedures. In the chapter which follows, the theoretical basis of the investigation is presented.

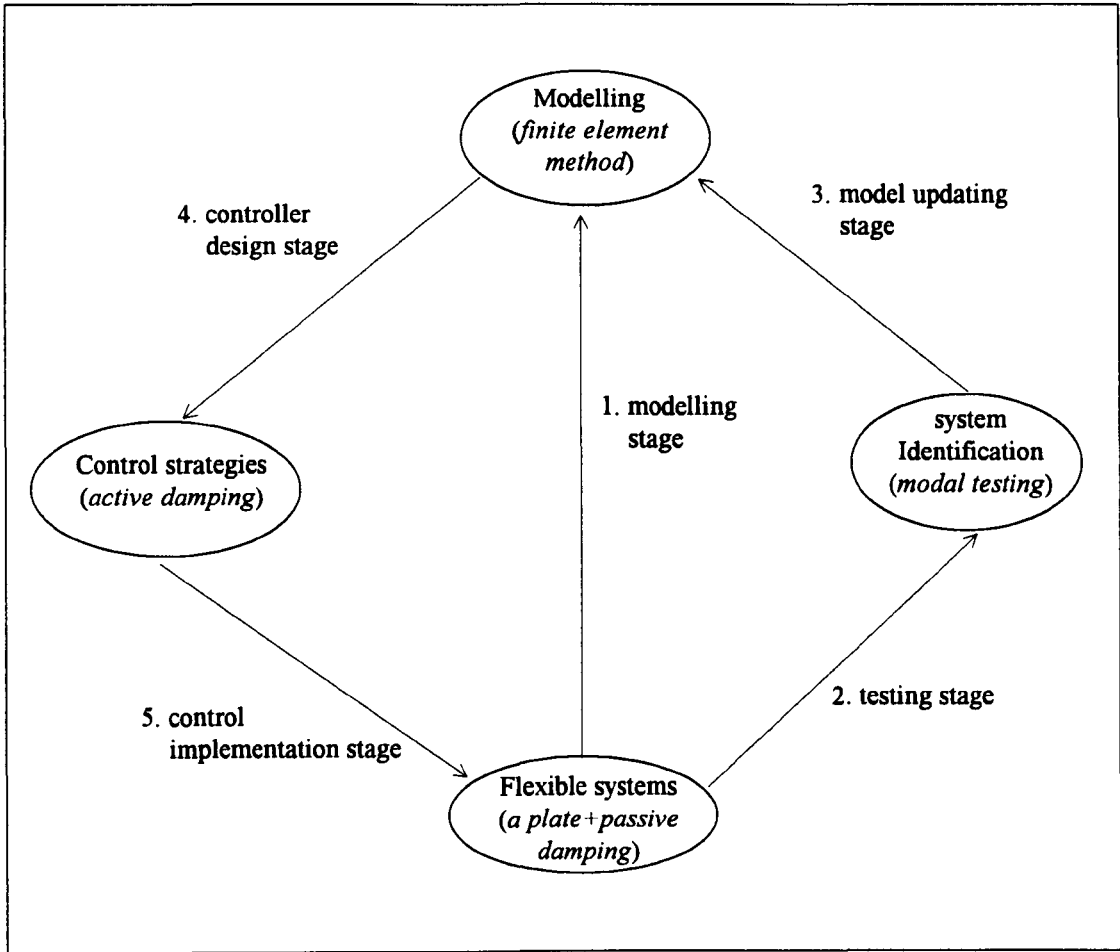


**Figure 2.2.** Strategies for active vibration control of flexible systems

# CHAPTER 3

## THEORY

### 3.1 Objectives

This chapter is intended to present three basic theories, finite element modelling, system identification and modal control techniques which are used in the present study. The key aims of this chapter are to describe the interrelationships between the above theories and to show the sequential order of procedures for developing a vibration control strategy. To achieve a flowing presentation of these techniques, details of the more complicated mathematical formulations are relegated to appendices. Nevertheless, all the key equations are retained in this chapter.

The main purposes for the study of each section of theory are summarised below. In the finite element modelling study, the goals are, first, development of a plate model with a constrained damping layer and second, verification of the finite element plate models by comparison with well-established work. In the system identification section, techniques for modal data extraction (natural frequencies and damping factors) and model updating are presented. Finally modal control using pole placement techniques is described. The treatment of modal control contained in this chapter is limited to the continuous-time case. In subsequent chapters a discrete-time approach will be developed and used for the eventual experimental implementation.

## 3.2 Finite element modelling

The analysis of a three-layer plate was introduced by Ross et al (1959). To produce extensional and shear damping, the host plate is covered with a damping layer and a second, relatively stiff plate acts as a constraining layer. The foundation of finite element modelling of multi-layer plates was described by Khatua and Cheung (1973). The shear strain of the middle layer (i.e. the damping layer) is formulated so as to relate to the extensional motion of the outer layers. Baz and Ro (1996) extended the finite element formulation to include distributed piezoelectric sensors and actuators whereby piezoelectric materials were used as the constraining layer. In the present study, the plate configuration is a simple three-layer plate where piezoelectric actuators are used to increase the extensional strain in the metallic constraining layer. Piezoelectric elements can then be added to the finite element model by treating them as elastic elements. The equation governing the behaviour of piezoelectric elements and including the coupling effects between mechanical and electrical properties is described in a later chapter. The following sub-sections are concerned with the formulation and verification of the finite element plate models which are generated from finite element code written in FORTRAN computer language format.

### 3.2.1 *The plate model*

Four-node rectangular plate elements are used to form the finite element plate model. An outline drawing of the three-layer rectangular element, along with the coordinate system, is shown in Figure 3.1(a). Viscoelastic material is used as the middle damping layer. Analysis of the base plate and the constraining layer requires assumptions of plate theory that can be found in any suitable textbook on fundamental plate theory or

finite element analysis of plates, for example, Dawe (1984, p. 281). In addition, it is assumed that the plane section of the viscoelastic layer remains in plane after deformation, and that there is no shear strain in the constraining layer and the base plate. The transverse displacement  $w$ , Figure 3.1(b), is considered at all points on the cross section of the three-layer plate. The bond for each layer is treated as a perfect bond.

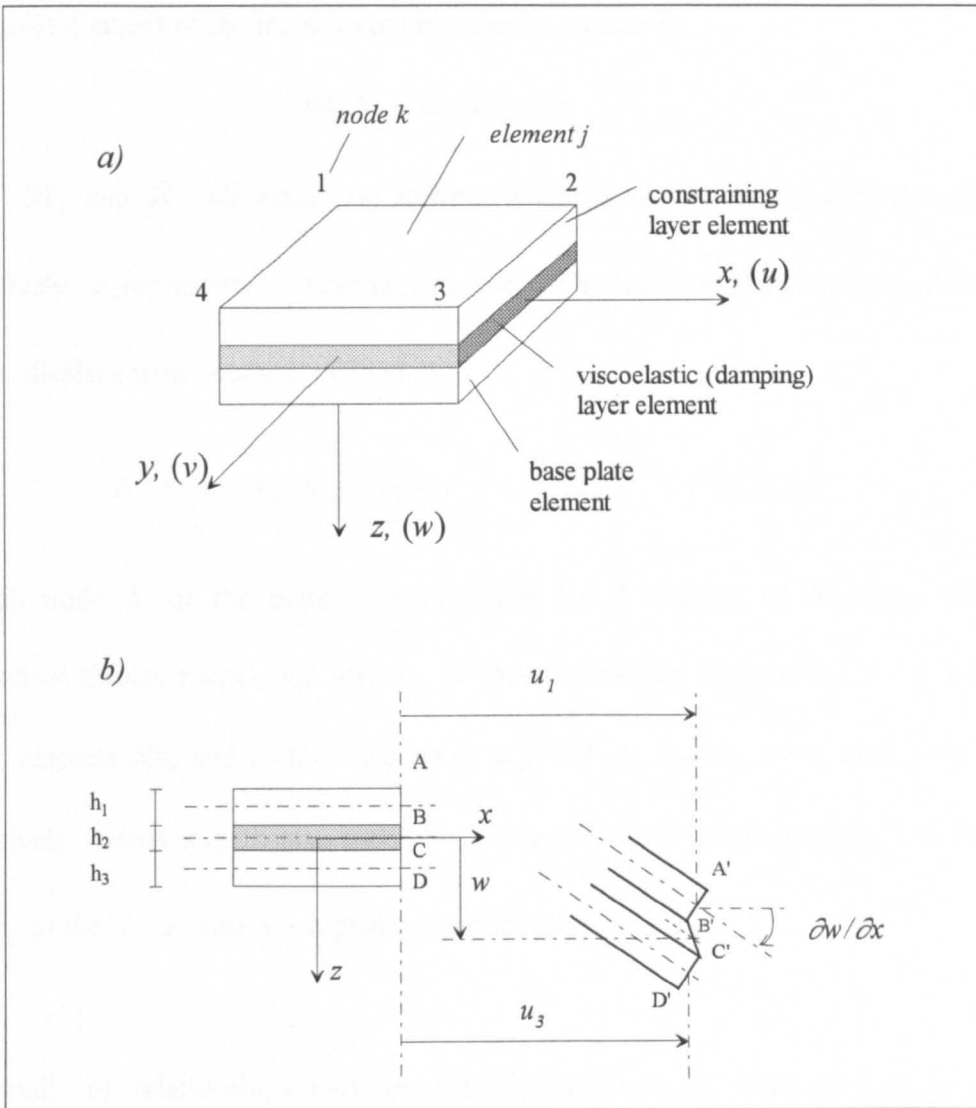


**Figure 3.1.** A rectangular element of the three-layer plate  
 a) co-ordinate system and nodes of the elements  
 b) displacement of the elements at  $x$ - $z$  plane

Since the finite element formulation of the plate treated with the constrained damping layer uses the potential energy method (i.e. strain energy) to form mass and stiffness matrices in the equations of motion, the longitudinal displacement of the viscoelastic layer must be evaluated in relation to the existing longitudinal displacements of the constraining layer and the base plate, as shown in Figure 3.1(b). Then the equation of motion of the rectangular element of the three-layer plate can be written as

$$\mathbf{M}_j \ddot{\Delta}_j + \overline{\mathbf{K}}_j \Delta_j = \mathbf{F}_j \quad (3.1)$$

where  $\mathbf{M}_j$  and  $\overline{\mathbf{K}}_j$  are mass and stiffness matrices of the rectangular plate element  $j$  respectively,  $\mathbf{F}_j$  represents an external force vector activated at the element nodes and the element displacement vector is defined as

$$\Delta_j = \left\{ u_{1k}, v_{1k}, u_{3k}, v_{3k}, w_k, \frac{\partial w}{\partial y_k}, \frac{\partial w}{\partial x_k} \right\}^T \quad k = 1, 2, 3, 4. \quad (3.2)$$

At each node  $k$  of the plate element, there are 7 degrees of freedom. These are longitudinal displacements,  $u_{1k}$  and  $v_{1k}$  of the constraining layer in the  $x-z$  and  $y-z$  planes, respectively, and of the base plate,  $u_{3k}$  and  $v_{3k}$  in the  $x-z$  and  $y-z$  planes, respectively, transverse displacement,  $w_k$  and rotational displacements,  $\partial w / \partial y_k$  and  $\partial w / \partial x_k$  in the  $y-z$  and  $x-z$  planes, respectively.

The details of relationships between the displacements of three-layer plate and the formulation of the mass and stiffness matrices in Equation (3.1), are given in Appendix A, section A1. Note that the stiffness matrix  $\overline{\mathbf{K}}_j$  is complex due to the complex shear modulus of the viscoelastic layer. Viscoelastic or rubber-like material is traditionally represented by its shear modulus in the form  $G(1+i\eta)$  where  $G$  is the storage modulus

and  $\eta$  is the loss factor (Lazan, 1968). The imaginary term represents the dissipation of energy or the damping properties of the material. This kind of damping is often referred to as hysteretic or structural damping (Ewins, 1984). Representation of material damping using the complex modulus has the advantage that it follows Hooke's law, the same as in the purely elastic case. Then the model associated with the viscoelastic material can be analysed using an existing elastic solution (Goodman, 1995).

### 3.2.2 Verification of plate model

To study the accuracy of the modelling techniques, two examples of verification are presented, one for the untreated plate and one for the three-layer plate model. In the first case, the equations of motion of the base plate are formulated and the eigensolutions are then found. The natural frequencies and mode shapes of base plate are obtained from these solutions. The natural frequencies are compared with those from the approximate analytical solutions presented by Warburton (1954). Mode shapes are then used to check that the number of elements is sufficient to obtain the corresponding natural frequencies. Note that, in general, the more elements which are used in representing a structure, the better will be the accuracy of the solutions (i.e. convergence to the exact solutions) (Dawe, 1984). To examine convergence of the solutions, the finite element plate model is divided, as a mesh, into 3 step sizes, 8 by 4, 16 by 8 and 32 by 16 elements along the  $x$  and  $y$  directions respectively (see Figure 3.2). The plate dimensions and material properties used in the numerical study are also given in Figure 3.2. The results from calculations of natural frequencies are illustrated as the deviation of the finite element model solutions from Warburton's solutions and are shown in Figure 3.3. The corresponding numerical data for the natural frequencies themselves are given in Table 3.1. In Appendix A, section A2,

Figure A.2 shows the first ten mode shapes corresponding to the natural frequencies. Warburton's solutions of plate vibrations satisfy exactly the boundary conditions for fixed and simply supported edges, but are only approximate for free edges. As a result the Warburton's solution predicts higher natural frequencies than the true values (Warburton, 1954). After refining the mesh size, the predicted natural frequencies of higher modes from the finite element model tended to take on lower values than Warburton's solutions. It may be inferred from the results that better predictions are obtained especially in higher modes of vibration as the number of elements is increased and deviations of predicted natural frequencies from Warburton's solutions remain within 1 percent for all sizes of mesh used.

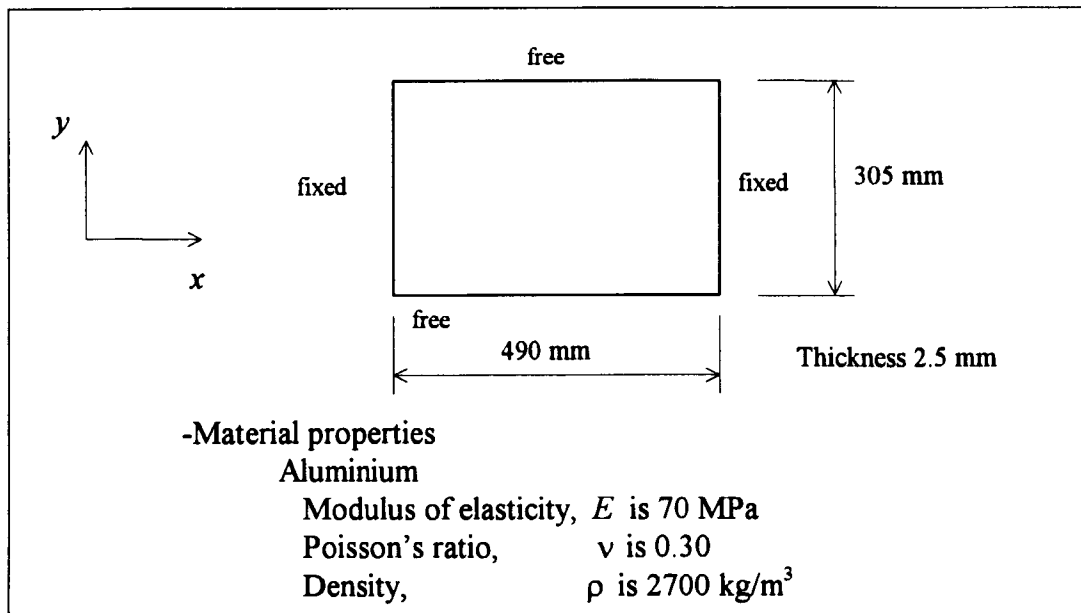


**Figure 3.2** Drawing of simplified plate

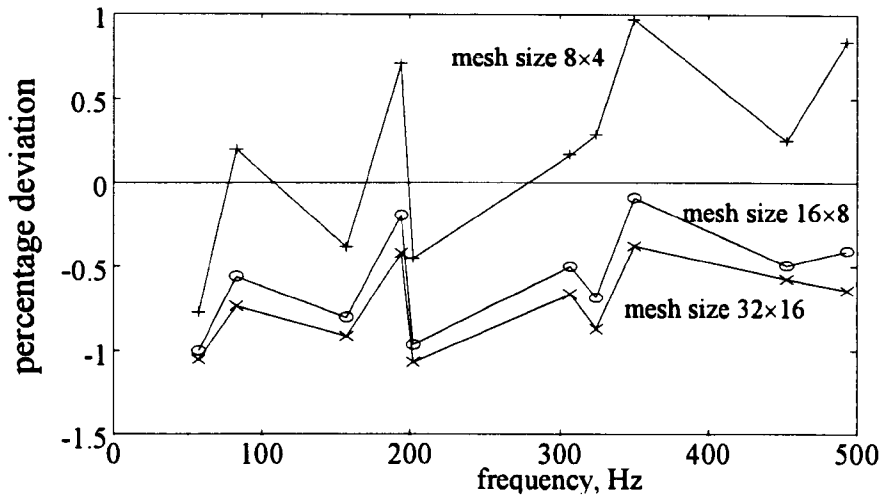


Figure 3.3. Deviation of first ten natural frequencies predicted by the finite element model from Warburton's solution

Table 3.1: A comparison of the first ten natural frequencies of panel plate from the finite element program and from Warburton's approximate solutions

mode number	The finite element method			Warburton's solution (Hz)
	8×4 elements	16×8 elements	32×16 elements	
1	56.54	56.41	56.38	56.98
2	82.09	81.47	81.33	81.93
3	156.43	155.77	155.60	157.03
4	195.26	193.52	193.08	193.89
5	200.98	199.94	199.74	201.89
6	308.29	306.25	305.75	307.78
7	325.60	322.46	321.86	324.67
8	353.50	349.77	348.77	350.09
9	453.98	450.62	450.23	452.84
10	497.59	491.48	490.30	493.46

In the second example of the model verification, a simply supported plate with a surface treatment is considered. Natural frequencies and modal loss factors obtained from the finite element program are compared with those predicted by the finite element model and the analytical solutions presented by Johnson and Kienholz (1982). The details of the plate used in their study are repeated here. Two identical 304.8 mm × 348.0 mm rectangular plates of 0.762 mm thickness are used as the host plate and as the constraining layer. The following material properties apply: Young's modulus  $E = 68.9$  GPa, Poisson's ratio  $\nu =$

0.30 and density  $\rho = 2740 \text{ kg/m}^3$ . The 0.254 mm thick viscoelastic layer, placed between the host plate and constraining layer, has the following material properties: shear modulus  $G = 0.896 \text{ MPa}$ , Poisson's ratio  $\nu_2 = 0.49$ , density  $\rho_2 = 999 \text{ kg/m}^3$  and loss factor  $\eta = 0.50$ . The boundary conditions are applied only to the base plate. The paper by Johnson and Kienholz presented the first five natural frequencies and modal loss factors from the analytical solution by Abdulhadi (see Johnson and Kienholz, 1982) and the commercial finite element program, NASTRAN, which uses the modal strain energy (MSE) method to obtain the solutions. The NASTRAN plate model was divided into 10 by 12 elements in the width and length directions respectively. A study of the convergence of the predictions is also considered for this case by first dividing the elements of the plate model into 8 by 8 and then into 10 by 12 elements in the width and length directions, respectively. The results are compared in Tables 3.2 and 3.3. Good agreement is obtained in that virtually all of the results from the finite element model are within 2 percent of the analytical solutions. Note that the results from the program are closer to the analytical solutions than the NASTRAN package. However, this accuracy has to be paid for in additional computation time.

### 3.2.3 Summary of finite element modelling

A plate treated with a constrained damping layer has been modelled using the finite element technique. The equations of motion are obtained wherein the stiffness matrix is complex so as to represent both storage and dissipation mechanisms in the three-layer plate. Later, piezoelectric actuator elements will be added directly in the form of elastic elements with coupling between the mechanical and electrical variables.

**Table 3.2:** A comparison of the first five natural frequencies from the finite element program, the analytical solutions and NASTRAN/MSE

The program, 8×8 elements (Hz)	The program, 10×12 elements (Hz)	The analytical solutions* (Hz)	Nastran/MSE* (Hz)
62.2	61.8	60.3	57.4
115.8	115.1	115.4	113.2
130.8	130.3	130.6	129.3
179.7	178.3	178.7	179.3
196.7	195.5	195.7	196.0

\* see Johnson and Kienholz (1982)

**Table 3.3:** A comparison of the first five modal loss factors from the finite element program, the analytical solutions and NASTRAN/MSE

The program, 8×8 elements	The program, 10×12 elements	The analytical solutions*	Nastran/MSE*
0.217	0.218	0.190	0.176
0.205	0.204	0.203	0.188
0.1996	0.1995	0.199	0.188
0.1810	0.1816	0.181	0.153
0.1766	0.1760	0.174	0.153

\* see Johnson and Kienholz (1982)

From the verification studies, the author's finite element models show good agreement with well-established solutions. As expected, the accuracy of models can be improved by increasing the number of elements in the models. However, more accurate modelling does not guarantee that the formulated models can account for the observed behaviour of structures owing to uncertainties such as imperfections in materials and in connections within the structures. To account for observed behaviour in real structures, some experimental testing must be performed. Differences between the model predictions and the observed behaviour of real structures can then be minimised through model updating techniques (Mottershead and Friswell, 1993). The following section is devoted to the details of system identification techniques to achieve refined models which characterise the behaviour of real structures.

### 3.3 System identification

In practice, performance predictions from mathematical models of structures usually differ from observed behaviour owing to the complexity of structures and connection methods, imperfections in materials and problems in establishing boundary conditions. Modal testing is used widely as a tool for obtaining information on the actual behaviour of structures. The data from testing can be used to construct directly or to provide corrections to existing mathematical models (Ewins, 1984). Usually, each model updating algorithm requires a different set of experimental data to implement the algorithm. The following subsections are concerned with considerations of suitable methods for modal data extraction and for model updating. The methods judged to be the most suitable will ultimately be applied in later numerical and experimental investigations.

#### 3.3.1 *Modal data extraction*

Modal testing is a technique for practical vibration analysis so that information used to describe the characteristics of structures under test can be extracted from measured data. The basic modal data obtained from identification studies are the natural frequencies, damping factors and mode shapes (the latter for systems with multiple degrees of freedom). A simplified introduction to modal data is included here for completeness.

To introduce the description of modal data, consider a single degree of freedom model of a mass-spring-damper system as shown in Figure 3.4.

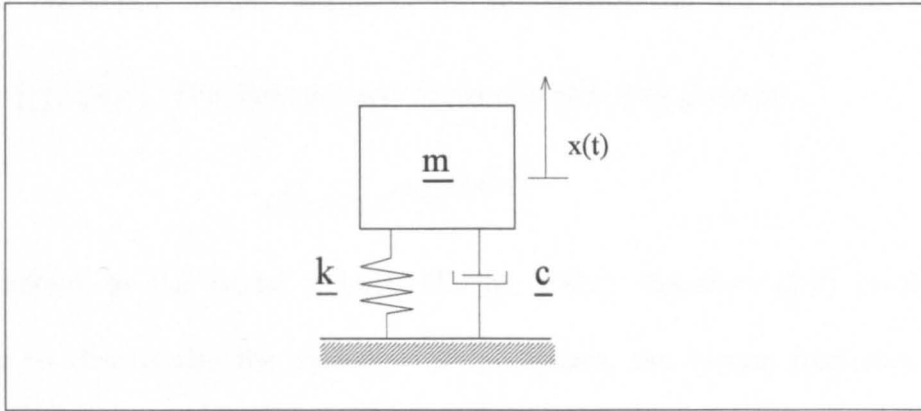


Figure 3.4. Schematic of a mass-spring-damper system

The equation of motion for free vibration is

$$\underline{m}\ddot{x}(t) + \underline{c}\dot{x}(t) + \underline{k}x(t) = 0 \quad (3.3)$$

where  $\underline{m}$  is the mass,  $\underline{c}$  is the damping coefficient,  $\underline{k}$  is the spring stiffness,  $x(t)$  is the displacement at time  $t$  and  $\dot{x}$  represents the time derivative of  $x$ . Then assume a general solution of the form:

$$x(t) = x_0 e^{st} \quad (3.4)$$

where  $x_0$  is constant and  $s$  is a complex number. Substitute Equation (3.4) into Equation (3.3) so that after some manipulation the following result is obtained:

$$(\underline{m}s^2 + \underline{c}s + \underline{k})e^{st} = 0 \quad (3.5)$$

If Equation (3.5) can be satisfied, then our assumption of the form of the solution, i. e. Equation (3.4), is correct. The solutions of Equation (3.5) are simply the roots of  $(\underline{m}s^2 + \underline{c}s + \underline{k}) = 0$ , i. e.

$$s_{1,2} = -\frac{\underline{c}}{2\underline{m}} \pm i \frac{\sqrt{\underline{c}^2 + 4\underline{k}\underline{m}}}{2\underline{m}} \quad (3.6)$$

$$= -\bar{\omega}\zeta \pm i\bar{\omega}\sqrt{1-\zeta^2} \quad (3.7)$$

where the undamped natural frequency is  $\bar{\omega} = \left(\frac{k}{m}\right)$  and the damping factor is  $\zeta = \underline{c}/c_o = \left(\frac{\underline{c}}{2\sqrt{km}}\right)$ . The time response of the system is then given by

$$x(t) = x_0 e^{-\bar{\omega}\zeta t} e^{i(\bar{\omega}\sqrt{1-\zeta^2})t} \quad (3.8)$$

which is known as the modal solution (Ewins, 1984). Equation (3.8) involves two parameters to characterise the dynamics of the system, the natural frequency  $\bar{\omega}$  and damping factor  $\zeta$ . For systems with multiple degrees of freedom, the solution can be formed as the superposition of the response of each degree of freedom.

Greater complexity of the modal solution occurs for the case of forced vibration of systems with multiple degrees of freedom. This class of model is generally used to represent a distributed structure. The mode shape is an additional parameter which is a component of the solution. Of these three parameters, natural frequency, damping factor and mode shape, mode shape is the most difficult to obtain in practice owing to incomplete models and the requirement for vast amounts of test data (Ewins, 1984). In the present study, model correction by pole placement (Inman and Minas, 1990) is used as the updating algorithm for the finite element model. The main reason for this choice is that the algorithm requires only estimates of natural frequencies and damping factors from experiments on the structure.

The so-called peak-picking method is the most convenient technique for identifying natural frequencies and damping factors of structures. Constraints inherent in the application of this method are that the frequency response functions of the structure should contain well-separated modes and that the percentage of damping should not be too low (less than 1%)

or too high (higher than 5%) such that it affects the accuracy of identified parameters. However, when structures with damping factors outside these limits do arise, the method may still be applied to obtain initial estimates before using other methods to refine the estimated parameters (Ewins, 1984). A summary of the method is given as part of Appendix B.

### 3.3.2 Updating the finite element model

The concept of the updating algorithm described by Inman and Minas (1990) is to modify the natural frequencies and damping factors to desired values using a pole placement technique. This procedure causes changes to the stiffness and damping matrices in the equations of motion. The pole placement technique in control system design was originally described for modal control schemes (Porter and Crossley, 1972). One advantage of using pole placement for model updating is that it is designed to minimise changes of the original matrices. The ideas behind the method are described below and the details of procedures are given in Appendix B, section B2.

The method requires the formulation of the equations of motion of a system with  $n$  degrees of freedom in the state-space form:

$$\dot{\mathbf{Y}} = \mathbf{A}\mathbf{Y} + \mathbf{B}\mathbf{u} \quad (3.9)$$

where a state-variable vector  $\mathbf{Y}_{2nx1}$  is related to a physical-variable vector  $\Delta_{nx1}$  by

$\mathbf{Y} = [\dot{\Delta} \quad \Delta]^T$ ,  $\mathbf{u}_{nx1}$  is an input vector, and matrices  $\mathbf{A}$  and  $\mathbf{B}$  are defined as

$$\mathbf{A} = \begin{bmatrix} -\mathbf{M}^{-1}\mathbf{D} & -\mathbf{M}^{-1}\mathbf{K} \\ \mathbf{I} & \mathbf{0} \end{bmatrix}_{2nx2n} \quad (3.10)$$

and

$$\mathbf{B} = \begin{bmatrix} \mathbf{B}_0 \\ \mathbf{0} \end{bmatrix}_{2nxn} \quad (3.11)$$

where  $\mathbf{D}_{n \times n}$  is a damping matrix,  $\mathbf{I}_{n \times n}$  is an identity matrix and  $\mathbf{B}_{0 \times n}$  is an input distribution matrix. The concept of a feedback controller designed by pole placement is used as the basis of this algorithm. An input vector  $\mathbf{u}$  is chosen for state-variable feedback (with appropriate gains) and written as

$$\mathbf{u} = \mathbf{GCY} \quad (3.12)$$

where  $\mathbf{G}_{n \times 2m}$  is a gain matrix and  $\mathbf{C}_{2m \times 2n}$  is a measurement matrix for which  $m$  is a number of modes to be updated. Therefore Equation (3.9) can be rewritten as

$$\dot{\mathbf{Y}} = (\mathbf{A} + \mathbf{BGC})\mathbf{Y}$$

or

$$\dot{\mathbf{Y}} = (\mathbf{A} + \Delta\mathbf{A})\mathbf{Y}. \quad (3.13)$$

Equation (3.13) implies that, subject to meeting controllability requirements, the characteristic roots of the plant matrix can be shifted to desired values through the appropriate choice of the gain matrix  $\mathbf{G}$ . Here,  $\Delta\mathbf{A}$  is a mass-normalised correction matrix available to modify the characteristics of the original plant matrix  $\mathbf{A}$  in order to match the identified natural frequencies and damping factors through changing the stiffness and damping matrices, respectively. However, the equations of motion in state-space form have to be formulated using a viscous damping matrix instead of the structural damping formulation using a complex stiffness matrix as in Equation (3.1). Thus, it is necessary to transform the imaginary term of the complex stiffness matrix to a real symmetrical viscous damping matrix. The algorithm to achieve this transformation (Minas and Inman, 1991) was originally derived for the identification of a non-proportional damping matrix from incomplete modal data. Details of this algorithm adapted to suit the present study, are given in Appendix B, section B3. The algorithm involves solving an over-determined system of linear equations to obtain a symmetrical matrix. A pseudo-inverse method is

used to obtain the solution. A difficulty arising with the method is the excessive dimensions of matrices and vectors which are likely to result. The dimension of the matrix requiring inversion is  $(2n^2) \times (n^2 + n)/2$ . This generally requires a significant amount of computational effort. As a result, it is desirable to consider reducing the number of degrees of freedom of the system equations. The Guyan reduction method (Guyan, 1965) is a method commonly employed to eliminate less significant variables and thus reduce the size of the matrices in the equations of motion. This algorithm is reviewed in Appendix B, section B4.

### 3.3.3 *Summary of system identification*

Natural frequencies and damping factors are modal parameters which need to be identified from experimental data. The peak-picking method was chosen and will be used to extract these parameters. Once these parameters have been obtained, the finite element plate model can be updated to account for the observed behaviour of the identified structure. The finite element plate model needs to be manipulated mathematically to obtain the appropriate form before the updating algorithm can be implemented. The diagram, Figure 3.5, summarises the model updating procedures. This does not include the iterative procedures used to assess convergence and which are discussed in the next chapter. The final models, when established, can then be used to perform active control design in a model-based approach.

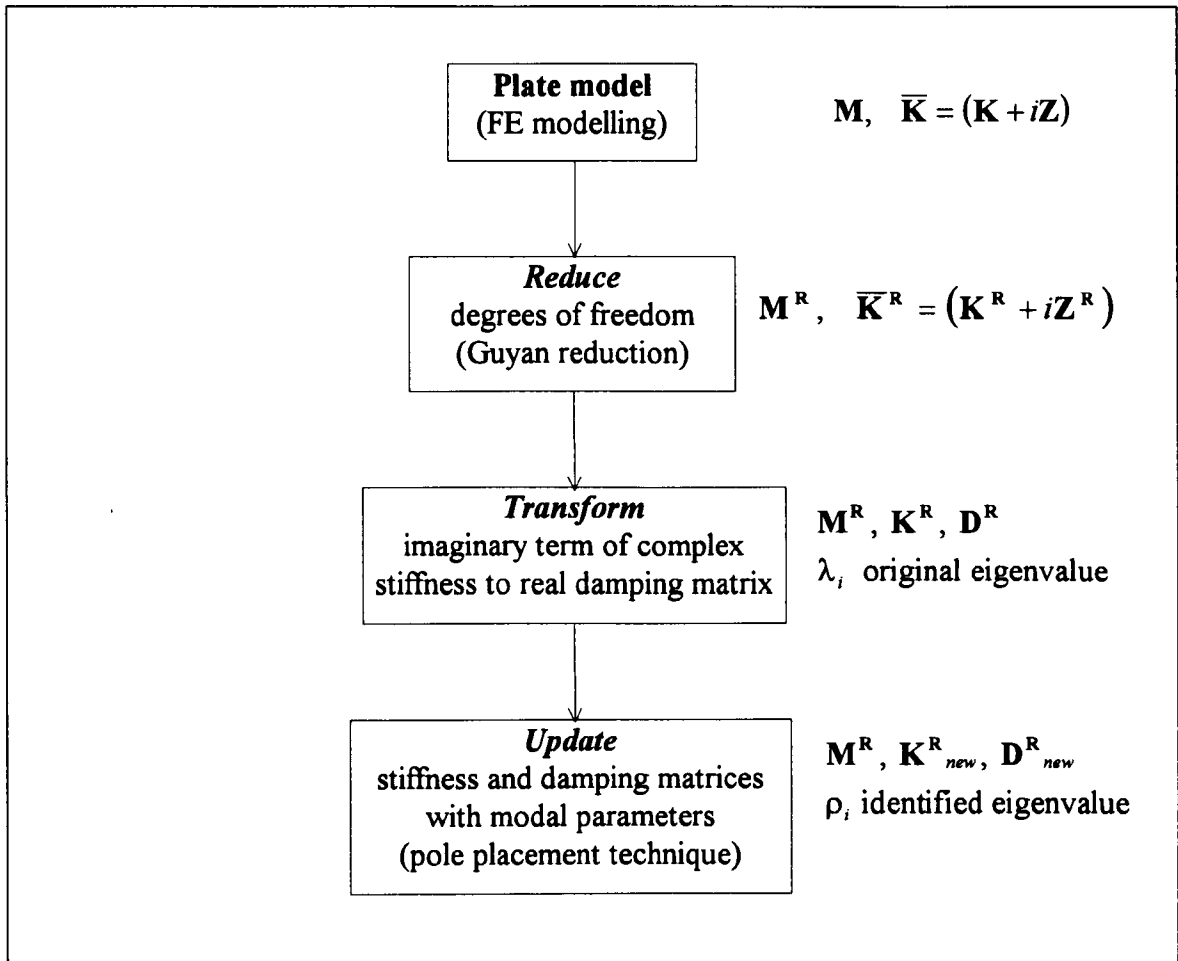


**Figure 3.5.** Flow chart showing procedures to obtain an updated model of the plate (iterative loops are not included, see Figure B.2 in Appendix B, section B2)

### 3.4 Modal control

As stated in Chapter 2, modal control using pole placement is to be used for active control in the present study. An active element used to perform control action consumes energy and generally multiple sensors and actuators are required if multiple modes are to be controlled. In the present study, modal control theory (Balas, 1978) associated with coupling of the control force is used. An advantage of coupling the force is to control a number of modes simultaneously using the minimum number of actuators. However,

spillover effects must obviously be taken into account. Modal control via pole placement, spillover effects, and their avoidance are presented in this section.

### 3.4.1 Pole placement

The technique used is similar to the updating algorithm presented in the sub-section 3.3.2 and Appendix B2, but the special case of a scalar input  $f(t)$  and an input vector  $\mathbf{b}$  is used here instead of the more general vector  $\mathbf{u}$  and the matrix  $\mathbf{B}$  used previously. Equation (3.9) then reduces to the form:

$$\dot{\mathbf{Y}} = \mathbf{A}\mathbf{Y} + \mathbf{b}f(t). \quad (3.14)$$

Note that the mass, damping and stiffness matrices formulated the plant matrix  $\mathbf{A}$  in Equation (3.10) now relate to the reduced-order model for which the damping and stiffness matrices have been updated with experimental data (i.e.  $\mathbf{M}^R, \mathbf{D}^R_{new}, \mathbf{K}^R_{new}$  in Figure 3.5). To control specific modes of vibration, Equation (3.14) needs to be transformed from physical co-ordinates,  $\mathbf{Y}$ , to modal co-ordinates,  $\xi$ , so that the system equations can be decomposed into a set of  $2r$  independent differential equations where  $r$  is the order of reduced-order model. The appropriate transformation requires the matrix of eigenvectors,  $\mathbf{U}$ , of the plant matrix,  $\mathbf{A}$ , such that

$$\mathbf{Y} = \mathbf{U}\xi. \quad (3.15)$$

Inserting Equation (3.15) into (3.14) and pre-multiplying by  $\mathbf{U}^{-1}$  gives:

$$\dot{\xi} = \Lambda\xi + \mathbf{w}f(t) \quad (3.16)$$

where  $\Lambda = \mathbf{U}^{-1}\mathbf{A}\mathbf{U}$  is a diagonal matrix which contains the eigenvalues of  $\mathbf{A}$  and  $\mathbf{w} = \mathbf{U}^{-1}\mathbf{b}$  is the mode-controllability vector. An element  $j$  of the vector  $\mathbf{w}$  quantifies

controllability of  $j$  th mode by the input  $f$ . Equation (3.16) can be partitioned into controlled modes  $c$  and residual or uncontrolled modes  $u$  or

$$\begin{Bmatrix} \dot{\xi}_c \\ \dot{\xi}_u \end{Bmatrix} = \begin{bmatrix} \Lambda_c & \mathbf{0} \\ \mathbf{0} & \Lambda_u \end{bmatrix} \begin{Bmatrix} \xi_c \\ \xi_u \end{Bmatrix} + \begin{Bmatrix} \mathbf{w}_c \\ \mathbf{w}_u \end{Bmatrix} f(t). \quad (3.17)$$

This equation implies the use of a truncated model for which the upper equation only (i.e. the controlled modes) is used in designing the controller. The force  $f(t)$  is chosen to be used in conjunction with state-variable feedback with appropriate weightings to alter the characteristics of the vibration modes,  $\Lambda_c$ , or

$$f = \mathbf{k}_c^T \xi_c \quad (3.18)$$

where  $\mathbf{k}_c$  is a  $c \times 1$  gain vector. Note that substitution of Equation (3.18) into Equation (3.17) results in force coupling in the system equation due to the presence of the coupling input matrix  $(\mathbf{w}_c \mathbf{k}_c^T)_{c \times c}$ . Modal decomposition attempts to de-couple a system of equations so that each mode can be controlled independently. The force coupling effect results in the possibility of benefiting from simultaneous control of several modes with a single actuator where the controllability element  $j$ , corresponding to the  $j$  th controlled mode, is non-zero. Nevertheless, this coupling force can effect the uncontrolled modes and produce undesirable effects. Details of gain selection and state-variable estimation to perform this algorithm are described in Appendix C, section C1.

### 3.4.2 Spillover effects

Balas (1978) showed that using a reduced set of equations for the controller and estimator causes, respectively, control and observation spillovers. Consider the diagram in Figure 3.6 below. Control spillover can result in excitation of the uncontrolled or residual

modes because of the force coupling which is presented. Similarly, if the measurement signal includes terms from the residual state variable  $\xi_u$ , then the estimator is contaminated with components from the uncontrolled modes.

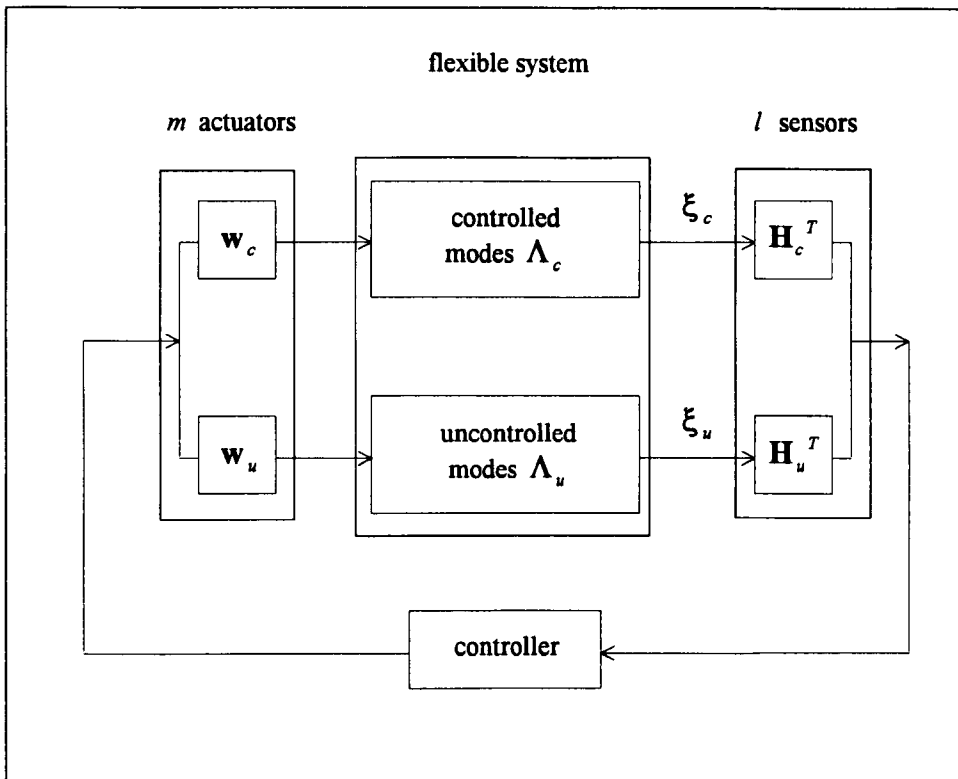


Figure 3.6. A diagram showing the effect of residual modes on a closed-loop control system (Balas, 1978)

However, these effects can be reduced by keeping the elements of gain vector  $k_c^T$  and the weighting matrix of the estimator low. Optimal designs such as the Linear Quadratic Regulator and Kalman filter (Franklin et al, 1998) can be used to achieve this aim. Placement of the actuator and sensor should be close to the nodal lines of the residual modes so that the residual modes are not significantly excited and the residual state variables in  $\xi_u$  are not strongly observed. Consideration of these effects in mathematical terms is given in Appendix C, section C2.

### 3.4.3 *Summary of modal control*

A pole placement technique for modal control has been presented. Subject to meeting controllability conditions the coupling force effect can, in principle, be used to control many modes of vibration with a single actuator. Spillover effects are a vitally important issue when implementing active vibration control of flexible systems since the controlled system's performance can be degraded or even destabilised by spillover effects. It will be shown that spillover effects can be reduced to acceptable levels through the introduction of passive constrained layer damping into the system.

## 3.5 Summary of Chapter 3

The theoretical basis of the present study has been presented. The chapter has been divided into three sections: finite element modelling, system identification and modal control. Validation of a finite element plate model has been demonstrated in this chapter by comparing model predictions with results presented in previously published works and good agreement has been reached. However, it has been implied that in order eventually to apply modal control algorithms, the finite element model will require experimental data from the structure under investigation. Obtaining suitable data using system identification techniques will be discussed in the chapter which follows. The next chapter is primarily concerned with passive control design of a constrained layer damping treatment and establishment of a refined finite element model to match observed behaviour of test plates. The model updating procedures and identification of modal parameters from experiments presented in this chapter then will be implemented practically.

# CHAPTER 4

## DESIGN OF PASSIVE CONTROL AND REFINED PLATE MODEL

### 4.1 Objectives

In the literature review chapter, passive control (in the form of a constrained layer damping treatment) of the vibrations of beams and plates was discussed as a means of attenuating levels of vibration. In the present chapter, the design of a constrained layer damping scheme to complement the active control of a panel plate is described. Predictions of plate frequency response functions (FRFs) from the finite element plate model are made for comparison with experimental results. The model updating algorithm using pole placement, presented in the previous chapter, will be implemented to match the models with the observed behaviour of test plates such that a refined model is obtained. The refined model will subsequently be used for active control design in the following chapter.

### 4.2 A frequency survey of test plates

Two identical aluminium rectangular plates were prepared for use in this investigation. The dimensions were 2.5 mm × 305 mm × 490 mm. One plate was treated with a passive constrained damping layer while the other plate was used as a benchmark so as to judge the influence of the damping treatment. The experimental arrangement involving the clamped-clamped plate is shown in Figure 4.1 where the excitation and measurement points are both at position 7, so as to excite and detect the first 10 modes of plate vibration. Figure 4.2 shows the division of the plate into 9 by 6 equal-length portions in  $x$  and  $y$  directions, respectively, and also the measurement positions used in the experiment. A shaker and load cell were connected underneath the plate and an

accelerometer was sited on top of the plate. Measured force and velocity, obtained by integration of the acceleration signal, were used as input and output signals, respectively, in order to obtain mobility frequency response functions (Ewins, 1984). The experimental facility is shown on Plate 1.

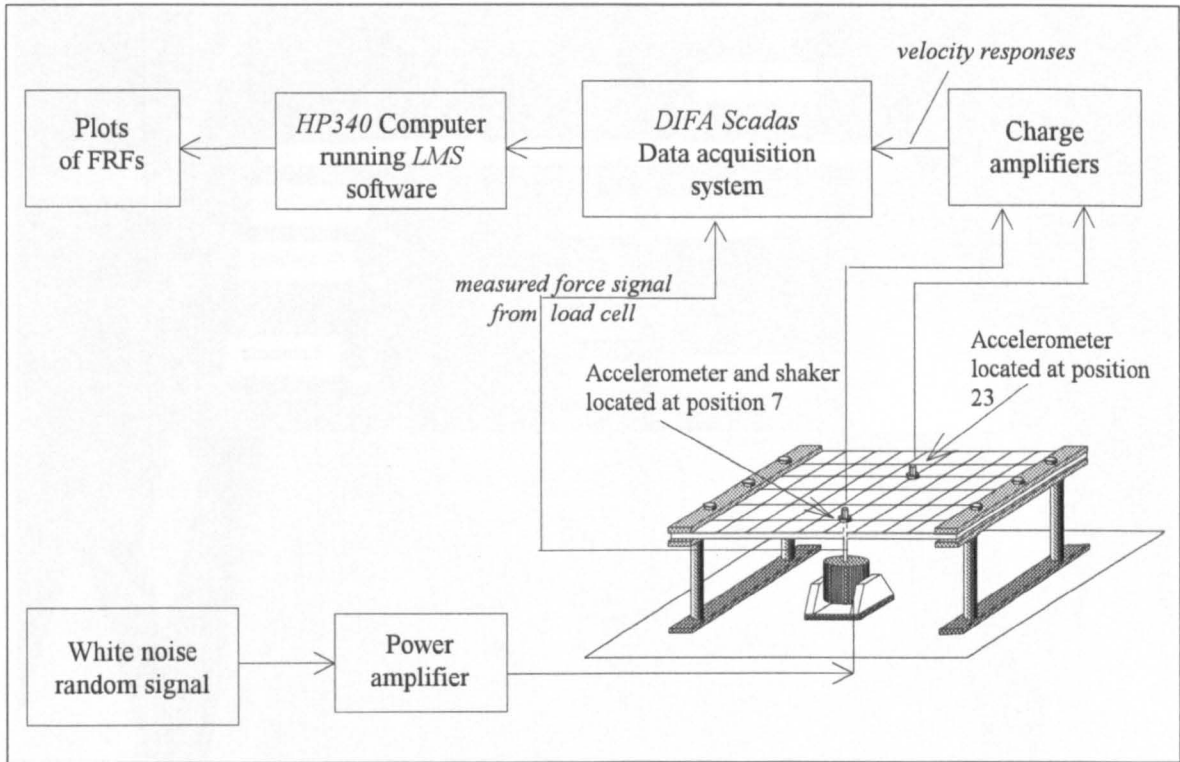


Figure 4.1. Experimental arrangement for the basic clamped-clamped plate

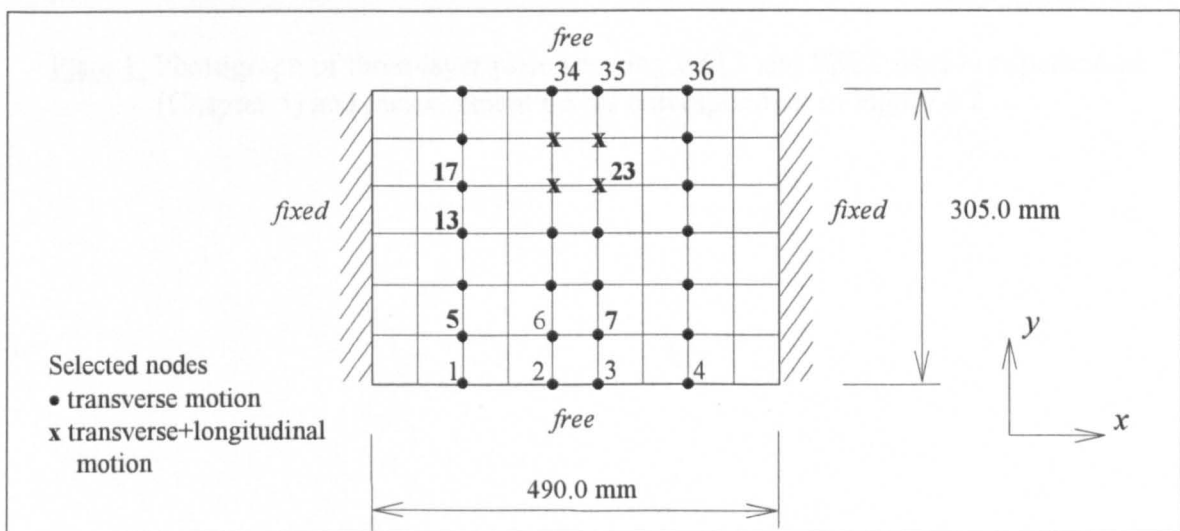


Figure 4.2. Measurement positions (number in bold) and selected nodes for model reduction of the panel plate

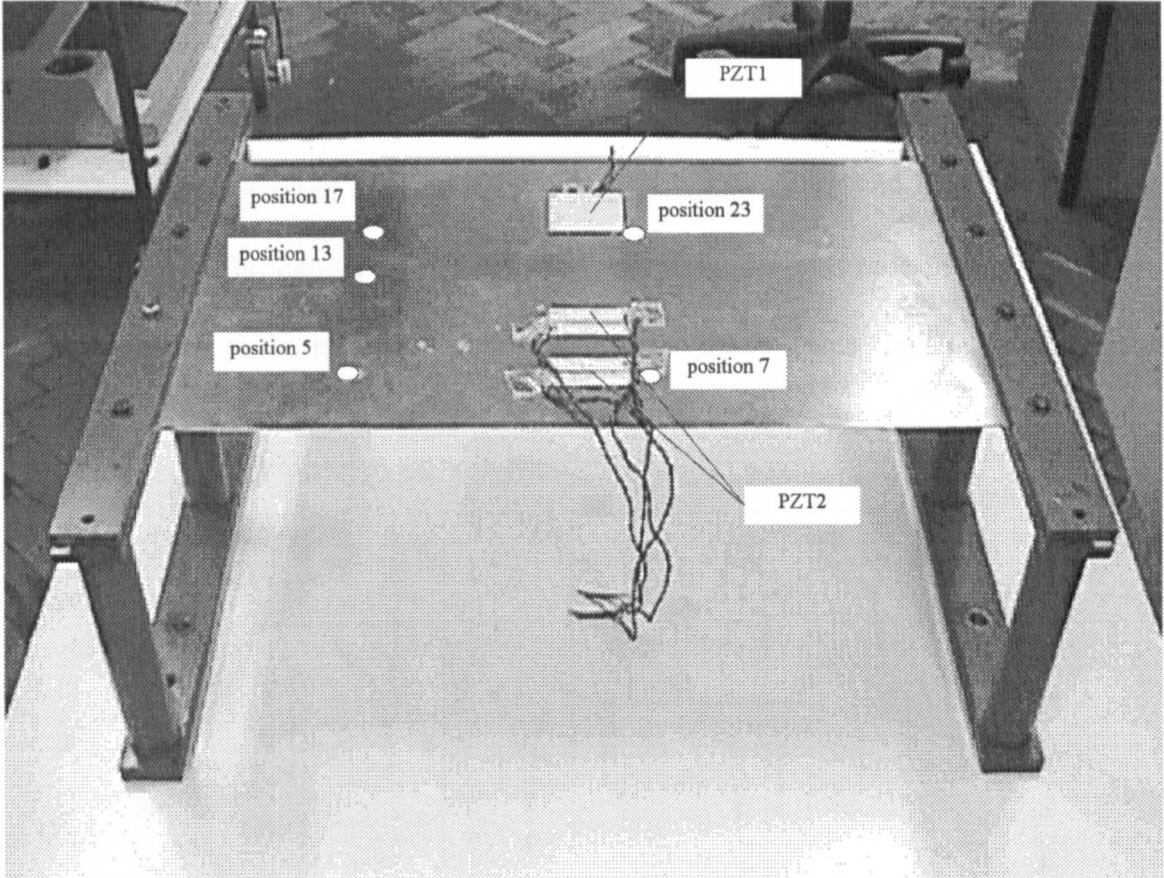
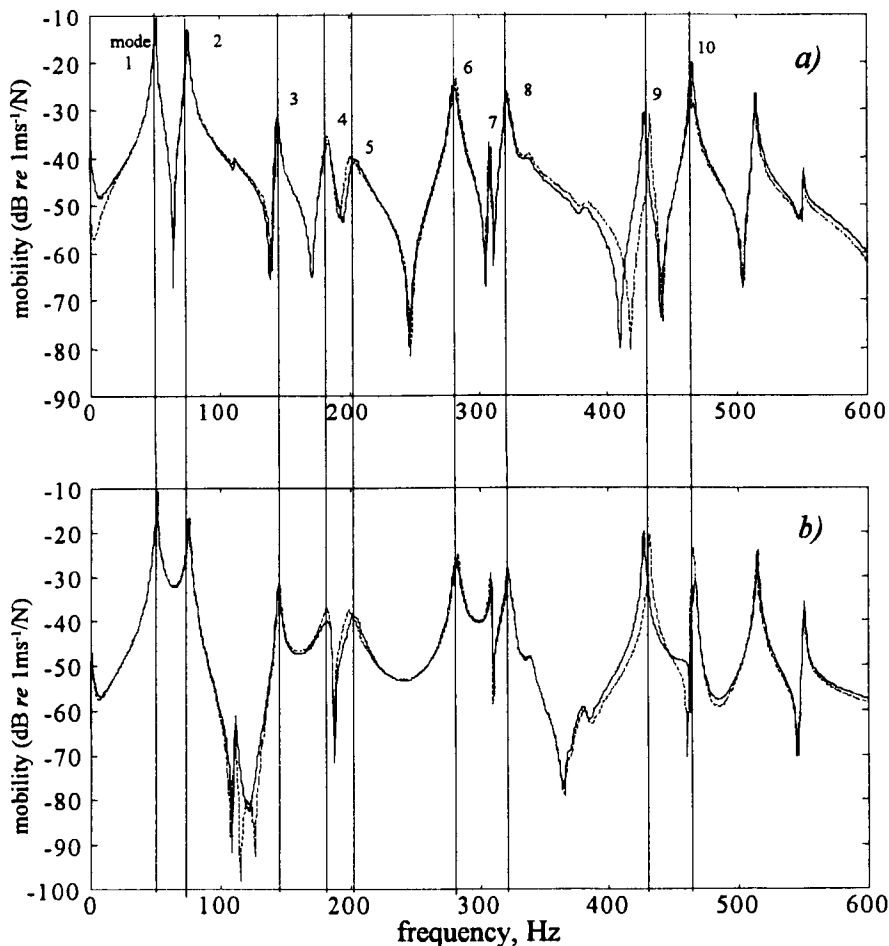
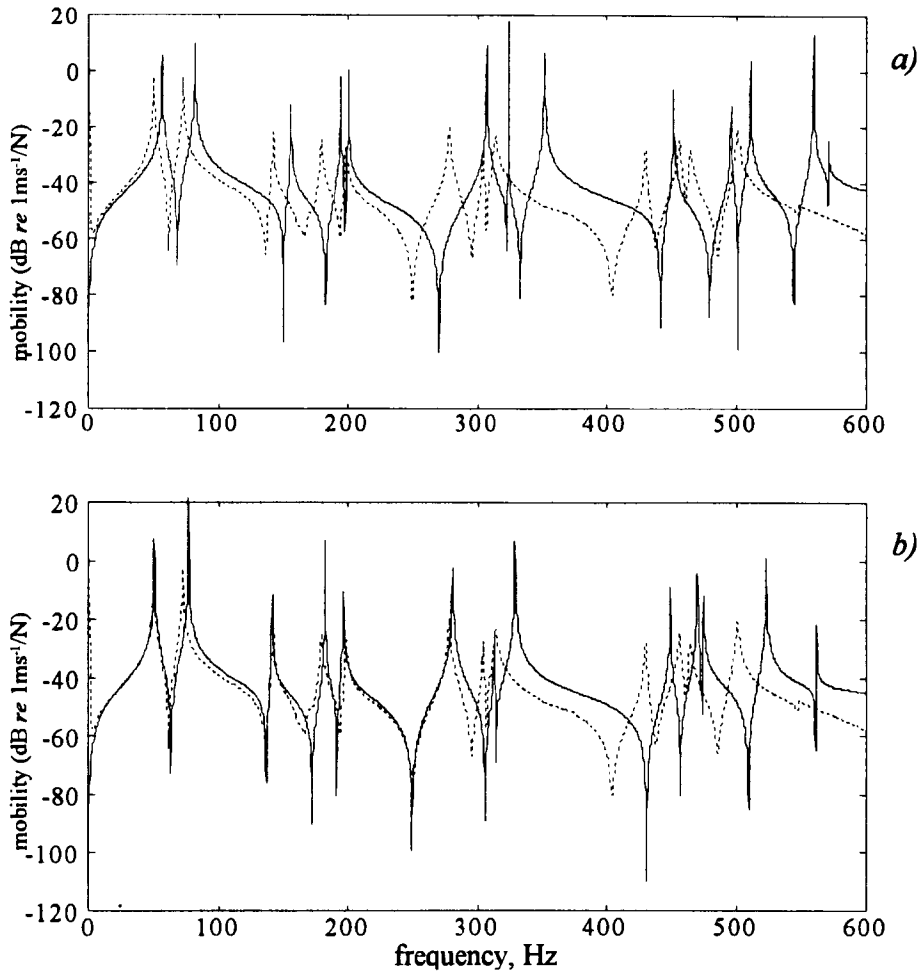


Plate 1. Photograph of three-layer plate showing PZT1 and PZT2 used in experiments (Chapter 5) and measurement points corresponding to Figure 4.2

The initial tests were designed to obtain the natural frequencies and damping factors of both lightly damped plates before introducing the damping layer to one of the plates. In addition, the test was designed to examine the repeatability of results following re-assembly of the test facility. FRFs from 2 different measurement points at positions 7 and 23 on both plates are plotted in Figures 4.3(a) and (b). It may be inferred from the results that both plates have the same characteristics and there is no significant sensitivity to re-assembly of the supported edges. Also, the first ten modes of plate vibration are relatively well-separated. Throughout this thesis, all FRF plots are specified using the notation  $FRF_{j_k}$  where  $j$  is the excitation point and  $k$  is the measurement point, as indicated in Figure 4.2.



**Figure 4.3.** Measured FRFs of two identical panel plates, — plate no.1 and - - - plate no.2  
 (a) point mobility forced and measured at point 7 (FRF7\_7)  
 (b) transfer mobility forced at point 7 and measured at point 23 (FRF7\_23)



**Figure 4.4.** Measured and Predicted FRFs (FRF7\_7) of the panel plate,

—— prediction, - - - - measurement

a) prediction from plate theory

b) prediction from plate theory with modified boundary conditions

The Measured FRF7\_7 is plotted in Figure 4.4(a) and compared with the corresponding prediction from the finite element plate model. A discrepancy occurs in that the predicted natural frequencies are higher than those measured. It is possible that the lower stiffness of the test plates in relation to the model stiffness results from rotation at the fixed edges of the test facility. After trial and error refinement of the plate model by introducing rotational stiffness at both fixed edges, such that the edges can slightly rotate about their axes, the FRF characteristics of the plate from the model prediction are closer to those of the test plates, as shown in Figure 4.4(b). However, the discrepancies between the finite

element model predictions and observed behaviour of the test plates can be reduced still further by updating the model such that the two essential properties, stiffness and damping of the plate, are updated to match the measured responses of the test plates. This will be shown later in the chapter. The predictions from finite element models used later on this thesis will be based on the models without the modification of boundary conditions.

### **4.3 Design of a constrained damping layer for a clamped-clamped plate**

One of the two test plates was treated with a surface damping treatment. As described in the literature survey on passive treatments for beams and plates in Chapter 2, the host plate was completely covered over its surface with a constrained damping layer to obtain vibration suppression over a broad band of frequencies, especially at higher frequencies where the damping mechanism performs most effectively. The characteristics of the viscoelastic and constraining layers must be chosen carefully so that the passive mechanism provides the most effective performance for both passive and active control functions. In this thesis, self-adhesive damping tape was used in conjunction with a thin metallic constraining layer. To simplify the calculation of the damping properties, the relationship between the damping and constraining layer was assumed to obey the relationship (Ross et al, 1959):

$$0.05 < 2h_{23} + h_{13} < 0.15. \quad (4.1)$$

where  $h_{23}$  and  $h_{13}$  are, respectively, the ratios of the damping and constraining layer thicknesses to the host plate thickness. The maximum loss factor introduced as a result of the damping treatment can be calculated from (Ross et al, 1959)

$$\eta_{\max} = \frac{3.5e_{13}h_{13}}{2 + 3.5e_{13}h_{13}} \cdot \frac{\eta}{1 + \sqrt{1 + \eta^2}} \quad (4.2)$$

where  $e_{13}$  is the ratio of the modulus of elasticity of the constraining layer to that of the host plate (i.e.  $e_{13} = E_1/E_3$ ). It is suggested by Ross and his colleagues that the maximum error from this approximate solution is about 15%. There are 4 parameters to choose in the design process, the two parameters  $h_2$ , thickness and  $\eta$ , a loss factor for the damping layer and the two parameters  $h_1$ , thickness and  $E_1$ , modulus of elasticity for the constraining layer. Equation (4.2) implies that the maximum damping is proportional to the loss factor  $\eta$  of the damping layer and the thickness and modulus of elasticity of the constraining layer with respect to the fixed value of the host plate thickness  $h_3$  and modulus of elasticity  $E_3$ . From commercially available materials, a 50.8  $\mu\text{m}$  (0.002 in) thick, model ISD112, viscoelastic layer from the 3M company was selected using the manufacturer's data sheets to provide a loss factor of approximately 1.0 over the frequency range from 0 to 600 Hz. A 0.254 mm (0.010 in) thick steel shim was used as the constraining layer giving an upper limit (Equation (4.1)) equal to 0.1422. The steel shim was used to provide a high modulus of elasticity for the constraining layer. Table 4.1 summarises the material properties for all three layers.

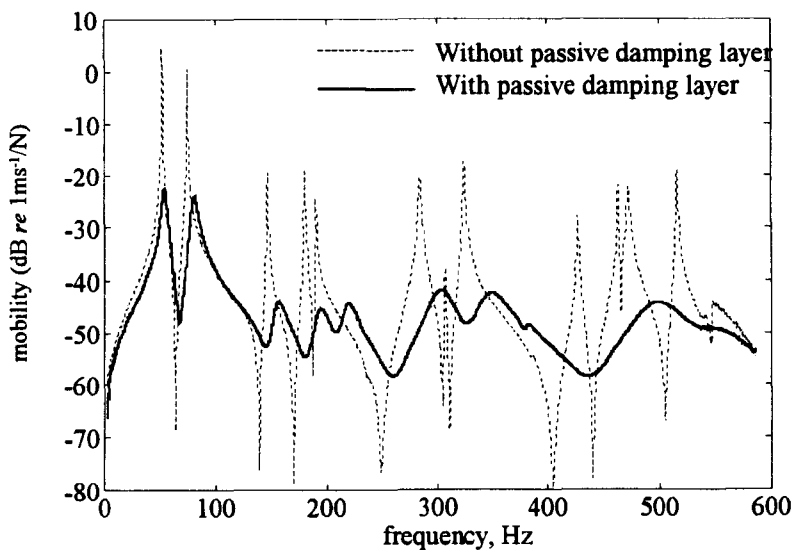
**Table 4.1** Material properties of the three-layer plate

Material	modulus of elasticity (MPa)	modulus of rigidity (MPa)	density ( $\text{kg/m}^3$ )	Poisson's ratio	shear loss factor
aluminium plate	$70 \times 10^3$	-	2700	0.3	-
ISD112 viscoelastic layer	29.8*	20*	1140	0.49	1.0*
steel constraining layer	$200 \times 10^3$	-	7000	0.3	-

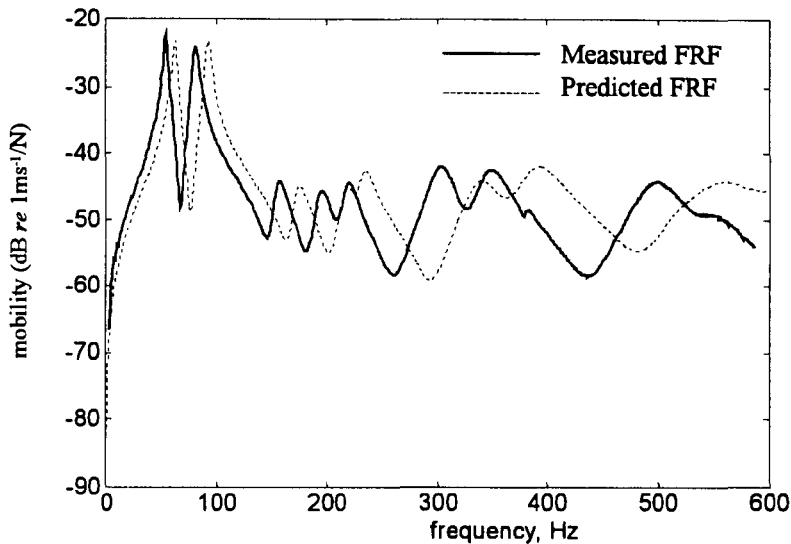
\* at the centre frequency of 600 Hz

Figure 4.5 shows the influence of the passive constrained damping layer when compared with the response of the untreated host plate. Note that the introduction of the damping layer produces around 25 dB attenuation of all the modes up to 600 Hz. However, the

long wavelengths associated with the first two modes still produce mobility peaks some 20 dB above those associated with the higher modes. It is these first two modes, one bending and one torsion, which require the use of active control to introduce significant additional attenuation of vibration levels. Before proceeding to describe active constrained layer damping, it is necessary to verify the finite element model of the passively damped plate. A comparison between the predicted FRF from the finite element three-layer plate model and the FRF measured experimentally, Figure 4.6, shows that the response levels predicted by the model are consistent with the results from the experiments. Nevertheless, there are discrepancies in the predicted natural frequencies. These discrepancies need to be minimised using updating techniques before the model can be used for active control system design.



**Figure 4.5.** Measured FRFs (FRF7\_7) of the panel plate with and without constrained damping layer



**Figure 4.6.** Measured and predicted FRFs (FRF7\_7) of the panel plate treated with constrained damping layer

#### 4.4 Model updating

In the comparison of predicted and measured FRFs of the passively damped plate shown in Figure 4.6, the FRF generated by the finite element model provides higher predicted natural frequencies than the experimental FRF. A pole placement technique described by Inman and Minas (1990) was used to update the finite element model so that both the predicted natural frequencies and damping factors are shifted to match the experimental data. In addition, the passive damping mechanism appropriate to the present study corresponds to representation of a loss factor,  $\eta$ , as frequency dependent value, and thus causes difficulties in dynamic analysis since the model involves both time and frequency variables. To obtain a suitable description of the dynamic model with a frequency-dependent loss factor, approximation procedures need to be considered. The loss factor is thus specified as a constant at the centre frequency of interest and the imaginary term (or energy dissipation term) of the complex stiffness matrix is updated to match the measured modal loss factors. Note that to suit the updating algorithm, the

complex stiffness matrix needs to be transformed to real stiffness and real symmetrical viscous damping matrices as described in sub-section 3.3.2. The diagram, Figure 4.7, summarises the procedures necessary to achieve a refined, reduced-order model of the three-layer plate.

#### *4.4.1 A tentative model*

The procedures shown in Figure 4.7 can be divided into three steps. The first three blocks in the diagram combine to form a tentative model for use in the updating procedures. Next, experimental natural frequencies and modal damping factors are obtained by performing modal system identification. Finally, the updating algorithm is implemented by iterative computation to obtain the refined finite element model of three-layer plate. This sub-section is aimed at describing the derivation of the tentative model prior to the application of the updating algorithm. The second and third steps are presented in the following sub-sections.

First, the analytical finite element model of three-layer plate is obtained by discretising the plate into 9 by 6 elements along the length and width directions, respectively, as shown in Figure 4.2. The resulting model accounts for the first 10 modes of vibration to an accuracy of within 1% when compared with models with higher numbers of elements (see Figure 3.3). When there is any doubt, plots of mode shapes can be produced to assess the accuracy of the model and to determine if the number of elements is sufficient to account for higher mode deformations (see Figure A.1 in Appendix A). The plots of the first six mode shapes are reproduced here in Figure 4.8. These modes will be identified from experimental data in the following sub-section.

The number of degrees of freedom  $n$  of the three-layer plate model is 420. However, such dimensions of the resulting system equations result in a vast amount of computational effort in implementing the updating algorithm. Consequently, Guyan reduction is performed by maintaining the transverse displacement of selected nodes (see Figure 4.2) together with the longitudinal displacements of the constraining layer at four selected nodes. These four nodes will be used in subsequent active control strategies as the locations for a piezoelectric actuator. In this way, the number of degrees of freedom is reduced from  $n = 420$  to  $r = 36$ . The selection of these master nodes needs to ensure the production of a suitable reduced-order model over the bandwidth of interest and also correspondence with the measurement points and an actuator location in the test procedures. Guidelines for node selection can be found in Shah and Raymund (1982).

As shown in the formulation of the updating algorithm in Chapter 3, the representation of a viscous damping matrix in an equation of motion is required to implement the algorithm. The equation of motion with reduced-order mass and complex stiffness matrices is solved for its eigensolutions  $(\lambda_i, \mathbf{q}_i, i = 1, r)$ . The solutions are then used together with Equations (B12) to (B15) to transform the imaginary term  $\mathbf{Z}^R$  of the reduced-order complex stiffness matrix  $\bar{\mathbf{K}}^R$  to an  $r \times r$  equivalent viscous damping matrix  $\mathbf{D}^R$ . It is worth noting that the dynamic responses of this plate model are modified from the original model owing to ignorance of the inertia term in the transformation when using Guyan reduction (Friswell and Mottershead, 1995) and use of the pseudo-inverse in Equation (B15). The established model eventually will be updated with identified parameters from experiments to match the observed behaviour of the plate structure.

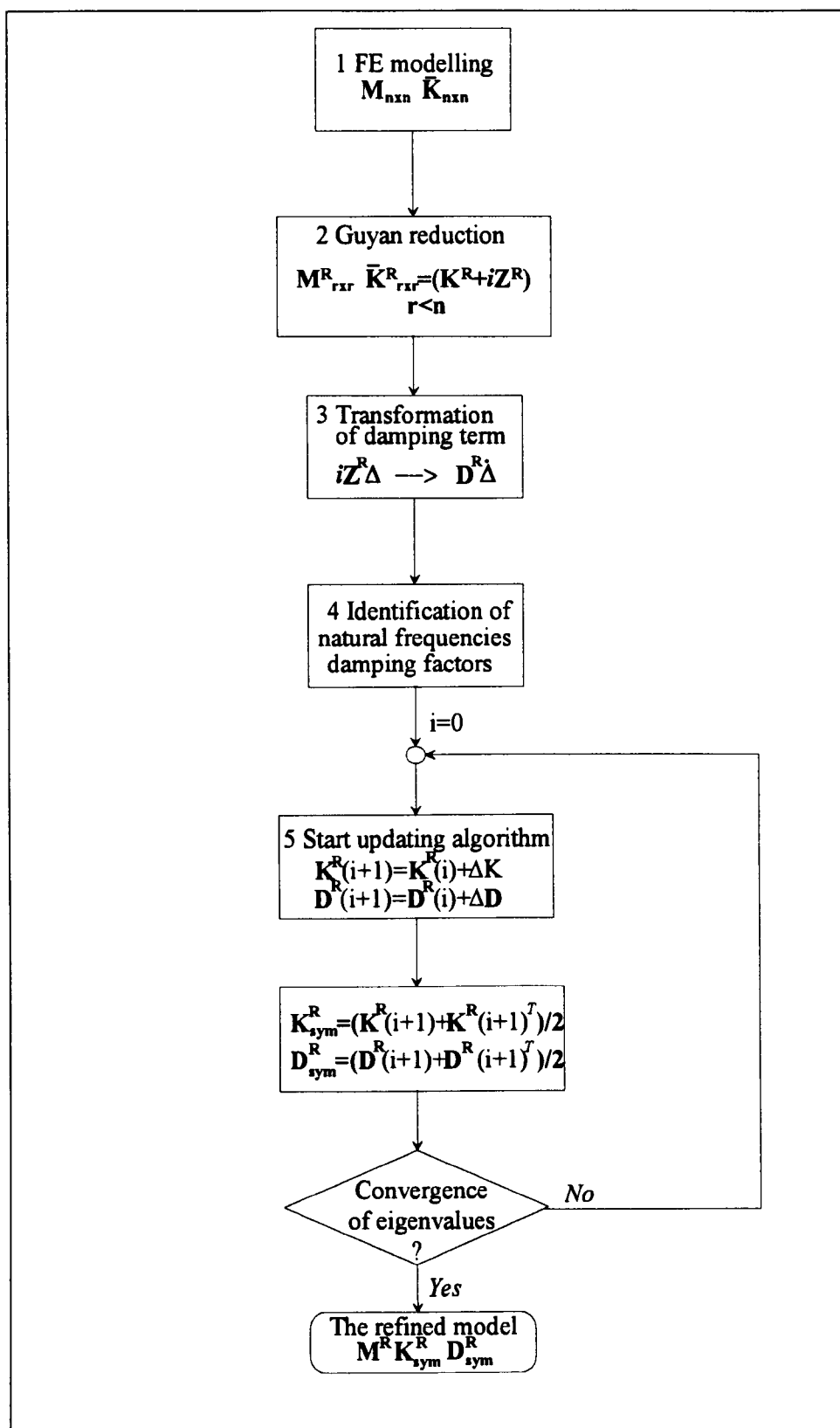
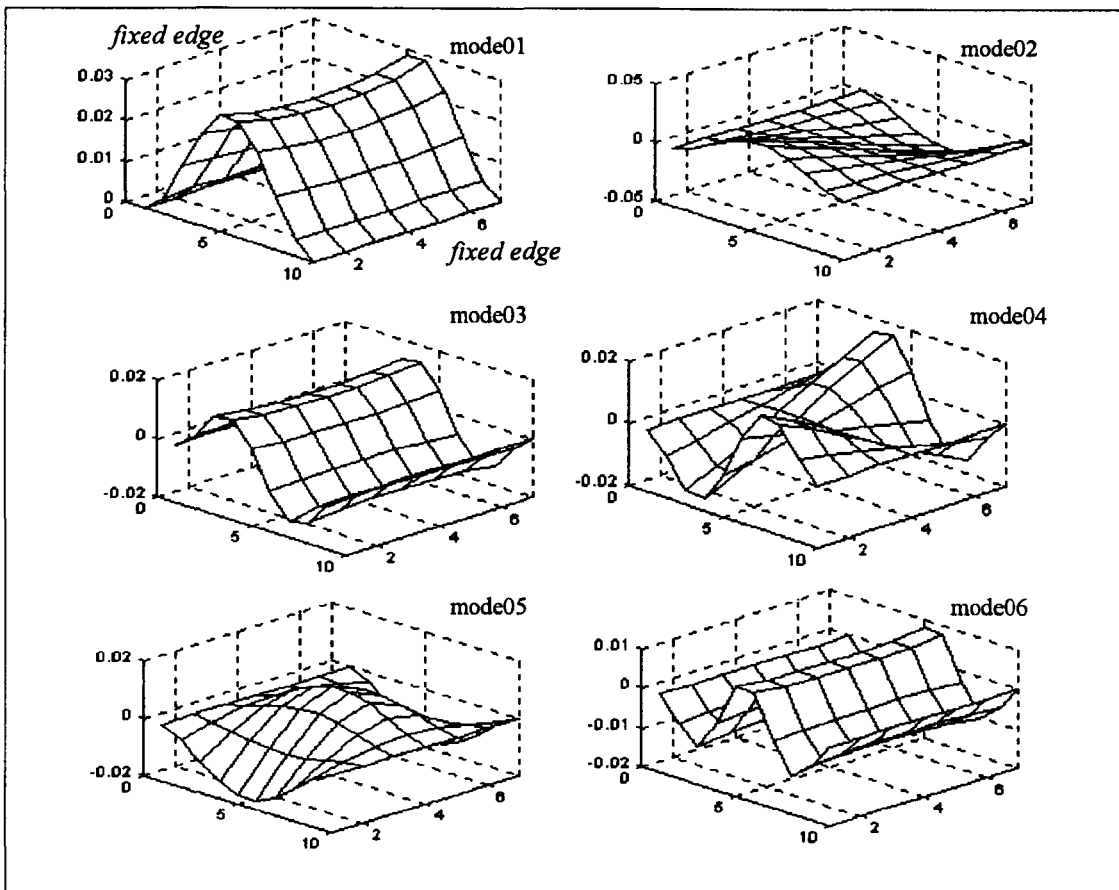


Figure 4.7. Flow chart showing procedures to achieve the refined model



**Figure 4.8.** The first six mode shapes of the clamped-clamped plate

#### 4.4.2 Identification of natural frequencies and damping factors from the test plate

Natural frequencies and damping factors extracted from the observed behaviour of the test plate covered with viscoelastic and constraining layers are used to update the three-layer plate model resulting from finite element analysis. The frequency range of interest is from 0 to 600 Hz and the corresponding modal damping factors from a frequency survey are generally less than 0.05. Hence, a simple peak-picking method can be used to obtain measured natural frequencies and damping factors (Ewins, 1984 and LMS user manual, 1993). Owing to the unavailability of mode 7 which is obscured by modes 6 and 8, only the first 6 modes can be identified. Table 4.2 gives the identified natural

frequencies and percentage damping factors of the first 6 modes of the three-layer plate together with the model predictions.

**Table 4.2** Measured and predicted first six natural frequencies and damping factors of the three-layer plate

mode	1	2	3	4	5	6
predicted natural frequency (Hz)	62.50	92.23	172.93	217.07	233.02	339.06
measured natural frequency (Hz)	54.53	81.50	157.47	195.59	220.60	304.02
predicted % damping	3.50	3.05	3.81	3.87	2.83	4.86
measured % damping	3.44	3.51	4.13	3.66	3.41	3.57

#### 4.4.3 Model updating, iteration and the refined model

Given the availability of a tentative finite element model and measured modal data, the updating algorithm can be implemented as shown in stage 5 of the flowchart, Figure 4.7. A complication arises in that the correction terms of the damping matrix ( $\Delta \mathbf{D}$ ) and of the stiffness matrix ( $\Delta \mathbf{K}$ ) are not guaranteed to be symmetrical such that the orthogonality properties of the modal model are satisfied (Ewins, 1984). These properties are required to enable decomposition of the system equations used in modal control. Because of the requirement for symmetrical stiffness and damping matrices, the updating procedure needs to be repeated until the updated eigenvalues are acceptable when compared with the identified eigenvalues (see Figure 4.7). A series of FRFs from five different accelerometer locations was plotted to show performance of the updating algorithm. These accelerometer locations are shown in Figure 4.2. Points 7 and 23 are nominated for use as sensing feedback locations in active control system design since they provide high observability indices of the first two modes which will be demonstrated in the next chapter. The other points (5, 13 and 17 in Figure 4.2) are chosen to be far from the maximum curvatures of modes 1 and 2. Note that the accelerometer location at point 13 is located on the nodal line of modes 2 and 4 and that point 5 is located near the nodal line of

mode 5. The experimental results also confirmed model predictions from these measurement locations. Figures 4.9 to 4.13 show a comparison of FRFs before and after updating the finite element three-layer plate model. In Figures 4.9 to 4.13, the dashed lines represent the measured FRFs and the solid lines represent the FRFs from prediction of (a) before updating and of (b) after updating the model. These results clearly show that the predicted FRFs of the first 6 modes are concurrent with the measured FRFs while the higher modes (i.e. those not updated) are unchanged. Although mismatches of the higher modes are clearly evident, the accuracy of the updated models is sufficient for use in an active design scheme where it is the accuracy of the controlled pole locations which is of paramount importance.

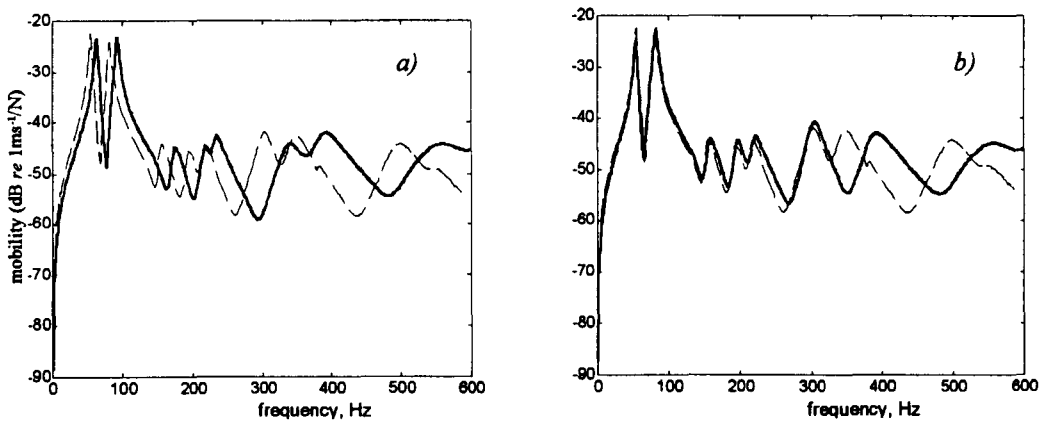


**Figure 4.9.** Comparison of model predictions with experimental results before and after updating the model: FRF7\_7 a) before updating  
b) after updating the model

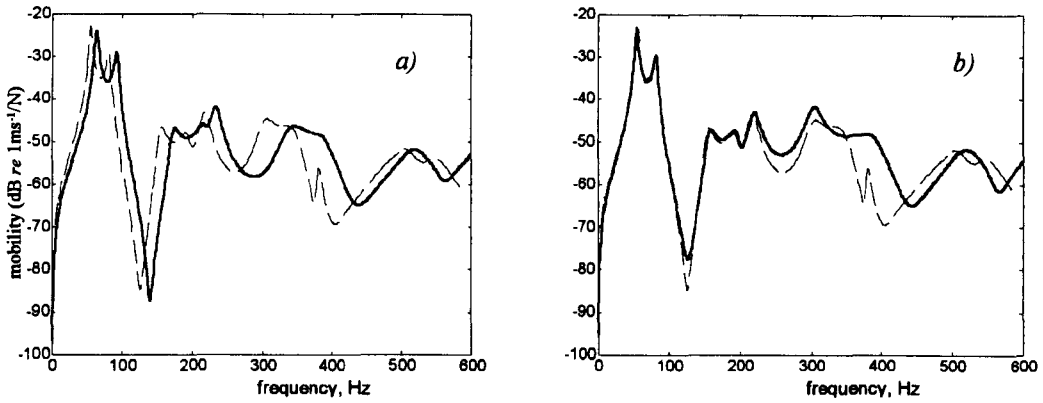


Figure 4.10. Comparison of model predictions with experimental results before and after updating the model: FRF7\_23 a) before updating  
b) after updating the model

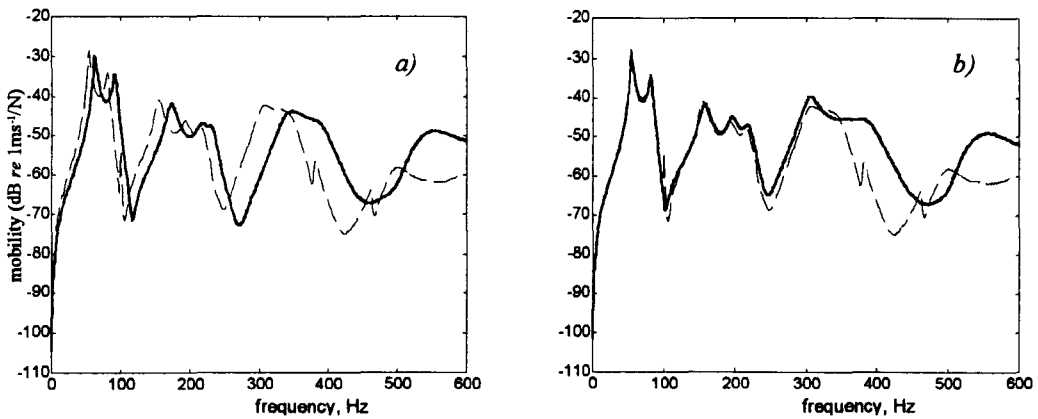


Figure 4.11 Comparison of model predictions with experimental results before and after updating the model: FRF7\_11 a) before updating  
b) after updating the model

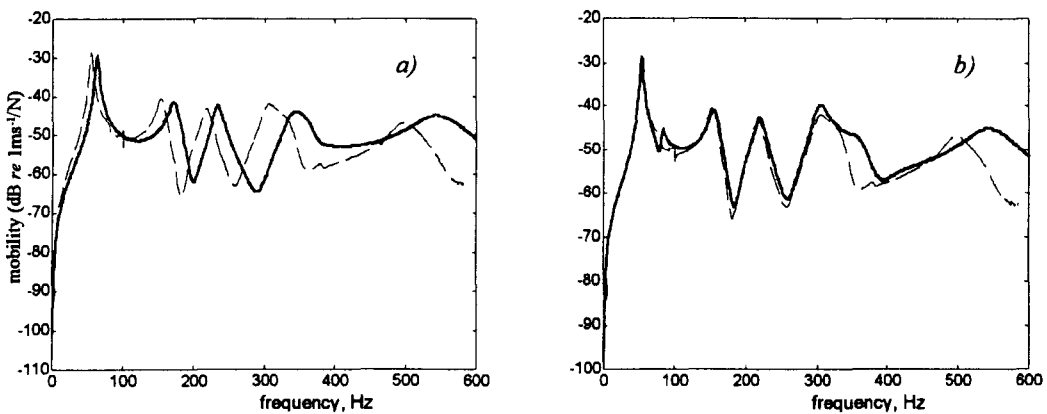
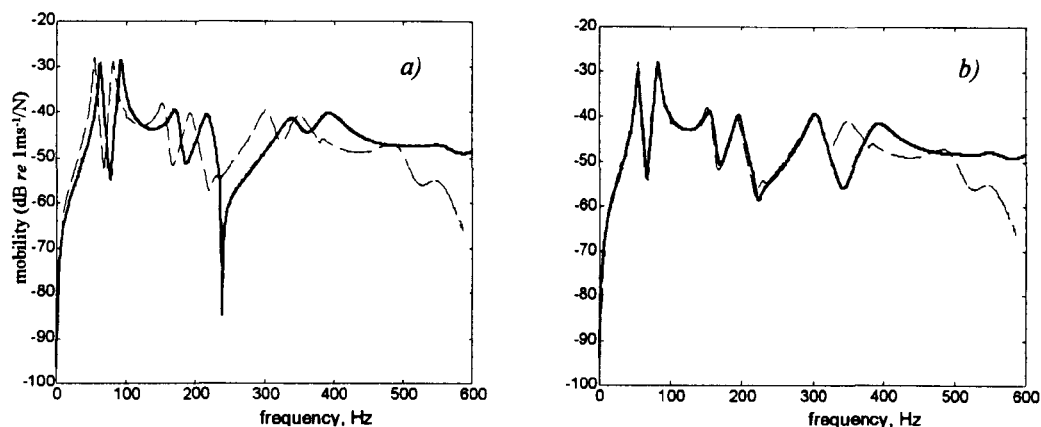


Figure 4.12. Comparison of model predictions with experimental results before and after updating the model: FRF7\_13 a) before updating  
b) after updating the model



**Figure 4.13.** Comparison of model predictions with experimental results before and after updating the model: FRF7\_5 a) before updating b) after updating the model

#### 4.5 Summary of Chapter 4

The design of a passive constrained layer damping treatment for the host plate has been described. A self-adhesive damping tape with a steel shim was used as the damping and constraining layers, respectively. Experimental results showed that the introduction of passive damping to the host plate reduces vibration amplitudes for the first 10 modes by around 25 dB. However, the first two modes, one bending and one torsional, have long wavelengths such that their vibration levels are around 20 dB higher than those of higher frequency modes. An active control scheme is thus required to provide improved vibration suppression at these two lower modes. Predictions of responses from the finite element three-layer plate model have been compared with measurements. It was found that the analytical finite element model needs to be updated using identified natural frequencies and damping factors from experiments to match the observed behaviour of the test plates. As a result, a refined finite element model of the three-layer plate has been produced to provide the basis for active control design. The next chapter is concerned with active control strategies and both numerical simulations and experimental results are presented.

# **CHAPTER 5**

## **NUMERICAL SIMULATIONS AND EXPERIMENTAL VERIFICATION OF ACTIVE CONTROL**

### **5.1 Objectives**

The refined finite element model of the plate covered with a constrained damping layer, established in the previous chapter, is now used to design modal controllers to implement active control of the three-layer plate. Spillover effects arising from the use of a reduced-order model are overcome by suitable choices of sensor and actuator placements and control and estimator gains. Numerical simulations of active control schemes are performed prior to experimental implementation in order to optimise the performance. Numerical results will be compared with those from testing. Various arrangements of sensors and actuators will also be studied to compare their performance in vibration suppression. Initially, a single input/single output (SISO) controller was designed before proceeding to evaluating controllers involving multiple inputs and multiple outputs.

### **5.2 Controller design**

To begin with, the simplest possible configuration of sensor and actuator was considered: a single accelerometer and a single lead zirconate ceramic (PZT) actuator, respectively. Consequently, a single input and single output (SISO) controller was designed initially. The state estimator and control law were designed in the continuous-time domain and then converted to the discrete-time domain for digital implementation.

Placement of the sensor and actuator and their influence on the design of the closed-loop control system are described below.

### 5.2.1 Placement of sensor and actuator

Plots of mode shapes (see Figure 4.8) were used to identify positions for the sensor and actuator such that, respectively, they detect and excite the maximum transverse displacements associated with the first two modes whilst also keeping to the nodal lines of the higher modes so as to minimise spillover effects. The modal controllability and observability vectors were also used to refine the choices of the sensor and actuator locations.

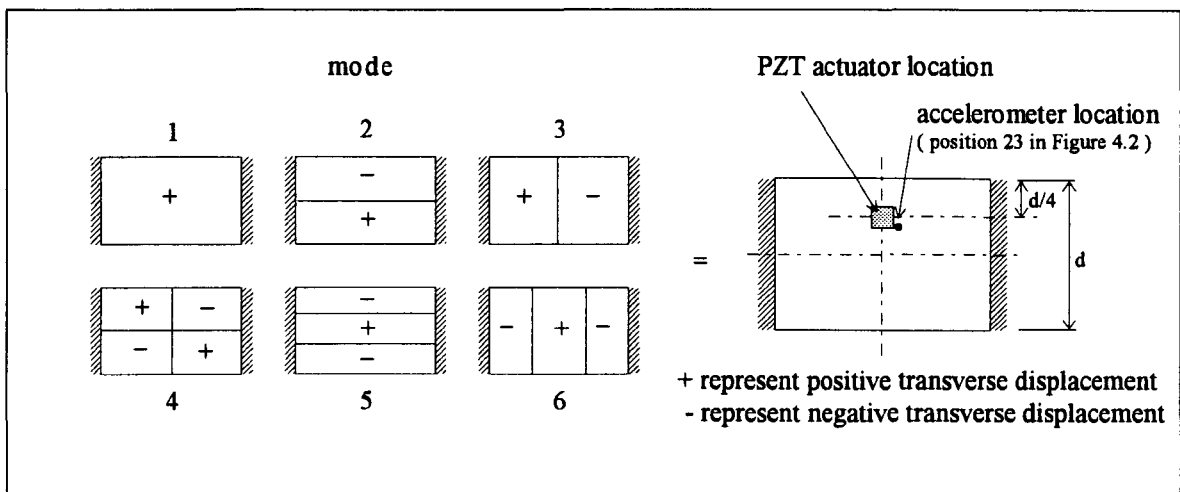


**Figure 5.1.** Location of PZT actuator and accelerometer to control the first two modes of the panel plate

The first six mode shapes were considered and the sensor and actuator were chosen to occupy the middle of the upper half portion of the plate as illustrated in Figure 5.1. The dimensions of the PZT actuator were chosen based upon the results obtained by finite element modelling and experimental observations. A 50 mm  $\times$  50 mm PZT patch was used as the actuator. Table 5.1 gives the controllability and observability indices for these

sensor and actuator locations from the first six elements of the mode controllability vector  $\mathbf{w}$  (see Equation 3.16) and the mode observability vector  $\mathbf{g}$  (see Appendix C1), respectively. Controllability and observability indices are low for modes 3 and 4 where the actuator and sensor are placed near their nodal lines, but are high for modes 1 and 2 where the actuator and sensor locations are in the region of maximum transverse motion so as to provide large induced shear strain in the damping layer. This procedure for obtaining suitable sensor and actuator locations is straightforward for simple structures such as plates and beams. However, it would be a tedious task for more complex structures and automatic procedures for placing sensors and actuators should be considered instead (Choe and Baruh, 1992; Baruh and Choe, 1990, respectively).

**Table 5.1** Controllability and observability indices

mode	controllability	observability
1	$6.30 \pm 1.0601 \times 10^1 i$	$-1.145 \times 10^{-1} \pm 1.557 \times 10^{-1} i$
2	$-5.05 \pm 9.09 i$	$3.66 \times 10^{-2} \pm 8.67 \times 10^{-2} i$
3	$-1.500 \times 10^{-8} \pm 7.30 \times 10^{-8} i$	$-1.442 \times 10^{-2} \pm 5.16 \times 10^{-4} i$
4	$-5.97 \times 10^{-8} \pm 3.39 \times 10^{-8} i$	$-6.15 \times 10^{-3} \pm 7.94 \times 10^{-3} i$
5	$-8.43 \times 10^{-1} \pm 2.49 \times 10^{-1} i$	$-1.256 \times 10^{-1} \pm 3.53 \times 10^{-2} i$
6	$2.16 \times 10^2 \pm 2.51 \times 10^2 i$	$-2.81 \times 10^{-2} \pm 1.527 \times 10^{-2} i$

## 5.2.2 Control law and estimator design

### 5.2.2.1 Continuous-time design

For the state-space equations with a single input and single output, the control gain vector  $\mathbf{k}_c^T$  (see Equation (3.18)) and weighting gain vector  $\Phi$  (see Equation (C7)) can be assigned using a pole placement technique. However, to optimise actuator power consumption and damping of the assigned modes, Linear Quadratic Regulator (LQR) and Gaussian (LQG) algorithms are used to obtain optimal control and estimator gains,

respectively, so that the spillover effects are not sufficient to destabilise the actively controlled system. The LQR is the solution provided by solving a general optimal control problem to find the control gains. However, a drawback is that the entire set of state variables must be measured. The LQG controller is provided by the solution of an extended optimal control problem where white noise disturbance inputs are included and incomplete state measurements can be used to construct the full state vector through computing the appropriate estimator gains (Burl, 1999). The LQR design is aimed at minimising the cost function

$$\mathbf{J} = \int (\xi' \mathbf{Q} \xi + f' \mathbf{R} f) dt \quad (5.1)$$

where  $\mathbf{Q}$  and  $\mathbf{R}$  are weighting matrices. One choice of  $\mathbf{Q}$  and  $\mathbf{R}$  is to make them symmetrical (semi-symmetrical for  $\mathbf{Q}$ ) positive definite matrices. For a SISO modal state-space equation,  $\mathbf{R}$  is a scalar and can be set to unity while  $\mathbf{Q}$  is of the form

$$\begin{bmatrix} a_1 & 0 & 0 & 0 \\ 0 & a_1 & 0 & 0 \\ 0 & 0 & a_2 & 0 \\ 0 & 0 & 0 & a_2 \end{bmatrix} \quad (5.2)$$

where  $a_1$  and  $a_2$  are real constants, chosen so as to maintain two pairs of complex conjugate eigenvalues. Increasing  $a_1$  and  $a_2$  results in an increase in the damping of the assigned eigenvalues which correspond to the original modes 1 and 2 respectively. The control gains must not be so high such that control spillover affects the results. The influence of a truncated model on the assigned eigenvalues of a closed-loop system will be discussed later.

Traditionally the estimator gains are chosen to provide poles to the left of the assigned poles in the left-hand half of the s-plane. Equations (3.17), (3.18) and (C7) can be rewritten in terms of the error of the estimation process

$$\dot{\mathbf{e}} = \left( \hat{\xi}_c - \dot{\xi}_c \right) = \left( \Lambda_c - \Phi \mathbf{H}_c^T \right) \mathbf{e} + \Phi \mathbf{H}_u^T \xi_u \quad (5.3)$$

The decay of the estimator error is thus dependent on the eigenvalues of  $\left( \Lambda_c - \Phi \mathbf{H}_c^T \right)$ . If the estimator gains are chosen to be high so as to achieve rapid decay of the error terms, then contamination of the uncontrolled modes is also amplified, resulting in a significant observation spillover effect. The effect of spillover on the assigned close-loop poles can be studied by reconsidering Equation (C8) ( a combination of a modal state-space equation involving the controlled modes, uncontrolled modes and state estimation error (Balas, 1978; Firoozian and Stanway, 1988)):

$$\begin{Bmatrix} \dot{\xi}_c \\ \mathbf{e} \\ \dot{\xi}_u \end{Bmatrix} = \begin{bmatrix} \Lambda_c + \mathbf{w}_c \mathbf{k}_c^T & \mathbf{w}_c \mathbf{k}_c^T & \mathbf{0} \\ \mathbf{0} & \Lambda_c - \Phi \mathbf{H}_c^T & \Phi \mathbf{H}_u^T \\ \mathbf{w}_u \mathbf{k}_c^T & \mathbf{w}_u \mathbf{k}_c^T & \Lambda_u \end{bmatrix} \begin{Bmatrix} \xi_c \\ \mathbf{e} \\ \xi_u \end{Bmatrix}. \quad (5.4)$$

As indicated in sub-section 3.4.2, the assigned eigenvalues are disturbed by the residual terms of the observation signal. Both the actual closed-loop eigenvalues and the stability of the control system including spillover effects can be investigated by obtaining the eigensolutions of Equation (5.4).

### 5.2.2.2 Discrete-time design

In the discrete-time domain, the controlled mode state-space equations of motion corresponding to Equation (3.17) can be obtained from (for example, see Ogata, 1987)

$$\Lambda_c^d = e^{\Lambda_c T_s}, \mathbf{w}_c^d = \left( e^{\Lambda_c T_s} - \mathbf{I} \right) \Lambda_c^{-1} \mathbf{w}_c \quad (5.5)$$

where  $\Lambda_c^d$  is the discrete-time form of  $\Lambda_c$  and  $T_s$  is sampling time. An advantage of controller design in modal co-ordinates is that the exponential of the plant matrix  $\Lambda_c$  is straightforward to compute because it contains only diagonal elements. Elements in the discrete-time control gain  $\mathbf{k}_c^T$  are then calculated from (Porter and Crossley, 1972)

$$\mathbf{k}_j^d = \frac{\prod_{k=1}^c (\exp(\rho_k T_s) - \exp(\lambda_j T_s))}{\left( w_{c,j}^d \prod_{\substack{k \neq j \\ k=1}}^c (\exp(\lambda_k T_s) - \exp(\lambda_j T_s)) \right)} \quad j=1,2,\dots,c \quad (5.6)$$

where  $\lambda_{j,k}$  is eigenvalue of the mode to be controlled,  $\rho_k$  is assigned eigenvalues obtained from the LQR design,  $c$  is the number of controlled modes and  $w_{c,j}^d$  is the  $j$ th element of  $\mathbf{w}_c^d$ . The estimator state-space equation (Equation (C7)) is rewritten here

$$\hat{\xi}_c(t) = (\Lambda_c - \Phi \mathbf{H}_c^T) \hat{\xi}_c(t) + \Phi z(t) + \mathbf{w}_c f(t) \quad (5.7)$$

For compactness, define  $\bar{\mathbf{G}} = (\Lambda_c - \Phi \mathbf{H}_c^T)$ . Then the discrete-time estimator takes the form

$$\hat{\xi}_c(k+1) = \bar{\mathbf{G}}^d \hat{\xi}_c(k) + \Phi^d z(k) + \bar{\mathbf{w}}_c^d f(k) \quad (5.8)$$

where  $\bar{\mathbf{G}}^d = e^{\bar{\mathbf{G}}T_s}$ ,  $\Phi^d = (e^{\bar{\mathbf{G}}T_s} - \mathbf{I})\bar{\mathbf{G}}^{-1}\Phi$ ,  $\bar{\mathbf{w}}_c^d = (e^{\bar{\mathbf{G}}T_s} - \mathbf{I})\bar{\mathbf{G}}^{-1}\mathbf{w}_c$  and  $k$  is the sampling index.

### 5.3 Description of numerical experiments

Numerical simulation of an active controlled system is implemented to study the performance of the controller designs. In what follows, a simple configuration of control device arrangement, a single accelerometer and single PZT actuator, is examined using simulation procedures. A series of simulation results will be given in the next section and

compared with experimental results. Various configurations of controller are studied in the next section.

In accordance with the discussion in sub-section 5.2.1, the disturbance (shaker position) and measurement points are at points 7 and 23, respectively, on the three-layer test plate as shown in Figure 5.2. The control excitation is applied to a PZT actuator placed in the middle of upper portion of plate. The controller and estimator gains are designed to produce high damping of the first two eigenvalues and to ensure stability of the closed-loop system in the face of spillover effects. The assigned eigenvalues, along with controller and estimator gains are given in Table 5.2. The assigned poles are obtained by using the LQR design to minimise the control gain and to achieve high damping. The LQG design is used to obtain the optimal estimator gain such that the error from estimation decays faster than the response due to the assigned poles. The main consideration in designing the controller is to minimise spillover problems. The complete closed-loop control system for numerical experiments, is shown in Figure 5.3.

In controller design, the control law and estimator are implemented using complex numbers - a formulation which is not suitable for experimental implementation by real-time digital control. To overcome this problem, the state-space estimator equation is converted to its transfer function form so that real and imaginary terms can be computed separately in terms of real numbers, as illustrated in Figure 5.3. This significantly reduces the number of lines required for program execution and results in faster calculations for real-time control.

Table 5.2 Poles and corresponding gains of controller and estimator

mode	original poles(rad/s)	assigned poles(rad/s)	control gain	estimator gain
1	$-11.78 \pm 343i$	$-105.6 \pm 339i$	$-4.88 \pm 5.61i$	$-1313 \pm 387i$
2	$-17.96 \pm 512i$	$-74.6 \pm 498i$	$5.08 \pm 3.80i$	$-720 \pm 302i$

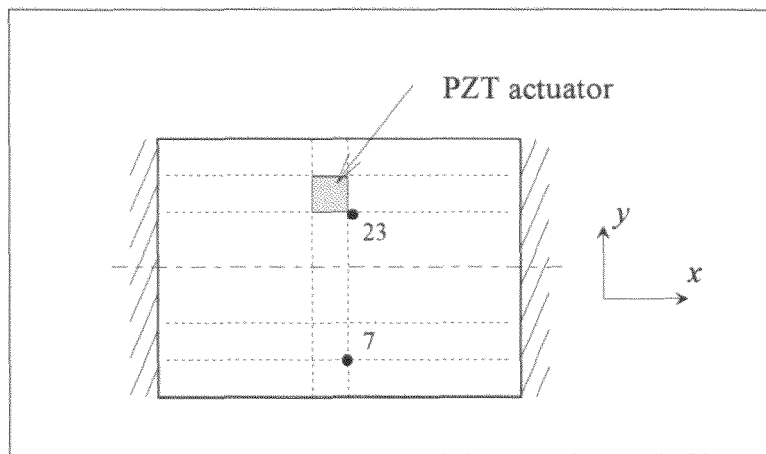
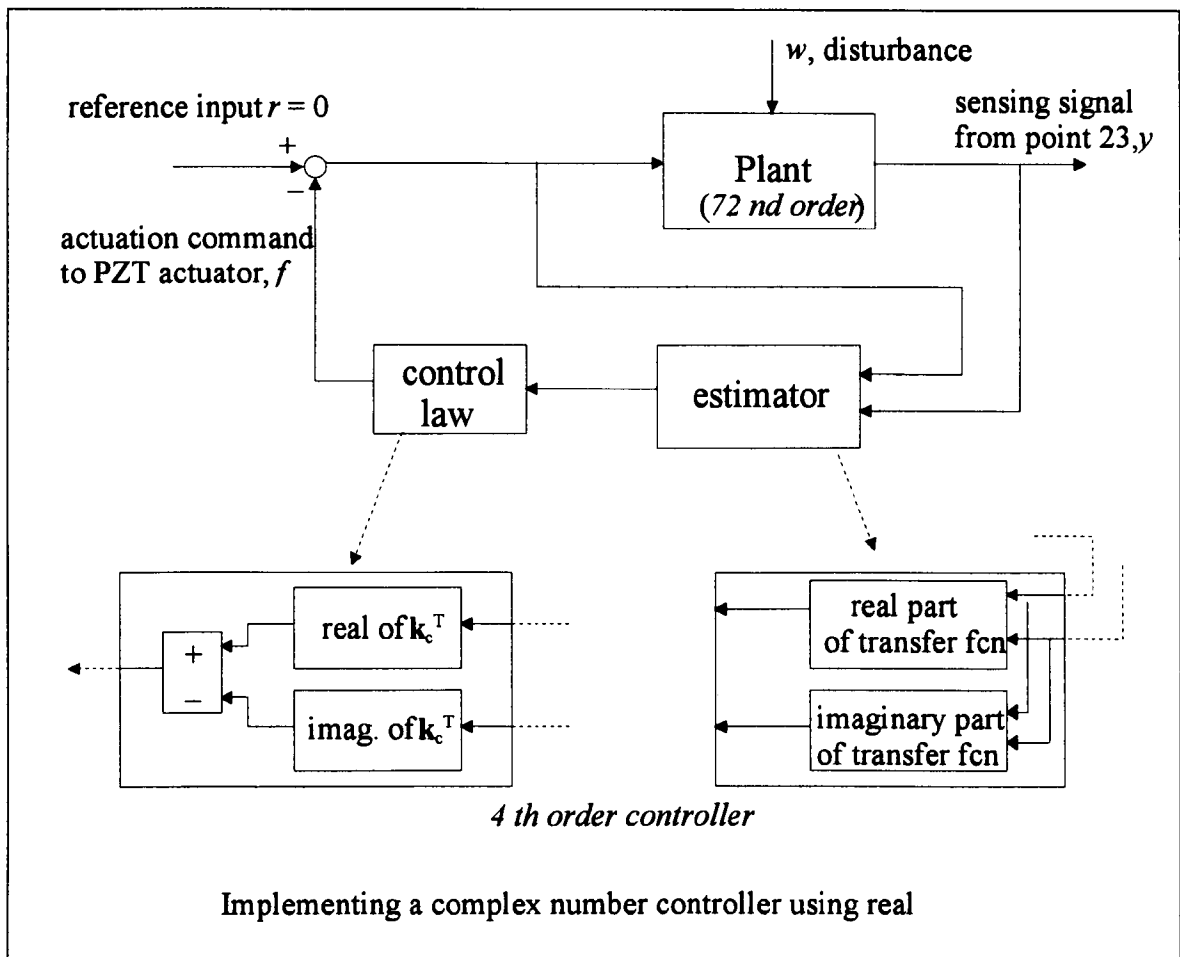


Figure 5.2. Actuator location and excitation and measurement points (7,23) used in simulation of active constrained layer damping



**Figure 5.3.** Block diagram of digital control simulation to match with real-time interface using SIMULINK software

For the numerical simulations, a 72<sup>nd</sup>-order plant equation together with a truncated, 4<sup>th</sup>-order controller is used to investigate the performance of active controlled system and the influence of spillover effects. FRFs from numerical simulations of the SISO configuration of the actively controlled system shown in Figure 5.2 are plotted in Figure 5.4. FRFs are obtained from the velocity response at measurement point 23 divided by the applied force at disturbance position 7. The disturbance is a white noise random signal in the frequency range from 0 to 600 Hz. Compared to the passively damped plate, the FRF of the actively controlled one shows significant attenuation of vibration levels of the first two modes.

However, higher frequency modes tend to be excited so that their amplitudes increase slightly. Experimental verification of the simulation results and study of other control configurations to obtain effective performance and overcome spillover effects are presented in the following section where simulation procedures described in this section will be used to obtain numerical results for a comparison with experimental results.

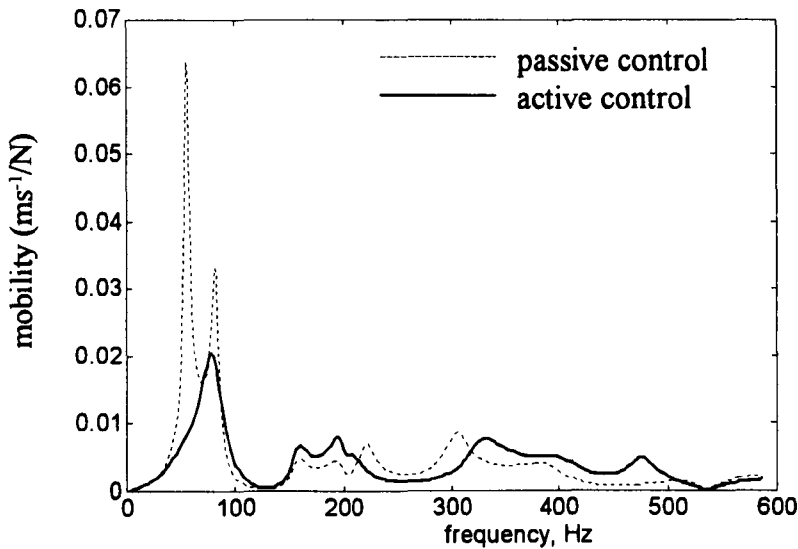


**Figure 5.4.** Simulation results: predicted FRFs (FRF7\_23) of three-layer plate with and without active control for a single PZT actuator and a single accelerometer

#### 5.4 Experimental verification

Various arrangements of accelerometers and PZT actuators on the three-layer test plate will be studied and the results from experiments will be compared to those from numerical simulations. The first one of three arrangements of sensors and actuators on the plate are shown in Figure 5.5. The general arrangement of the test facility is shown in Figure 5.6. A source of disturbance signal to a shaker is white noise random. Implementation of the digital controller is performed using a commercial package

('dSPACE' DS1102) which has up to 4 analogue-to-digital (A/D) input channels and 4 digital-to-analogue (D/A) output channels. In general, to avoid aliasing of a sampled signal, the sampling frequency must be greater than twice the highest natural frequency of interest, which in this case is around 600 Hz (for example, see Franklin et al, 1998). In the present study it was found that a sampling frequency of 10 kHz provided a suitable compromise between sufficiently accurate discretisation of the analogue signal for real-time control and the capabilities of the digital signal processor. This sampling rate ensures that the spillover from the uncontrolled higher frequency modes (mode up to 600 Hz), included in the analysis, will not occur. The control interface card is designed to operate with SIMULINK software (Dabney and Harman, 1996).

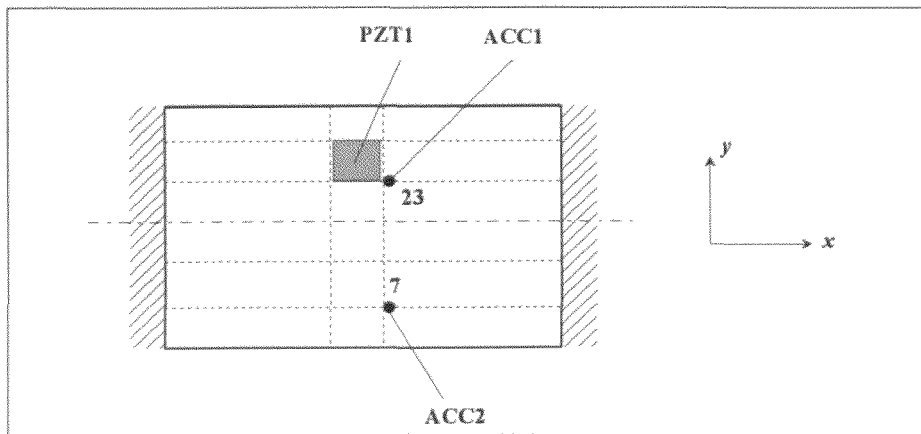


Figure 5.5. Arrangement of the clamped-clamped plate with a square PZT element used as actuator and 2 accelerometers for sensing

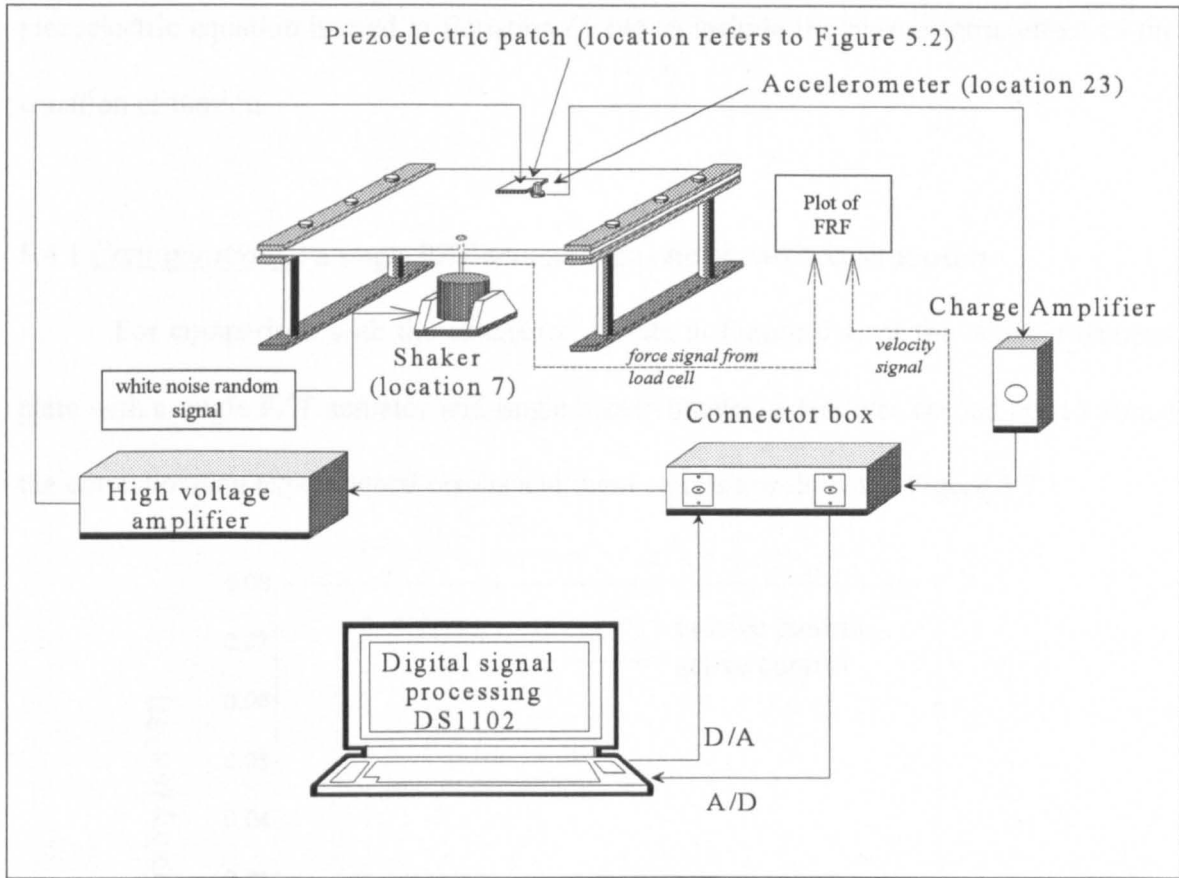


Figure 5.6. Arrangement of the closed-loop clamped-clamped plate with electronic equipment for digital control implementation

The PZT actuator (model PC5H type VI from the MATROC company) is approximately 1 mm thick to react effectively to a maximum voltage of from 1 to 2 kV (Physik Instrumente, 1999). The relationship between force and voltage applied for the PZT actuator is derived as (Physik Instrumente, 1999)

$$\begin{aligned}
 f(t) &= \sigma_a A_a = \left( E_a \frac{d_{31}}{t_a} V(t) \right) \cdot b_a t_a \\
 &= -0.702 V(t) \quad (\text{Newton per Volt}) \quad (5.9)
 \end{aligned}$$

where  $\sigma_a$  is the stress developed in the PZT,  $A_a$  is the cross-section area of the PZT,  $b_a$  is the width of the PZT,  $t_a$  is thickness of the PZT,  $E_a$  is the modulus of elasticity of the PZT ( $= 1/15.1 \times 10^{-12} \text{ Nm}^{-2}$ ) and  $d_{31}$  is the piezoelectric constant ( $= -212 \times 10^{-12} \text{ mV}^{-1}$ ). This

piezoelectric equation is used in Equation (3.14) to include the piezoelectric effect to the equation of motion.

#### 5.4.1 *Configuration 1*: a single PZT actuator and one or two accelerometers

For comparison with the simulation results in Figure 5.4, of the actively damped plate with a single PZT actuator and single accelerometer, a test was carried out to obtain the corresponding experimental results and these results are shown in Figure 5.7.

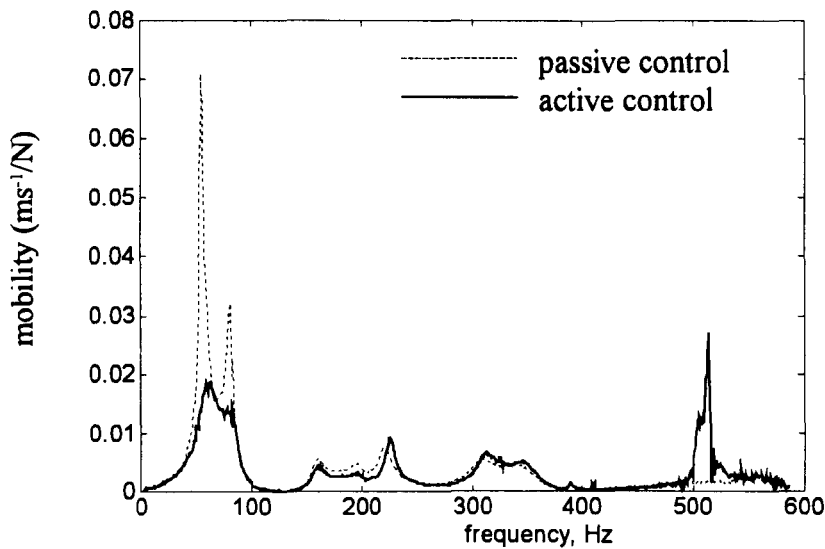


**Figure 5.7.** Measured FRFs (FRF7\_23) of three-layer plate with and without active control using PZT1 and ACC1 (Figure 5.5)

The introduction of active control results in significant attenuation of the two lowest modes, which was predicted by the simulation results. However the simulation results in Figure 5.4 indicated that these two modes would coalesce into a single mode. This did not happen in practice with the two modes remaining distinct. Note that the excitation of the mode just above 500 Hz occurred.

The second test used two accelerometers as sensors for the estimator. The arrangement of sensors is shown in Figure 5.5. Results from the test are shown in Figure 5.8(a). Initially, using two sensors for constructing modal variables may improve the stability of the controlled system but the level of vibration in the first mode is higher than that using a single accelerometer. The reason for this is that perturbations of assigned poles in the closed-loop system (Equation (5.4)) owing to observation spillover between controllers using one and two sensors are different. If the voltage gain in the controller with two sensors is amplified until levels of the controlled modes equal to those of the single sensor case, the similar results are obtained as shown in Figure 5.8(b) such that the excitation of the mode just above 500 Hz occurs. Comparisons of both active and passive control schemes in relation to the response of the bare plate are shown in Figures 5.9 to 5.13 with different points of measurement, as defined in Figure 4.2. The attenuation of the first and second modes is increased through the active damping control by about 10 dB and 5 dB, respectively.

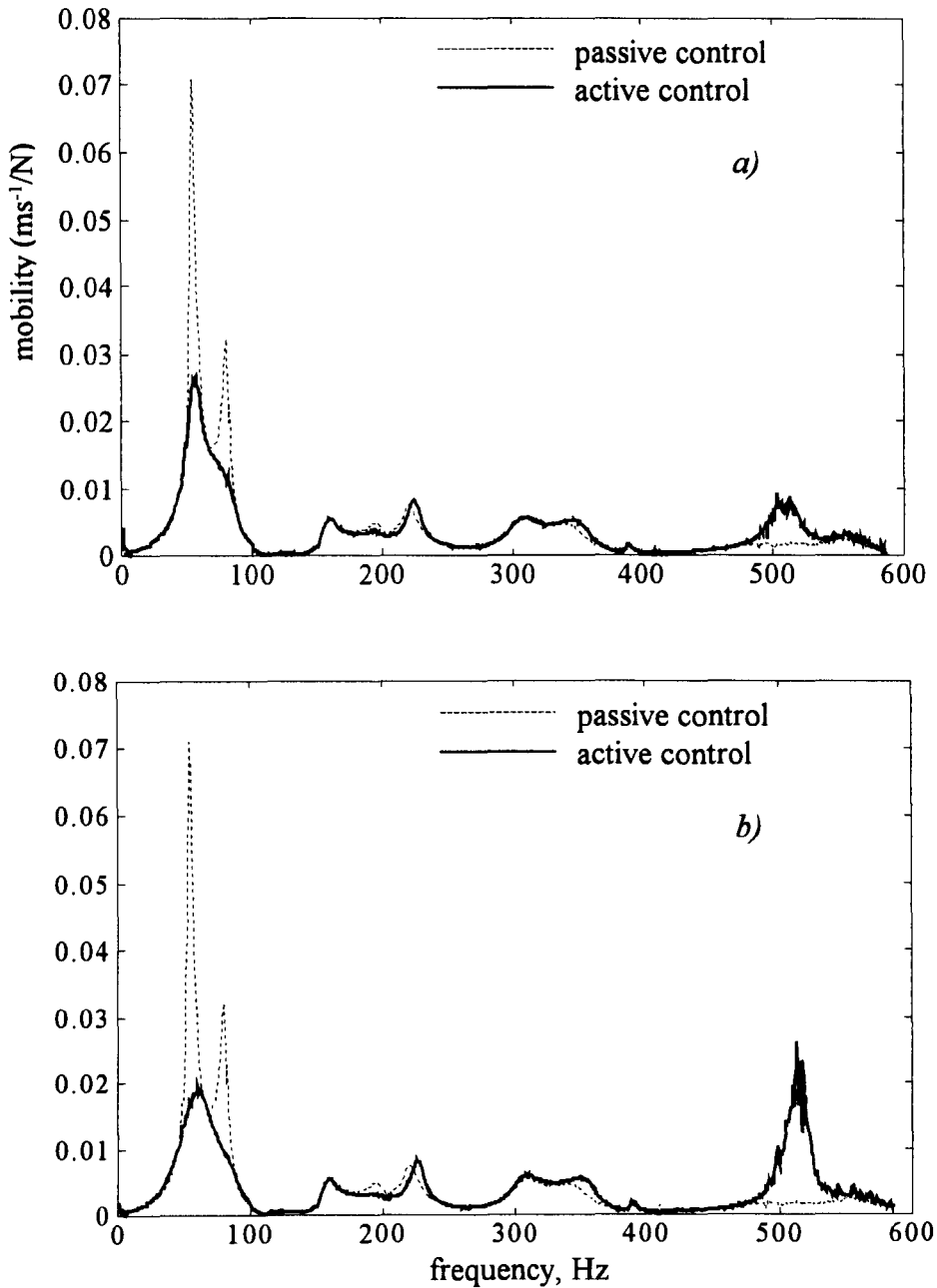


**Figure 5.8.** Measured FRFs (FRF7\_23) of three-layer plate with and without active control using PZT1 and ACC1 and 2 (Figure 5.5)  
 a) gain as designed  
 b) with an amplified gain factor = 1.6

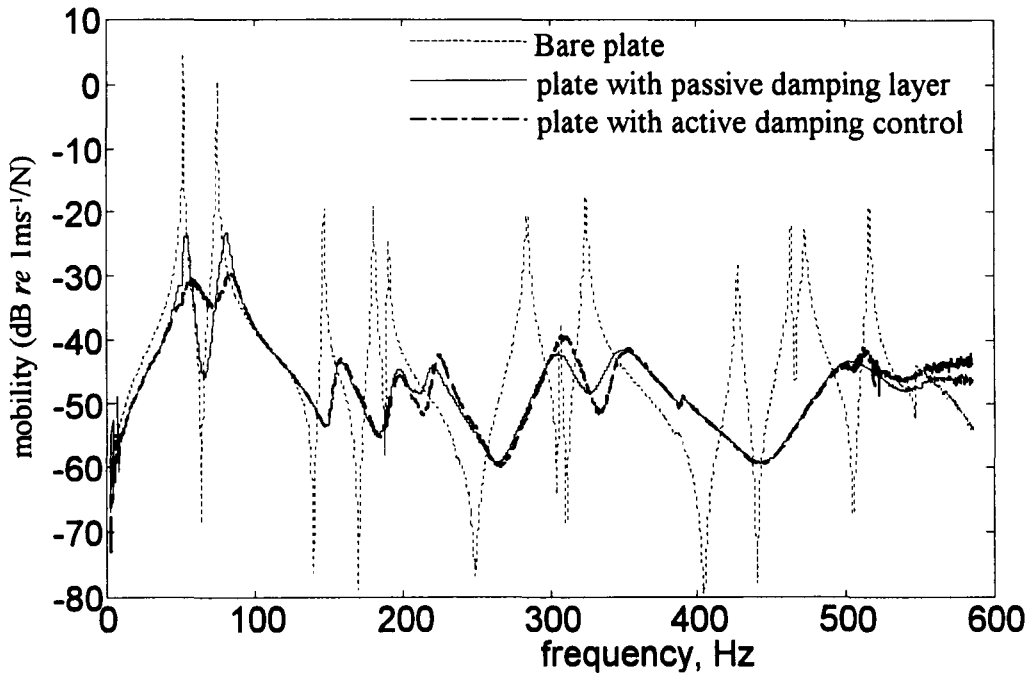


Figure 5.9. FRF7\_7: a comparison of passive and active schemes in relation to untreated plate

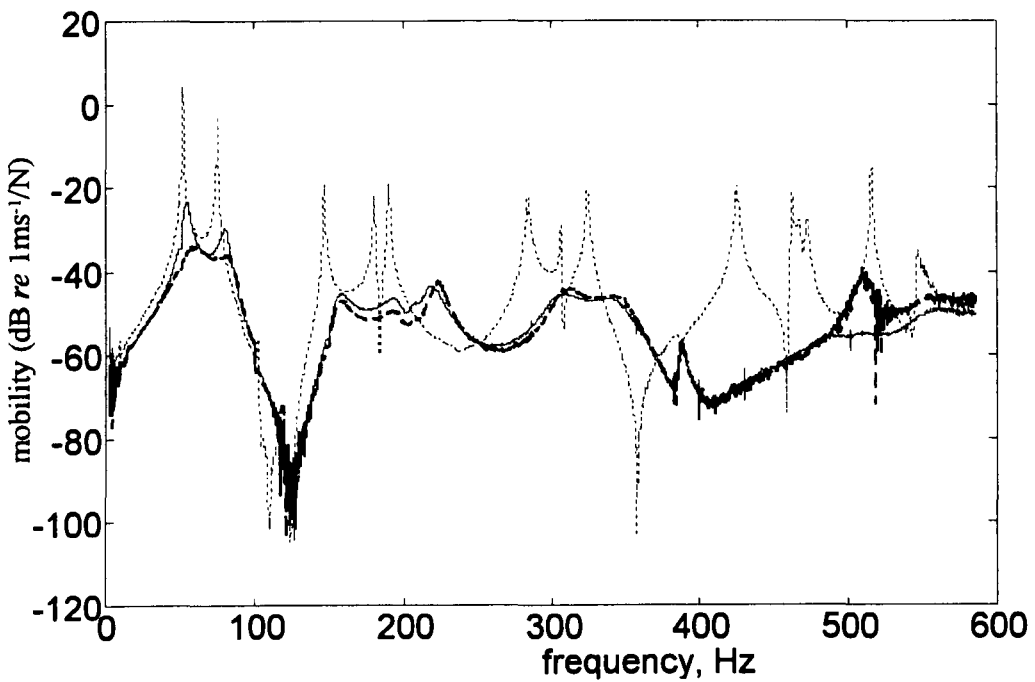


Figure 5.10. FRF7\_23: a comparison of passive and active schemes in relation to untreated plate

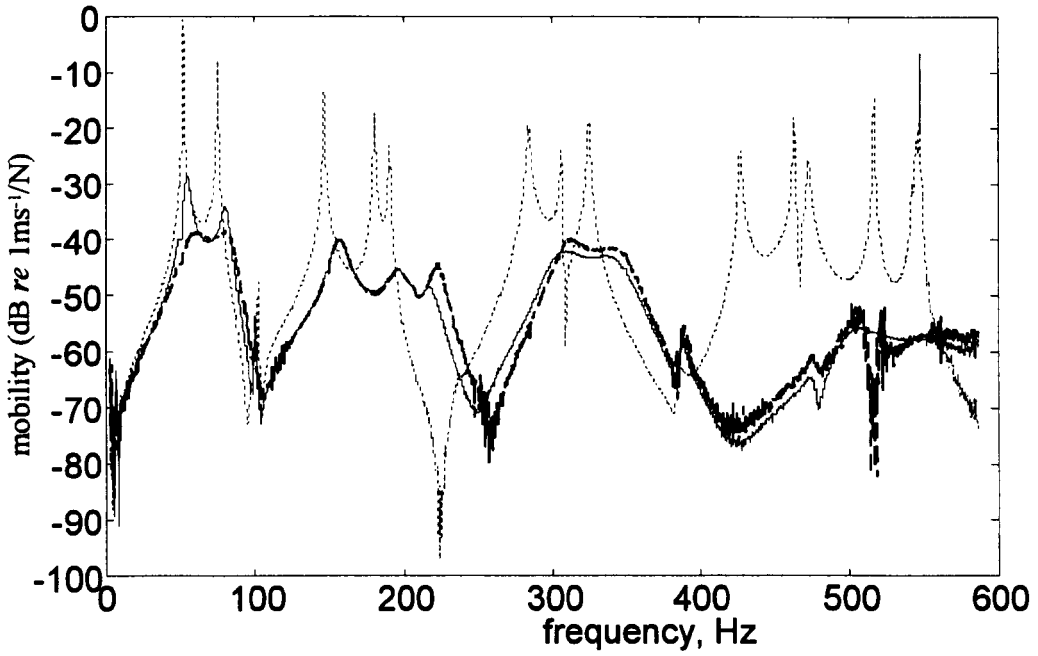


Figure 5.11. FRF7\_17: a comparison of passive and active schemes in relation to untreated plate

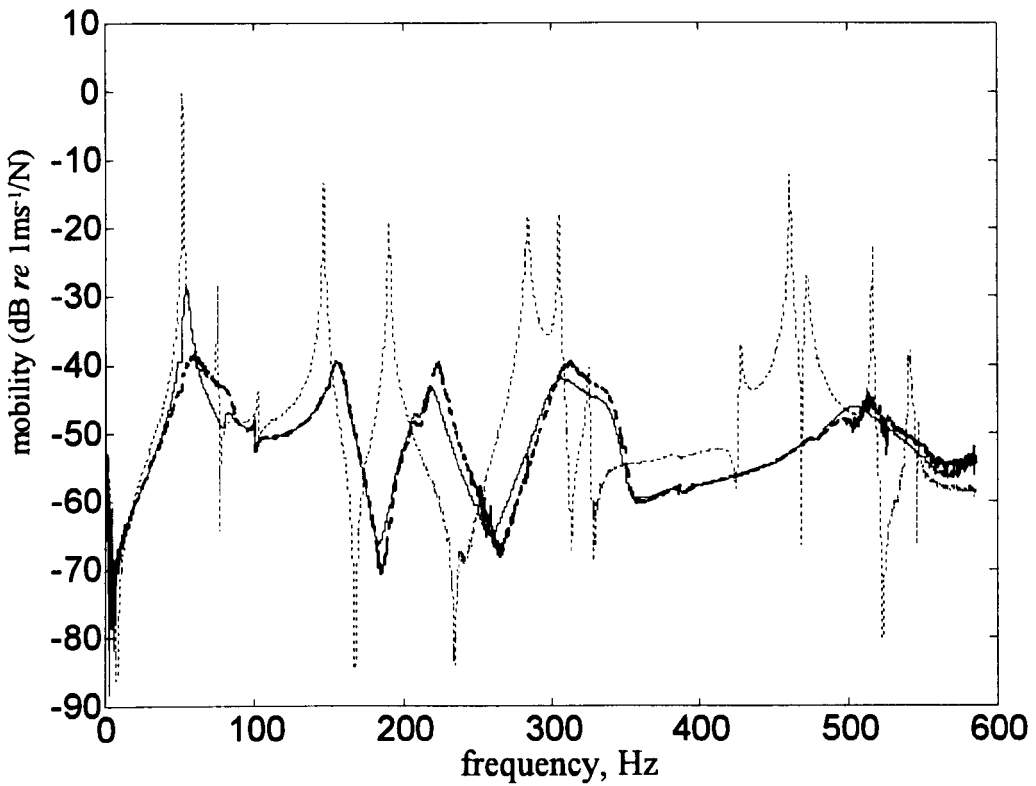


Figure 5.12. FRF7\_13: a comparison of passive and active schemes in relation to untreated plate

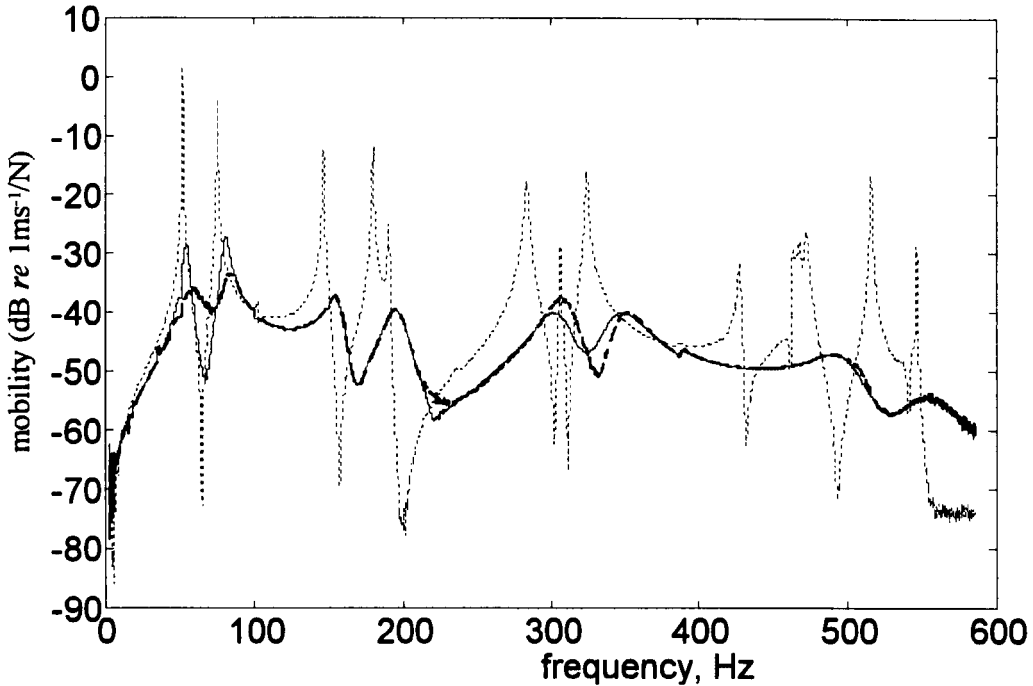
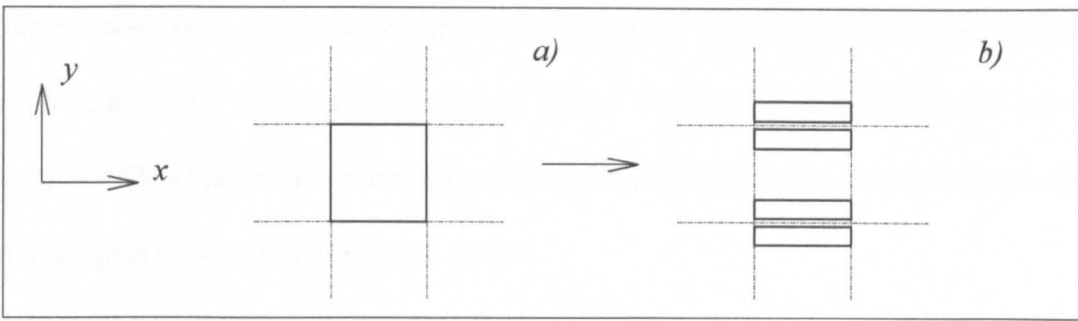


Figure 5.13. FRF7\_5: a comparison of passive and active schemes in relation to untreated plate

#### 5.4.2 *Configuration 2*: a PZT actuator operating in $x$ direction only

In the previous tests (sub-section 5.4.1), a 50 mm  $\times$  50 mm element of PZT material was used as an actuator which operates in both the  $x$  and  $y$  directions. In principle, the intention of the active control strategy is to increase the induced shear strain in the  $x$  direction where bending curvature of the first two modes occur. Actuation of the PZT actuator in the  $y$  direction causes an excessive load of the actuator and may excite higher frequency modes of vibration as already shown in Figures 5.7 and 5.8(b). To activate dominantly the PZT actuator in the  $x$  direction only, the length of the PZT should be longer than 3.5 times its width and thickness (Morgan Matroc, 1999). Thus, to use the same area of PZT actuator in the previous configuration, a 50 mm  $\times$  50 mm PZT patch is cut into 4 strips of equal width and attached to the plate as shown in Figure 5.14.



**Figure 5.14.** Configuration of PZT actuator  
 a) for operation in  $x$  and  $y$  directions  
 b) for operation in  $x$  direction only

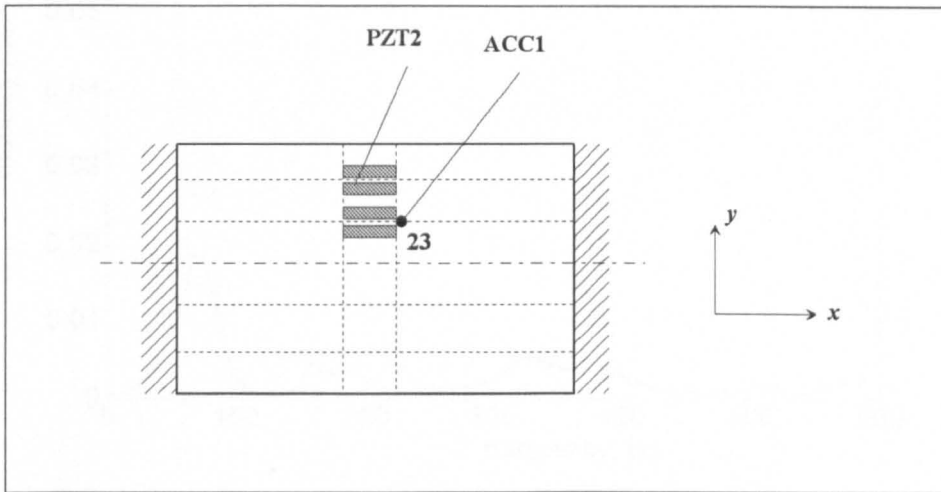


**Figure 5.15.** Arrangement of the clamped-clamped plate with 4-strip PZT elements used as actuator and a single accelerometer for sensing

The arrangement of sensor and actuator for this arrangement is shown in Figure 5.15. The simulation results in Figure 5.16 show the influence of activating the PZT element in the  $x$  direction only. The results demonstrate that superior suppression of vibrations is obtained. In addition, the power consumption for the PZT actuator decreases when actuation is in one direction only, as shown by the plots of applied voltage *versus* time in Figure 5.17, which the disturbance time history is swept sine with a frequency range from 0 to 600 Hz. The simulation results in Figure 5.16 are confirmed with plots of FRFs from experiments in Figure 5.18. With the PZT actuator operating in the  $x$  direction only, the controlled system

is more stable and levels of vibrations can be attenuated more than those in the case of the two-direction PZT actuator. Figure 5.19 shows FRFs from experiments of the one-direction PZT actuator case where the control gain is increased by a factor of 2.4 times the designed gain (of the result in Figure 5.18).

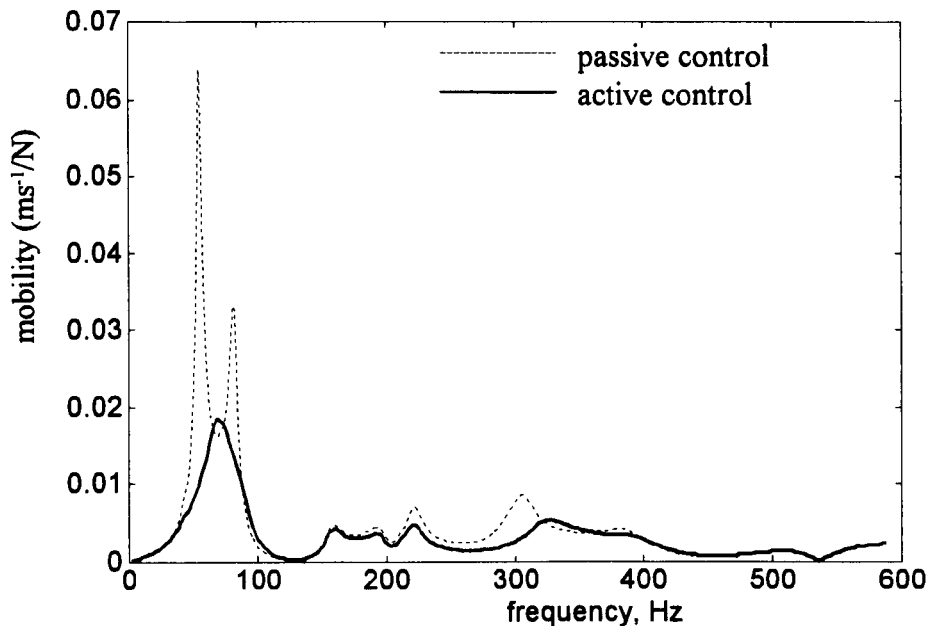


Figure 5.16. Simulation results: predicted FRFs (FRF7\_23) of three-layer plate with and without active control for PZT actuator operating in  $x$  direction only (Figure 5.15)

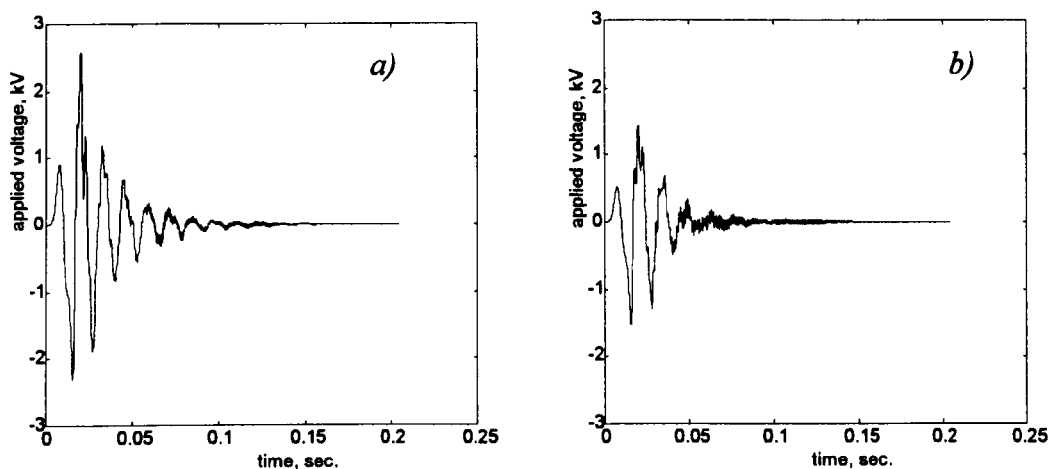
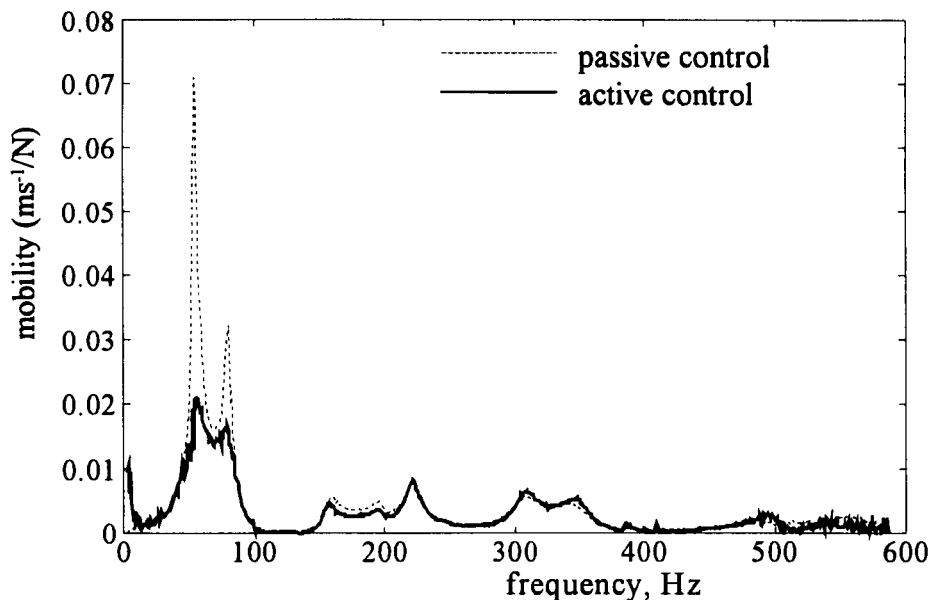
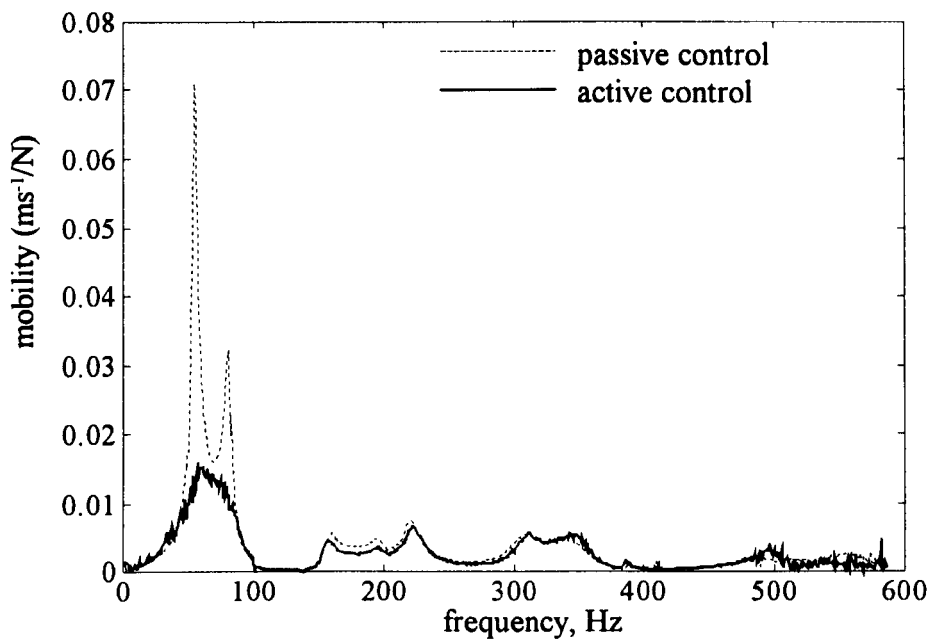


Figure 5.17. Simulation results: applied voltage for PZT actuator  
 a) operating in both  $x$  and  $y$  directions  
 b) operating in  $x$  direction only



**Figure 5.18.** Measured FRFs (FRF7\_23) of three-layer plate with and without active control using 4-strip PZT2 and ACC1 (Figure 5.15)



**Figure 5.19.** Measured FRFs (FRF7\_23) of three-layer plate with and without active control using 4-strip PZT2 and ACC1 (Figure 5.15) with an amplified gain factor = 2.4

### 5.4.3 Configuration 3: two PZT actuators with a single-channel voltage amplifier and one accelerometer

The application of two PZT actuators was studied in an attempt to achieve better vibration suppression than was possible using a single PZT actuator. The configuration of sensors and actuators is shown in Figure 5.20. The first test is performed by using PZT actuators, PZT1 and 2, and a single accelerometer, ACC1 in Figure 5.20. Both PZT actuators are supplied with the same command force from a single channel high-voltage amplifier, i.e. the control system is still a SISO system. The result, as expected, shows that suppression of the second, torsional, mode, where positive and negative displacements occurred simultaneously, is worse when using the non-collocated sensor and actuators. Figures 5.21(a) and (b) show the experimental results from testing. The results in Figure 5.21(a) arise from using the control gain as designed and in Figure 5.21(b) from using a gain 1.4 times of the designed gain. The first bending mode is suppressed in amplitude but the levels of the second (i.e. torsional), and sixth modes increase as the control gain increases.

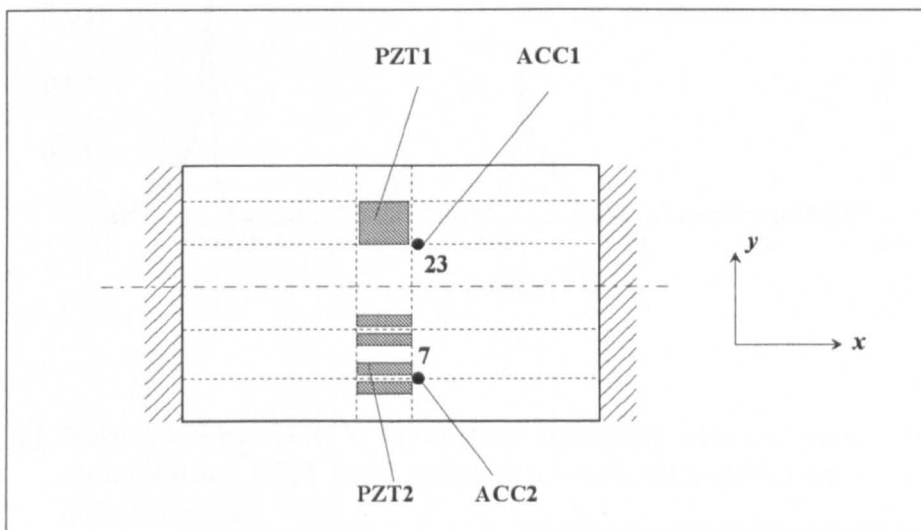


**Figure 5.20.** Arrangement of the clamped-clamped plate with 2 PZT actuators (one square element and one 4-strip element) and 2 accelerometers for sensing

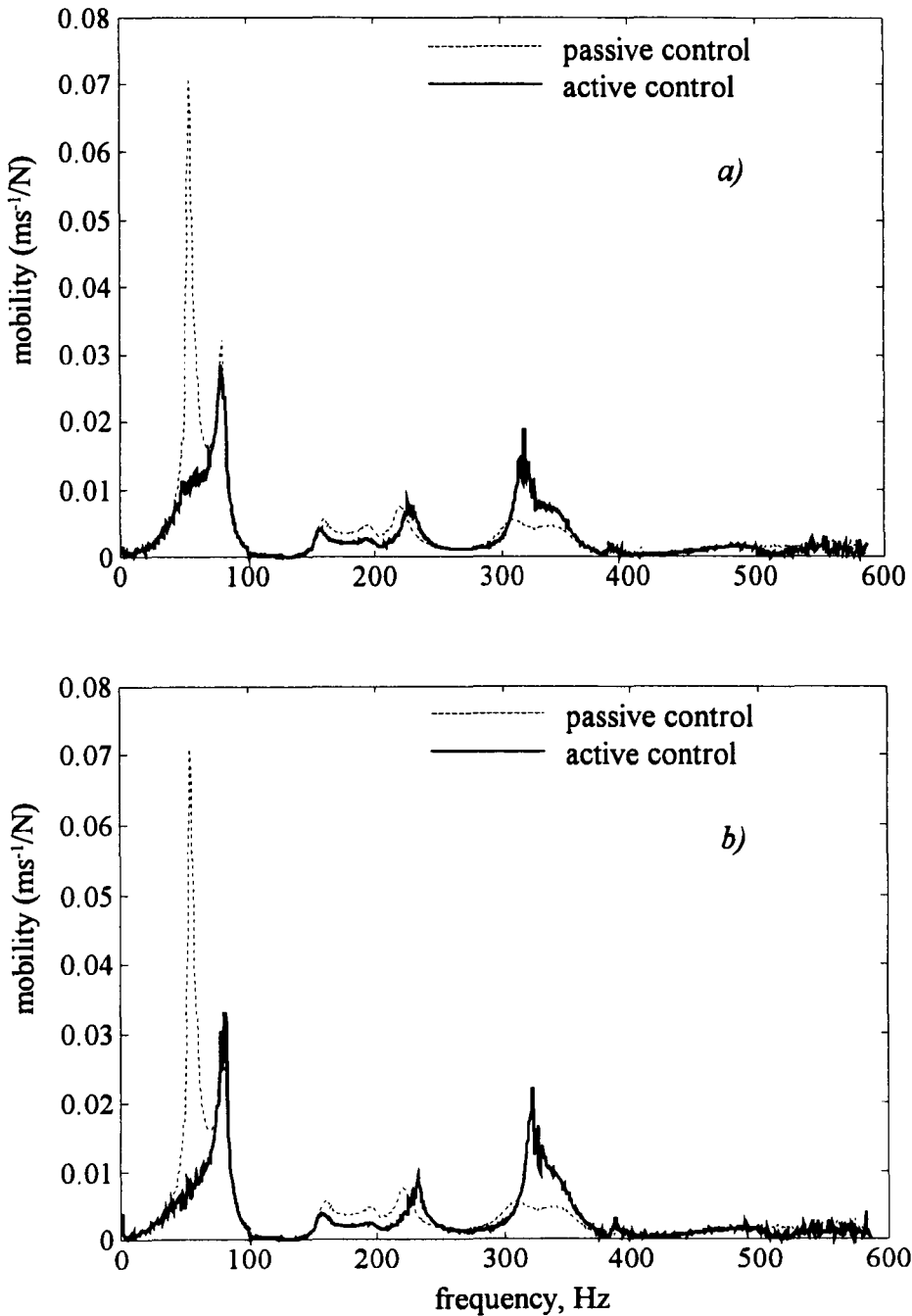


**Figure 5.21.** Measured FRFs (FRF7\_23) of three-layer plate with and without active control using PZT1 and 2 with a single-channel amplifier and ACC1 (Figure 5.20)

- a) gain as designed
- b) with an amplified gain factor = 1.4

Consequently, the next tests are aimed to the use of two PZT actuators incorporating with a two-channel high-voltage amplifier to perform a MIMO control system such that each PZT actuator is commanded independently by each control law.

#### 5.4.4 Configuration 4: two PZT actuators with a two-channel amplifier and one or two accelerometers

The test arrangement is the same as in the previous test and shown in Figure 5.20 except in the use of the two-channel high-voltage amplifier. Initially, two PZT actuators, PZT1 and 2, and single accelerometer, ACC1, are used to implement active control. Measured FRFs from experiments show that the amplitude of the first mode is well-suppressed but this does not occur for the second mode, especially when the control gains increase, as shown in Figures 5.22(a) and (b). From simulations of this test, it is also shown that levels of the first two vibration modes are about to increase as the control gains increase. Figure 5.23 shows the numerical results corresponding to the experiments.

The reason for this increase in the amplitudes of the first two modes could arise from spillover effects in the closed-loop system. As a result, the controller was redesigned to obtain lower estimator gains. Two other tests were performed where the configurations of test plate are the same as the previous test but in one the sensor location was changed from point 7 to point 23 (see Figure 5.20) and for the other case with two sensors at points 7 and 23. FRFs predicted from the models of these two redesigned control systems are shown in Figures 5.24 and 5.25 and the corresponding experimental results are shown in Figures 5.26 and 5.27, respectively. The plots show that the magnitudes of the first two vibration modes are reduced significantly as the control gains are increased. Table 5.3

presents the redesigned estimator gains such that the designed gains are reduced by changing sensor locations. The most effective vibration suppression of the first two controlled modes is obtained using two PZT actuators, two sensors and a two-channel amplifier. The resulting maximum amplitudes of first two modes do not exceed  $0.01 \text{ ms}^{-1}/\text{N}$  (Figure 5.27(b)).

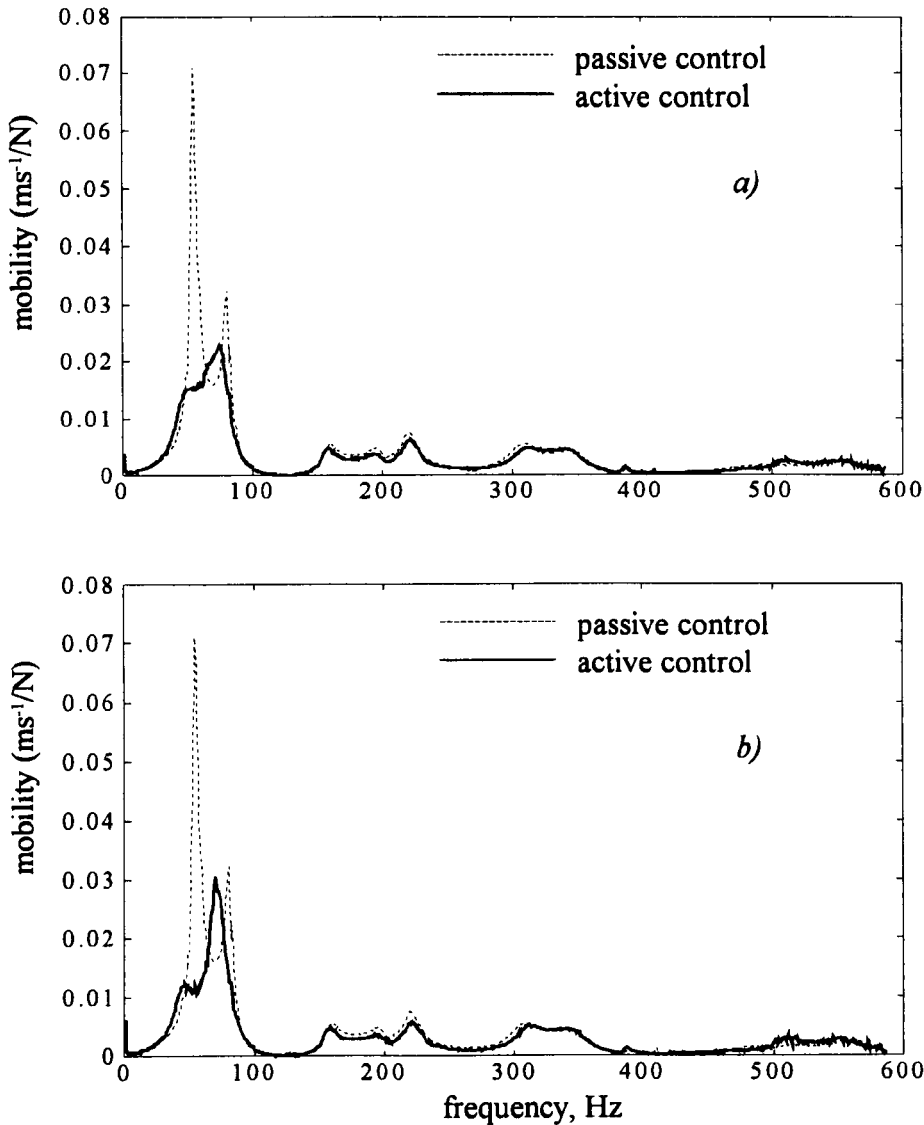


**Figure 5.22.** Measured FRFs (FRF7\_23) of three-layer plate with and without control using PZT1 and 2 with a 2-channel amplifier and ACC1 (Figure 5.20)  
 a) gain as designed  
 b) with an amplified gain factor = 1.4

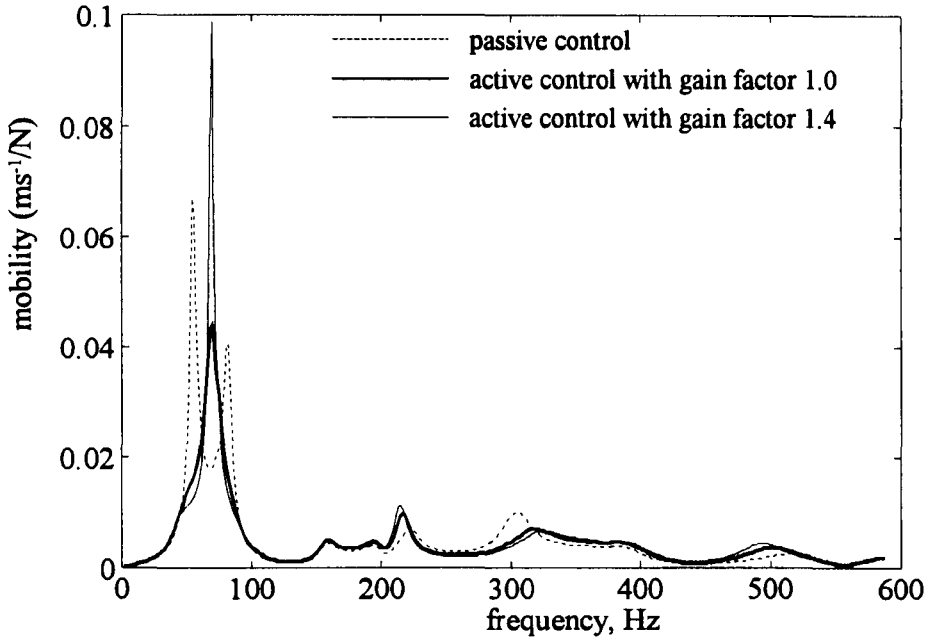
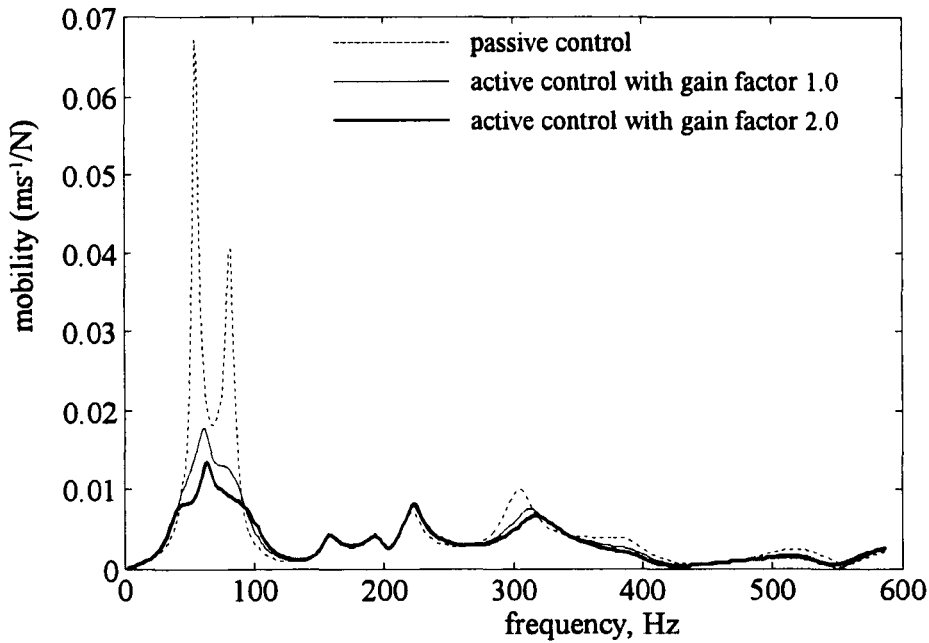


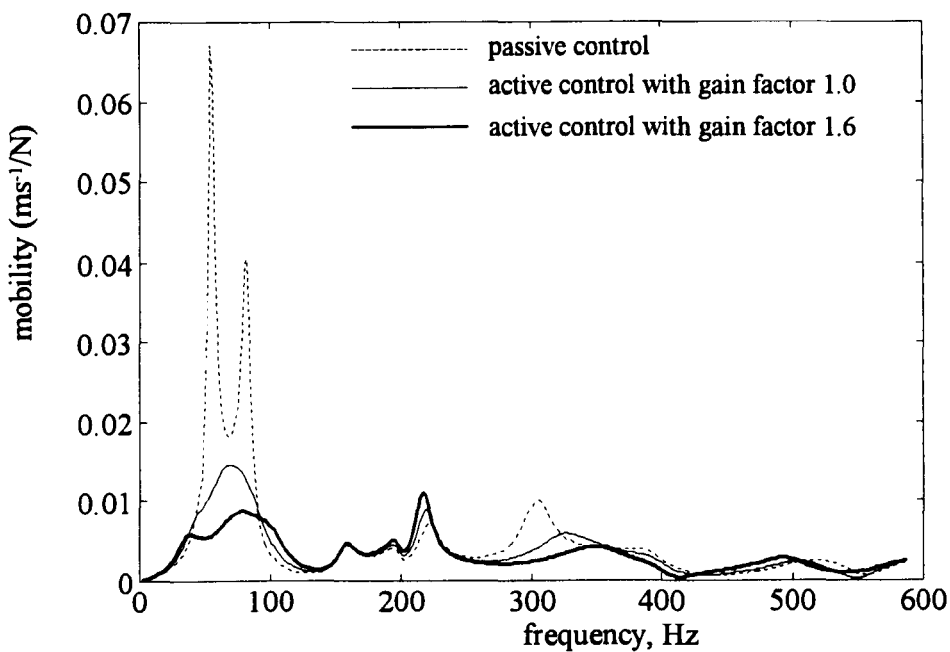
Figure 5.23. Simulation results: FRFs (FRF7\_23) of three-layer plate with and without active control using PZT1 and 2 with a 2-channel amplifier and ACC1 (Figure 5.20)

Table 5.3 Re-designed estimator gains

Case	1) PZT1&2, ACC1	2) PZT1&2, ACC2	3) PZT1&2, ACC1&2	
Estimator for model	65.4±296.6i	44.1±251.0i	66.6±256.5i	51.4±289.9i
gain : for mode2	-337.1±284.6i	218.6±161.4i	-127.8±100.1i	246.2±174.7i



**Figure 5.24.** Simulation results: FRFs (FRF7\_23) of three-layer plate with and without active control using PZT1 and 2 with a 2-channel amplifier and ACC2 (Figure 5.20)



**Figure 5.25.** Simulation results: FRFs (FRF7\_23) of three-layer plate with and without active control using PZT1 and 2 with a 2-channel amplifier and ACC1 and 2 (Figure 5.20)

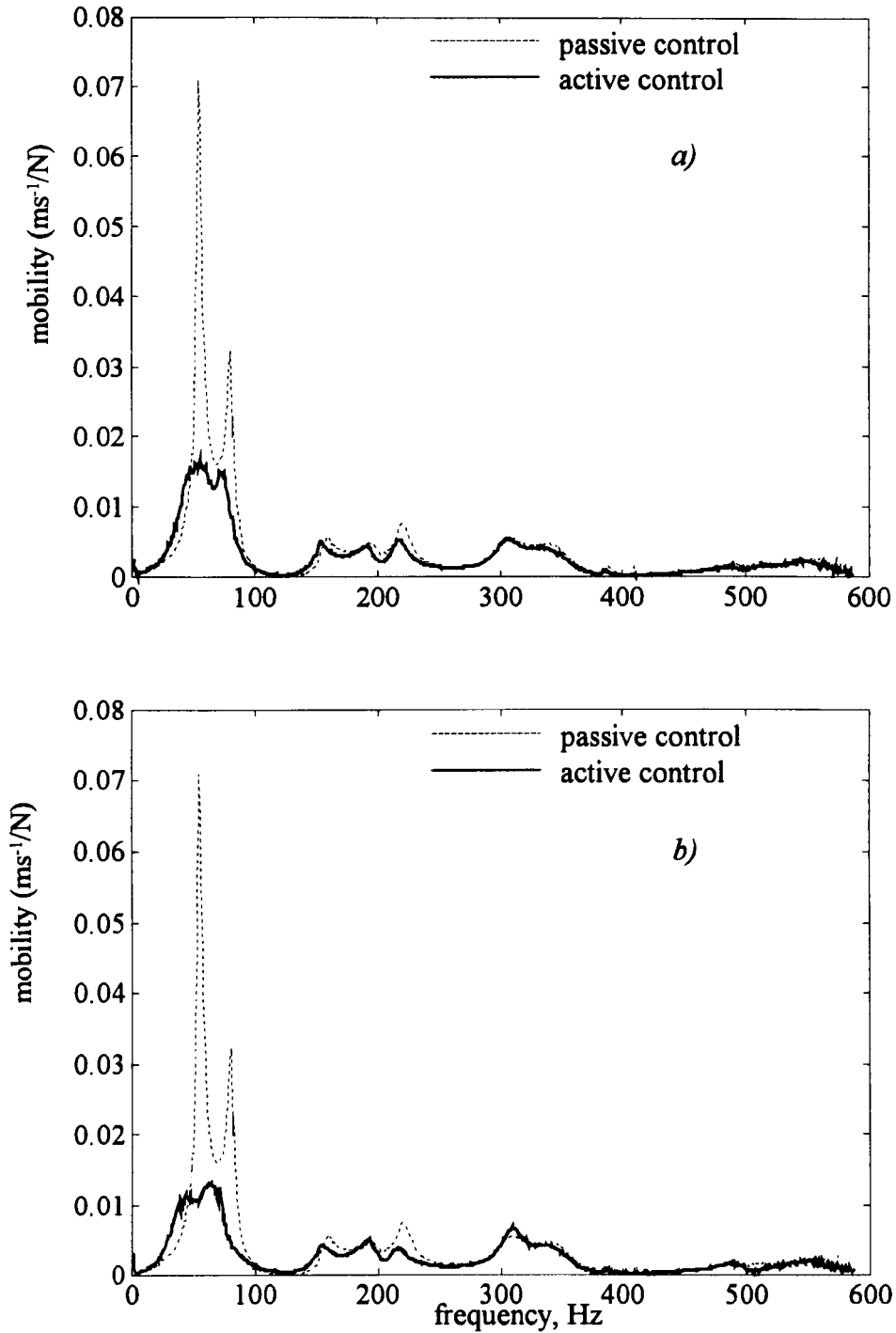


**Figure 5.26.** Measured FRFs (FRF7\_23) of three-layer plate with and without active control using PZT1 and 2 with a 2-channel amplifier and ACC2 (Figure 5.20)

a) gain as designed

b) with an amplified gain factor = 2.0

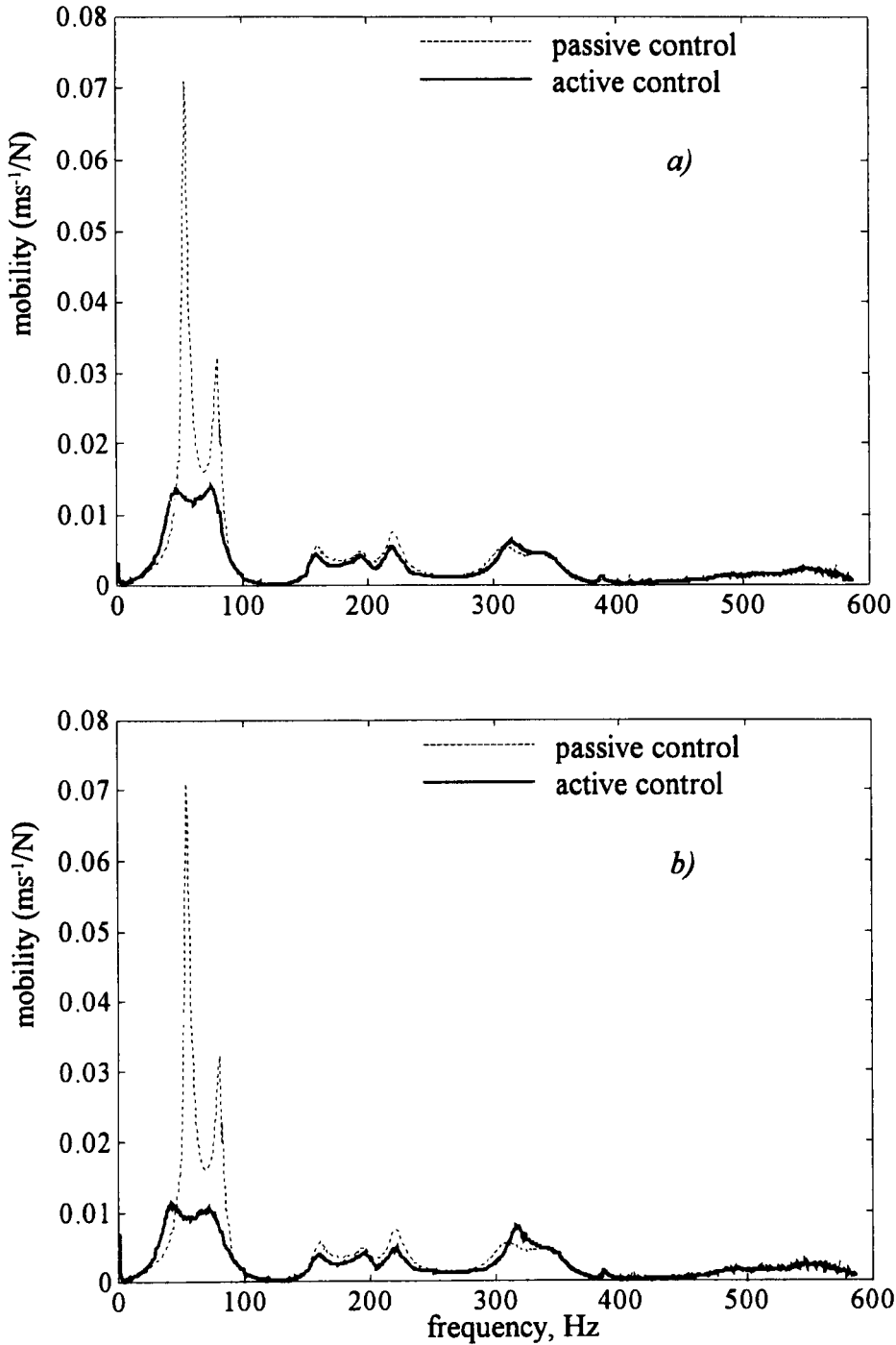


**Figure 5.27.** Measured FRFs (FRF7\_23) of three-layer plate with and without active control using PZT1 and 2 with a 2-channel amplifier and ACC1 and 2 (Figure 5.20)

a) gain as designed

b) with an amplified gain factor = 1.6

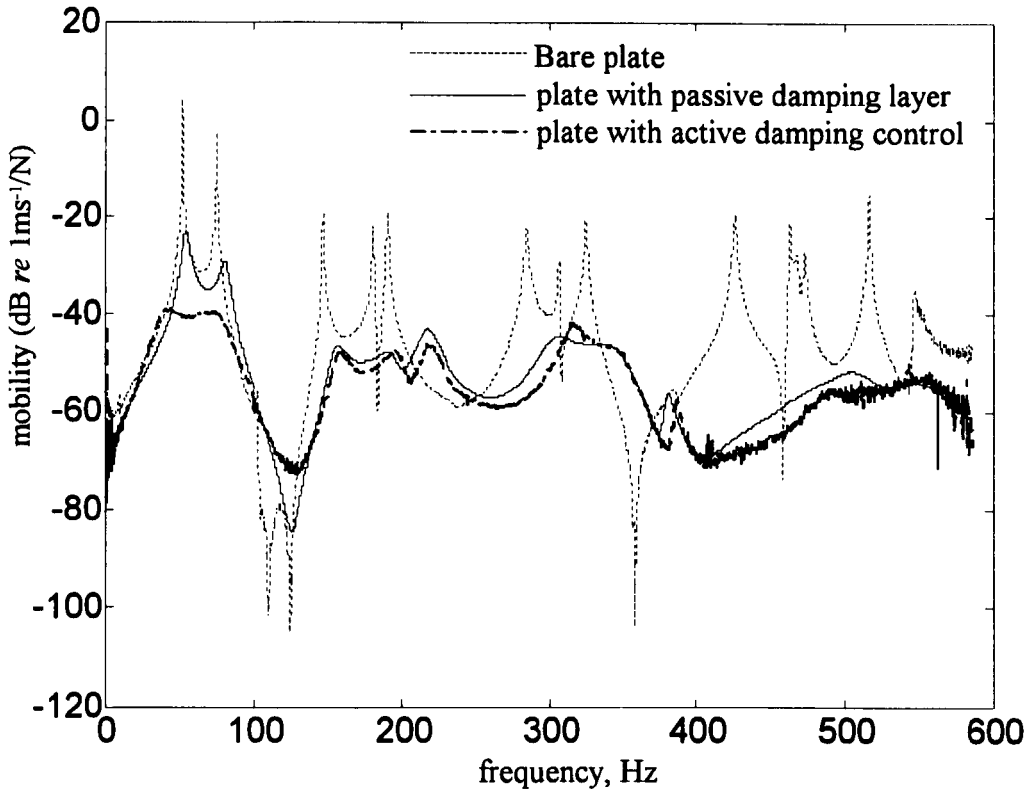


**Figure 5.28.** FRF7\_23: A comparison of passive and active schemes in relation to untreated plate: the best case of using 2 PZTs with a 2-channel amplifier and 2 ACCs

In Figure 5.27, it is worthy of note that the level of mode 6 slightly increases as the control gains increase. This arises because mode 6 is the third bending mode where maximum curvature occurs in the middle of the plate, the same as for mode 1. However, this problem could be solved by including mode 6 as a controlled mode. In summary, Figure 5.28 shows a comparison of FRFs from the actively controlled, passively controlled schemes and the result from the bare plate. The active control results provide the best performance using two PZT actuators along with a two-channel amplifier and two accelerometers (Figure 5.27(b)). Compared with passive control, the attenuation of the first two modes through the active control is increased by 15 dB and 10 dB, respectively.

## **5.5 Summary of Chapter 5**

The design of an active controller was presented to obtain the discrete-time controller to implement digital control of the three-layer plate in which the first two modes were controlled. The control and estimator gains were obtained from optimal selection using LQR and LQG control algorithms, respectively, so that spillover effects are effectively avoided. Suitable placement of sensors and actuators is also essential in order to overcome spillover effects. Numerical simulations were performed before performing experiments, so as to consider the performance of active control systems under controlled conditions. Various configurations of the control strategies were studied - a single PZT actuator operating in the  $x$  direction only - two PZT actuators associated with single- or two-channel amplifiers and with one or two accelerometers. In the simplest case - a single PZT patch and single accelerometer, the effective vibration suppression of the three-layer plate was obtained with reduction of vibration levels through the active control of about 10 dB and 5 dB for the first and second modes, respectively. The best performance of vibration suppression was obtained in the case of two PZT actuators along with two-channel amplifier and two accelerometers such that better attenuation of vibration amplitudes was achieved, 15 dB and 10 dB, respectively, in the first and second modes compared to passive control. Furthermore, lower power consumption was required. However, note that the latter schemes required additional hardware.

# CHAPTER 6

## CONCLUSIONS AND RECOMMENDATIONS FOR FUTURE WORK

### 6.1 Conclusions

In this thesis, a study of the active constrained layer damping treatment of a clamped-clamped plate has been described. This study has involved both numerical and experimental investigations. The strategy adopted was based upon the development of a model-based approach to control system design. The aim has been to minimise the amount of control hardware required whilst avoiding spillover problems which are liable to degrade performance. The combination of passive and active schemes in the active damping treatment has advantages where inherent damping in the passive damping layer improves the robustness of the actively controlled system and the active function is to enhanced vibration suppression of the lower frequency modes which are characterised by long wavelengths.

Initially, finite element analysis was used to form the dynamic model of plate treated with the constrained damping layer so that design and performance of both passive and active control could be examined before the implementation stage. The formulated finite element models in this study showed good agreement with well-established solutions. A passive constrained damping layer was introduced and its influence on vibration levels was investigated. Not unexpectedly it was found that the higher frequency modes benefited significantly from the introduction of the passive layer, a self-adhesive damping tape with a thin steel shim on the top: modes 3 to 10 in the range from 150 to 600 Hz were attenuated

by approximately 25 dB. The first two modes (bending, torsional) below 100 Hz were attenuated by a similar amount. However, peak mobility levels for modes 1 and 2 were still some 20 dB above those of the higher order modes and an active strategy was developed to deal with this problem.

It was demonstrated that more accurate modelling does not guarantee that the formulated models can account for the observed behaviour of test plates owing to uncertainties such as imperfection of materials and connection within the plates. An updating algorithm involving pole placement was applied to match the formulated finite element model with the observed behaviour of the treated plate so that the refined model could be used in active control system design. To match the formulation of the state-space equations of motion used in the updating algorithm, the identification technique has been developed to transform a complex stiffness matrix, representing damping of the three-layer plate, to real symmetrical stiffness and viscous damping matrices. The first six natural frequencies and modal damping factors of the three-layer test plate were identified experimentally using the peak-picking method to provide the data required to implement the updating algorithm.

The development of the active control system involved the transformation of the original finite element model of the plate into a modal state-space description to be implemented in discrete time. To illustrate some of the key problems involved in this transformation and the solutions which were devised, the mathematical treatment has been described in some detail. The end result of the various computations was a fourth-order estimator/controller. Numerical experiments indicated that such an arrangement was capable of attenuating modes 1 and 2 (in conjunction with a 72 nd order model of the plate) without incurring

significant problems due to spillover. This was achieved using only a single sensor and single actuator channel.

The experimental study confirmed the results of the numerical simulations. Various configurations of the control strategies were investigated - a single PZT actuator and single accelerometer - a single PZT actuator activating in  $x$  direction only - two PZT actuators associated with single- or two-channel amplifiers and one or two accelerometers. In the simplest configuration - a single PZT patch and single accelerometer, further reduction of vibration levels in the passively damped plate through the active control is about 10 dB and 5 dB for the first and second modes, respectively. The best performance of vibration suppression was found in the case of using two PZT actuators incorporating with a two-channel amplifier and two accelerometers such that high attenuation of vibration levels was achieved, 15 dB and 10 dB in the first and second modes, respectively. The influence of sensor locations to performance of the controlled system has been studied. Lower estimator gains can be obtained by changing the sensor locations so as to minimise spillover effects and to result in better vibration suppression. Also two configurations of PZT actuator were investigated. A single PZT patch arranged to provide actuation in mutually perpendicular directions, and an arrangement of four PZT patches driven by a single amplifier but designed to activate the plate in a single direction only. Both configurations were effective at controlling modes 1 and 2 but the single PZT patch produced significant excitation of a mode above 500 Hz.

Note that two further papers have been submitted for publication. There are included as Appendices D and E.

## **6.2 Recommendations for future work**

Other configurations of a hybrid (passive/active) scheme should be considered to compare their effectiveness in vibration suppression. For example, Lam et al (1997) studied a cantilever beam treated with an active constrained damping layer but instead of placing a PZT actuator on top of a metallic constraining layer, the PZT element is placed directly on the host cantilever beam on the opposite side to the passive damping layer. Lam and her colleagues showed that the voltage applied to the actuator given this configuration is reduced when compared to the case of placing the actuator on top of the constraining layer. The reason is that control action is applied directly to the beam without passing through a viscoelastic layer. However, to maximise the performance of the passive damping treatment, a combined scheme can use two PZT patches - one passively shunted PZT (Hagood and von Flotow, 1991) is placed on top of the constraining layer to increase induced shear strain in the damping layer and a second PZT is used to perform fully active control using the same configuration adopted by Lam et al. To achieve better performance in vibration suppression, active control strategies could be applied to both PZT patches but there are additional hardware requirements.

In addition, future work could be aimed at comparing the performance of the time-domain control algorithm described here with robust frequency domain methods which have recently been developed for use with plate-like structures (Sadri et al, 1999). In the investigation by Sadri et al (1999), multi-variable controllers, linear quadratic Gaussian (LQG) and H-infinity algorithms, were implemented numerically and experimentally to examine and compare their performance in suppressing vibrations of a cantilevered plate. They found that the H-infinity controller using frequency-dependent weighting functions

performs better than the LQG controller in terms of vibration attenuation and also robustness to spillover due to uncontrolled and unmodelled modes.

Alternatively instead of introducing damping onto the host plate to avoid excessive vibrations, active isolation (Jenkins et al, 1993) may be considered for an application at the clamped edges so that the plate can be isolated from external disturbances.

# APPENDIX A

## FINITE ELEMENT MODELLING

### A1 Plate model

#### A1.1 Relationships between displacements

For convenience Figure 3.1(b) is reproduced here as Figure A.1.

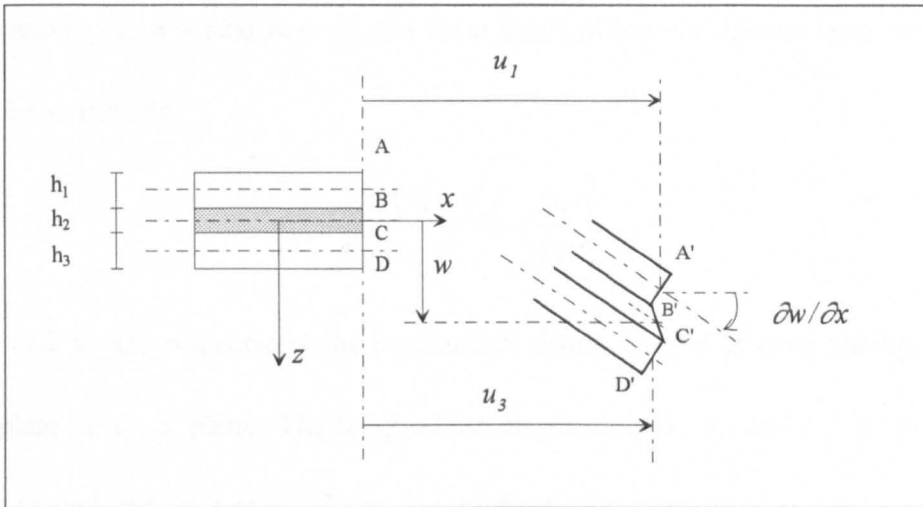


Figure A.1. Displacement of a rectangular element of the three-layer plate in  $x$ - $z$  plane

From Figure A.1, the shear strain of viscoelastic layer can be formulated as

$$\gamma_x = \frac{\partial u}{\partial z} + \frac{\partial w}{\partial x} \quad (\text{A1})$$

where

$$\frac{\partial u}{\partial z} = \frac{u_C - u_B}{h_2} \quad (\text{A2})$$

Substitute Equation (A2) into (A1) to obtain

$$\begin{aligned}
\gamma_x &= \frac{u_C - u_B}{h_2} + \frac{\partial w}{\partial x} \\
&= \frac{1}{h_2} \left[ \left( u_3 + \frac{h_3}{2} \frac{\partial w}{\partial x} \right) - \left( u_1 + \frac{h_1}{2} \frac{\partial w}{\partial x} \right) \right] + \frac{\partial w}{\partial x} \\
&= \frac{(u_3 - u_1)}{h_2} + \left[ \frac{1}{h_2} \left( \frac{h_3 + h_1}{2} \right) + 1 \right] \frac{\partial w}{\partial x} \\
\gamma_x &= \frac{d}{h_2} \left[ \frac{(u_3 - u_1)}{d} + \frac{\partial w}{\partial x} \right] \tag{A3}
\end{aligned}$$

where

$$d = h_2 + \frac{1}{2}(h_3 + h_1) \tag{A4}$$

and  $h_1, h_2$  and  $h_3$  represent the thicknesses of constraining layer, viscoelastic core and host plate respectively. In a similar manner, the shear strain of the viscoelastic layer in the  $y - z$  plane can be written as

$$\gamma_y = \frac{d}{h_2} \left[ \frac{(v_3 - v_1)}{d} + \frac{\partial w}{\partial y} \right] \tag{A5}$$

where  $v_1$  and  $v_3$  are respectively the longitudinal displacements of constraining layer and the host plate in  $y - z$  plane. The longitudinal displacements,  $u_2$  and  $v_2$ , of viscoelastic layer are formulated in terms of the longitudinal displacements,  $u_1$  and  $v_1$  of the constraining layer and,  $u_3$  and  $v_3$  of the host plate as

$$u_2 = \frac{u_B + u_C}{2} = \frac{1}{2} \left[ (u_1 + u_3) + \frac{(h_3 - h_1)}{2} \frac{\partial w}{\partial x} \right] \tag{A6}$$

and

$$v_2 = \frac{1}{2} \left[ (v_1 + v_3) + \frac{(h_3 - h_1)}{2} \frac{\partial w}{\partial y} \right] \tag{A7}$$

## A1.2 Shape functions

To formulate the plate element properties and the mass and stiffness matrices of the equations of motion, the displacement field needs to be expressed in terms of nodal displacements. Appropriate shape functions must be developed to establish this relationship.

According to Figure 3.1(b), the 4-node three-layer plate element has 7 degrees of freedom at each node, 4 longitudinal, 1 transverse and 2 rotational displacements. The longitudinal displacement field comprises of the bilinear polynomial terms that satisfy both linear displacement and compatibility condition of element boundaries (Dawe, 1984). Thus the longitudinal displacement field is expressed as

$$\begin{aligned}u_1 &= a_1 + a_2x + a_3y + a_4xy \\v_1 &= a_5 + a_6x + a_7y + a_8xy \\u_3 &= a_9 + a_{10}x + a_{11}y + a_{12}xy \\v_3 &= a_{13} + a_{14}x + a_{15}y + a_{16}xy\end{aligned}\tag{A8}$$

where  $a_1, a_2, \dots, a_{16}$  are the generalised displacements. For plate bending, the transverse displacement field extends the displacement field of a beam element which corresponds the product of two perpendicular beam displacement fields i.e., a product of cubic fields. However, there are four redundant higher terms that can be omitted from the assumed polynomial displacement field. Therefore the transverse displacement field is reduced from 16 to 12 generalised displacements and is written as

$$\begin{aligned}w &= b_1 + b_2x + b_3y + b_4x^2 + b_5xy + b_6y^2 + b_7x^3 + b_8x^2y \\&\quad + b_9xy^2 + b_{10}y^3 + b_{11}x^3y + b_{12}xy^3\end{aligned}\tag{A9}$$

where  $b_1, b_2, \dots, b_{12}$  are the generalised displacements. This transverse displacement field is for a simple rectangular element. Nevertheless, due to inter-element continuity, extra terms can be added to improve the smoothness of element boundaries (Dawe, 1984). The rotational displacement fields of  $\partial w/\partial y$  and  $\partial w/\partial x$  can be obtained by differentiating Equation (A9) respect to  $y$  and  $x$ , in order. The displacement fields of Equations (A8) and (A9) in terms of generalised displacements  $a_i$  and  $b_i$ , can be expressed in terms of nodal displacements of the rectangular plate element  $j$ ,  $\Delta_j$  in Equation (2) as

$$\left\{ u_1, v_1, u_3, v_3, w, \frac{\partial w}{\partial y}, \frac{\partial w}{\partial x} \right\}^T = \left[ \mathbf{N}_1, \mathbf{N}_2, \mathbf{N}_3, \mathbf{N}_4, \mathbf{N}_5, \mathbf{N}_{5,y}, \mathbf{N}_{5,x} \right]^T \left\{ \Delta_j \right\} \quad (\text{A10})$$

where  $\mathbf{N}_1, \mathbf{N}_2, \mathbf{N}_3, \mathbf{N}_4, \mathbf{N}_5, \mathbf{N}_{5,y}$  and  $\mathbf{N}_{5,x}$  are the shape function vectors corresponding to the displacement fields of  $u_1, v_1, u_3, v_3, w, \partial w/\partial y$  and  $\partial w/\partial x$  respectively and are the functions of point co-ordinates  $x$  and  $y$ . Formulation of shape function vectors can be found in any suitable finite element textbook, for example, Dawe (1984). Finally, displacements at any point of the plate element can be described in terms of the nodal displacements shown in Equation (A10).

### A1.3 Equations of motion

The mass and stiffness matrices in the equation of motion for element  $j$  can be written as a linear combination of the characteristics in each layer. These combinations are shown below

$$\mathbf{M}_j = \left( \mathbf{M}_{bc} + \mathbf{M}_{pc} \right) + \left( \mathbf{M}_{bv} + \mathbf{M}_{pv} \right) + \left( \mathbf{M}_{bp} + \mathbf{M}_{pp} \right) \quad (\text{A11})$$

$$\mathbf{K}_j = (\mathbf{K}_{bc} + \mathbf{K}_{pc}) + (\mathbf{K}_{bv} + \mathbf{K}_{sv} + \mathbf{K}_{pv}) + (\mathbf{K}_{bp} + \mathbf{K}_{pp}) \quad (\text{A12})$$

where the first subscripts,  $b$ ,  $s$  and  $p$  stand for bending, shear and in-plane motion respectively and the second subscripts,  $c$ ,  $v$  and  $p$  stand for the constraining layer, the viscoelastic layer and the host plate respectively.

Stiffness matrices in Equation (A12) are derived from the strain energy by which the strains (pseudo strains) used for computing of all the layers are listed in the same sequential order of Equation (A12) as in the following expression:

$$\{\chi\} = \left[ \left\{ \left( -\frac{\partial^2 w}{\partial x^2}, -\frac{\partial^2 w}{\partial y^2}, \frac{2\partial^2 w}{\partial x \partial y} \right)_b, \left( \frac{\partial u_1}{\partial x}, \frac{\partial v_1}{\partial y}, \frac{\partial u_1}{\partial y} + \frac{\partial v_1}{\partial x} \right)_p \right\}_c, \right. \\ \left. \left\{ \left( -\frac{\partial^2 w}{\partial x^2}, -\frac{\partial^2 w}{\partial y^2}, \frac{2\partial^2 w}{\partial x \partial y} \right)_b, (\gamma_x, \gamma_y)_s, \left( \frac{\partial u_2}{\partial x}, \frac{\partial v_2}{\partial y}, \frac{\partial u_2}{\partial y} + \frac{\partial v_2}{\partial x} \right)_p \right\}_v, \right. \\ \left. \left\{ \left( -\frac{\partial^2 w}{\partial x^2}, -\frac{\partial^2 w}{\partial y^2}, \frac{2\partial^2 w}{\partial x \partial y} \right)_b, \left( \frac{\partial u_3}{\partial x}, \frac{\partial v_3}{\partial y}, \frac{\partial u_3}{\partial y} + \frac{\partial v_3}{\partial x} \right)_p \right\}_p \right] \quad (\text{A13})$$

The components of the mass and stiffness matrices in Equations (A11) and (A12) can be obtained from

$$\mathbf{K} = \int_{-b-a}^b \int_a^a \mathbf{B}^T \mathbf{D} \mathbf{B} dx dy \quad (\text{A14}) \\ \mathbf{M} = \int_{-b-a}^b \int_a^a \mathbf{N}^T \mathbf{P} \mathbf{N} dx dy$$

where  $\mathbf{B}$  is the pseudo strain matrix related to Equation (A13),  $\mathbf{N}$  is the shape function matrix of displacements,  $\mathbf{D}$  is the stiffness property matrix and  $\mathbf{P}$  is the mass density matrix. More details of the formulation can be found in works by Baz and Ro (1996) and Khatua and Cheung (1973).

## **A2 Verification using Warburton's method**

The natural frequencies of a bare plate obtained from finite element predictions are compared with those of Warburton's analytical solution. Warburton's solutions of plate vibrations are derived from the Rayleigh method by applying appropriate characteristic beam functions in  $x$  and  $y$  directions of a plate in which these functions satisfy exactly the boundary conditions for fixed and simply supported edges, but are only approximate for free edges. As a result the method predicts higher natural frequencies than true values. The reason for this is that the assumption of an incorrect wave equation is equivalent to the introduction of constraints to the free edges (Warburton, 1954). After refining mesh size, natural frequencies of higher modes from the finite element method are tended to be lower values than Warburton's solutions. All mode shape in Figure A.2 is from calculations of the plate model with  $9 \times 6$  mesh size. However, these mode shape configurations are the same as mesh size  $8 \times 4$ ,  $16 \times 8$  and  $32 \times 16$ . This means that the number of elements is enough to obtain the correct natural frequencies, predicting up to ten modes of the plate vibrations.

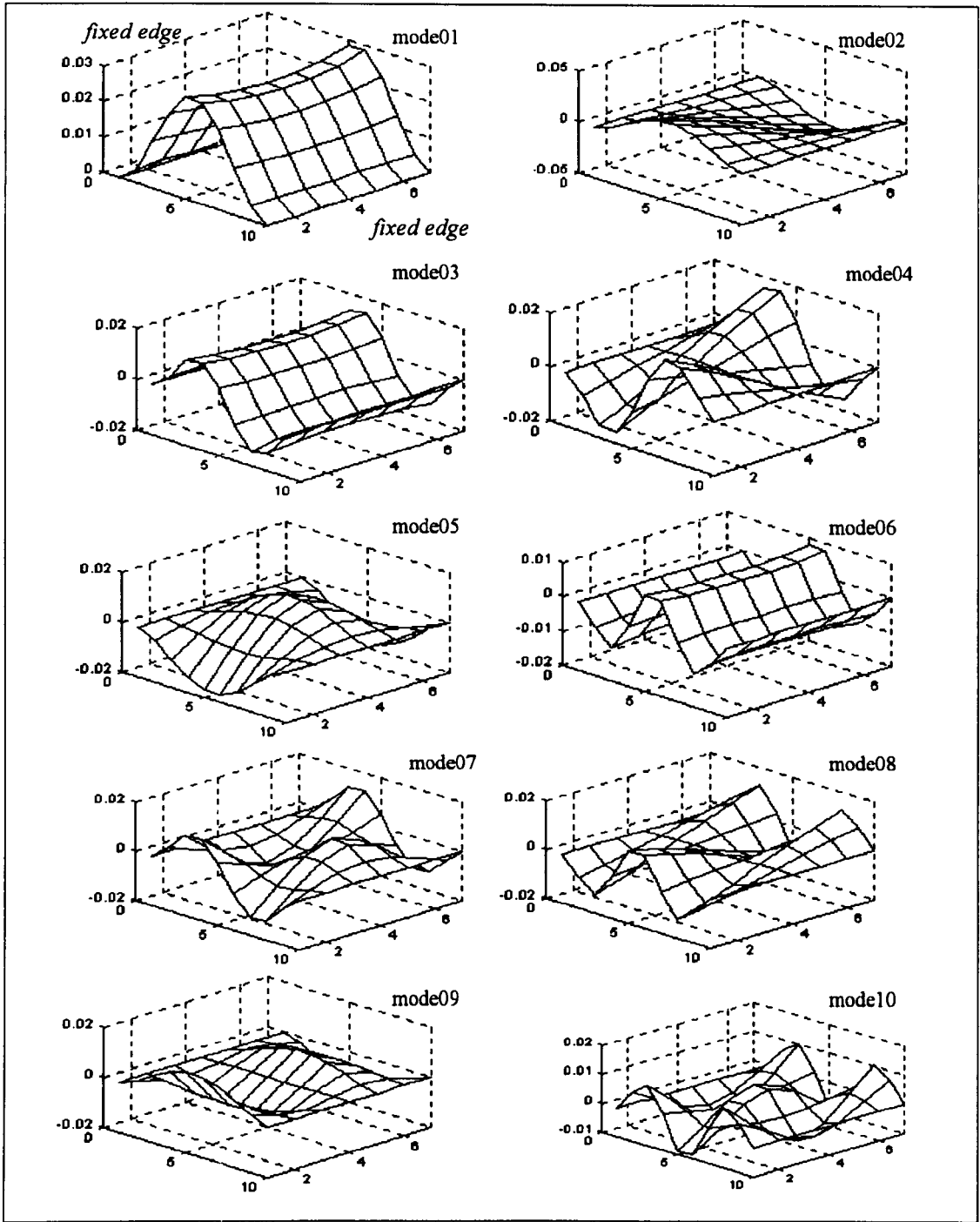


**Figure A.2.** The first ten mode shapes of 9x6 mesh size panel plate corresponding to their natural frequencies

# APPENDIX B

## SYSTEM IDENTIFICATION

### B1 Peak picking method

The following procedures are necessary in order to extract the natural frequency  $\bar{\omega}$  and the damping factor  $\zeta$  from structures using measured frequency response functions.

1. The frequency response function (FRF), consists of an output response divided by an input stimulus. At each mode, the frequency at a maximum peak is considered as the resonant frequency (see Figure B.1(a)) and approximates to the natural frequency.
2. If the FRF is a velocity output response divided by a force stimulus, the so-called mobility function  $\alpha(i\omega)$ , then the damping factor  $\zeta$  can be estimated from

$$\zeta = \frac{(\omega_2 - \omega_1)}{2\bar{\omega}} \quad (\text{B1})$$

where  $\omega_2$  and  $\omega_1$  are frequencies at the half-power points for which  $\omega_2$  is located to the right of the natural frequency and corresponds to the calculated amplitude of the maximum magnitude of the FRF at the mode divided by  $\sqrt{2}$  or  $|\alpha(i\bar{\omega})|/\sqrt{2}$ . A similar definition is applied for  $\omega_1$  but located at the left of the natural frequency (see Figure B.1(b)). The structural damping or loss factor  $\eta$  is related to the damping factor  $\zeta$  by (Ungar, 1971)

$$\eta = 2\zeta. \quad (\text{B2})$$

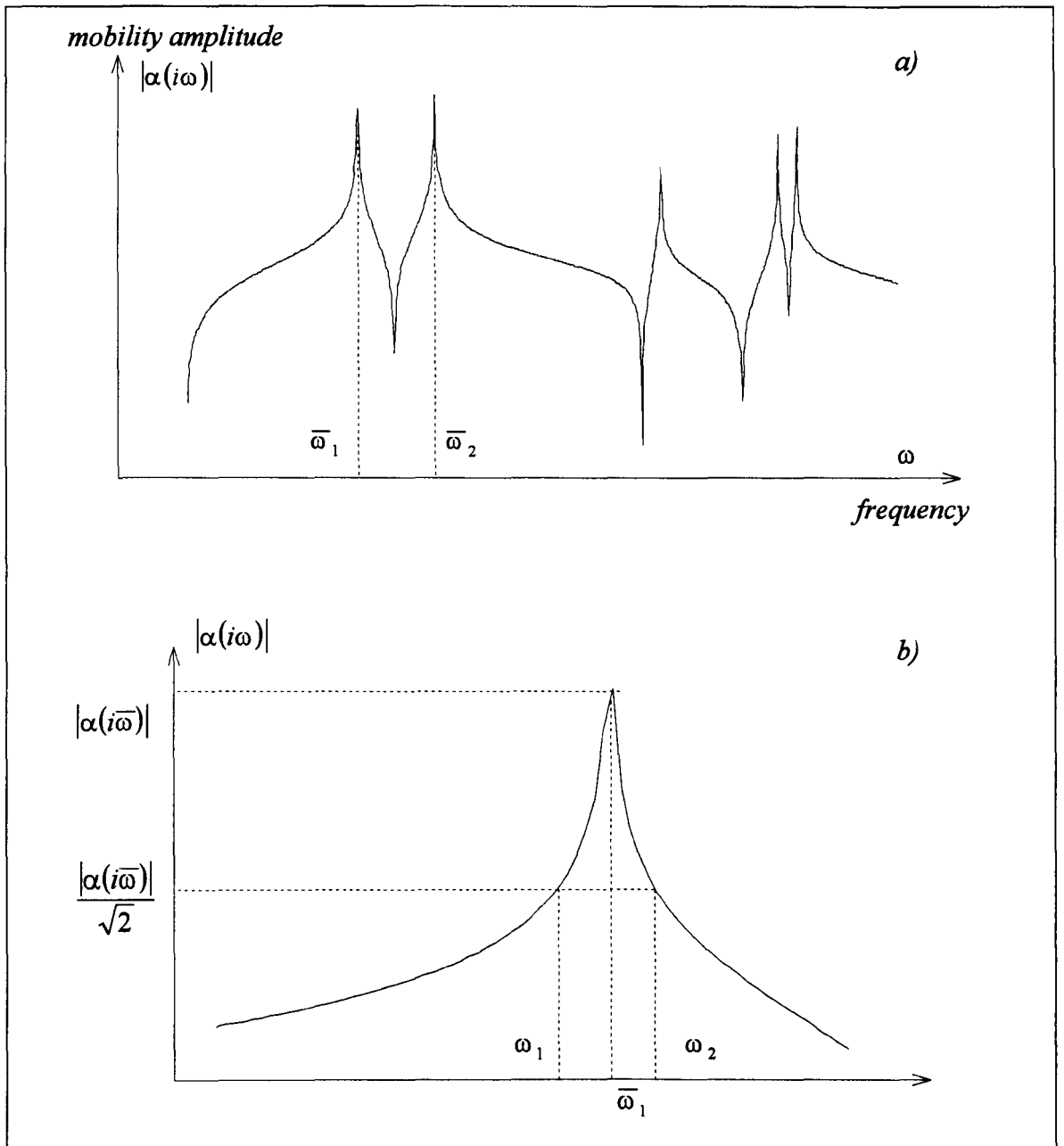


**Figure B.1.** Illustration of peak picking method  
a) location of natural frequencies  
b) definition of half-power points

## B2 Model updating

Recall from Equations (3.9) and (3.12) that

$$\dot{\mathbf{Y}} = \mathbf{A}\mathbf{Y} + \mathbf{B}\mathbf{u} \quad (\text{B3})$$

and

$$\mathbf{u} = \mathbf{G}\mathbf{C}\mathbf{Y} \quad (\text{B4})$$

or in state-space form

$$\begin{Bmatrix} \ddot{\Delta} \\ \dot{\Delta} \end{Bmatrix} = \begin{bmatrix} -\mathbf{M}^{-1}\mathbf{D} & -\mathbf{M}^{-1}\mathbf{K} \\ \mathbf{I} & \mathbf{0} \end{bmatrix} \begin{Bmatrix} \dot{\Delta} \\ \Delta \end{Bmatrix} + \begin{bmatrix} \mathbf{B}_0 \\ \mathbf{0} \end{bmatrix} \mathbf{GC} \begin{Bmatrix} \dot{\Delta} \\ \Delta \end{Bmatrix}$$

or

$$\begin{Bmatrix} \ddot{\Delta} \\ \dot{\Delta} \end{Bmatrix} = \begin{bmatrix} -\mathbf{M}^{-1}\mathbf{D} & -\mathbf{M}^{-1}\mathbf{K} \\ \mathbf{I} & \mathbf{0} \end{bmatrix} \begin{Bmatrix} \dot{\Delta} \\ \Delta \end{Bmatrix} + \begin{bmatrix} \Delta\mathbf{A}_1 & \Delta\mathbf{A}_2 \\ \mathbf{0} & \mathbf{0} \end{bmatrix} \begin{Bmatrix} \dot{\Delta} \\ \Delta \end{Bmatrix} \quad (\text{B5})$$

where  $\Delta\mathbf{A}_1$  and  $\Delta\mathbf{A}_2$  are the  $n \times n$  mass-normalised correction matrices of damping and stiffness, respectively. Define  $\mathbf{A}_1 = -\mathbf{M}^{-1}\mathbf{D} + \Delta\mathbf{A}_1$  and  $\mathbf{A}_2 = -\mathbf{M}^{-1}\mathbf{K} + \Delta\mathbf{A}_2$  and then the updated damping and stiffness matrices can be obtained from

$$\begin{aligned} \mathbf{D}_{new} &= -\mathbf{MA}_1 \\ \mathbf{K}_{new} &= -\mathbf{MA}_2 \end{aligned} \quad (\text{B6})$$

where  $\mathbf{D}_{new}$  and  $\mathbf{K}_{new}$  are the updated damping and stiffness matrices, respectively. The matrix  $\mathbf{B}_0$  is chosen to be an  $n \times n$  identity matrix  $\mathbf{I}_n$  to provide a controllable system (Inman and Minas, 1990). The characteristic of the plant matrix  $\mathbf{A}$  can be changed if the measurement matrix  $\mathbf{C}$  is chosen to correspond to the  $m$  row eigenvectors of the matrix  $\mathbf{A}^T$  or

$$\mathbf{C} = \begin{bmatrix} \mathbf{v}_1^T \\ \mathbf{v}_1^* \\ \mathbf{v}_2^T \\ \mathbf{v}_2^* \\ \vdots \\ \mathbf{v}_m^T \\ \mathbf{v}_m^* \end{bmatrix}_{2m \times 2n} \quad (\text{B7})$$

where  $\mathbf{v}_i$  is the eigenvector of any mode  $i$  which need to be updated and  $*$  denotes the complex conjugate transpose. The changes in the updated eigenvalues depend on the

appropriate choice of the gain matrix  $\mathbf{G}$ . The entries of the matrix  $\mathbf{G}$  are given by Porter and Crossley (1972):

$$G_{ki} = P_{ik} (\rho_i - \lambda_i) / \sum_{k=1}^n (P_{ik})^2 \quad (k = 1, 2, \dots, n; i = 1, 2, \dots, 2m) \quad (\text{B8})$$

where the mode-controllability element  $P_{ik}$  is the product of eigenvector  $\mathbf{v}_i^T$  and the column  $k$  of matrix  $\mathbf{B}$ ,  $\rho_i$  is the desired eigenvalue of mode  $i$  and  $\lambda_i$  is the original eigenvalue of mode  $i$ . This algorithm is developed for single mode control with gain minimisation. There is no change to non-updated modes in this original development. However, for multi-mode updating, this algorithm can be applied but updated eigenvalues may not necessarily be converted to the desired values. Then the procedures must be repeated until all updated eigenvalues converge to the desired values. Unfortunately, the updated stiffness matrix  $\mathbf{K}_{new}$  and damping matrix  $\mathbf{D}_{new}$  are not guaranteed to be symmetrical and are likely to occur with complex elements in the matrices. Symmetry of the matrices is required so that the orthogonality properties of the modal model are satisfied (Ewins, 1984). These properties are required to enable decomposition of the system equations used in the modal control algorithm. To obtain the real symmetrical updated matrices, first complex terms are omitted and then the skew-matrix property is used for satisfying the symmetry condition:

$$\begin{aligned} \mathbf{D}_{sym} &= (\mathbf{D}_{new} + \mathbf{D}_{new}^T) / 2 \\ \mathbf{K}_{sym} &= (\mathbf{K}_{new} + \mathbf{K}_{new}^T) / 2 \end{aligned} \quad (\text{B9})$$

The above procedures are displayed as a block diagram in Figure B.2.

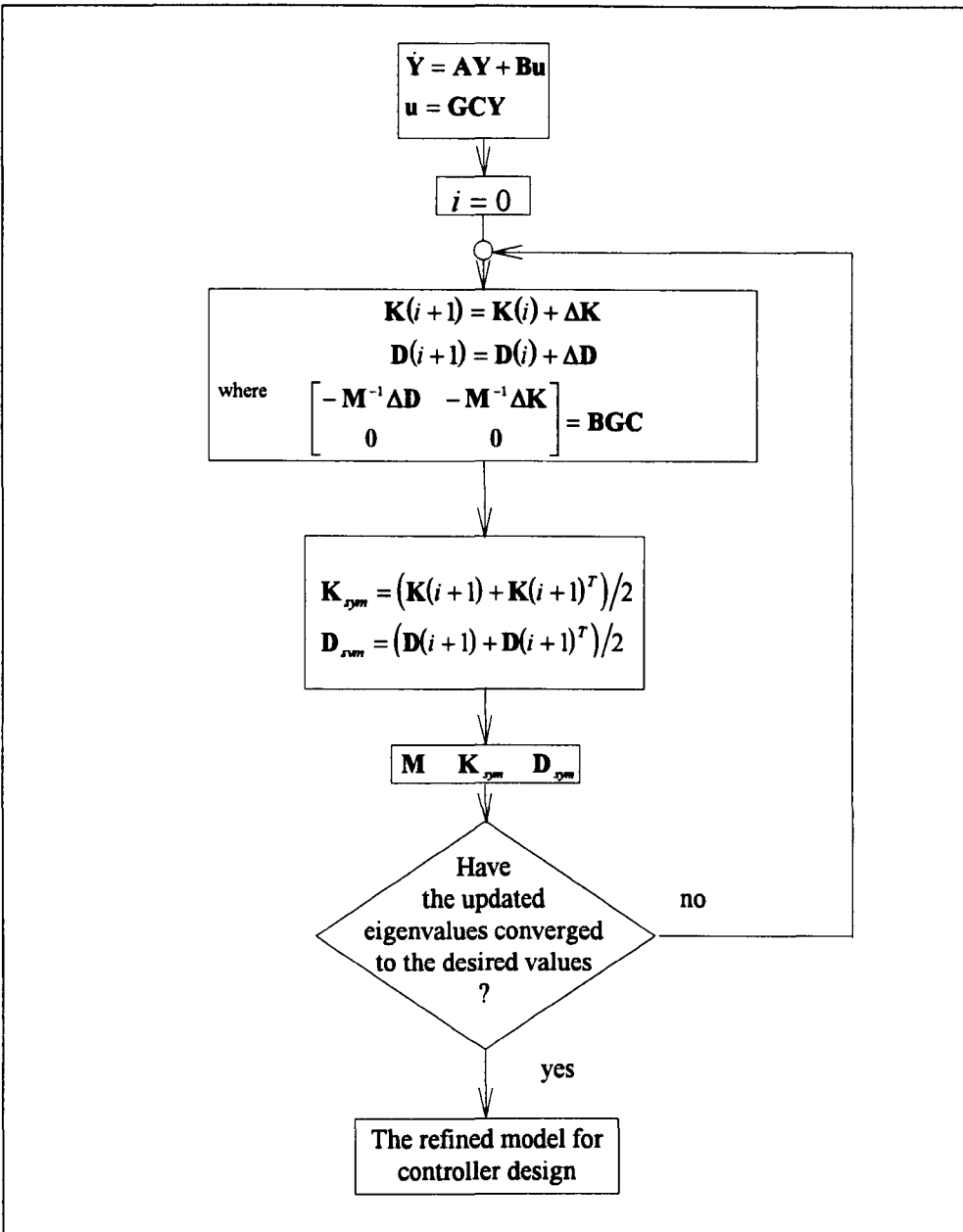


Figure B.2. Flow chart of procedures in the model updating algorithm

### B3 Transformation of structural damping matrix to viscous damping matrix

The imaginary term of the complex stiffness matrix (i.e. a complete global matrix formulated by combining a number of element matrices in Equation (3.1)) can be transformed to correspond to the viscous damping matrix where the viscous damping

coefficients are now frequency dependent. Consider the general form of equations of motion of  $n$  degrees of freedom without external forcing:

$$\mathbf{M}\ddot{\Delta} + \mathbf{D}\dot{\Delta} + \mathbf{K}\Delta = \mathbf{0} \quad (\text{B10})$$

The eigensolution of Equation (B10) is of the form

$$(\lambda_i^2 \mathbf{M} + \lambda_i \mathbf{D} + \mathbf{K})\mathbf{q}_i = \mathbf{0} \quad (\text{B11})$$

or

$$\mathbf{D}\mathbf{q}_i = -\left(1/\lambda_i\right)(\lambda_i^2 \mathbf{M} + \mathbf{K})\mathbf{q}_i \quad (\text{B12})$$

where  $\lambda_i$  is the eigenvalue representing the  $i^{\text{th}}$  mode of vibration or, mathematically

$\lambda_i = -\bar{\omega}_i \zeta_i + i\bar{\omega}_i \sqrt{1 - \zeta_i^2}$  where  $\bar{\omega}_i$  is the natural frequency and  $\zeta_i$  is the damping ratio,

and  $\mathbf{q}_i$  is the corresponding eigenvector which is obtained from the eigensolutions of Equation (3.1) given no external forcing. Note that the stiffness matrix  $\mathbf{K}$  in Equation (B12) is the same as the real term in the complex stiffness matrix of Equation (3.1).

Define  $\mathbf{p}_i = -\left(1/\lambda_i\right)(\lambda_i^2 \mathbf{M} + \mathbf{K})\mathbf{q}_i$  and then Equation (B12) can simply be expressed as

$$\mathbf{q}_i^* \mathbf{D} = \mathbf{p}_i^* \quad (\text{B13})$$

If the elements in the upper triangular portion of the  $n \times n$  damping matrix  $\mathbf{D}$  are re-arranged as a variable vector  $\mathbf{d}$ , Equation (B13) can then be rewritten as

$$\mathbf{W}\mathbf{d} = \mathbf{g} \quad (\text{B14})$$

where  $\mathbf{W}$  and  $\mathbf{g}$  are, respectively, the  $2n \times (n^2 + n)/2$  re-arranged matrix with, as entries, the real and imaginary elements of  $\mathbf{q}_i^*$  and the  $2n \times 1$  re-arranged vector of real and imaginary elements of  $\mathbf{p}_i^*$  (Minas and Inman, 1991). To solve for the vector  $\mathbf{d}$ , the terms  $\lambda_i$  and  $\mathbf{q}_i$  are eigensolutions identified from the plate equation of motion using complex stiffness notation. From Equation (B14), the determination of the vector  $\mathbf{d}$  is necessary to formulate

the matrix  $\mathbf{W}$  to be a square matrix of  $(n^2+n)/2$  orders so that the inverse of the matrix  $\mathbf{W}$  is available. A number of modes  $i=1, m$  where  $m$  is less than  $n$  is used to construct the square matrix  $\mathbf{W}$  and the corresponding vector  $\mathbf{g}$ . However; the eigensolutions in the state-space form of Equation (B10) may not occur in complex conjugate pairs. To ensure consistency over all modes, an over-determined system of linear equations must be solved. The size of the matrix  $\mathbf{W}$  comprising vectors  $\mathbf{q}_i^*$ ,  $i=1, n$  is  $2n^2 \times (n^2+n)/2$ . The pseudo inverse technique is used to solve Equation (B14) so that

$$\mathbf{d} = (\mathbf{W}^T \mathbf{W})^{-1} \mathbf{W}^T \mathbf{g}. \quad (\text{B15})$$

#### B4 Guyan reduction

Consider equations of motion of a series of mass-spring systems:

$$\mathbf{M}\ddot{\Delta} + \mathbf{K}\Delta = \mathbf{f}. \quad (\text{B16})$$

Let

$$\Delta = \begin{Bmatrix} \Delta_1 \\ \Delta_2 \end{Bmatrix} \quad (\text{B17})$$

where  $\Delta_1$  and  $\Delta_2$  are sub-vectors of the displacement vector  $\Delta$ . Then Equation (B16) is partitioned as

$$\begin{bmatrix} \mathbf{M}_{11} & \mathbf{M}_{12} \\ \mathbf{M}_{21} & \mathbf{M}_{22} \end{bmatrix} \begin{Bmatrix} \ddot{\Delta}_1 \\ \ddot{\Delta}_2 \end{Bmatrix} + \begin{bmatrix} \mathbf{K}_{11} & \mathbf{K}_{12} \\ \mathbf{K}_{21} & \mathbf{K}_{22} \end{bmatrix} \begin{Bmatrix} \Delta_1 \\ \Delta_2 \end{Bmatrix} = \begin{Bmatrix} \mathbf{f}_1 \\ \mathbf{f}_2 \end{Bmatrix}. \quad (\text{B18})$$

If sub-vector  $\Delta_2$  is to be eliminated or considered as the sub-vector of displacements with least strain energy, then regardless of kinetic energy, the force  $\mathbf{f}_2$  is considered to be zero.

Then the second set of Equation (B18) without the inertia terms can be written as

$$\mathbf{K}_{21}\Delta_1 + \mathbf{K}_{22}\Delta_2 = \mathbf{0} \quad (\text{B19})$$

thus

$$\Delta_2 = -\mathbf{K}_{22}^{-1}\mathbf{K}_{21}\Delta_1 \quad (\text{B20})$$

From this relationship in Equation (B20), a co-ordinate transformation of full co-ordinates  $\Delta$  to reduced co-ordinates  $\Delta_1$  or  $\Delta = \mathbf{T}\Delta_1$ , can be defined as

$$\mathbf{T} = \begin{bmatrix} \mathbf{I} \\ -\mathbf{K}_{22}^{-1}\mathbf{K}_{21} \end{bmatrix} \quad (\text{B21})$$

This co-ordinate transformation is called static transformation owing to ignorance of the inertia terms (Friswell and Mottershead, 1995). If we insert this co-ordinate transformation into Equation (B18) and pre-multiply by  $\mathbf{T}^T$ , the reduced-variable equations of motion are

$$\mathbf{T}^T\mathbf{M}\mathbf{T}\ddot{\Delta}_1 + \mathbf{T}^T\mathbf{K}\mathbf{T}\Delta_1 = \mathbf{T}^T \begin{Bmatrix} \mathbf{f}_1 \\ \mathbf{f}_2 \end{Bmatrix} \quad (\text{B22})$$

where the reduced stiffness matrix is

$$\mathbf{K}^R = \mathbf{T}^T\mathbf{K}\mathbf{T} = (\mathbf{K}_{11} - \mathbf{K}_{12}\mathbf{K}_{22}^{-1}\mathbf{K}_{21}) \quad (\text{B23})$$

and the reduced mass matrix is

$$\mathbf{M}^R = \mathbf{T}^T\mathbf{M}\mathbf{T} = \mathbf{M}_{11} - \mathbf{K}_{12}\mathbf{K}_{22}^{-1}\mathbf{M}_{21} - \mathbf{M}_{12}\mathbf{K}_{22}^{-1}\mathbf{K}_{21} + \mathbf{K}_{12}\mathbf{K}_{22}^{-1}\mathbf{M}_{22}\mathbf{K}_{22}^{-1}\mathbf{K}_{21}. \quad (\text{B24})$$

# APPENDIX C

## MODAL CONTROL

### C1 Modal control

#### C1.1 Pole placement

Recall from Equation (3.16), the single-input modal control system:

$$\dot{\xi} = \Lambda\xi + \mathbf{w}f(t) \quad (\text{C1})$$

The scalar input  $f(t)$  can be chosen to shift  $m$  eigenvalues ( $m \leq r$ ) by state-variable feedback as shown by Porter and Crossley (1972):

$$f(t) = \sum_{i=1}^m k_i \mathbf{v}_i^T \mathbf{Y} \quad (\text{C2})$$

or

$$\begin{aligned} f(t) &= \left( \sum_{i=1}^m k_i \mathbf{v}_i^T \mathbf{U} \right) \xi \\ &= \mathbf{k}_c^T \xi \end{aligned} \quad (\text{C3})$$

where  $k_i$  is the control gain and  $\mathbf{v}_i$  is the eigenvector of  $\mathbf{A}^T$ . The gain  $k_i$  can be obtained from the following algorithm

$$k_i = \frac{\prod_{k=1}^m (\rho_k - \lambda_i)}{\left( w_i \prod_{\substack{k \neq i \\ k=1}}^m (\lambda_k - \lambda_i) \right)} \quad i = 1, 2, \dots, m \quad (\text{C4})$$

where  $\lambda_{i,k}$  is an original eigenvalue of  $\mathbf{A}$ ,  $\rho_k$  is a desired eigenvalue and  $w_i$  is the  $i$ th element of  $\mathbf{w} = \mathbf{U}^{-1}\mathbf{b}$ .

In summary, any mode of vibration can be controlled by choosing the desired eigenvalue  $\rho_k$  so that the output response converges to the steady state in a finite time. However, if the desired value is too far from the original pole, it means that the control force needs a high gain in order to achieve this result. The high gain force can lead to saturation of an actuator and thus cause the system to behave in non-linear fashion.

### C1.2 State estimator

Every state variable in Equation (C3) cannot usually be obtained directly due to difficulties in measurement and limitations on the number of sensors. Thus state estimation is required in order to reconstruct indirectly all state variables from the output signal.

Given a vector of observation  $\mathbf{z}_{k \times 1}$ , where  $l$  is the number of available measurements, the relationship of this vector in the form of physical co-ordinates  $\mathbf{Y}_{2 \times r \times 1}$  is

$$\mathbf{z} = \mathbf{L}\mathbf{Y} \quad (\text{C5})$$

where  $\mathbf{L}_{k \times 2r}$  is the output matrix. In modal co-ordinates, Equation (C5) is written as

$$\mathbf{z} = \mathbf{L}\mathbf{U}\boldsymbol{\xi} = \begin{bmatrix} \mathbf{H}_c^T & \mathbf{H}_u^T \end{bmatrix} \begin{Bmatrix} \boldsymbol{\xi}_c \\ \boldsymbol{\xi}_u \end{Bmatrix} \quad (\text{C6})$$

where the size of  $\mathbf{H}_c$  and  $\mathbf{H}_u$  is  $c \times 1$  and  $u \times 1$  respectively. At this stage, observability of state variables can be checked by forming a matrix  $\mathfrak{O}_{2 \times r \times l} = \mathbf{U}^T \mathbf{L}^T$ . Using an estimator, a set of  $c$  controlled mode equations can be formulated as

$$\hat{\boldsymbol{\xi}}_c = (\boldsymbol{\Lambda}_c + \mathbf{w}_c \mathbf{k}_c^T) \hat{\boldsymbol{\xi}}_c + \boldsymbol{\Phi}(\mathbf{z} - \mathbf{h}(\hat{\boldsymbol{\xi}}_c, t)) \quad (\text{C7})$$

where  $\hat{\xi}_c$  is the estimated vector of  $\xi_c$ ,  $\mathbf{k}_c^T$  is control gain in the form of Equation (C3),  $\mathbf{h}(\hat{\xi}_c, t) = \mathbf{H}_c^T \hat{\xi}_c$  is the estimated vector of  $\mathbf{z}$ , and  $\Phi_{\text{est}}$  is a weighting matrix. There are several methods to obtain the weighting matrix, for example Ackermann's formula and Kalman's Linear Filter (Franklin et al, 1998).

## C2 The effects of truncated models with the state estimator

In order to study the effect of residual modes in a closed-loop system, Equations (3.17), (3.18) and an error equation  $\mathbf{e} = \hat{\xi}_c - \xi_c$  is rearranged as

$$\begin{Bmatrix} \dot{\xi}_c \\ \dot{\mathbf{e}} \\ \dot{\xi}_u \end{Bmatrix} = \left[ \begin{array}{cc|c} (\Lambda_c + \mathbf{w}_c \mathbf{k}_c^T) & \mathbf{w}_c \mathbf{k}_c^T & \mathbf{0} \\ \mathbf{0} & (\Lambda_c - \Phi \mathbf{H}_c^T) & \Phi \mathbf{H}_u^T \\ \mathbf{w}_u \mathbf{k}_c^T & \mathbf{w}_u \mathbf{k}_c^T & \Lambda_u \end{array} \right] \begin{Bmatrix} \xi_c \\ \mathbf{e} \\ \xi_u \end{Bmatrix} \quad (\text{C8})$$

or simply written as

$$\begin{Bmatrix} \dot{\mathbf{R}}_c \\ \dot{\xi}_u \end{Bmatrix} = \begin{bmatrix} \mathbf{H}_{11\text{cxc}} & \mathbf{H}_{12\text{cxu}} \\ \mathbf{H}_{21\text{uxc}} & \mathbf{H}_{22\text{uxu}} \end{bmatrix} \begin{Bmatrix} \mathbf{R}_c \\ \xi_u \end{Bmatrix} \quad (\text{C9})$$

where  $\mathbf{R}_c$  is the reduced order co-ordinate system.

Balas (1978) divided the effects of the residual modes into control and observation spillovers. Observation spillover is the measured signal contaminated by the uncontrolled modes. In the same way, control spillover is the feedback signal that excites the uncontrolled modes. To see the effect of control spillover, it is assumed that there is no residual estimation term (i.e.  $\mathbf{H}_u^T$  or  $\mathbf{H}_{12}$  equal zero). The eigenvalues of Equation (C8) then is given by  $(\Lambda_c + \mathbf{w}_c \mathbf{k}_c^T)$ ,  $(\Lambda_c - \Phi \mathbf{H}_c^T)$  and  $\Lambda_u$ . This means that the residual modes are excited at their natural frequencies by the control force  $f(t) = \mathbf{w}_u \mathbf{k}_c^T \mathbf{R}_c$  (see

Figure 3.6). In the presence of observation spillover, the eigenvalues of Equation (C8) are continuous functions of the parameters in  $\mathbf{H}_u^T$  which have the poles of  $(\Lambda_c + \mathbf{w}_c \mathbf{k}_c^T)$ ,  $(\Lambda_c - \Phi \mathbf{H}_c^T)$  and  $\Lambda_u$  (Balas, 1978). The original poles disturbed by the parameters could cause instabilities in the system because the poles of the residual modes may have little or no stability margin in lightly damped structures.

## **APPENDIX D**

**COPY OF A PAPER SUBMITTED TO  
JOURNAL OF SOUND AND VIBRATION**

TITLE:  
ACTIVE CONSTRAINED LAYER DAMPING OF  
CLAMPED-CLAMPED PLATE VIBRATIONS  
(*Revised manuscript*)

AUTHORS:  
C. CHANTALAKHANA AND R. STANWAY\*

ADDRESS:  
*Department of Mechanical Engineering, University of Sheffield, Mappin Street  
Sheffield S1 3JD, United Kingdom*

THIS PAPER CONTAINS 36 PAGES, 4 TABLES AND 20 FIGURES.

SUMMARY

Surface damping treatments are often effective at suppressing higher frequency vibrations in thin-walled structures such as beams, plates and shells. However the effective suppression of lower frequency modes usually requires the addition of an active vibration control scheme to augment the passive treatment. Advances in the technologies associated with so-called smart materials are dramatically reducing the cost, weight and complexity of active structural control and make it feasible to consider active schemes in an increasing number of applications.

In this paper the authors present a numerical and experimental study of the application of active constrained layer damping to a clamped-clamped plate. Specifically, a passive constrained viscoelastic damping layer is augmented with an active scheme employing a PZT patch as the actuator. In the opening sections of the paper, emphasis is placed upon establishing a suitable model of the plate. Starting with an established finite element formulation it is shown how model updating and model reduction are required to produce a low-order state-space model which can be used as the basis for active control. The effectiveness of the formulation is then demonstrated in a numerical study. Finally, in the description of the experimental study, it is shown how modes in the frequency range from 0 to 600 Hz are effectively suppressed: the two lowest modes (bending and torsional) through active control using only a single sensor and single actuator in the feedback loop, the higher modes (around ten in number) by the constrained passive damping layer. The paper's original contribution lies in the experimental demonstration that given a sufficiently accurate model of the plate and passive constrained damping layer, together with a suitable active feedback control algorithm, spillover effects are not significant even when using a single sensor and single actuator. The experimental traces show, in some instances, minor effects due to spillover. However, it can be concluded that the presence of the passive layer introduces sufficient damping into the residual modes to avoid any major problems when using only the minimum amount of active control hardware.

---

\* Author to whom correspondence should be addressed.

## 1. INTRODUCTION

The application of active control techniques to suppress vibrations in flexible structures poses some special problems. These problems arise primarily from the distributed nature of such structures and the resulting large number of degrees of freedom which are required in a mathematical model to account for observed behaviour. If a lumped parameter model is derived then this generally needs to be reduced in order prior to controller design. Balas [1] investigated the so-called spillover effects which result from ignoring higher order modes when implementing active feedback control. It was shown that spillover effects are liable to degrade or even de-stabilise the response of the closed-loop system. Various techniques for reducing the influence of spillover effects have been proposed. One effective technique in which modal transformations were employed so as to control each mode independently was described by Meirovitch and his colleagues [2]. It was demonstrated that no spillover occurs if the number of actuators is equal to the order of the lumped parameter model and the number of sensors is capable of identifying all of the controlled modes. Furthermore the performance of so-called independent modal-space control (IMSC) was shown to be superior in almost every respect to techniques which seek to exploit the coupling in a flexible structure in order to minimise the number of actuators and sensors. Unfortunately the hardware requirements for the independent control of modes can be daunting and alternative techniques have been investigated with the aim of reducing spillover effects whilst also reducing the number of actuators and sensors.

Early attempts at achieving these joint aims almost invariably involved experiments using various cantilevered beams with piezoelectric elements to implement the control. Bailey and Hubbard [3] overcame spillover effects by employing a distributed parameter

control algorithm. A drawback with this method concerned the need to provide a measurement of the angular velocity of the beam's tip. Since such a measurement was not available the experiments were limited to control of the fundamental mode. An alternative approach was proposed by Fanson and Caughey [4]. These authors described experiments to control the first six bending modes of a cantilevered beam using so-called positive position feedback (PPF). It was shown that using PPF the effect of spillover is to stabilise rather than de-stabilise the closed-loop system. In a further example involving a cantilevered beam, Baz and his colleagues [5] showed how the attributes of IMSC and PPF could be combined to provide effective real-time control of structural vibrations using a smaller number of actuators.

In the early 1990s, reports began to appear of an alternative approach to controlling structural vibrations: using active techniques to augment the damping provided by a passive constrained layer added to the host structure. It had long been recognised that passive constrained layer damping is most effective at suppressing vibrations of the higher frequency modes. Using a hybrid approach, it appeared feasible to use active control to suppress the lower modes while the passive layer would reduce spillover from the higher frequency modes. Baz and Ro [6] demonstrated the feasibility of this concept using the ubiquitous cantilevered beam but soon progressed to more complex structures such as plates and shells. Using a cantilevered plate, partially treated with an active constrained damping layer, Baz and Ro [7] showed how the bending mode could be controlled effectively using a simple proportional control arrangement. A comparison of active, passive and hybrid (i.e. active constrained layer damping treatments) appeared in the study by Veley and Rao [8]. A cantilevered beam and also a plate clamped on all four sides were used as host structures to examine and compare active, passive and hybrid control

strategies. The design objectives were to minimise the weight of the structures and also to achieve high levels of damping. The results showed that the hybrid approach is superior to the active control of an untreated plate in that a given damping ratio can be achieved using less than half the mass.

The present study is concerned with a clamped-clamped aluminium plate which was first investigated by Azvine and his colleagues [9]. This plate is a simplified version of an instrument box cover found in a military aircraft. Azvine's brief was to investigate active constrained layer damping treatments as a means of suppressing bending and torsional vibrations which were causing the instrument box to malfunction in service. Negative velocity feedback was used along with non-collocated sensors and actuators in an attempt to control the first two modes of vibration. Using two actuators, the benefits of the constraining layer were clearly demonstrated: higher feedback gains could be used to give lower resonant peaks without causing instability. However, this study indicated the need for better models of the host plate, the passive constraining layer and the piezoelectric actuators together with a more effective control algorithm based upon this model. At the same time, it was essential for the eventual application that the amount of hardware be minimised. Consequently, in the present investigation, it was decided to investigate whether effective control could be achieved using only a single actuator and single sensor.

In what follows here, the authors describe this novel approach to controlling both the bending and torsional vibrations of the clamped-clamped plate. Initially, the technique of Baz and Ro [7] is extended to produce a finite element model of the plate together with the passive constraining layer. Using system identification techniques, the model is validated using data from the test facility. Model reduction and model updating are then

applied to produce a compact model which is capable of accounting for observed behaviour. Following a comprehensive numerical study, active constrained layer damping treatments is implemented experimentally and a comprehensive set of test results is presented.

## 2. FINITE ELEMENT MODELLING

### 2.1 STRATEGY

The strategy adopted by the authors is to develop a model-based approach to the investigation of active constrained layer damping of a clamped-clamped plate. Modelling of the plate and its passive damping treatment is conveniently performed using finite element analysis in order to determine the equations of motion in terms of mass, damping and stiffness matrices. Active control is more conveniently formulated in state-space notation which requires transformation of the finite element model [10]. This transformation is straightforward in principle but can be difficult in practice. The choice of model order is crucial if observed behaviour is to be accounted for without requiring excessive matrix dimensions. To obtain an acceptable compromise, formal model reduction techniques [11] will be used here. Also, it has been found necessary to use model updating algorithms [12] in order to obtain sufficiently close correspondence between model predictions and observed behaviour.

### 2.2 MATHEMATICAL MODEL

The system under consideration involves the host plate to which is added a viscous elastic layer and a further metallic constraining layer. The modelling technique follows Khuata and Cheung [13] and Baz and Ro [7]. Rectangular plate elements are used as shown in

Figure 1. The co-ordinate system is illustrated in Figure 1(a) and the displacements in Figure 1(b). The analysis of the host plate and the metallic constraining layer employs the assumptions of thin plate theory that can be found in any suitable textbook on fundamental plate theory or finite element analysis, for example, Dawe [14]. In addition, it is assumed that the plane section of the viscoelastic layer remains in plane after deformation, and that there is no shear strain in the constraining layer and host plate. At each node  $k$  of element  $j$ , there are 7 degrees of freedom, 4 longitudinal, 1 transverse and 2 rotational displacements. These displacements can be gathered together to form a vector:

$$\Delta_j = \left\{ u_{1k}, v_{1k}, u_{3k}, v_{3k}, w_k, \frac{\partial w}{\partial y_k}, \frac{\partial w}{\partial x_k} \right\}^T \quad k = 1,2,3,4 \quad (1)$$

where  $v_{1k}$  and  $v_{3k}$  are longitudinal displacements of the constraining layer and base plate, respectively, in the  $y$ - $z$  plane. Given this displacement vector, the equation of motion is formed as

$$\mathbf{M}_j \ddot{\Delta}_j + \overline{\mathbf{K}}_j \Delta_j = \mathbf{F}_j \quad (2)$$

where  $\mathbf{M}_j$  and  $\overline{\mathbf{K}}_j$  are, respectively, the mass and stiffness matrices of element  $j$  and  $\mathbf{F}_j$  is an external force vector acting at the  $j$ th element. The arrays  $\mathbf{M}_j$  and  $\overline{\mathbf{K}}_j$  are formulated by the strain energy method [7,13]. The shear modulus of the viscoelastic damping material is given by  $G(1+i\eta)$  where  $G$  is the shear modulus and  $\eta$  is the loss factor which is frequency dependent. Consequently,  $\overline{\mathbf{K}}$  is a complex stiffness matrix whose imaginary part serves as a loss energy or damping term. Full details (including experimental validation) of this finite element plate model are given in reference [15].

### 3. PASSIVE CONTROL OF PLATE VIBRATIONS

The plate used originates from a vibration control problem described by Azvine and his colleagues [9]. In the present investigation, the original panel is modelled as a plate clamped along opposite edges.

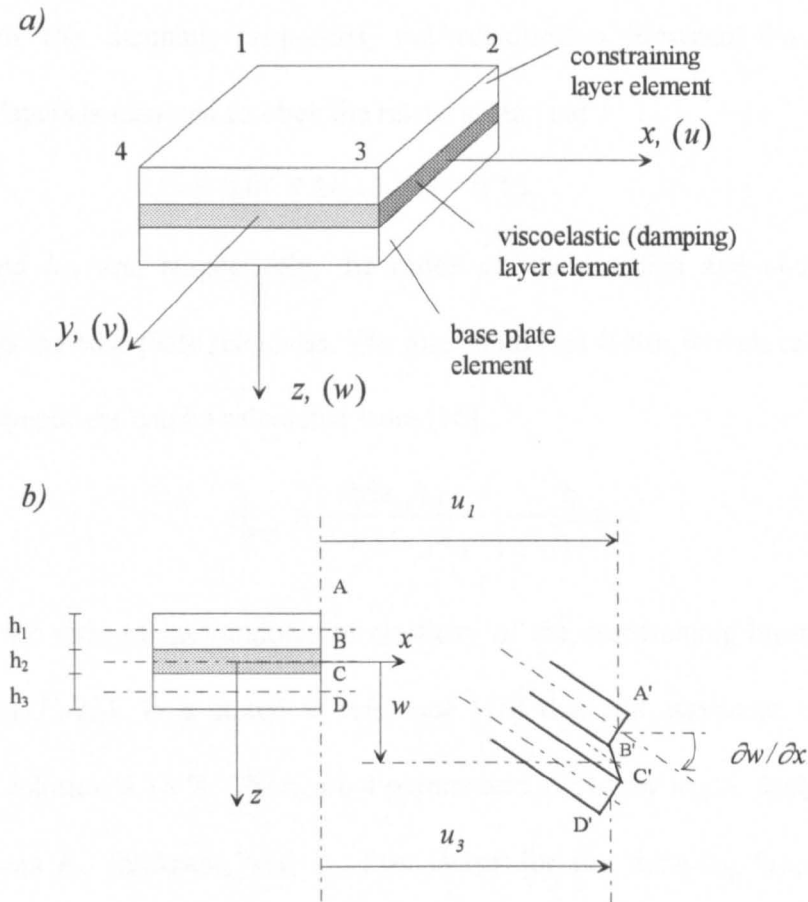


Figure 1. A rectangular element of the three-layer plate  
 a) co-ordinate system and nodes of the elements  
 b) displacement of the elements at x-z plane

The plate is aluminium and has the dimensions 2.5 mm  $\times$  305 mm  $\times$  490 mm. The experimental arrangement of the clamped-clamped plate is shown in Figure 2. Preliminary experiments indicated that given excitation and measurement points at node 7, the first 10 modes can be excited and detected. These modes will be identified experimentally and

compared with model predictions before consideration of model updating. Passive damping, through the addition of viscoelastic and constraining layers, must aim to attenuate levels of plate vibration. Ross and his colleagues [16] provided guidelines for designing suitable surface treatments for plates. In the present study, self-adhesive damping tape is used in conjunction with a thin metallic constraining layer. To simplify the calculation of the damping properties, the relationship between the damping and constraining layers is assumed to obey the relationship [16]

$$0.05 < 2h_{23} + h_{13} < 0.15. \quad (3)$$

where  $h_{23}$  and  $h_{13}$  are, respectively, the ratios of the damping and constraining layer thicknesses to the base plate thickness. The maximum loss factor introduced as a result of the damping treatment can be calculated from [16]

$$\eta_{\max} = \frac{3.5e_{13}h_{13}}{2 + 3.5e_{13}h_{13}} \cdot \frac{\eta}{1 + \sqrt{1 + \eta^2}} \quad (4)$$

where  $e_{13}$  is the ratio of the modulus of elasticity of the constraining layer to that of the base plate (or  $E_1/E_3$ ). It is stated in reference [16] that the maximum error from this approximate solution is 15 %. There are 4 parameters to choose in the design process, the two parameters  $h_2$ , thickness, and  $\eta$ , loss factor for the damping layer and the two parameters  $h_1$ , thickness, and  $E_1$ , modulus of elasticity for the constraining layer. Equation (4) implies that the maximum damping is proportional to the loss factor  $\eta$  of the damping layer and the thickness and modulus of elasticity of the constraining layer with respect to the fixed values of the base plate thickness  $h_3$  and modulus of elasticity  $E_3$ . From commercially available materials, a 50.8  $\mu\text{m}$  (0.002 in) thick ISD112 viscoelastic layer from the 3M company was selected from the manufacturer's data sheet to provide a loss factor of approximately 1.0 in the frequency range from 0 to 600 Hz. A 0.254 mm (0.010

in) thick steel shim was used as the constraining layer giving an upper limit (Equation (3)) equal to 0.1422. The steel shim was used to provide a high modulus of elasticity for the constraining layer. Table 1 gives the material properties for all three layers.

Figure 3 shows the influence of the passive constrained damping layer when compared with the response of the undamped host plate. Note that the introduction of the damping layer produces around 25 dB attenuation of all the modes up to 600 Hz. However, the vibrations associated with the first two modes still produce mobility peaks some 20 dB above those associated with the higher modes. It is these first two modes, one bending and one torsion, which require the use of active control to introduce significant additional attenuation of vibration levels. Before proceeding to describe active constrained layer damping it is necessary to refine the finite element model of the passively damped plate. A comparison between the predicted Frequency Response Function (FRF) from the finite element model and the FRF measured experimentally, Figure 4, shows that the response levels predicted by the model are consistent with the results from the experiments. However, there are discrepancies in the predicted natural frequencies. The discrepancies in natural frequencies probably stem from imperfect clamping at the two ends (see Figure 2) where rotational stiffness is present. These discrepancies will be minimised using updating techniques before the model is used for control system design.

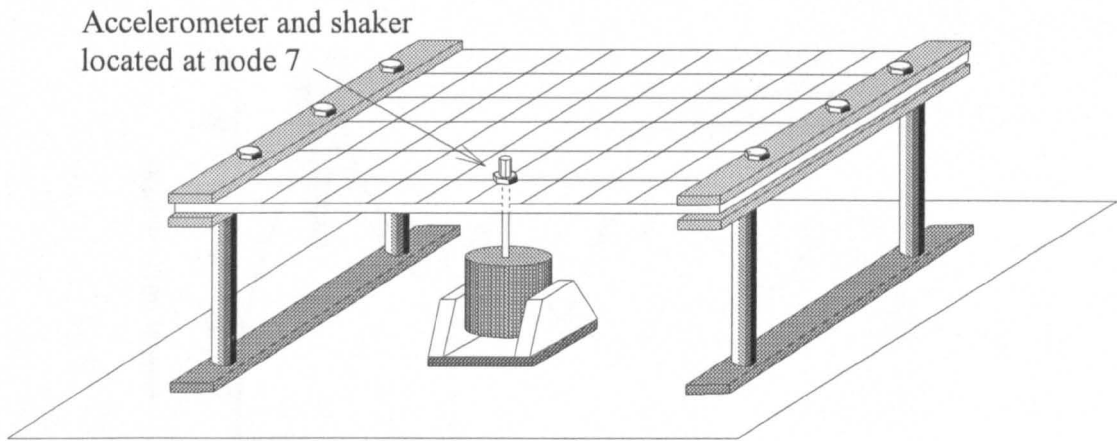


Figure 2. Experimental arrangement of the clamped-clamped plate for passive constrained layer damping experiments

Table 1

Material properties of three-layer plate

Material	modulus of elasticity (MPa)	modulus of rigidity (MPa)	density (kg/m <sup>3</sup> )	Poisson's ratio	shear loss factor
aluminium plate	$70 \times 10^3$	-	2700	0.3	-
ISD112 viscoelastic layer	$29.8^*$	$20^*$	1140	0.49	$1.0^*$
steel constraining layer	$200 \times 10^3$	-	7000	0.3	-

\* at the centre frequency of 600 Hz

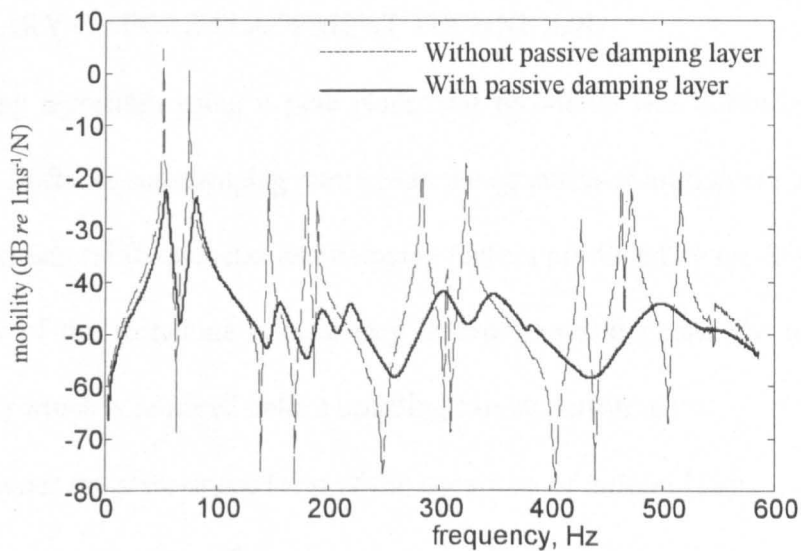


Figure 3. Measured FRFs of the panel plate with and without constrained damping layer

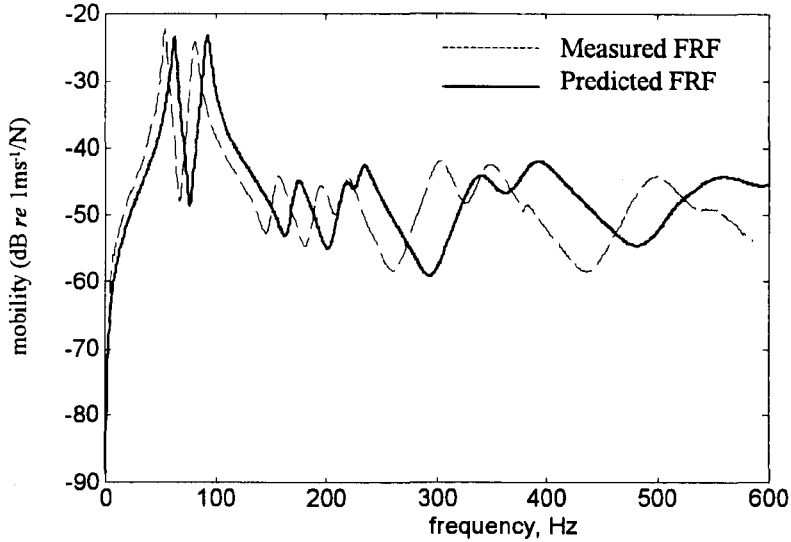


Figure 4. Measured and predicted FRFs (point mobility, the same point for acting force and velocity response) of the panel plate covered with constrained damping layer

#### 4. MODEL UPDATING

In the FRFs shown in Figure 4, the FRF predicted by the finite element model is shifted to the right of the experimental FRF. A pole placement technique was used to update the finite element model so that both the predicted natural frequencies and modal damping factors are modified so as to match the experimentally measured data.

##### 4.1 SUMMARY OF POLE PLACEMENT TECHNIQUE

One updating algorithm using a pole placement technique was described by Inman and Minas [17]. Stiffness and damping matrices in the equation of motion are updated to match the identified natural frequencies and damping factors produced by experimental testing. A brief review of the technique is necessary in order to understand the transformation of Equation (2) which is required before updating can be performed.

Consider the state-space form of the equations of motion [10]:

$$\begin{Bmatrix} \ddot{\Delta} \\ \dot{\Delta} \end{Bmatrix} = \begin{bmatrix} -\mathbf{M}^{-1}\mathbf{D} & -\mathbf{M}^{-1}\mathbf{K} \\ \mathbf{I} & \mathbf{0} \end{bmatrix} \begin{Bmatrix} \dot{\Delta} \\ \Delta \end{Bmatrix} + \begin{bmatrix} \mathbf{B}_0 \\ \mathbf{0} \end{bmatrix} \mathbf{f} \quad (5)$$

where  $\mathbf{D}$  is an  $n \times n$  damping matrix,  $\mathbf{I}$  is an  $n \times n$  identity matrix,  $\mathbf{B}_0$  is an  $n \times n$  input matrix and  $\mathbf{f}$  is an  $n \times 1$  input vector. If the vector  $\mathbf{f}$  is used to provide the feedback signal, then

$$\mathbf{f} = \mathbf{GC} \begin{Bmatrix} \dot{\Delta} \\ \Delta \end{Bmatrix} \quad (6)$$

where  $\mathbf{G}$  is an  $n \times 2m$  gain matrix,  $\mathbf{C}$  is an  $2m \times 2n$  measurement matrix containing  $2m$  rows of eigenvectors and  $m$  is the number of modes to be updated. Note that these modes occur as complex conjugate pairs. A method of calculating the elements of  $\mathbf{G}$  is given by Porter and Crossley [18]. A suitable choice of the matrix  $\mathbf{B}_0$  to provide controllability of all the modes is the identity matrix  $\mathbf{I}$  [17]. Then the second term on the right hand side of Equation (5) acts as a correction term and Equation (5) can be rewritten as

$$\begin{Bmatrix} \ddot{\Delta} \\ \dot{\Delta} \end{Bmatrix} = \begin{bmatrix} -\mathbf{M}^{-1}\mathbf{D} & -\mathbf{M}^{-1}\mathbf{K} \\ \mathbf{I} & \mathbf{0} \end{bmatrix} \begin{Bmatrix} \dot{\Delta} \\ \Delta \end{Bmatrix} + \begin{bmatrix} \Delta\mathbf{A}_1 & \Delta\mathbf{A}_2 \\ \mathbf{0} & \mathbf{0} \end{bmatrix} \begin{Bmatrix} \dot{\Delta} \\ \Delta \end{Bmatrix} \quad (7)$$

where  $\Delta\mathbf{A}_1$  and  $\Delta\mathbf{A}_2$  are the  $n \times n$  mass-normalised correction matrices of the damping and stiffness matrices, respectively, and are obtained from the inner product of  $\mathbf{B}_0(\mathbf{GC})$ .

Define  $\mathbf{A}_1 = -\mathbf{M}^{-1}\mathbf{D} + \Delta\mathbf{A}_1$  and  $\mathbf{A}_2 = -\mathbf{M}^{-1}\mathbf{K} + \Delta\mathbf{A}_2$ , then the updated damping and stiffness matrices can be obtained from

$$\begin{aligned} \mathbf{D}_{new} &= -\mathbf{MA}_1 \\ \mathbf{K}_{new} &= -\mathbf{MA}_2 \end{aligned} \quad (8)$$

where  $\mathbf{D}_{new}$  and  $\mathbf{K}_{new}$  are the updated damping and stiffness matrices, respectively. In Equation (7) it is assumed that the damping matrix  $\mathbf{D}$  represents viscous damping. Consequently it is necessary to transform the imaginary term of the complex stiffness matrix of the plate model as formulated in Equation (2) to an equivalent viscous damping matrix.

#### 4.2. TRANSFORMATION OF THE IMAGINARY TERM OF THE COMPLEX STIFFNESS MATRIX TO AN EQUIVALENT VISCOUS DAMPING MATRIX

The imaginary term of the complex stiffness matrix can be transformed to approach the viscous damping matrix where the viscous damping coefficients are now frequency dependent. The algorithm used to achieve this damping transformation is adapted from work by Minas and Inman [19] and was originally used for identifying a non-proportional damping matrix from experimental data. Details of the transformation have been presented by Chantalakhana and Stanway [15]. Although this transformation is straightforward in principle, difficulties in the present application arise owing to the dimensions of the matrices, which are involved. Essentially, the pseudo-inverse of an over-determined system of linear equations incorporating a  $2n^2 \times (n^2 + n)/2$  order matrix needs to be computed. Consequently the mass and complex stiffness matrices of the finite element plate model need to be reduced in size. To overcome this problem, the authors used the Guyan reduction technique [20] to reduce the order of system equations before implementing the transformation.

#### 4.3. VALIDATION OF THE UPDATED MODEL

In this section, the pole placement algorithm for updating the model is implemented in order to study its performance. Experimental data are required to implement the algorithm. The diagram in Figure 5 summarises the procedures necessary to achieve a refined, reduced-order model of the three-layer plate.

#### 4.3.1 TENTATIVE MODEL

Details of first three stages in implementing the flow-chart in Figure 5 are described below. The finite element model is obtained by discretising the three-layer plate as 9 by 6 elements along the length and width directions, respectively, as shown in Figure 6.

The number of degrees of freedom  $n$  of the original finite element plate model is 420. Guyan reduction is performed by maintaining the transverse displacements of selected nodes (see Figure 6) and the longitudinal displacements of the constraining layer at four selected nodes. These nodes will be used in the active control strategies which are described later. In this way the number of degrees of freedom is reduced from  $n=420$  to  $r=36$ . The selection of these master nodes needs to ensure a suitable reduced-order model over the bandwidth of interest and also maintain correspondence with the measurement points used in the experimental procedures. Guidelines for this node selection can be found in Shah and Raymund [21]. The equation of motion with reduced mass and complex stiffness matrices is then solved to obtain the eigensolutions. These solutions are then used to transform the imaginary term  $\mathbf{Z}^R$  of the reduced complex stiffness matrix  $\bar{\mathbf{K}}^R$  to an  $r \times r$  equivalent viscous damping matrix  $\mathbf{D}^R$ . The dynamic responses of this reduced-order plate model deviate from the original model owing to ignorance of the inertia term in the transformation using Guyan reduction [22] and the pseudo-inverse used in the damping transformation algorithm. The reduced-order model eventually will be updated with parameters identified from experiments in order to match the model predictions to the observed behaviour of the plate structure.

#### 4.3.2 IDENTIFICATION OF NATURAL FREQUENCIES AND DAMPING FACTORS

Identified natural frequencies and damping factors are used to update the finite element plate model. The frequency range of interest is from 0 to 600 Hz where modal damping factors are generally less than 0.05. Hence, a simple peak picking method can be used for identification [23,24]. Care must be taken when using the method since peak picking requires well-separated modes. Many plate configurations have coincident modes but this feature does not occur within the frequency range of interest of the plate used here. Note that, in Figure 3, mode 7 at around 300 Hz disappears when the passive layer is applied to the plate. Owing to the unavailability of mode 7, only the first 6 modes are identified. Table 2 gives the identified natural frequencies and percentage damping factors of the first 6 modes compared with those from the model predictions. Specifically, the predictions are obtained from the  $r$ -order reduced model which is updated with the eigenvalues of the full  $n$ -order plate model. Then the predicted natural frequencies and damping factors are the same for both models.

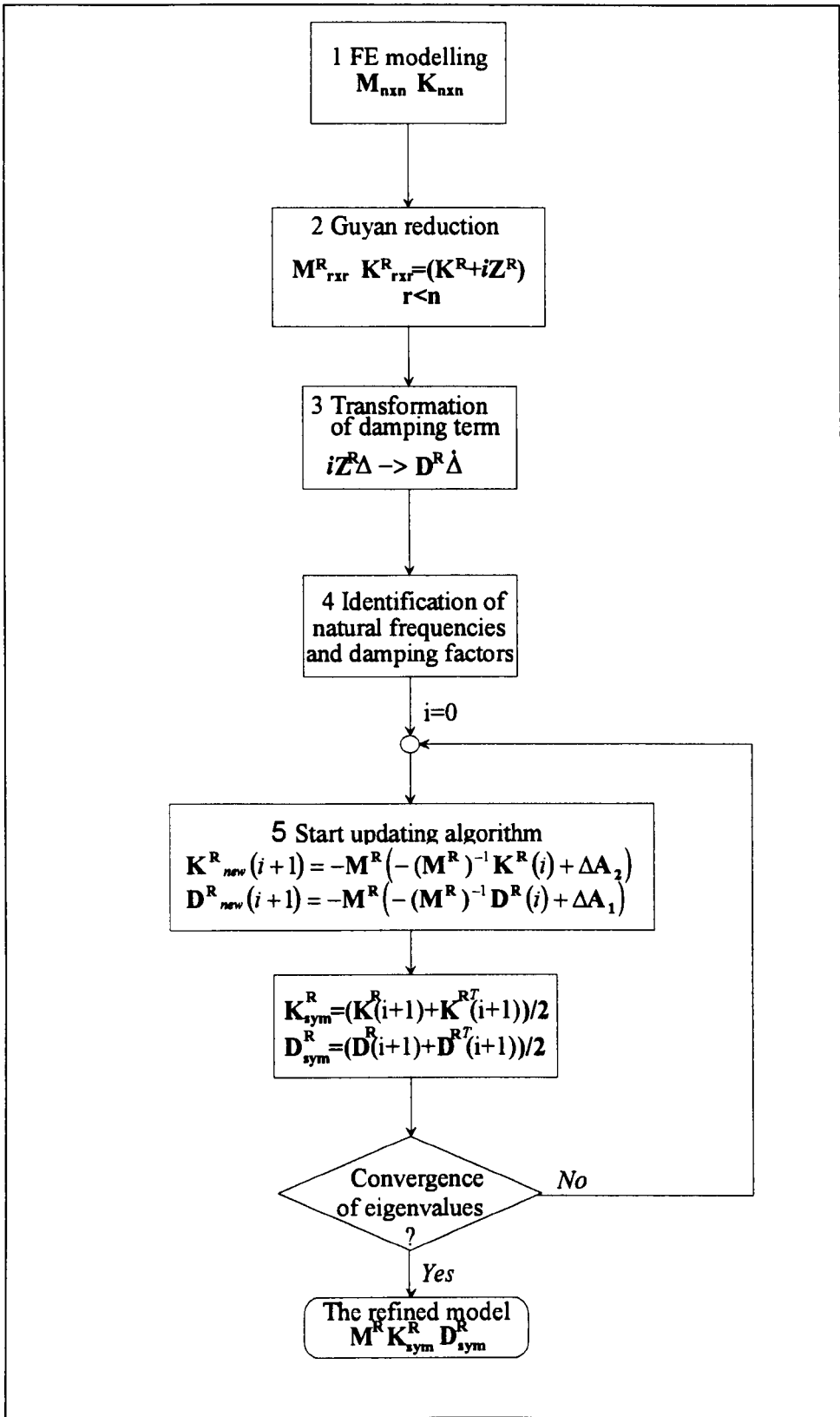


Figure 5. Procedures to achieve the refined model constructed using finite element analysis

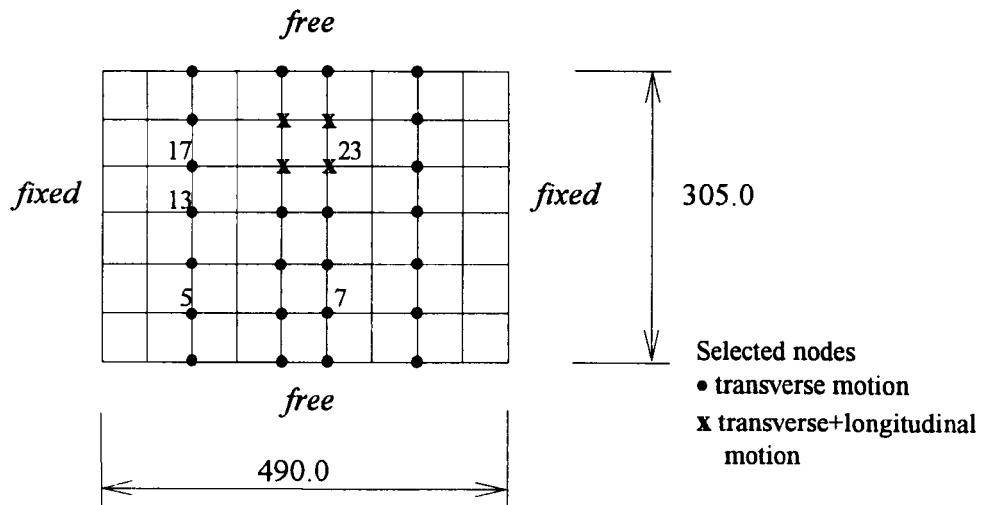


Figure 6. Division of plate to finite elements and selected nodes for model reduction

Table 2  
Measured and predicted first six natural frequencies  
and damping factors of three-layer plate

mode	1	2	3	4	5	6
predicted natural frequency (Hz)	62.50	92.23	172.93	217.07	233.02	339.06
measured natural frequency (Hz)	54.53	81.50	157.47	195.59	220.60	304.02
predicted % damping	3.50	3.05	3.81	3.87	2.83	4.86
measured % damping	3.44	3.51	4.13	3.66	3.41	3.57

#### 4.3.3 MODEL UPDATING ITERATION AND REFINED MODEL

Unfortunately, the mass-normalised correction terms of the damping matrix ( $\Delta\mathbf{A}_1$ ) and of the stiffness matrix ( $\Delta\mathbf{A}_2$ ) are not guaranteed to be symmetrical such that the orthogonality properties of the modal model are satisfied [23]. These properties are required to enable decomposition of the system equations used in modal control. Because of the requirement for symmetrical stiffness and damping matrices, the updating procedures need to be repeated until the updated eigenvalues are acceptable when compared with the identified eigenvalues (see Figure 5). Figures 7 and 8 show a comparison of FRFs before and after updating the finite element three-layer plate model.

The notation used is  $FRF_{j\_k}$  where  $j$  is the excitation point and  $k$  is the measurement point, as indicated in Figure 6. In Figures 7 and 8 the dashed lines represent the measured FRFs and the solid lines represent the FRFs from prediction (a) before updating and (b) after updating the model. These results clearly show that the first six modes of the predicted FRFs are concurrent with the measured FRFs and the higher modes (i.e. those not updated) are unchanged. Although mismatches of the higher modes are clearly present, the accuracy of the updated models is sufficient to use in an active design scheme where it is the accuracy of controlled pole locations which is required.

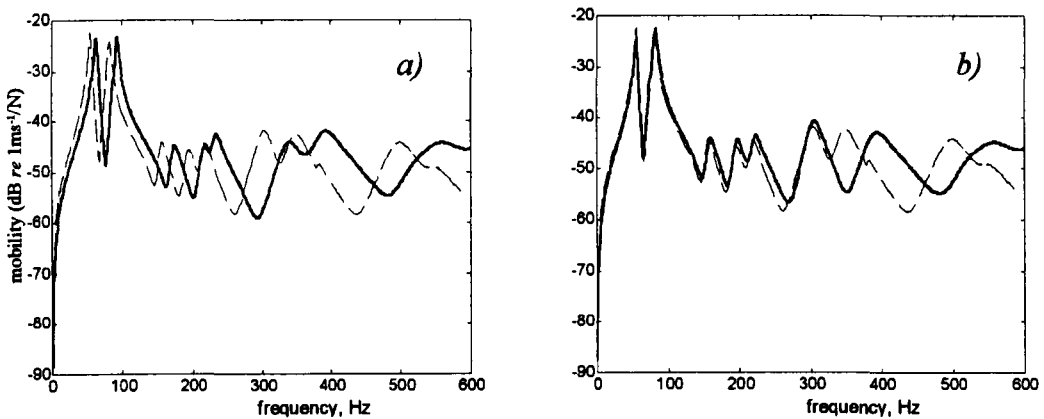


Figure 7. FRF7\_7 a) before updating  
b) after updating the model

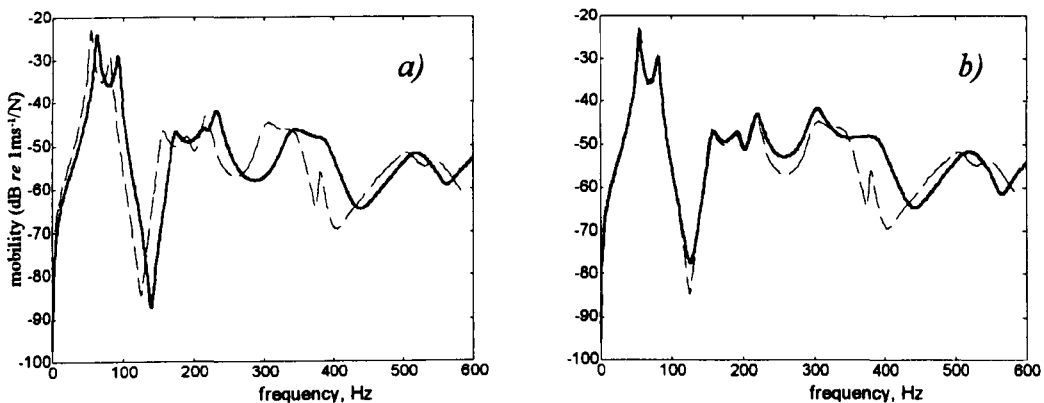


Figure 8. FRF7\_23 a) before updating  
b) after updating the model

## 5. MODAL CONTROL

From the results in Section 3 (Figures 3 and 4), the FRFs of the plate treated with a passive constrained damping layer show that an additional active control scheme is required to provide adequate attenuation the first two modes of vibration of the plate. An active element used to perform control action consumes energy and generally multiple sensors and actuators are required if multiple modes are to be controlled. In the present study, modal control theory [1] associated with coupling of the control force is used. An advantage of coupling the force is to control a number of modes simultaneously using the minimum number of actuators. However, spillover effects must obviously be taken into account.

### 5.1 MODAL STATE-SPACE FORM OF EQUATIONS OF MOTION

For the reduced-order finite element plate model with  $r$  degrees of freedom, the corresponding state-space equation of motion is written as a set of  $2r$  first order differential equations :

$$\begin{Bmatrix} \ddot{\Delta} \\ \dot{\Delta} \end{Bmatrix} = \begin{bmatrix} \mathbf{0} & \mathbf{M}^R \\ \mathbf{M}^R & \mathbf{D}^R \end{bmatrix}^{-1} \begin{bmatrix} \mathbf{M}^R & \mathbf{0} \\ \mathbf{0} & -\mathbf{K}^R \end{bmatrix} \begin{Bmatrix} \dot{\Delta} \\ \Delta \end{Bmatrix} + \begin{bmatrix} \mathbf{0} & \mathbf{M}^R \\ \mathbf{M}^R & \mathbf{D}^R \end{bmatrix}^{-1} \begin{Bmatrix} \mathbf{0} \\ \mathbf{F} \end{Bmatrix} \quad (9)$$

where  $\Delta$  is an  $r \times 1$  displacement vector,  $\mathbf{M}^R$ ,  $\mathbf{D}^R$  and  $\mathbf{K}^R$  are  $r \times r$  mass, damping and stiffness matrices, respectively, and  $\mathbf{F}$  is an  $r \times 1$  force vector acting at the nodal points. For the special case of a single input force, Equation (9) may written in the form

$$\dot{\mathbf{Y}} = \mathbf{A}\mathbf{Y} + \mathbf{b}f \quad (10)$$

where  $\mathbf{Y}_{2r \times 1} = \begin{bmatrix} \dot{\Delta}^T & \Delta^T \end{bmatrix}^T$ ,  $\mathbf{A}_{2r \times 2r}$  is a plant matrix,  $\mathbf{b}_{2r \times 1}$  is an input vector and  $f$  is a scalar input. Let  $\mathbf{Y} = \mathbf{U}\xi$ , where  $\xi_{2r \times 1}$  is a modal state variable vector and  $\mathbf{U}_{2r \times 2r}$  is a transformation matrix containing  $2r$  columns of the eigenvectors of  $\mathbf{A}$ . After substituting

this transformation into Equation (10) and pre-multiplying by  $\mathbf{U}^{-1}$ , then Equation (10) becomes

$$\dot{\xi} = \Lambda \xi + \mathbf{w}f \quad (11)$$

where  $\Lambda = \mathbf{U}^{-1} \mathbf{A} \mathbf{U}$  is a diagonal matrix containing  $2r$  eigenvalues of  $\mathbf{A}$  along its diagonal elements,  $\mathbf{w} = \mathbf{U}^{-1} \mathbf{b}$  is a modal controllability vector in which an element  $j$  of  $\mathbf{w}$  quantifies controllability of the  $j$ th mode by the input  $f$ . This transformation results in the decoupling of Equation (10). If Equation (11) is partitioned as  $c$  controlled mode equations and  $u$  residual or uncontrolled mode equations, then Equation (11) can be re-arranged as

$$\begin{Bmatrix} \dot{\xi}_c \\ \dot{\xi}_u \end{Bmatrix} = \begin{bmatrix} \Lambda_c & \mathbf{0} \\ \mathbf{0} & \Lambda_u \end{bmatrix} \begin{Bmatrix} \xi_c \\ \xi_u \end{Bmatrix} + \begin{Bmatrix} \mathbf{w}_c \\ \mathbf{w}_u \end{Bmatrix} f \quad (12)$$

The  $c$  controlled eigenvalues can be shifted to their desired values by feeding back the vector of state variables  $\xi_c$ , as a scalar input  $f$  with appropriate weightings

$$f = \mathbf{k}_c^T \xi_c \quad (13)$$

where  $\mathbf{k}_c$  is a  $c \times 1$  gain vector.

The scalar feedback input  $f$  in Equation (13) is formed from the modal state variable vector  $\xi_c$  which needs to be computed from physical measurements. A state estimator [10] is implemented in conjunction with the modal controller to obtain estimates of all controlled state variables.

## 5.2 SPILLOVER EFFECTS

Balas [1] showed that using a reduced set of equations for the controller and estimator causes, respectively, control and observation spillover. A scalar input force  $f$  can excite the controllable residual modes (see Equation (12)) because of the force coupling which is present. Similarly, if the measurement signal includes terms from the residual state variable

$\xi_u$ , then the estimator is contaminated by amplified noise. These spillover effects can cause instability in the controlled structure. However, these effects can be reduced by keeping the elements of the control and estimator gain vectors low. Optimal designs such as the linear quadratic regulator and Kalman filter [25] can be used to achieve this. Placement of the actuator and sensor should be close to the nodal lines of residual modes so that the residual modes are not significantly excited and the residual state variables in  $\xi_u$  are not strongly observed.

## 6. DESIGN OF CONTROLLER

In what follows, the simplest possible configuration of sensor and actuator is considered: a single accelerometer and a single lead zirconate ceramic (PZT) actuator, respectively. The state estimator and the control law are designed in the continuous-time domain and then transformed to the discrete-time domain for digital implementation. Placement of the sensor and the actuator are described below.

### 6.1 PLACEMENT OF SENSOR AND ACTUATOR

Plots of mode shapes are used to identify positions for the sensor and actuator such that they detect and excite the maximum transverse displacements of the first two modes whilst also keeping to the nodal lines of the higher modes so as to minimise spillover effects. The modal controllability and observability vectors are used to refine the selection of the sensor and actuator locations.

The first six mode shapes are considered and then the sensor and actuator are located in the middle of the upper half portion of the plate as illustrated in Figure 9. The dimensions of the PZT actuator are chosen based upon the results obtained by finite

element modelling and experimental observations. A 50 mm × 50 mm PZT patch is used as the actuator. Table 3 gives the controllability and observability indices of these sensor and actuator locations from the first six elements of the mode controllability vector  $w$  and the mode observability vector [10], respectively. Controllability and observability indices are low for modes 3 and 4 where the actuator and sensor are placed near their nodal lines, but are high for modes 1 and 2 where the actuator and sensor locations are in the region of maximum transverse motion so as to provide large induced shear strain in the damping layer.

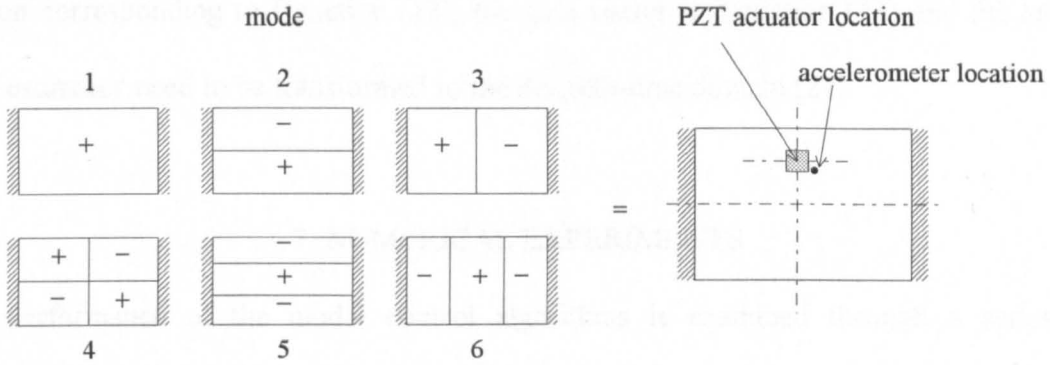


Figure 9. Location of PZT actuator and accelerometer to control the first two modes of the panel plate

Table 3  
Controllability and observability indices

mode	controllability	observability
1	$6.30 \pm 1.0601 \times 10^1 i$	$-1.145 \times 10^{-1} \pm 1.557 \times 10^{-1} i$
2	$-5.05 \pm 9.09 i$	$3.66 \times 10^{-2} \pm 8.67 \times 10^{-2} i$
3	$-1.500 \times 10^{-8} \pm 7.30 \times 10^{-8} i$	$-1.442 \times 10^{-2} \pm 5.16 \times 10^{-4} i$
4	$-5.97 \times 10^{-8} \pm 3.39 \times 10^{-8} i$	$-6.15 \times 10^{-3} \pm 7.94 \times 10^{-3} i$
5	$-8.43 \times 10^{-1} \pm 2.49 \times 10^{-1} i$	$-1.256 \times 10^{-1} \pm 3.53 \times 10^{-2} i$
6	$2.16 \times 10^2 \pm 2.51 \times 10^2 i$	$-2.81 \times 10^{-2} \pm 1.527 \times 10^{-2} i$

## 6.2 CONTROL LAW AND ESTIMATOR DESIGN

For the state-space equations with a single input and single output (SISO), the control gain vector  $\mathbf{k}_c^T$  in Equation (13) and estimator gain can be assigned using a pole placement technique. However, to optimise actuator power consumption and damping of the desired modes, linear quadratic regulator (LQR) and gaussian (LQG) algorithms [26] are used to obtain optimal control and estimator gains, respectively, so that the spillover effects are not sufficient to destabilise the actively controlled system. To implement the digital controller of modal control algorithm, the controlled mode state-space equations of motion corresponding to Equation (12), the gain vector in Equation (13) and the modal state estimator need to be transformed to the discrete-time domain [27].

## 7. NUMERICAL EXPERIMENTS

The performance of the modal control algorithms is examined through a series of numerical experiments. Controller and estimator gains are designed to produce maximum damping of the first two eigenvalues and ensure stability of the closed-loop system in the face of spillover effects. The desired eigenvalues, along with controller and estimator gains are given in Table 4. The desired poles are obtained by using the LQR design to minimise the control gains and to achieve high damping. The LQG design is used to obtain the optimal estimator gains. The main consideration in designing the controller is to minimise spillover problems.

Table 4  
Poles and gains of designed controller

mode	original poles(rad/s)	desired poles(rad/s)	control gain	estimator gain
1	$-11.78 \pm 343i$	$-105.6 \pm 339i$	$-4.88 \pm 5.61i$	$-1313 \pm 387i$
2	$-17.96 \pm 512i$	$-74.6 \pm 498i$	$5.08 \pm 3.80i$	$-720 \pm 302i$

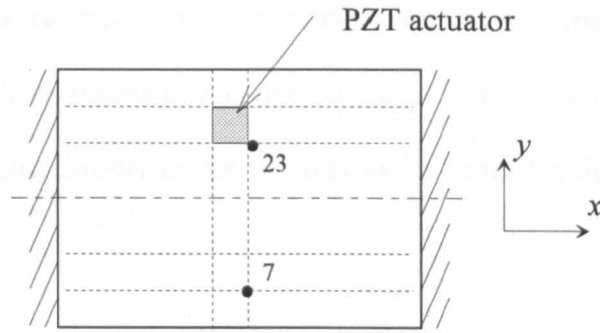
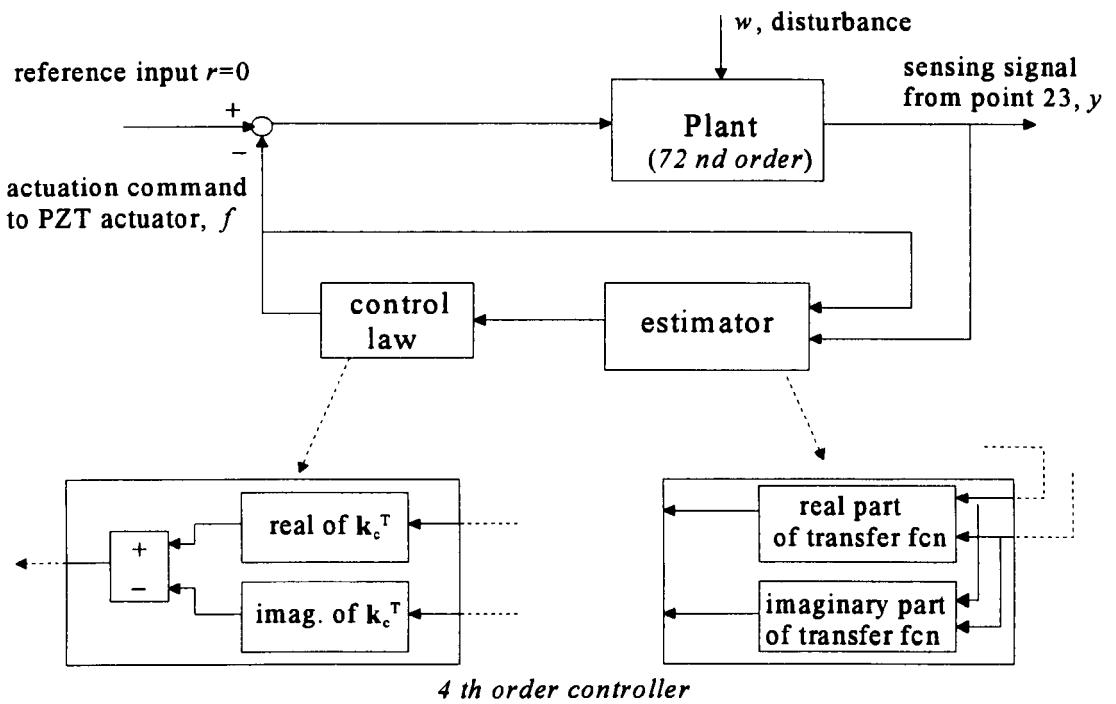


Figure 10. Actuator location and excitation and measurement points (7,23) used in simulation of active constrained layer damping

In accordance with the discussion in Section 6.1, the disturbance (shaker position) and measurement points are at points 7 and 23, respectively, as shown in Figure 10. The control excitation is applied to the PZT actuator placed in the middle of the upper portion of the three-layer plate. The complete closed-loop control system is shown in Figure 11.

The PZT actuator model is initially designed to activate in both the  $x$  and  $y$  directions (see Figure 10) and the predicted FRFs are shown in Figure 12 where the FRFs relate the integrated velocity from the accelerometer to the disturbance force derived from the load cell. The FRF simulation results in Figure 13 show the influence of activating the PZT model in the  $x$  direction only. The results demonstrate that superior suppression of vibrations is obtained by activating in the  $x$  direction only since actuation of the PZT in the  $y$  direction is liable to induce excitation of higher modes and thus affect the closed-loop poles. In addition, the power consumption for the PZT actuator decreases when actuation is in one direction only, as shown by the plots of applied voltage *versus* time in Figure 14 where the disturbance time history is swept sine with a frequency range from 0 to 600 Hz. Also superimposed on Figures 12 and 13 are simulation results produced using a controller designed upon the basis of the reduced-order model prior to updating. In both cases the

use of the updated model produces superior suppression of the first two modes. Also in Figure 12 there are indications of spillover causing excitation of the modes at around 200 and 500 Hz. Given these results it was decided to proceed with the experimental study using the updated, reduced-order model as the basis for controller design.



Implementing a complex number controller using real numbers

Figure 11. Block diagram of digital control simulation to match with real-time interface using SIMULINK software

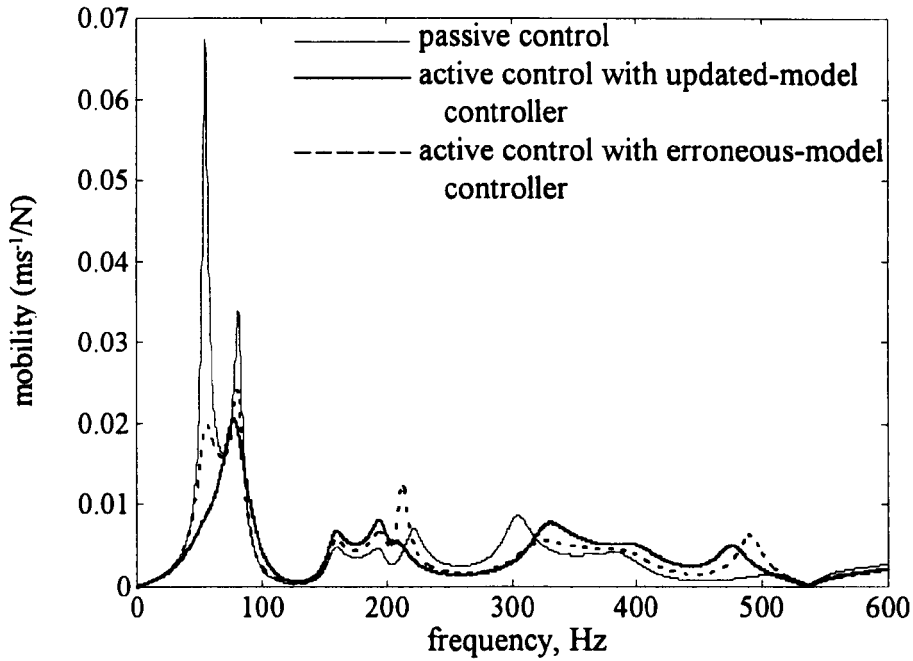


Figure 12. Simulation results: predicted FRFs of three-layer plate with and without active control for PZT actuator operating in both  $x$  and  $y$  directions

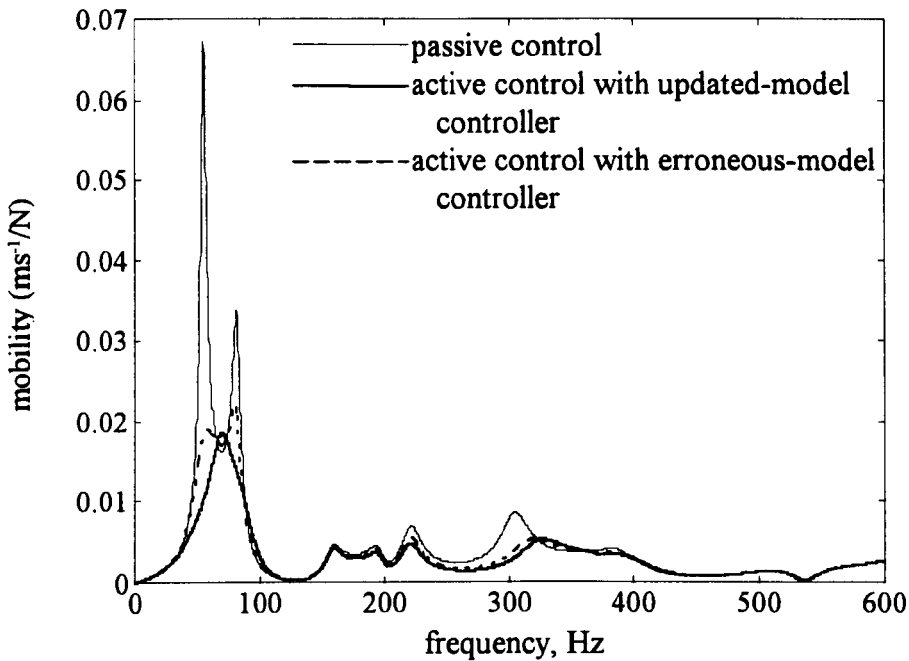


Figure 13. Simulation results: predicted FRFs of three-layer plate with and without active control for PZT actuator operating in  $x$  direction only

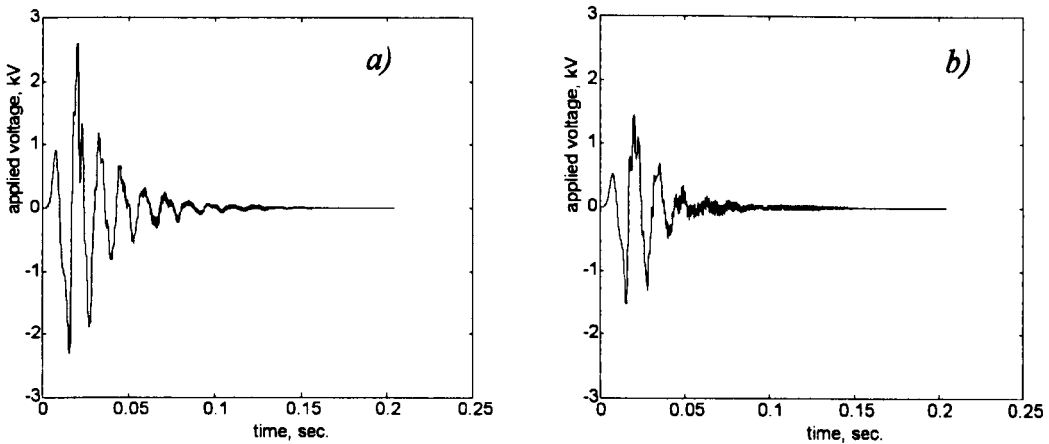


Figure 14. Simulation results: applied voltage for PZT actuator  
 a) operating in both  $x$  and  $y$  directions  
 b) operating in  $x$  direction only

## 8. EXPERIMENT FACILITY AND RESULTS

The general arrangement of the test facility is shown in Figure 15. Implementation of the digital controller is performed using a commercial package ('dSPACE' DS1102) which uses one analogue-to-digital input channel and one digital-to-analogue output channel. In general, to avoid aliasing of a sampled signal, the sampling frequency must be greater than twice the highest natural frequency, which in this case is around 600 Hz [25]. In the present study it was found that a sampling frequency of 10 kHz provided a suitable compromise between sufficiently accurate discretisation of the analogue signal for real-time control and the capabilities of the digital signal processor. This sampling rate also ensures that the spillover effects from the uncontrolled higher frequency modes will not occur. The control interface card is designed to operate with SIMULINK software [28]. Processing of the sensor signal to compute the command force is written in block diagram form in SIMULINK. This programming format is restricted to operations in real numbers and hence the complex matrices of the state-space controller have to be transformed into

complex transfer functions (see Figure 11). Real and imaginary terms can then be computed separately in terms of real numbers.

To activate the PZT actuator in the  $x$  direction only, a 50 mm  $\times$  50 mm element of PZT material is cut into 4 strips of equal width and attached to the plate as shown in Figure 16. The PZT actuator is approximately 1 mm thick to react effectively to a maximum voltage of from 1 to 2 kV [29]. The relationship between force and voltage applied for the PZT actuator is derived as [29]

$$\begin{aligned} f(t) &= \sigma_a A_a = \left( E_a \frac{d_{31}}{t_a} V(t) \right) b_a t_a \\ &= -0.702 V(t) \quad (\text{Newton per Volt}) \end{aligned} \quad (14)$$

where  $\sigma_a$  is the stress developed in the PZT,  $A_a$  is the cross-section of the PZT,  $b_a$  is the width of the PZT,  $t_a$  is thickness of the PZT,  $E_a$  is the modulus of elasticity of the PZT ( $= 1/15.1 \times 10^{-12} \text{ Nm}^{-2}$ ) and  $d_{31}$  is the piezoelectric constant ( $= -212 \times 10^{-12} \text{ mV}^{-1}$ ).

Figures 17 and 18 show FRFs from experiments for different PZT actuator configurations and can be compared directly with the simulation results shown in Figures 12 and 13. Close agreement between simulations and experiments is evident. The introduction of active control results in significant attenuation of the two lowest modes, which was predicted by the simulation results. However the simulation results in Figures 12 and 13 indicated that these two modes would coalesce into a single mode. This did not happen in practice with the modes remaining distinct. The experimental results also show the excitation of the mode just above 500 Hz which occurs when the actuator is arranged to operate in both  $x$  and  $y$  directions.

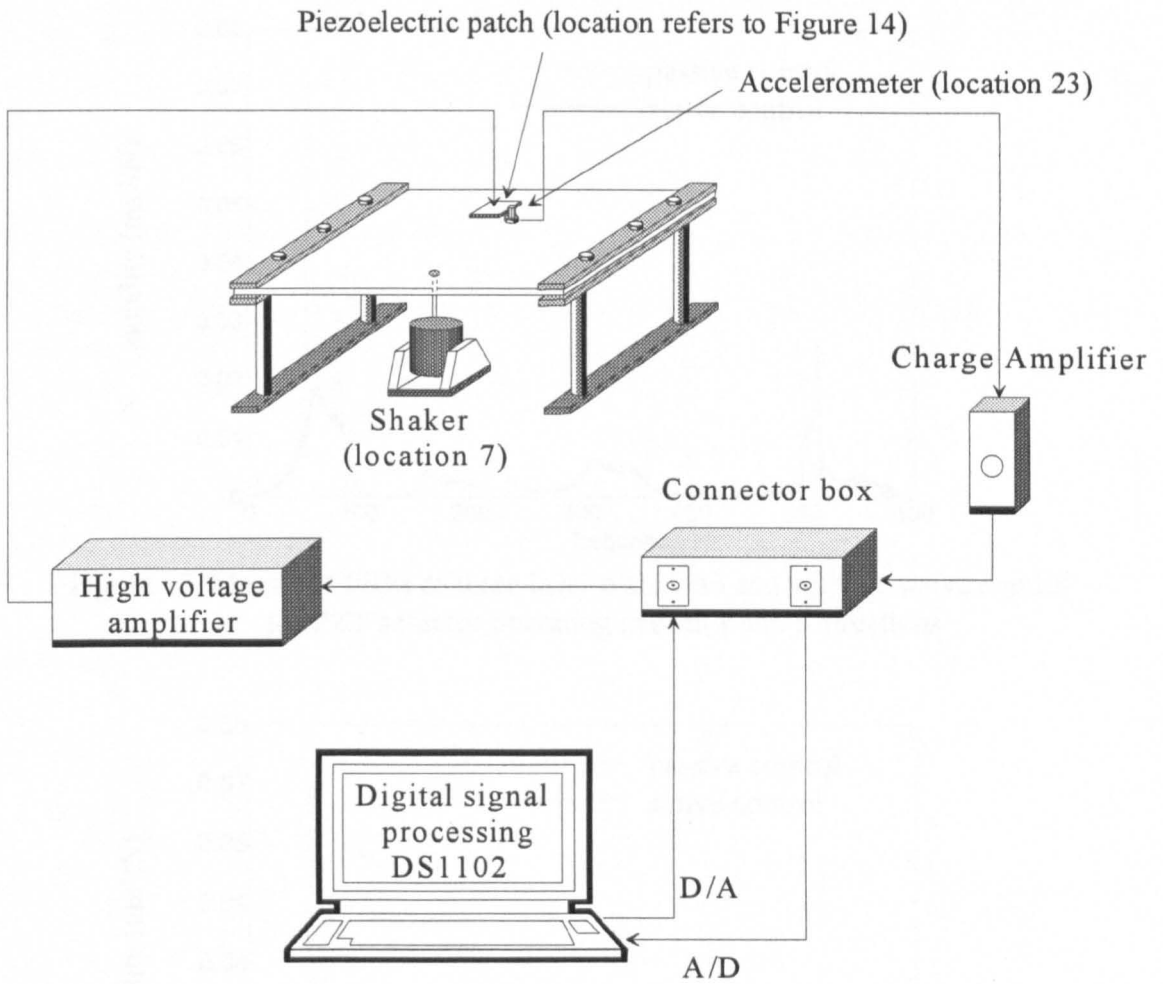


Figure 15. Arrangement of clamped-clamped plate with electronic equipment for digital control implementation

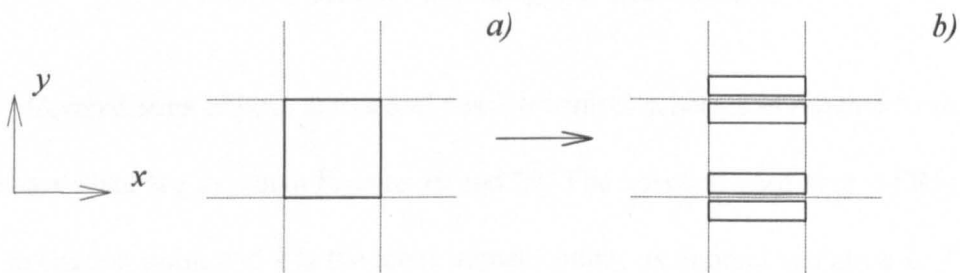


Figure 16. Configuration of PZT actuator  
 a) for operation in  $x$  and  $y$  directions  
 b) for operation in  $x$  direction only

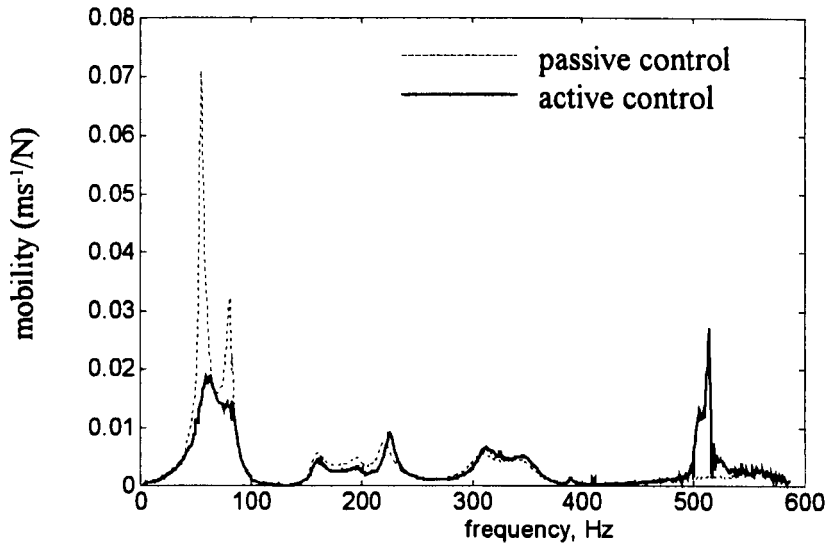


Figure 17. Measured FRFs of three-layer plate with and without active control for PZT actuator operating in both  $x$  and  $y$  directions

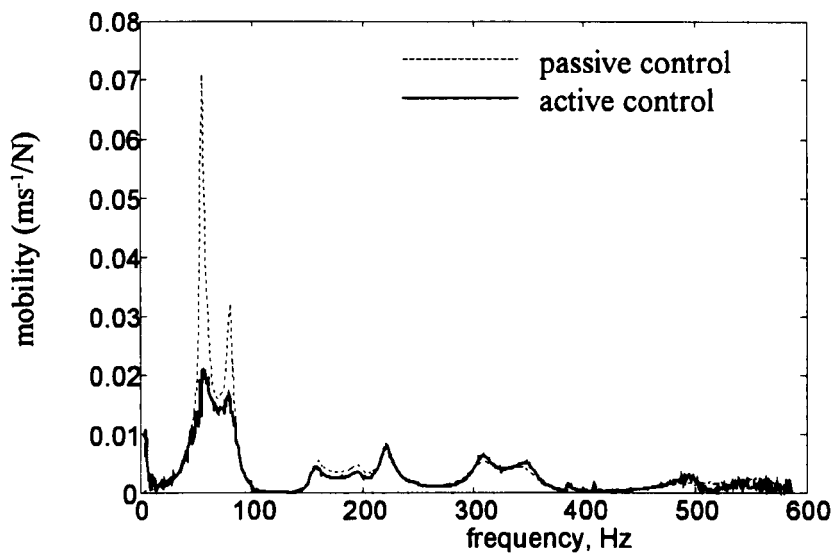


Figure 18. Measured FRFs of three-layer plate with and without active control for PZT actuator operating in  $x$  direction only

Comparisons of both active and passive control schemes in relation to the response of the bare plate are shown in Figures 19 and 20. The notation used here is  $FRF_{j_k}$  where  $j$  is the excitation point and  $k$  is the measurement point, as defined in Figure 6. The FRF of the actively damped plate using the two-direction PZT actuator is shown in Figure 19 and Figure 20 is of the one-direction PZT case. The attenuation of the first and second modes

is increased through the active damping control by about 10 dB and 5dB, respectively. Noise is associated with the FRFs measured from the response of the actively controlled plate using the one-direction PZT actuator, especially at low and high frequencies. This may arise from the unsynchronised operation of the four-strip PZT actuator designed to operate in one direction only. The results in Figures 19 to 20 show clearly the influence of passive and active constrained layer damping on the dynamic response of the plate.

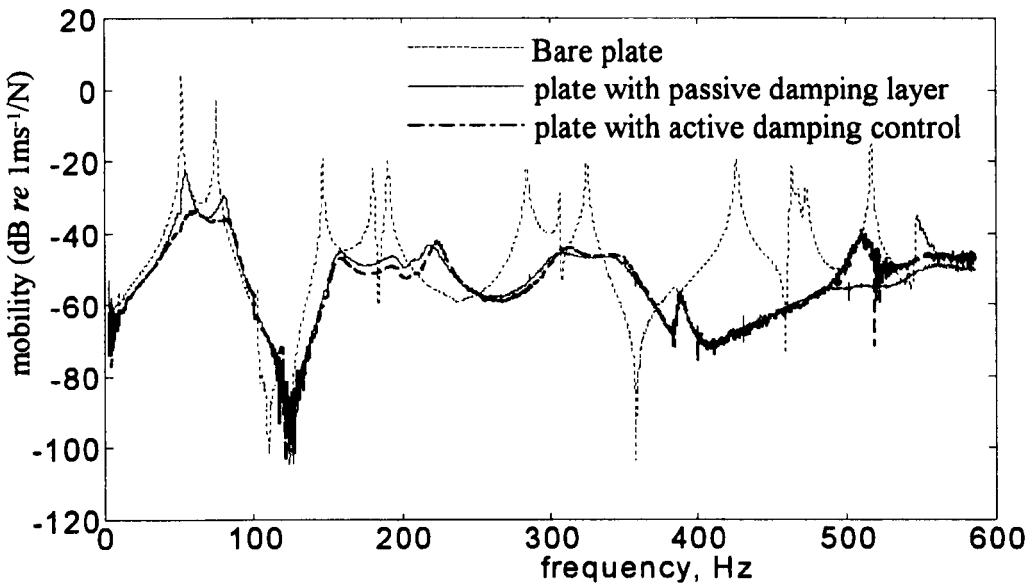


Figure 19. FRF7\_23 (PZT operating in 2 directions)

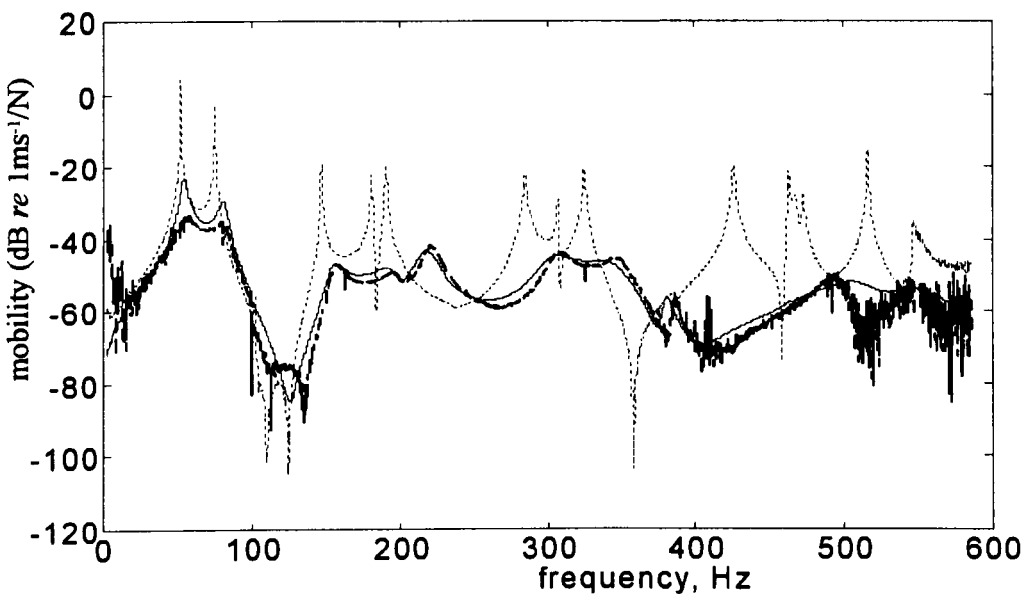


Figure 20. FRF7\_23 (PZT operating in 1 direction)

## 9. CONCLUSIONS

In this paper the authors have described both numerical and experimental investigations into the active constrained layer damping of a clamped-clamped plate. The strategy adopted has involved the development of a model-based approach to control system design. The aim has been to minimise the amount of control hardware required whilst avoiding spillover problems which are liable to degrade performance.

Initially a passive constrained damping layer was introduced and its influence on vibration levels was investigated. Not unexpectedly it was found that the higher modes benefited significantly from the introduction of the passive layer: modes 3 to 10 in the range from 150 to 600 Hz were attenuated by approximately 25 dB. The first two modes (bending, torsional) below 100 Hz were attenuated by a similar amount. However peak mobility levels for modes 1 and 2 were still some 20 dB above those of the higher order modes and an active strategy was developed to deal with this problem.

The development of the active control system involved the transformation of the original finite element model of the plate into a modal state-space description to be implemented in discrete time. To illustrate some of the key problems involved in this transformation and the solutions which were devised, the mathematical treatment has been described in some detail. The end result of the various computations was a fourth-order estimator/controller. Numerical experiments indicated that such an arrangement was capable of attenuating modes 1 and 2 (in conjunction with a 72<sup>nd</sup> order model of the plate) without incurring problems due to spillover. This was achieved using only a single sensor and single actuator channel.

The experimental study confirmed the results of the numerical simulations. Two configurations of actuator were investigated - a single PZT patch arranged to provide

actuation in mutually perpendicular directions, and an arrangement of four PZT patches driven by a single amplifier but designed to activate the plate in a single direction only. Both configurations were effective at controlling modes 1 and 2 but the single PZT patch produced significant excitation of a mode above 500 Hz.

Two mobility/frequency plots have been used to summarise the effects of passive and active constrained layer damping and actuators operating in one and two directions. By using the four-patch arrangement the excitation of the mode above 500 Hz, which occurs using a single patch, can be avoided. Also, using the four PZT patches collocated with the sensor produces the greatest attenuation of modes 1 and 2 but the mobility/frequency plot is noisier, especially at high and low frequencies. Overall the experiments show that the passive layer introduces sufficient damping into the higher modes to avoid any serious problems due to spillover effects.

Future work will be aimed at comparing the performance of the time-domain control algorithm with robust frequency domain methods which have recently been developed for use with plate-like structures [30].

## 10. ACKNOWLEDGEMENTS

The authors would like to thank the European Research Office of the US Army for partial funding of the control equipment under contract number N68171-98-M-5388.

## REFERENCES

1. M. J. BALAS 1978 *IEEE Transactions on Automatic and Control* **AC-23**, 673-679.  
Feedback control of flexible systems.

2. L. MEIROVITCH, H. BARUH and H. OZ 1983 *Journal of Guidance and Control* **6**, 302-310. A comparison of control techniques for large flexible systems.
3. T. BAILEY and J. E. HUBBARD Jr. 1985 *Journal of Guidance and Control* **8**, 605-611. Distributed piezoelectric-polymer active vibration control of a cantilever beam.
4. J. L. FANSON and T. K. CAUGHEY 1990 *AIAA Journal* **28**, 717-724. Positive position feedback control for large space structures.
5. A. BAZ, S. POH and J. FEDOR 1992 *ASME Journal of Vibration and Acoustics* **114**, 96-103. Independent modal space control with positive position feedback.
6. A. BAZ and J. RO 1993 *Conference of Engineering Sciences Society*, Charlottesville, VA. Partial treatment of flexible beams with active constrained layer damping.
7. A. BAZ and J. RO 1996 *Smart Materials and Structures* **5**, 272-280. Vibration control of plates with active constrained layer damping.
8. D. E. VELEY and S. S. RAO 1996 *Smart Materials and Structures* **5**, 660-671. A comparison of active, passive and hybrid damping in structural design.
9. B. AZVINE, G. R. TOMLINSON, R. J. WYNNE and O. SENSBURG 1994 *4th International Conference on Adaptive Structures*, Cologne. Vibration suppression of flexible structures using active damping
10. R. FIROOZIAN and R. STANWAY 1988 *Mechanical Systems and Signal Processing* **2**, 243-264. Active vibration control of turbomachinery: a numerical investigation of modal controllers.
11. P. AVITABILE, J. O'CALLAHAN and J. MILANI 1989 *7th IMAC*, 1109-1115. Comparison of system characteristics using various model reduction techniques.
12. J. E. MOTTERSHEAD and M. I. FRISWELL 1993 *Journal of Sound and Vibration* **167**, 347-375. Model updating in structural dynamics: a survey.

13. T. P. KHATUA and Y. K. CHEUNG 1973 *International Journal for Numerical Methods in Engineering* **6**, 11-24. Bending and vibration of multilayer sandwich beams and plates.
14. D. J. DAWE 1984 *Matrix and Finite Element Displacement Analysis of Structures* New York: Oxford University Press.
15. C. CHANTALAKHANA and R. STANWAY 1998 *Proceedings of the 4th European and 2nd MIMR Conference, Harrogate, UK*, 195-204. Control of plate vibrations using smart technology.
16. D. ROSS, E. E. UNGAR and E. M. KERWIN, Jr. 1959 *Structural Damping, Sec. 3, The American Society of Mechanical Engineers*. Damping of plate flexural vibrations by means of viscoelastic laminae.
17. D. J. INMAN and C. MINAS 1990 *Control and Dynamic Systems* **37**, 327-363. Matching analytical models with experimental modal data in mechanical systems.
18. B. PORTER and R. CROSSLEY 1972 *Modal Control Theory and Applications*. London: Taylor and Francis.
19. C. MINAS and D. J. INMAN 1989 *Transactions of the American Society of Mechanical Engineers, Journal of Vibration and Acoustics* **113**, 219-224. Identification of a nonproportional damping matrix from incomplete modal information.
20. R. J. GUYAN 1965 *AIAA Journal* **3**, 380. Reduction of stiffness and mass matrices.
21. V. N. SHAH and M. RAYMUND 1982 *International Journal for Numerical Methods in Engineering* **18**, 89-98. Analytical selection of masters for the reduced eigenvalue problem.
22. M. I. FRISWELL and J. E. MOTTERSHEAD 1995 *Finite Element Model Updating in Structural Dynamics*. The Netherlands: Kluwer Academic Publishers.

23. D. J. EWINS 1986 *Modal Testing: Theory and Practice*. Herts, England: Research Studies Press Ltd.
24. LMS 1993 *LMS CADA-PC User Manual*.
25. G. F. FRANKLIN, J. D. POWELL and M. WORKMAN 1998 *Digital Control of Dynamic Systems (3rd edition)*. California, USA.: Addison Wesley Longman, Inc.
26. J. B. BURL 1999 *Linear Optimal Control*. California, USA.: Addison Wesley Longman, Inc.
27. K. OGATA 1987 *Discrete-time Control Systems*. London: Englewood Cliffs, Prentice-Hall.
28. J. B. DABNEY and T. L. HARMAN 1996 *The Student Edition of SIMULINK*. New Jersey: Prentice Hall
29. Physik Instrumente (PI) Tutorial Manual. 1999 *Web page:*  
*<http://www.physikinstrumente.com/tutorial>*
30. A. M. SADRI, R. J. WYNNE and J. R. WRIGHT 1999 *Proceeding of the Institution of Mechanical Engineers*. **213**, 489-504. Robust strategies for active vibration control of plate-like structures: theory and experiment.

#### APPENDIX A: NOTATION.

$A_a$	cross-section area of the PZT actuator ( $m^2$ )
$b_a$	width of the PZT actuator (m)
$B_0$	input matrix ( $nxn$ )
$C$	measurement matrix ( $2mx2n$ )
$d_{31}$	piezoelectric constant ( $mV^{-1}$ )
$e_{13}$	ratio of the modulus of elasticity between the constraining layer and the base plate

$E_{1,3}$	modulus of elasticity of the constraining layer and the base plate respectively ( $\text{N/m}^2$ )
$E_a$	modulus of elasticity of the PZT actuator ( $\text{N/m}^2$ )
$f(t)$	force varied in time (N)
$\mathbf{f}$	input vector ( $n \times 1$ )
$G$	modulus of rigidity ( $\text{N/m}^2$ )
$\mathbf{G}$	gain matrix ( $n \times 2m$ )
$h_{1,2,3}$	thickness of the constraining layer, viscoelastic and base plate respectively (m)
$h_{23}, h_{13}$	thickness ratio between the viscoelastic layer and the base plate and the constraining layer and the base plate respectively
$\mathbf{I}$	identity matrix ( $r \times r$ )
$j, k, l, m, n, r$	integer
$\mathbf{M}_j, \bar{\mathbf{K}}_j$	mass and complex stiffness matrices for the $j$ th element ( $\text{kg}, \text{N/m}^2$ )
$\mathbf{M}, \mathbf{D}, \mathbf{K}$	global mass, damping and stiffness matrices ( $n \times n$ )
$\mathbf{M}^R, \bar{\mathbf{K}}^R$	reduced-order mass and complex stiffness matrices ( $r \times r$ )
$t$	time
$t_a$	thickness of the PZT actuator (m)
$u_{1k,3k}$	longitudinal displacement in $x$ axis at node $k$ of the rectangular element of the constraining layer and the base plate respectively (m)
$\mathbf{U}$	eigenvector matrix ( $2r \times 2r$ )
$v_{1k,3k}$	longitudinal displacement in $y$ axis at node $k$ of the rectangular element of the constraining layer and the base plate respectively (m)
$V(t)$	applied voltage across the PZT actuator (Volt)
$w_k$	transverse displacement in $z$ axis at node $k$ of the rectangular element (m)
$\frac{dw}{dy}_k, \frac{dw}{dx}_k$	rotational displacement about $x$ axis and $y$ axis respectively (rad)
$\mathbf{Y}$	state vector ( $2r \times 1$ )
$\mathbf{Z}^R, \mathbf{K}^R$	reduced-order imaginary and real terms, respectively, of the complex stiffness matrices ( $r \times r$ )

$\eta$	loss factor of viscoelastic layer
$\nu_3$	Poisson ratio of the base plate
$\rho_3$	density of the base plate ( $\text{kg/m}^3$ )
$\sigma_a$	stress developed in the PZT actuator ( $\text{N/m}^2$ )
$\xi$	modal co-ordinate vector ( $2r \times 1$ )
$\Lambda$	eigenvalue matrix ( $2r \times 2r$ )
$\Delta_j$	displacement vector of the rectangular element $j$ ( $28 \times 1$ )
$\Delta \mathbf{A}_{1,2}$	mass-normalised correction matrices for the damping and stiffness matrices respectively
$i$	complex operator, $\sqrt{-1}$
$[ ]^T$	denotes matrix transpose
$[ ]^{-1}$	denotes matrix inverse
$[ ]^*$	denotes complex conjugate matrix transpose
$[ ]_c$	subscript for controlled terms
$[ ]_u$	subscript for uncontrolled terms
$[\dot{x}]$	denotes differentiation of $x$ variable with respect to time

## **APPENDIX E**

**COPY OF A PAPER SUBMITTED TO  
SMART MATERIALS AND STRUCTURES**

TITLE:  
ACTIVE CONSTRAINED LAYER DAMPING OF PLATE VIBRATIONS:  
A NUMERICAL AND EXPERIMENTAL STUDY OF MODAL CONTROLLERS

AUTHORS:  
C. CHANTALAKHANA AND R. STANWAY\*

ADDRESS:  
*Department of Mechanical Engineering, University of Sheffield, Mappin Street  
Sheffield S1 3JD, United Kingdom*

THIS PAPER CONTAINS 36 PAGES, 4 TABLES AND 25 FIGURES.

SUMMARY

In this paper the authors address the problem of suppressing the vibrations of a clamped-clamped plate using an active constrained layer damping treatment. This treatment involves adding viscoelastic and metallic constraining layers to the host plate and then augmenting this arrangement with an active feedback scheme using piezo-electric actuators. The basis of the control strategy is an effective model of the plate together with the passive damping treatment. The paper summarises the modelling procedures including the finite element formulation, model reduction and model updating. By this means a low-order model, capable of accounting for observed behaviour, is developed.

Emphasis is placed upon the design and implementation of active modal controllers based upon the reduced and updated model. Four actuator/sensor configurations are examined in both numerical and experimental studies. It is shown that effective control of the first two modes of vibration (bending and torsion) can be achieved using only a single actuator and single sensor. However, the most effective configuration involves two actuators and two sensors operating as two independent control channels. It is shown that through suitable design, the active constrained layer damping treatment is capable of avoiding problems due to spillover effects.

---

\* Author to whom correspondence should be addressed.

## 1. INTRODUCTION

A previous study by Azvine and his colleagues (1994) examined the vibrations of a clamped-clamped plate using an active constrained layer damping treatment (ACLD). The plate was a simplified version of an instrument box cover found in a military aircraft. Excessive bending and torsional vibrations were causing the instrument box to malfunction in service. Consequently, Azvine's brief was to investigate ACLD treatments as a means of suppressing these undesirable levels of vibration.

The ACLD approach involves augmenting a conventional passive constrained layer damping treatment with active control, the latter typically implemented using piezoelectric actuators. The feasibility of applying an ACLD treatment was demonstrated by Baz and Ro (1993) who initially examined a cantilevered beam before progressing to more complex structures such as a cantilevered plate (Baz and Ro, 1996). It is now well established that the passive constrained damping layer is effective at suppressing higher frequency modes of vibration while the active scheme can be designed to suppress the lower frequency modes. Furthermore the presence of the passive treatment introduces sufficient inherent damping so as to minimise the influence of spillover effects which are liable to degrade or even de-stabilise mechanical structures under active control. A recent study (Velez and Rao, 1996) compared ACLD treatments with purely active and purely passive schemes using both a cantilevered beam and a plate clamped on all four sides. It was shown that the ACLD is superior to active schemes in that desired levels of damping can be introduced using with significantly less additional weight.

Whereas there remains little doubt about the capabilities of ACLD as an effective technique for vibration control of thin-walled structures, there is still considerable scope for the development of control algorithms. In particular, the study by Azvine et al (1994)

demonstrated the need for improved models of the host plate, the viscoelastic and constraining layers and a more effective control algorithm based upon the use of these models.

A previous paper by the present authors (Chantalakhana and Stanway, 2000) described a technique for modelling the clamped-clamped plate and showed preliminary experimental results using a modal controller based upon the improved model. In what follows here, the authors will summarise the modelling procedures before focusing on a comprehensive series of numerical and experimental investigations into control of the plate vibrations.

## **2. SUMMARY OF MODELLING PROCEDURES**

### **2.1 Introduction**

It was decided at the outset to develop a model-based approach to controlling the vibrations of the clamped-clamped plate. The starting point was a finite-element of the host plate extended to account for the behaviour of the added viscoelastic and metallic constraining layers. To obtain a model suitable as the basis for controller design, it was necessary to apply model reduction techniques. In order to obtain sufficiently close correspondence between the predictions of the reduced-order model and experimental measurements, it was necessary to apply model updating algorithms. The modelling procedures are described in detail by Chantalakhana and Stanway (2000) and are summarised in the sub-sections which follow.

## 2.2 Clamped-clamped plate: physical arrangement

The basic experimental facility is shown in Figure 1. Essentially the plate is made of aluminium and has the dimensions 2.5 mm × 305 mm × 490 mm and is firmly clamped along the two shorter sides. To the host plate was added a viscoelastic layer (3M Company, type ISD112) of thickness 50.8 μm (0.002 in). A steel shim of thickness 254 μm (0.010 in) was used as the constraining layer. The material properties for all three layers are given in Table 1. For preliminary experiments to examine the dynamics of the plate, a single shaker and accelerometer were located at node 7, as shown in Figure 1. With this arrangement it was established that at least ten modes of vibration could be excited and detected.

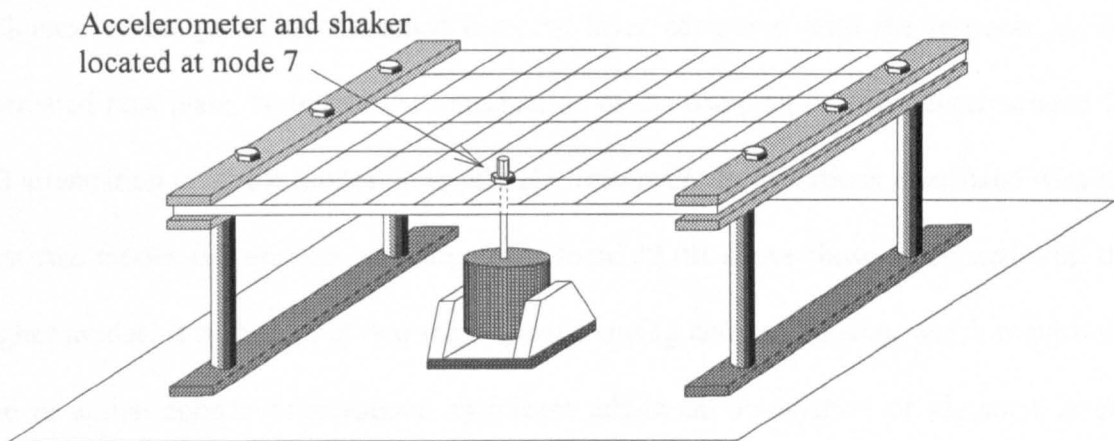


**Figure 1.** Experimental arrangement of the clamped-clamped plate for passive constrained layer damping experiments

**Table 1**

Material properties of three-layer plate

Material	modulus of elasticity (MPa)	modulus of rigidity (MPa)	density (kg/m <sup>3</sup> )	Poisson's ratio	shear loss factor
aluminium plate	70x10 <sup>3</sup>	-	2700	0.3	-
ISD112 viscoelastic layer	29.8*	20*	1140	0.49	1.0*
steel constraining layer	200x10 <sup>3</sup>	-	7000	0.3	-

\* at the centre frequency of 600 Hz

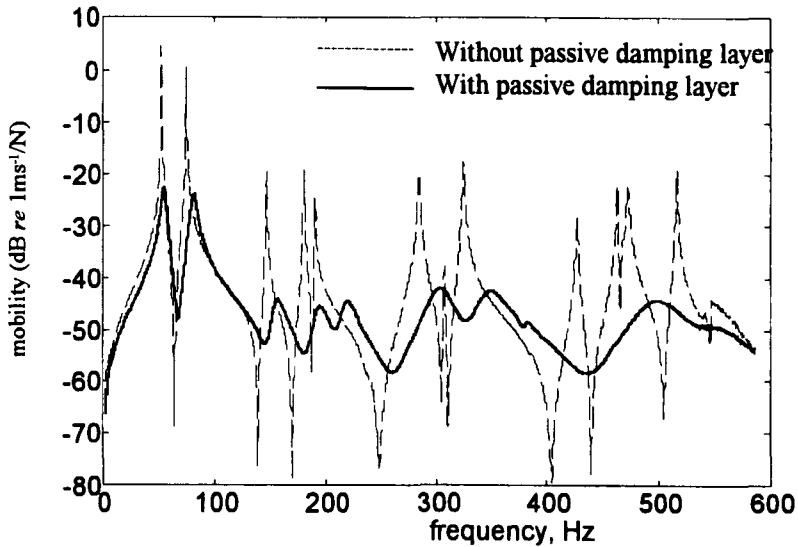


**Figure 2.** Measured FRFs of the panel plate with and without constrained damping layer

Figure 2, which was generated during the preliminary experiments, shows the influence of the passive constrained damping layer compared with the response of the untreated host plate. Note that the introduction of the damping layer produces around 25 dB attenuation of all the modes up to 600 Hz. However, the vibrations associated with the first two modes still produce mobility peaks some 20 dB above those associated with the higher modes. It is these first two modes, one bending and one torsion, which require the use of active control to introduce significant additional attenuation of vibration levels. Before proceeding to describe active constrained layer damping it is necessary to refine the finite element model of the passively damped plate.

### 2.3 Finite element model

The finite element modelling technique follows the approach described by Baz and Ro (1996). Rectangular elements are used and at each node there are 7 degrees of freedom, 4

longitudinal, 1 transverse and 2 rotational displacements. The equation of motion is formed as

$$\mathbf{M}_j \ddot{\Delta}_j + \overline{\mathbf{K}}_j \Delta_j = \mathbf{F}_j \quad (1)$$

where  $\mathbf{M}_j$  and  $\overline{\mathbf{K}}_j$  are, respectively, the mass and stiffness matrices of element  $j$  and  $\mathbf{F}_j$  is an external force vector acting at the  $j^{\text{th}}$  element. Note that  $\overline{\mathbf{K}}$  is a complex stiffness matrix whose imaginary term serves as a loss energy or damping term. Full details of the formulation and validation of this finite element model are given by Chantalakhana and Stanway (1998). A comparison between the predicted FRF from the finite element model and the FRF measured experimentally, Figure 3, shows that the response levels predicted by the model are consistent with the results from the experiments. However, note that the predicted natural frequencies are shifted to the right of the experimental results. Figure 4 shows the first six mode shapes of the clamped-clamped plate obtained from solving eigensolutions of Equation (1) in which the plate is divided as 9 by 6 elements along the length and width directions, respectively.

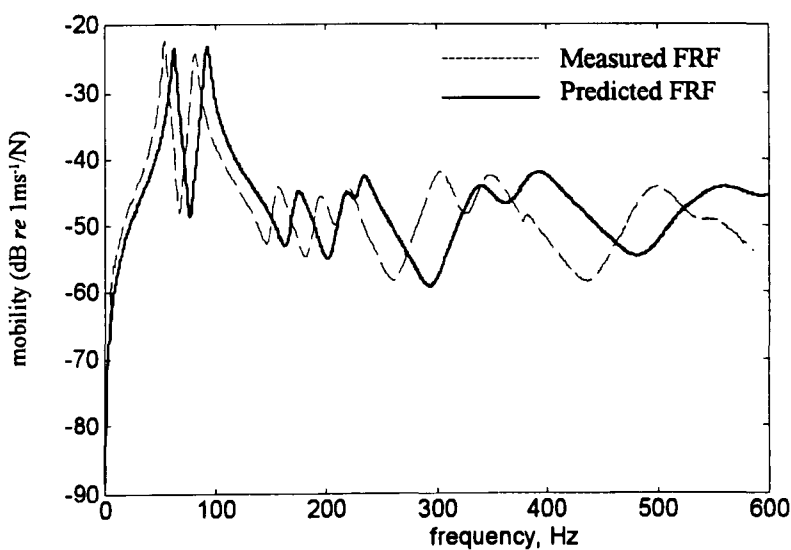


**Figure 3.** Measured and predicted FRFs (point mobility, the same point for acting force and velocity response) of the panel plate covered with constrained damping layer

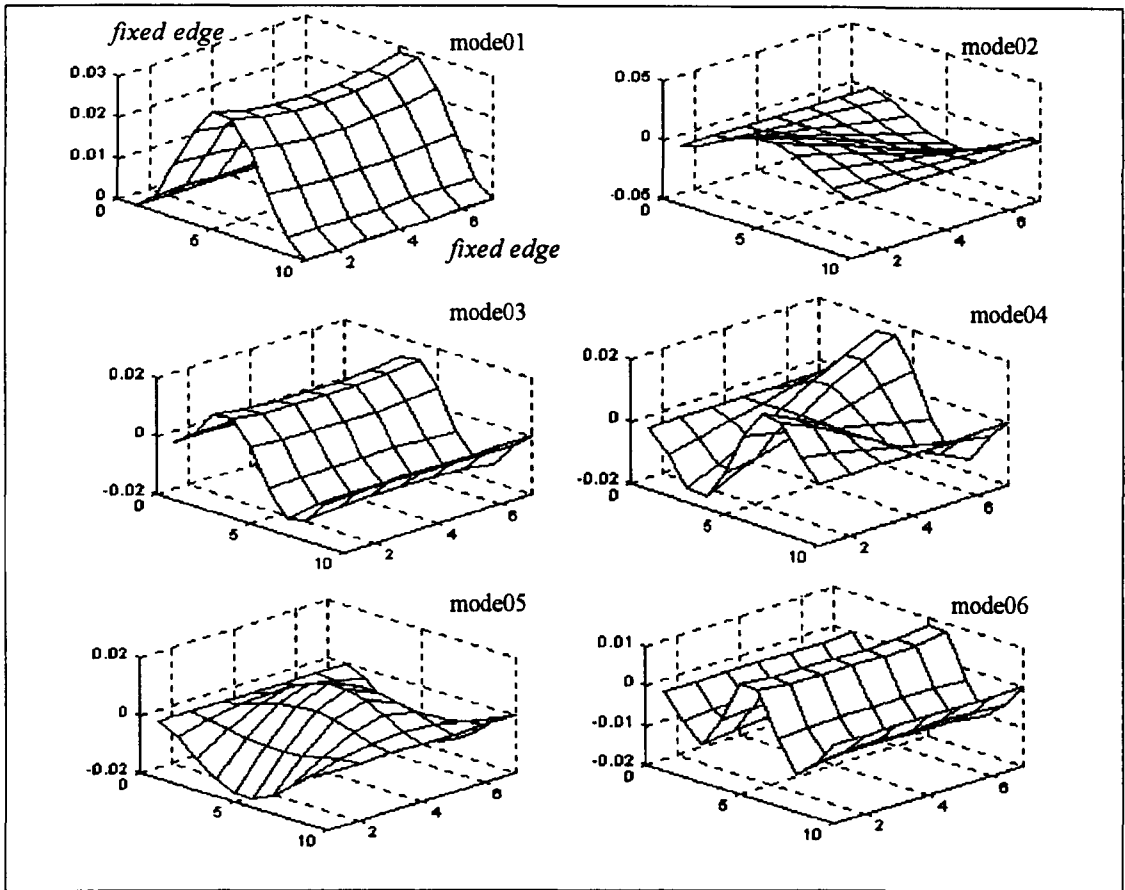


**Figure 4.** The first six mode shapes of the clamped-clamped plate

## 2.4 Model updating

It was noted in sub-section 2.3 that the FRF predicted by the finite element model is shifted to the right of the experimental FRF. In order to produce a closer match between predicted and observed FRFs, a model updating procedure was applied. The algorithm used, based upon a pole placement technique, was originally described by Inman and Minas (1990), where full details can be found.

This model updating algorithm requires that the imaginary term in the complex stiffness matrix  $\bar{\mathbf{K}}$ , in Equation (1), be transformed to a viscous damping matrix. A complication arises in that the resulting viscous damping coefficients are frequency dependent. The algorithm used to achieve this damping transformation was adapted from

work by Minas and Inman (1989). Although the transformation is straightforward in principle, difficulties arose in the present application owing to the dimensions of the matrices which are involved. Essentially, the pseudo-inverse of an over-determined system of linear equations incorporating a  $2n^2 \times (n^2+n)/2$  order matrix needs to be computed. Given that the number of degrees of freedom,  $n$ , in the original finite element model is 420, it was necessary to reduce the size of the mass and complex stiffness matrices in Equation (1) before implementing the transformation.

The Guyan technique (1965) was used for model reduction. In this way the number of degrees of freedom was reduced from 420 to 36. Figure 5 shows selected nodes and displacements nominated for the reduced-order model. The master nodes in the reduced-order model were chosen to ensure an adequate reduced-order model over bandwidth of interest and also to maintain correspondence with the measurement locations used in the subsequent experimental work.

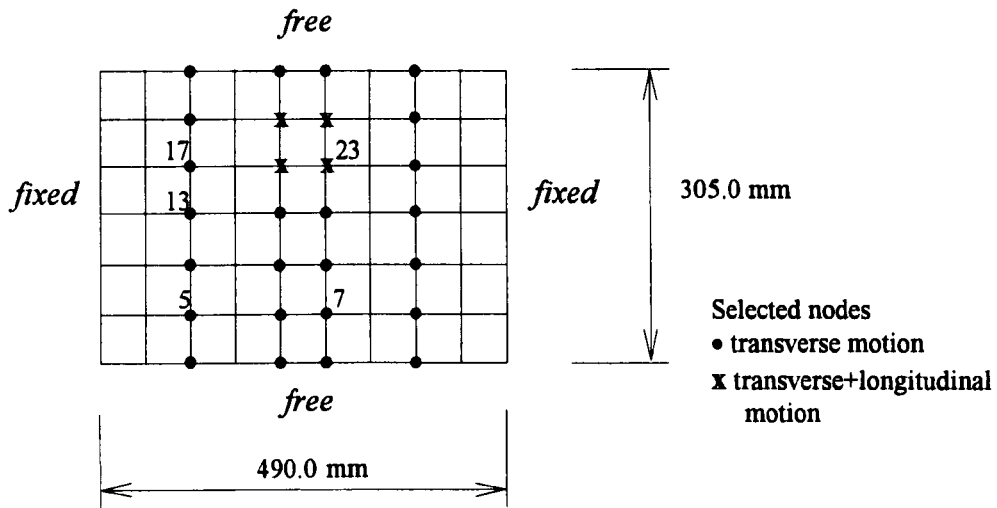


**Figure 5.** Division of plate to finite elements and selected nodes for model reduction

Following model reduction and transformation of the complex stiffness matrix,  $\bar{\mathbf{K}}$ , model updating was applied to improve correspondence between predicted and observed

FRFs. The updating procedure requires estimates of the natural frequencies and damping factors obtained from the experimental facility. Since the modes of the clamped-clamped plate are well separated, it is possible to use a peak-picking method to identify the natural frequencies and damping ratios (LMS, 1993). Table 2 gives the identified natural frequencies and percentage damping factors of the first 6 modes compared with those predicted by the finite element model. These predictions were obtained from the reduced model (of order  $r$ ) which is to be updated with the eigenvalues of the full plate model (of order  $n$ ).

**Table 2**  
 Measured and predicted first six natural frequencies  
 and damping factors of three-layer plate

mode	1	2	3	4	5	6
predicted natural frequency (Hz)	62.50	92.23	172.93	217.07	233.02	339.06
measured natural frequency (Hz)	54.53	81.50	157.47	195.59	220.60	304.02
predicted % damping	3.50	3.05	3.81	3.87	2.83	4.86
measured % damping	3.44	3.51	4.13	3.66	3.41	3.57

A typical result of model updating is shown in Figure 6. This result shows that the first six modes in the predicted FRFs are concurrent with the measured FRFs. Higher modes are not updated and thus remain unchanged. In the sections which follow, it will be shown that the updated model forms a suitable basis for the design of an active modal controller which complements the damping introduced by the passive constrained layer treatment.

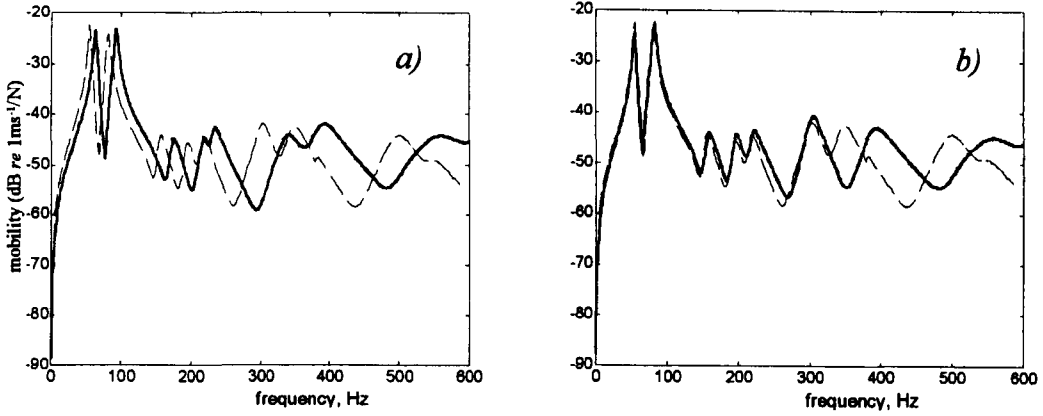


**Figure 6. FRF7\_7 a) before updating  
b) after updating the model**

### 3. CONTROL AND NUMERICAL EXPERIMENTS

#### 3.1 Modal control

The well-established finite element model of three-layer plate summarised in the previous section, will be used here as the basis for the design of active control schemes. The number of degrees of freedom of the model has been reduced by eliminating insignificant variables. The model has also been updated so that observed behaviour of the test plate matches the model predictions. Modal control via pole placement is the method to be used for control. Spillover effects and their avoidance are emphasised.

##### 3.1.1 State-space equations

For a finite element plate model reduced to  $r$  degrees of freedom, the corresponding state-space equation of motion can be written as a set of  $2r$  first order differential equations :

$$\begin{Bmatrix} \ddot{\Delta} \\ \dot{\Delta} \end{Bmatrix} = \begin{bmatrix} \mathbf{0} & \mathbf{M}^R \\ \mathbf{M}^R & \mathbf{D}^R \end{bmatrix}^{-1} \begin{bmatrix} \mathbf{M}^R & \mathbf{0} \\ \mathbf{0} & -\mathbf{K}^R \end{bmatrix} \begin{Bmatrix} \dot{\Delta} \\ \Delta \end{Bmatrix} + \begin{bmatrix} \mathbf{0} & \mathbf{M}^R \\ \mathbf{M}^R & \mathbf{D}^R \end{bmatrix}^{-1} \begin{Bmatrix} \mathbf{0} \\ \mathbf{F} \end{Bmatrix} \quad (2)$$

where  $\Delta$  is an  $r \times 1$  displacement vector,  $\mathbf{M}^R$ ,  $\mathbf{D}^R$  and  $\mathbf{K}^R$  are  $r \times r$  the reduced-order mass, damping and stiffness matrices, respectively, and  $\mathbf{F}$  is an  $r \times 1$  force vector acting at the

nodal displacements. For the special case of a single input force, Equation (2) may be written in the form

$$\dot{\mathbf{Y}} = \mathbf{A}\mathbf{Y} + \mathbf{b}f \quad (3)$$

where  $\mathbf{Y}_{2r \times 1} = [\dot{\Delta}^T \quad \Delta^T]^T$ ,  $\mathbf{A}_{2r \times 2r}$  is a plant matrix,  $\mathbf{b}_{2r \times 1}$  is an input vector or  $\mathbf{b} = [(\mathbf{M}^{-1}\mathbf{F})^T \quad \mathbf{0}]^T$  and  $f$  is a scalar input. Let  $\mathbf{Y} = \mathbf{U}\boldsymbol{\xi}$ , where  $\boldsymbol{\xi}_{2r \times 1}$  is a modal state variable vector and  $\mathbf{U}_{2r \times 2r}$  is a transformation matrix containing  $2r$  columns of the eigenvectors of  $\mathbf{A}$ . After substituting this transformation into Equation (3) and pre-multiplying by  $\mathbf{U}^{-1}$ , then Equation (3) becomes

$$\dot{\boldsymbol{\xi}} = \boldsymbol{\Lambda}\boldsymbol{\xi} + \mathbf{w}f \quad (4)$$

where  $\boldsymbol{\Lambda} = \mathbf{U}^{-1}\mathbf{A}\mathbf{U}$  is a diagonal matrix containing  $2r$  eigenvalues of  $\mathbf{A}$  along its diagonal elements,  $\mathbf{w} = \mathbf{U}^{-1}\mathbf{b}$  is a modal controllability vector in which an element  $j$  of  $\mathbf{w}$  quantifies controllability of the  $j$ th mode by the input  $f$ . This transformation results in the decoupling of Equation (3). If Equation (4) is partitioned as  $c$  controlled mode equations and  $u$  residual or uncontrolled mode equations, then Equation (4) can be rearranged as

$$\begin{Bmatrix} \dot{\boldsymbol{\xi}}_c \\ \dot{\boldsymbol{\xi}}_u \end{Bmatrix} = \begin{bmatrix} \boldsymbol{\Lambda}_c & \mathbf{0} \\ \mathbf{0} & \boldsymbol{\Lambda}_u \end{bmatrix} \begin{Bmatrix} \boldsymbol{\xi}_c \\ \boldsymbol{\xi}_u \end{Bmatrix} + \begin{Bmatrix} \mathbf{w}_c \\ \mathbf{w}_u \end{Bmatrix} f \quad (5)$$

The  $c$  eigenvalues can be shifted to their desired values by feeding back the vector of state variables  $\boldsymbol{\xi}_c$ , as a scalar input  $f$  with appropriate weightings

$$f = \mathbf{k}_c^T \boldsymbol{\xi}_c \quad (6)$$

where  $\mathbf{k}_c$  is a  $c \times 1$  gain vector.

Note that substitution of Equation (6) into Equation (5) results in force coupling in the system equation due to a coupling input matrix  $(\mathbf{w}_c \mathbf{k}_c^T)_{c \times c}$ . Modal decomposition attempts to decouple a system of equations so that each mode can be controlled independently. The force coupling effect results in the benefit of simultaneous control of

several modes with possibly a single actuator where the controllability element  $j$ , corresponding to the  $j$  th controlled mode, is non-zero.

### 3.1.2 State estimator

The scalar feedback input  $f$  in Equation (6) is formed from the modal state variable vector  $\xi_c$  which needs to be computed from physical measurements. If  $\mathbf{z}_{lx1}$  is a vector of physical observations where  $l$  is a number of available measurements, the relationship between this vector and the vector of physical co-ordinates  $\mathbf{Y}_{2rx1}$  is

$$\mathbf{z} = \mathbf{L}\mathbf{Y} \quad (7)$$

where  $\mathbf{L}_{lx2r}$  is an output matrix. In modal co-ordinates, Equation (7) becomes

$$\mathbf{z} = \mathbf{L}\mathbf{U}\xi \quad (8)$$

or

$$\mathbf{z} = \left[ \mathbf{H}_c^T \quad \mathbf{H}_u^T \right] \begin{Bmatrix} \xi_c \\ \xi_u \end{Bmatrix}. \quad (9)$$

An observability vector can be defined at this stage as  $\mathbf{v} = \mathbf{U}^T \mathbf{L}^T$  which the  $j$  th element in the vector represents the observability of a modal state variable  $\xi_j$ . Using with Equations (6) and (9), a set of  $c$  controlled mode equations defines the modal state estimator :

$$\hat{\xi}_c = (\Lambda_c + \mathbf{w}_c \mathbf{k}_c^T) \hat{\xi}_c + \Phi(\mathbf{z} - \mathbf{h}(\hat{\xi}_c, t)) \quad (10)$$

where  $\hat{\xi}_c$  is the estimate of  $\xi_c$ ,  $\mathbf{h}(\hat{\xi}_c, t) = \mathbf{H}_c^T \hat{\xi}_c$  is the estimate of  $\mathbf{z}$ , and  $\Phi_{cxl}$  is a weighting matrix.

### 3.1.3 Spillover effects

Balas (1978) showed that using a reduced set of equations for the controller and estimator causes, respectively, control and observation spillover. A scalar input force  $f$  can excite

the controllable residual modes (see Equation (5)) because of the force coupling which is present. Similarly, Equation (10) shows that if the measurement signal includes terms from the residual state variable  $\xi_u$ , then the estimator is contaminated by values of  $\Phi(\mathbf{H}_u^T \xi_u)$ . These spillover effects can cause instability in the controlled structure. However, these effects can be reduced by keeping the elements of gain vector  $\mathbf{k}_c^T$  and the weighting matrix  $\Phi$  low. Optimal designs such as the linear quadratic regulator and Kalman filter (Franklin et al, 1998) can be used to achieve the low gains. Placement of actuator and sensor should be close to the nodal lines of residual modes so that the residual modes are not significantly excited and the residual state variables in  $\xi_u$  are not strongly observed.

### 3.1.4 Control law and estimator design

#### *Continuous-time design*

For the state-space equations with a single input and single output, the control gain vector  $\mathbf{k}_c^T$  (see Equation (6)) and weighting gain vector  $\Phi$  (see Equation (10)) can be assigned using a pole placement technique. However, to optimise actuator power consumption and damping of the assigned modes, Linear Quadratic Regulator (LQR) and Gaussian (LQG) algorithms are used to obtain optimal control and estimator gains, respectively, so that the spillover effects are not sufficient to destabilise the actively controlled system. The LQR is the solution provided by solving a general optimal control problem to find the control gains. However, a drawback is that the entire set of state variables must be measured. The LQG controller is provided by the solution of an extended optimal control problem where white noise disturbance inputs are included and incomplete state measurements can be

used to construct the full state vector through computing the appropriate estimator gains (Burl, 1999). The LQR design is aimed at minimising the cost function

$$\mathbf{J} = \int (\xi' \mathbf{Q} \xi + f' \mathbf{R} f) dt \quad (11)$$

where  $\mathbf{Q}$  and  $\mathbf{R}$  are weighting matrices. One choice of  $\mathbf{Q}$  and  $\mathbf{R}$  is to make them symmetrical (semi-symmetrical for  $\mathbf{Q}$ ) positive definite matrices. For a SISO modal state-space equation,  $\mathbf{R}$  is a scalar and can be set to unity while  $\mathbf{Q}$  is of the form

$$\begin{bmatrix} a_1 & \cdots & \cdots & 0 \\ \vdots & a_1 & & \vdots \\ \vdots & & a_2 & \vdots \\ 0 & \cdots & \cdots & a_2 \end{bmatrix} \quad (12)$$

where  $a_1$  and  $a_2$  are real constants, chosen so as to maintain two pairs of complex conjugate eigenvalues. Increasing  $a_1$  and  $a_2$  results in an increase in the damping of the assigned eigenvalues which correspond to the original modes 1 and 2 respectively. The control gains must not be so high such that control spillover affects the results. The influence of a truncated model on the assigned eigenvalues of a closed-loop system will be discussed later.

Traditionally the estimator gains are chosen to provide poles to the left of the assigned poles in the left-hand half of the  $s$ -plane. Equations (5), (6) and (10) can be rewritten in terms of the error of the estimation process

$$\dot{\mathbf{e}} = \left( \hat{\xi}_c - \dot{\xi}_c \right) = \left( \Lambda_c - \Phi \mathbf{H}_c^T \right) \mathbf{e} + \Phi \mathbf{H}_u^T \xi_u \quad (13)$$

The decay of the estimator error is thus dependent on the eigenvalues of  $(\Lambda_c - \Phi \mathbf{H}_c^T)$ . If the estimator gains are chosen to be high so as to achieve rapid decay of the error terms, then contamination of the uncontrolled modes is also amplified, resulting in a significant observation spillover effect. The effect of spillover on the assigned close-loop poles can be studied by considering Equations (5), (6) and (13) (a combination of a modal state-space

equation involving the controlled modes, uncontrolled modes and state estimation error (Balas, 1978)):

$$\begin{Bmatrix} \dot{\xi}_c \\ \mathbf{e} \\ \dot{\xi}_u \end{Bmatrix} = \begin{bmatrix} \Lambda_c + \mathbf{w}_c \mathbf{k}_c^T & \mathbf{w}_c \mathbf{k}_c^T & \mathbf{0} \\ \mathbf{0} & \Lambda_c - \Phi \mathbf{H}_c^T & \Phi \mathbf{H}_u^T \\ \mathbf{w}_u \mathbf{k}_c^T & \mathbf{w}_u \mathbf{k}_c^T & \Lambda_u \end{bmatrix} \begin{Bmatrix} \xi_c \\ \mathbf{e} \\ \xi_u \end{Bmatrix}. \quad (14)$$

As indicated in sub-section 3.1.3, the assigned eigenvalues are disturbed by the residual terms of the observation signal. Both the actual closed-loop eigenvalues and the stability of the control system including spillover effects can be investigated by obtaining the eigensolutions of Equation (14).

#### *Discrete-time design*

In the discrete-time domain, the controlled mode state-space equations of motion corresponding to Equation (5) can be obtained from (for example, see Ogata, 1987)

$$\Lambda_c^d = e^{\Lambda_c T_s}, \mathbf{w}_c^d = (e^{\Lambda_c T_s} - \mathbf{I}) \Lambda_c^{-1} \mathbf{w}_c \quad (15)$$

where  $\Lambda_c^d$  is the discrete-time form of  $\Lambda_c$  and  $T_s$  is sampling time. An advantage of controller design in modal co-ordinates is that the exponential of the plant matrix  $\Lambda_c$  is straightforward to compute because it contains only diagonal elements. Elements in the discrete-time control gain  $\mathbf{k}_c^T$  are then calculated from (Porter and Crossley, 1972)

$$k_j^d = \frac{\prod_{k=1}^c (\exp(\rho_k T_s) - \exp(\lambda_j T_s))}{\left( \mathbf{w}_{c,j}^d \prod_{\substack{k=1 \\ k \neq j}}^c (\exp(\lambda_k T_s) - \exp(\lambda_j T_s)) \right)} \quad j=1,2,\dots,c \quad (16)$$

where  $\lambda_{j,k}$  is eigenvalue of the mode to be controlled,  $\rho_k$  is assigned eigenvalues obtained from the LQR design,  $c$  is the number of controlled modes and  $w_{c,j}^d$  is the  $j$  th element of  $w_c^d$ . The estimator state-space equation (Equation (10)) is rewritten here

$$\hat{\xi}_c(t) = (\Lambda_c - \Phi H_c^T) \hat{\xi}_c(t) + \Phi z(t) + w_c f(t) \quad (17)$$

For compactness, define  $\bar{G} = (\Lambda_c - \Phi H_c^T)$ . Then the discrete-time estimator takes the form

$$\hat{\xi}_c(k+1) = \bar{G}^d \hat{\xi}_c(k) + \Phi^d z(k) + \bar{w}_c^d f(k) \quad (18)$$

where  $\bar{G}^d = e^{\bar{G}T_s}$ ,  $\Phi^d = (e^{\bar{G}T_s} - \mathbf{I})\bar{G}^{-1}\Phi$ ,  $\bar{w}_c^d = (e^{\bar{G}T_s} - \mathbf{I})\bar{G}^{-1}w_c$  and  $k$  is the sampling index. From Equations (15) to (18), the discrete modal controller can be formulated to implement digital control used in the following section.

### 3.2 Description of numerical experiments

Numerical simulations of an actively controlled system were performed to investigate the performance of the controller designs. In what follows, various configurations of control device arrangement are examined using simulation procedures. A series of simulation results is given and will be compared with experimental results in the next section.

#### Configuration 1: a single PZT actuator and single accelerometer

Plots of mode shapes were considered and the sensor and actuator were chosen to occupy the middle of the upper half portion of the plate as illustrated in Figure 7. The dimensions of the PZT actuator were chosen based upon the results obtained by finite element modelling and experimental observations. A 50 mm × 50 mm PZT patch was used as the actuator. A square shape of PZT patch results in generating forces in both  $x$  and  $y$

directions (Figure 7). With this location, the sensor and actuator, respectively, detect and excite the maximum transverse displacements associated with the first two modes whilst also keeping to the nodal lines of the higher modes so as to minimise spillover effects. Modal controllability and observability vectors were also used to refine the choices of the sensor and actuator locations (Chantalakhana and Stanway, 2000). The disturbance (shaker position) and measurement points are at points 7 and 23, respectively, on the three-layer test plate as shown in Figure 7. The control excitation is applied to a PZT actuator placed in the middle of upper portion of plate. The controller and estimator gains are designed to produce high damping of the first two eigenvalues and to ensure stability of the closed-loop system in the face of spillover effects. The assigned eigenvalues, along with controller and estimator gains are given in Table 3. The assigned poles are obtained by using the LQR design to minimise the control gain and to achieve high damping. The LQG design is used to obtain the optimal estimator gain such that the error from estimation decays faster than the response due to the assigned poles. The main consideration in designing the controller is to minimise spillover problems. The complete closed-loop control system for numerical experiments, is shown in Figure 8.

In controller design, the control law and estimator are implemented using complex numbers - a formulation which is not suitable for experimental implementation by real-time digital control. To overcome this problem, the state-space estimator equation is converted to its transfer function form so that real and imaginary terms can be computed separately in terms of real numbers, as illustrated in Figure 8. This significantly reduces the number of lines required for program execution and results in faster calculations for real-time control.

**Table 3**

Poles and corresponding gains of controller and estimator

mode	original poles(rad/s)	assigned poles(rad/s)	control gain	estimator gain
1	$-11.78 \pm 343i$	$-105.6 \pm 339i$	$-4.88 \pm 5.61I$	$-1313 \pm 387i$
2	$-17.96 \pm 512i$	$-74.6 \pm 498i$	$5.08 \pm 3.80I$	$-720 \pm 302i$

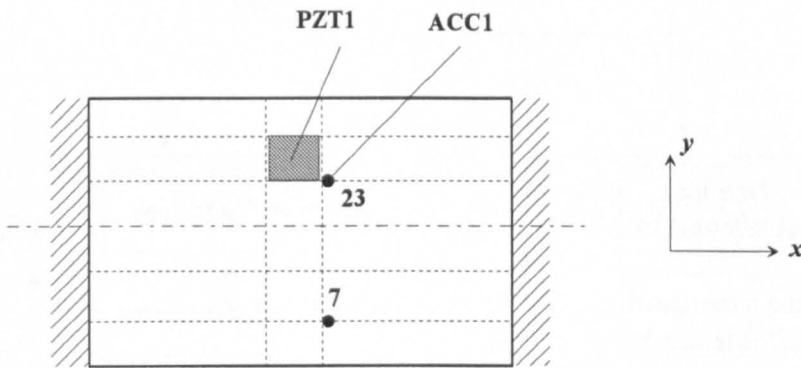
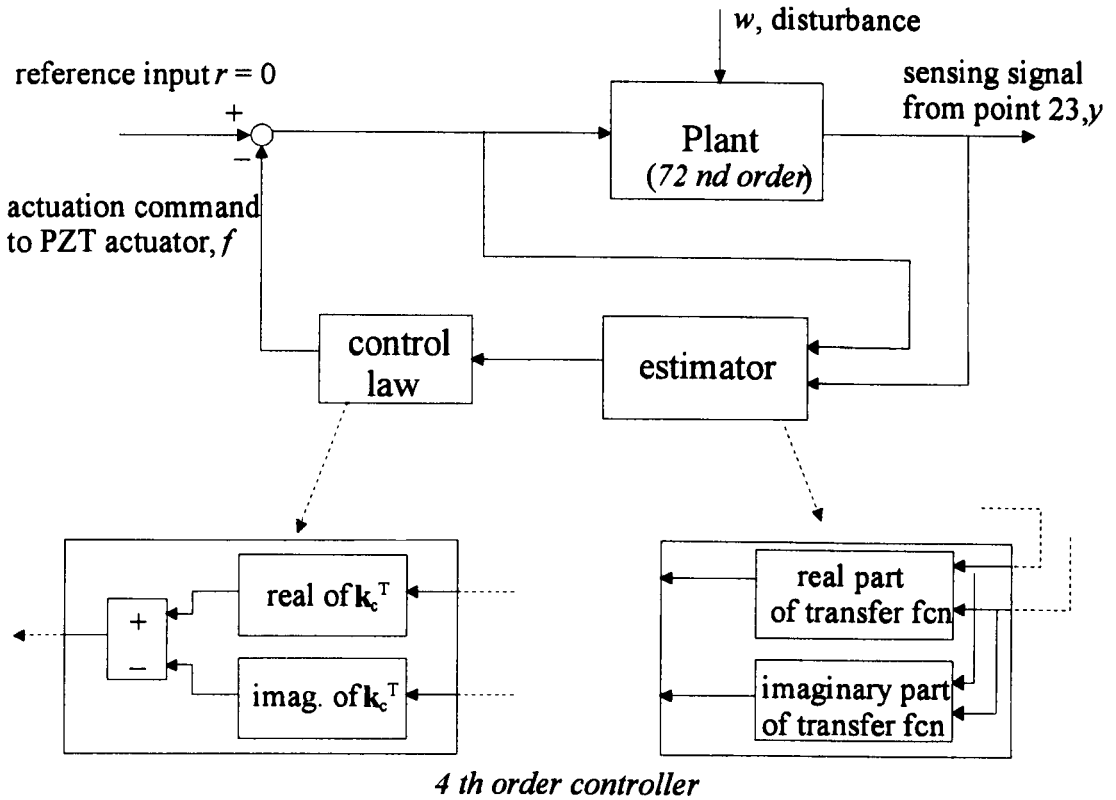


**Figure 7.** Arrangement of the clamped-clamped plate with a square PZT element used as actuator, an accelerometer for sensing at point 23 and shaker location at point 7 used in simulation of active constrained layer damping



### Implementing a complex number controller using real

**Figure 8.** Block diagram of digital control simulation to match with real-time interface using SIMULINK software

For the numerical simulations, a 72<sup>nd</sup>-order plant equation together with a truncated, 4<sup>th</sup>-order controller is used to investigate the performance of active controlled system and the influence of spillover effects. FRFs from numerical simulations of the SISO configuration of the actively controlled system shown in Figure 7 are plotted in Figure 9 where notation FRF7\_23 is referred to disturbance and measurement locations at points 7 and 23 respectively. Compared to the passively damped plate, the FRF of the actively controlled one shows significant attenuation of vibration levels of the first two modes. However, higher frequency modes tend to be excited so that their amplitudes increase

slightly. Experimental verification of the simulation results and study of other control configurations to obtain effective performance and overcome spillover effects are presented in the following sub-section where simulation procedures described in this section will be used to obtain numerical results for a comparison with experimental results in the next section.

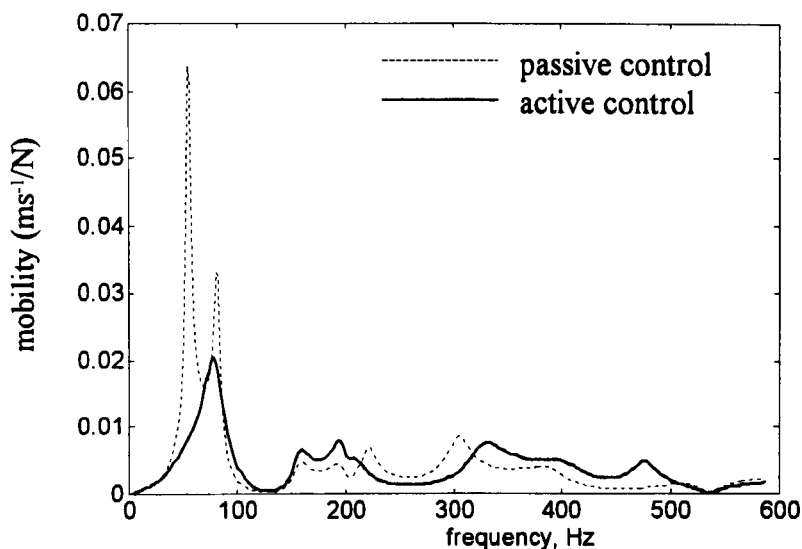


**Figure 9.** Simulation results: predicted FRFs (FRF7\_23) of three-layer plate with and without active control for a single PZT actuator and a single accelerometer

**Configuration 2:** a PZT actuator operating in the  $x$  direction only

In configuration 1, a 50 mm  $\times$  50 mm element of PZT material was used as an actuator which operates in both the  $x$  and  $y$  directions. In principle, the intention of the active control strategy is to increase the induced shear strain in the  $x$  direction where bending curvature of the first two modes occur. Actuation of the PZT actuator in the  $y$  direction causes an excessive load of the actuator and may excite higher frequency modes of vibration as already shown in Figures 9. To activate the PZT actuator in the  $x$  direction only, the length of the PZT should be longer than 3.5 times their width and thickness

(Morgan Matroc, 1999). Thus, a 50 mm × 50 mm PZT patch is cut into 4 strips of equal width and attached to the plate as shown in Figure 10.

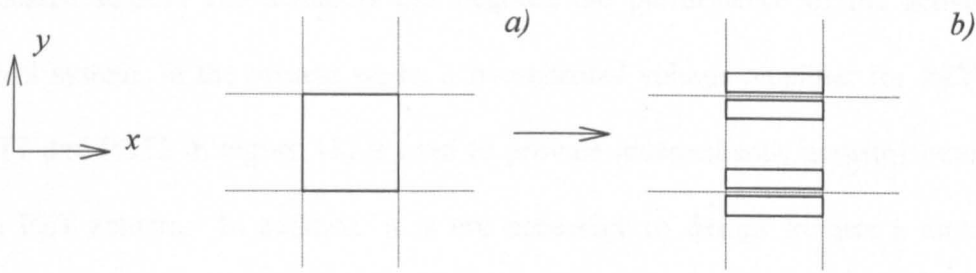


**Figure 10.** Configuration of PZT actuator  
 a) for operation in  $x$  and  $y$  directions  
 b) for operation in  $x$  direction only

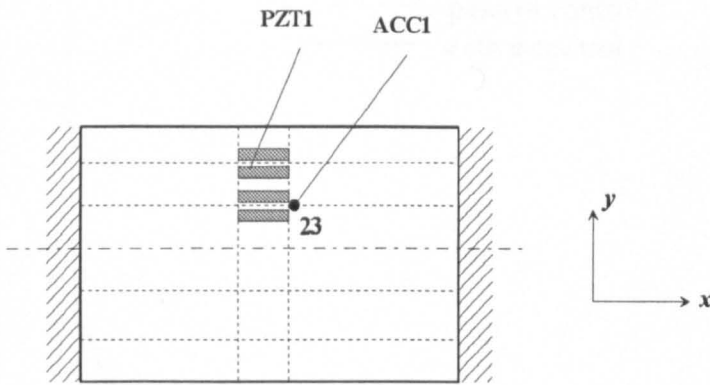


**Figure 11.** Arrangement of the clamped-clamped plate with 4-strip PZT elements used as actuator and a single accelerometer for sensing

The arrangement of sensor and actuator for this arrangement is shown in Figure 11. The simulation results in Figure 12 show the influence of activating the PZT element in the  $x$  direction only. The results demonstrate that superior suppression of vibrations is obtained. In addition, the power consumption for the PZT actuator decreases when actuation is in one direction only (Chantalakhana and Stanway, 2000).

Configuration 3: two PZT actuators with a two-channel amplifier and one accelerometer

As suggested by Azvine et al (1994), a negative velocity feedback controller using non-collocated sensors and actuators can degrade the performance of the active vibration control system. In the present study, a two-channel voltage amplifier for PZT actuators (PZT1 and PZT2 in Figure 13) is used to provide independently actuator commands for each PZT actuator. In addition, it is not necessary to design for use a multiple-input, multiple-output modal controller with collocated sensors and actuators.

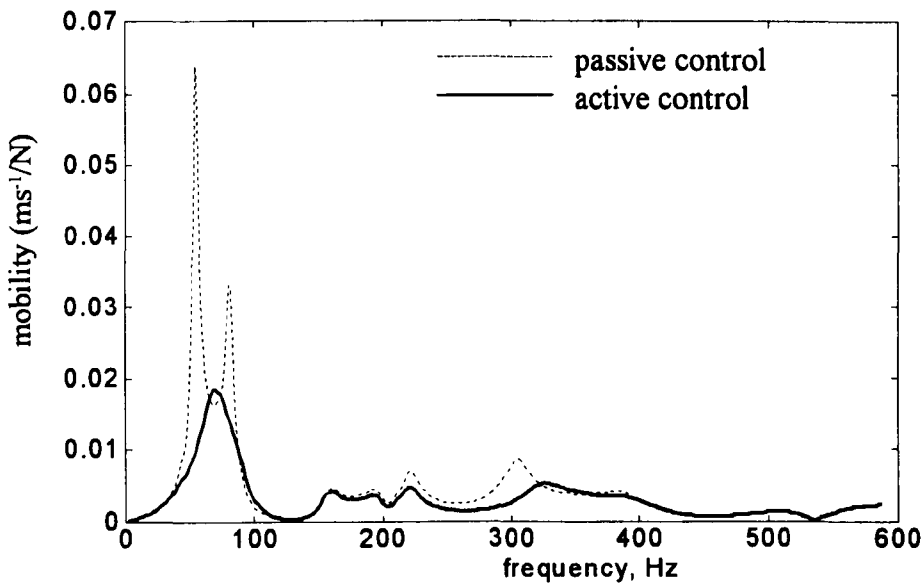


**Figure 12.** Simulation results: predicted FRFs (FRF7\_23) of three-layer plate with and without active control for PZT actuator operating in  $x$  direction only (Figure 11)

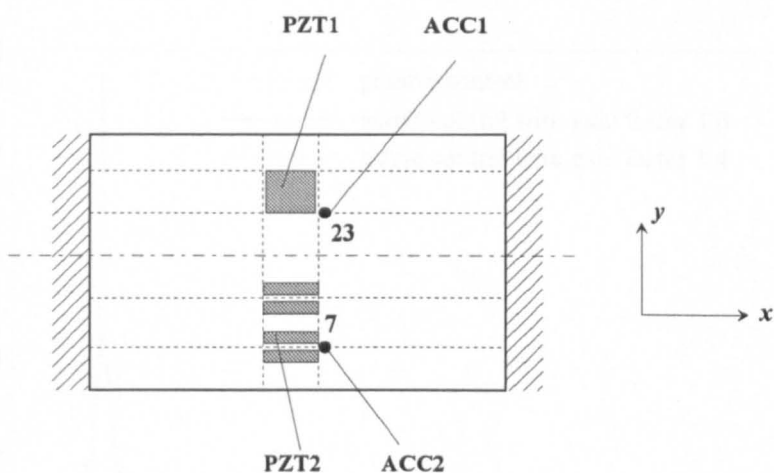


**Figure 13.** Arrangement of the clamped-clamped plate with 2 PZT actuators (one square element and one 4-strip element) and 2 accelerometers for sensing

Initially, two PZT actuators, PZT1 and 2, and single accelerometer, ACC1, are used in the numerical simulations. Predicted FRFs from simulations show that the amplitudes of the first two modes coalesce into a single mode and the vibrational amplitudes are not effectively suppressed, especially when the control gains increase, as shown in Figure 14.

The reason for this increase in the amplitudes of the first two modes could arise from spillover effects in the closed-loop system. As a result, the controller was redesigned to operate with lower estimator gains. The second test was performed where the configurations of test plate are the same as the previous test but in one configuration the sensor location was changed from point 7 to point 23 (see Figure 13). FRFs predicted from the models of the redesigned control system is shown in Figures 15. The amplitudes of first two modes are well-suppressed as the control gains increase. Table 4 presents the redesigned estimator gains such that the designed gains are reduced by changing the sensor location.

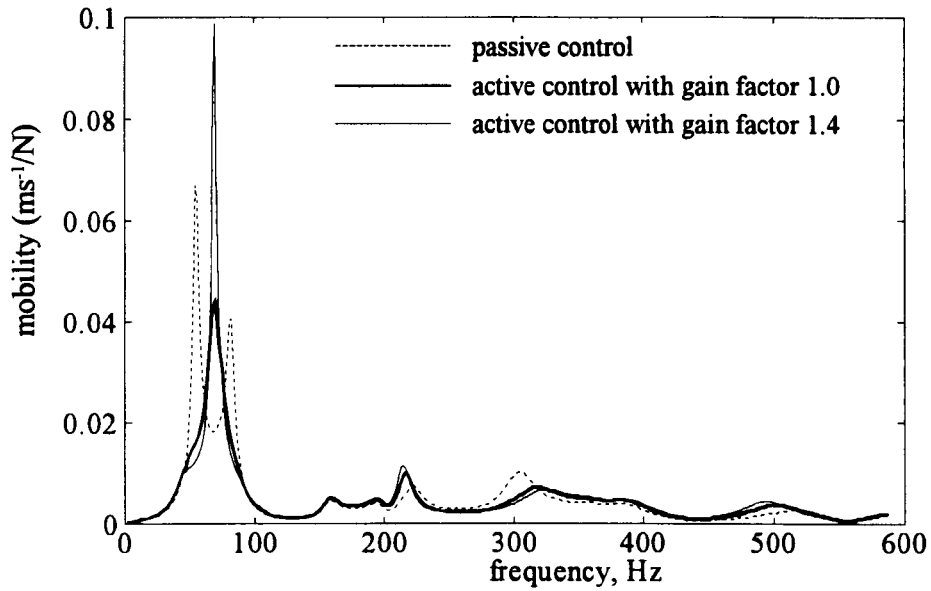


**Figure 14.** Simulation results: FRFs (FRF7\_23) of three-layer plate with and without active control using PZT1 and 2 with a 2-channel amplifier and ACC1 (Figure 13)

**Table 4**

Re-designed estimator gains

Case	1) PZT1&2, ACC1	2) PZT1&2, ACC2	3) PZT1&2, ACC1&2	
<i>Estimator</i> for mode1	65.4±296.6i	44.1±251.0i	66.6±256.5i	51.4±289.9i
<i>gain</i> : for mode2	-337.1±284.6i	218.6±161.4i	-127.8±100.1i	246.2±174.7i

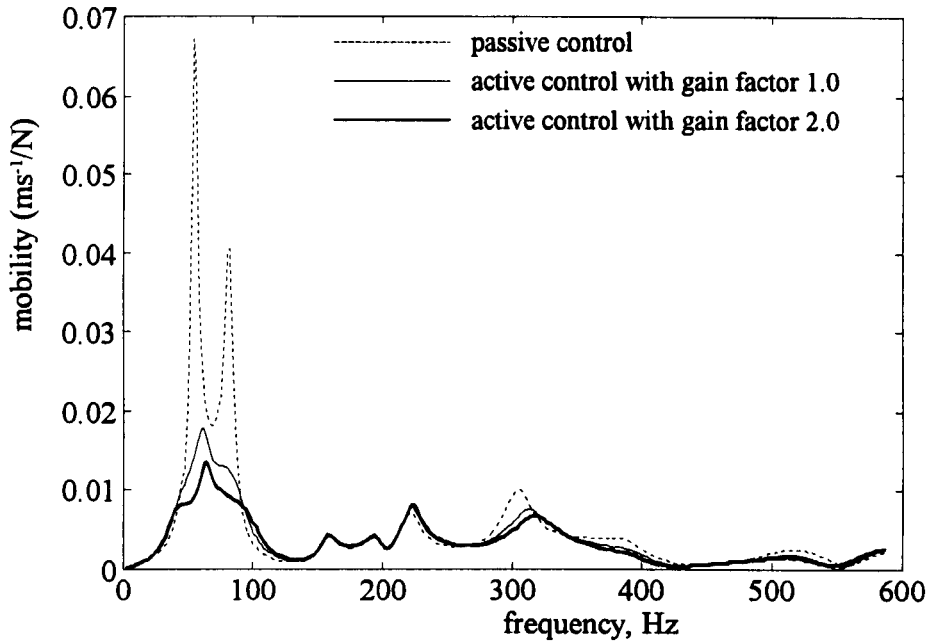


**Figure 15.** Simulation results: FRFs (FRF7\_23) of three-layer plate with and without active control using PZT1 and 2 with a 2-channel amplifier and ACC2 (Figure 13)

***Configuration 4:*** two PZT actuators with a two-channel amplifier and two accelerometers

In this test, two PZT actuators with a two-channel amplifier are used to perform active control as in *Configuration 3* but two accelerometers at points 7 and 23 are used for sensing. Compared to the case of using PZT1 and 2 with ACC1, the estimator gains also reduce in this configuration, PZT1 and 2 with ACC1 and 2 (Table 4). Figure 16 shows results from numerical simulations of this configuration. The best performance of vibration suppression is achieved using this configuration such that the amplitudes of the first two modes do not exceed  $0.01 \text{ ms}^{-1}/\text{N}$ . Note that the amplitude of mode 5, just above 200 Hz, increases slightly as the control gains increase.

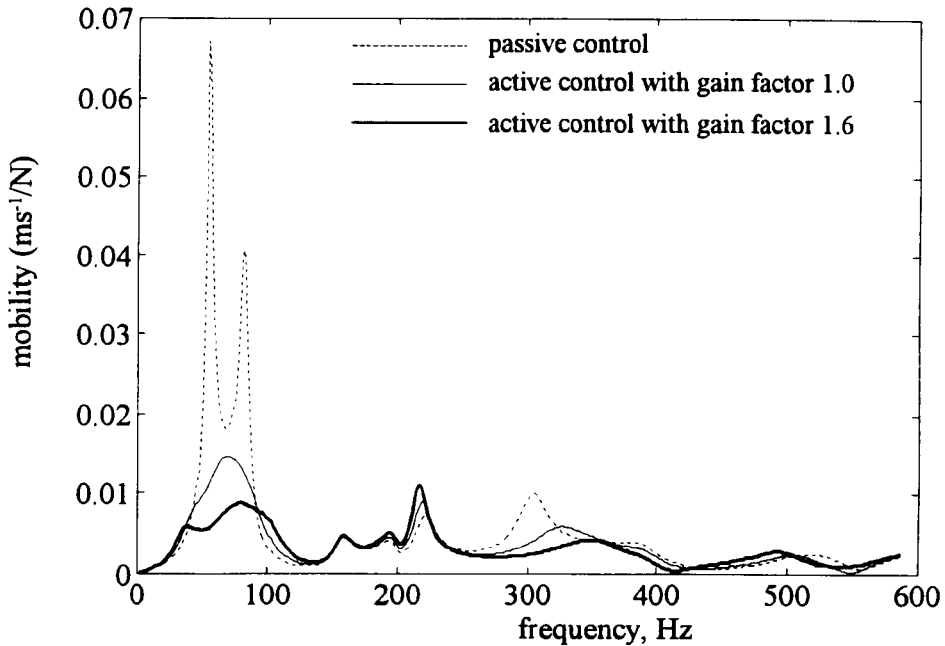


**Figure 16.** Simulation results: FRFs (FRF7\_23) of three-layer plate with and without active control using PZT1 and 2 with a 2-channel amplifier and ACC1 and 2 (Figure 13)

#### 4 EXPERIMENTAL VERIFICATION

In the previous section, various numerical simulations were used to study various configurations of accelerometers and PZT actuators on the three-layer test plate. In the present section, the results from experiments will be compared to those from numerical simulations. The general arrangement of the test facility is shown in Figure 17. Implementation of the digital controller is performed using a commercial package ('dSPACE' DS1102) which has up to 4 analogue-to-digital (A/D) input channels and 4 digital-to-analogue (D/A) output channels. In general, to avoid aliasing of a sampled signal, the sampling frequency must be greater than twice the highest natural frequency of interest, which in this case is around 600 Hz (for example, see Franklin et al, 1998). In the present study it was found that a sampling frequency of 10 kHz provided a suitable

compromise between sufficiently accurate discretisation of the analogue signal for real-time control and the capabilities of the digital signal processor. This sampling rate ensures that the spillover from the uncontrolled higher frequency modes (mode up to 600 Hz), included in the analysis, will not occur. The control interface card is designed to operate with SIMULINK software (Dabney and Harman, 1996).

The PZT actuator (model PC5H type VI from the MATROC company) is approximately 1 mm thick to react effectively to a maximum voltage of from 1 to 2 kV (Physik Instrumente, 1999). The relationship between force and voltage applied for the PZT actuator is derived as (Physik Instrumente, 1999)

$$\begin{aligned} f(t) &= \sigma_a A_a = \left( E_a \frac{d_{31}}{t_a} V(t) \right) \cdot b_a t_a \\ &= -0.702 V(t) \quad (\text{Newton per Volt}) \end{aligned} \quad (19)$$

where  $\sigma_a$  is the stress developed in the PZT,  $A_a$  is the cross-section area of the PZT,  $b_a$  is the width of the PZT,  $t_a$  is thickness of the PZT,  $E_a$  is the modulus of elasticity of the PZT ( $= 1/15.1 \times 10^{-12} \text{ Nm}^{-2}$ ) and  $d_{31}$  is the piezoelectric constant ( $= -212 \times 10^{-12} \text{ mV}^{-1}$ ).

#### 4.1 Experiment results using *Configuration 1*

For comparison with the simulation results in Figure 9, of the actively damped plate with a single PZT actuator and single accelerometer, a test was carried out to obtain the corresponding experimental results and these results are shown in Figure 18.

Close agreement between simulations and experiments is evident. The introduction of active control results in significant attenuation of the two lowest modes, which was predicted by the simulation results. However the simulation results in Figure 9 indicated that these two modes would coalesce into a single mode. This did not happen in practice

with the two modes remaining distinct. Note that there was significant excitation of the mode just above 500 Hz.

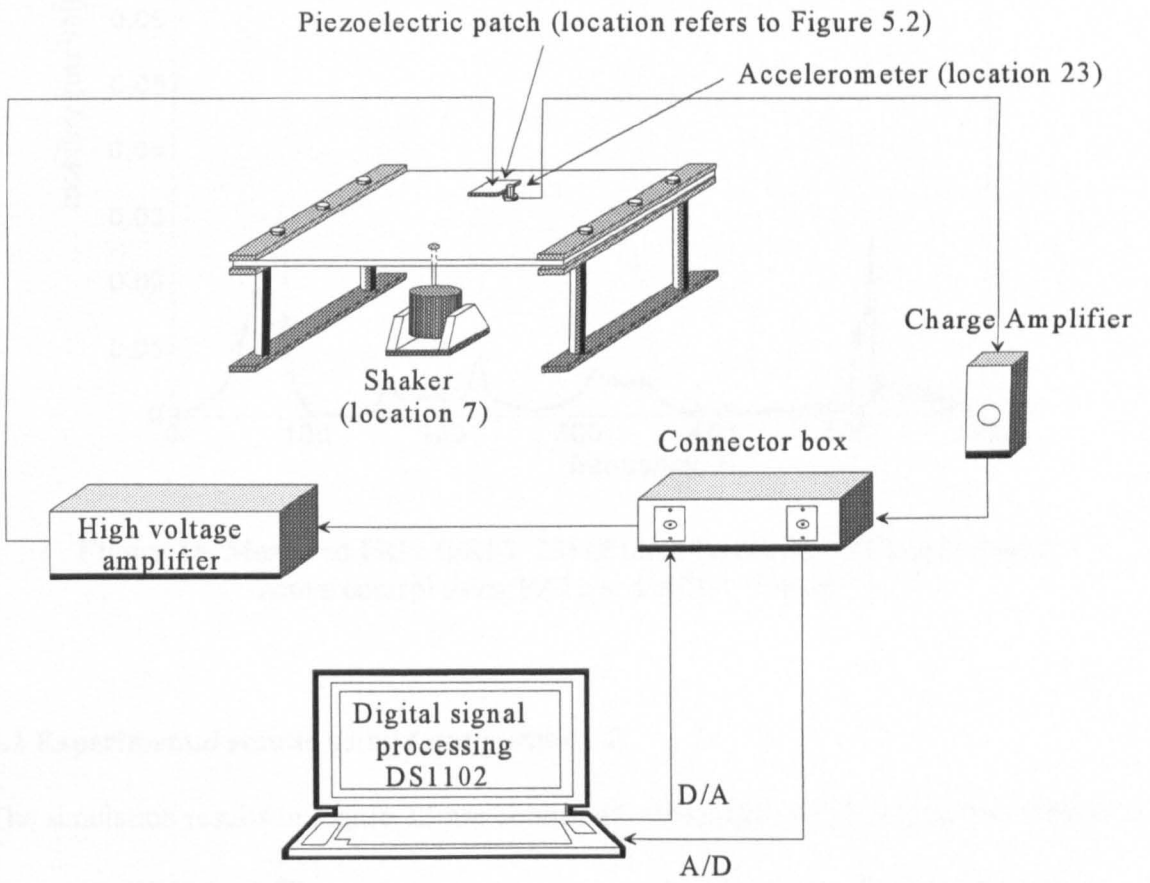


**Figure 17.** Arrangement of the closed-loop clamped-clamped plate with electronic equipment for digital control implementation

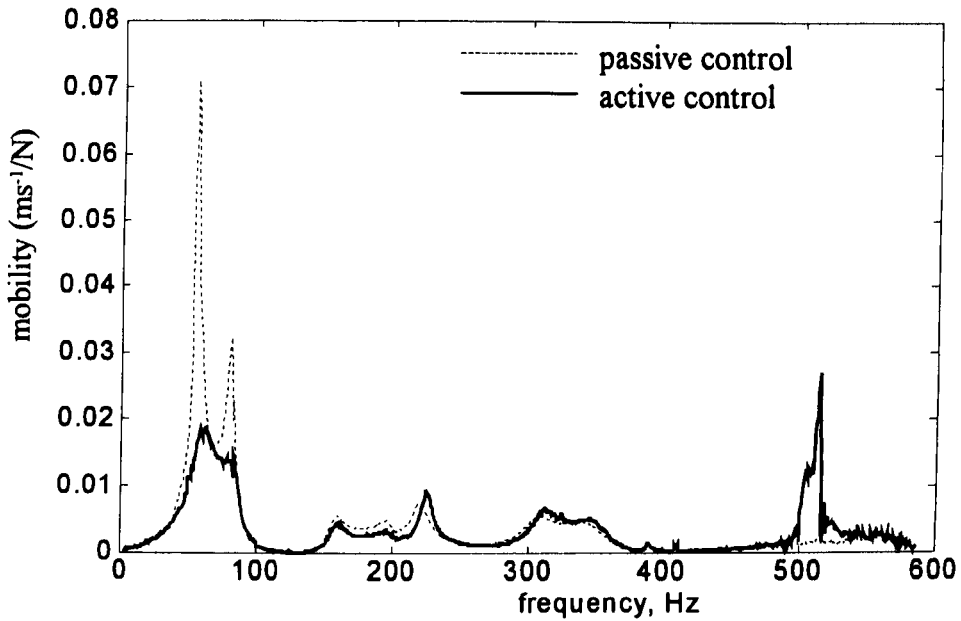


**Figure 18.** Measured FRFs (FRF7\_23) of three-layer plate with and without active control using PZT1 and ACC1 (Figure 7)

#### 4.2 Experimental results using *Configuration 2*

The simulation results in Figure 12 are confirmed with plots of FRFs from experiments in Figure 19. With the PZT actuator operating in the  $x$  direction only, the controlled system is more stable and levels of vibrations can be attenuated more than those in the case of the two-direction PZT actuator. Figure 20 shows FRFs from experiments of the one-direction PZT actuator case where the control gain is increased by a factor of 2.4 times the designed gain (of the result in Figure 19). Note also that the excitation of the mode just above 500 Hz is dramatically reduced in relation to the results obtained using *Configuration 1*.

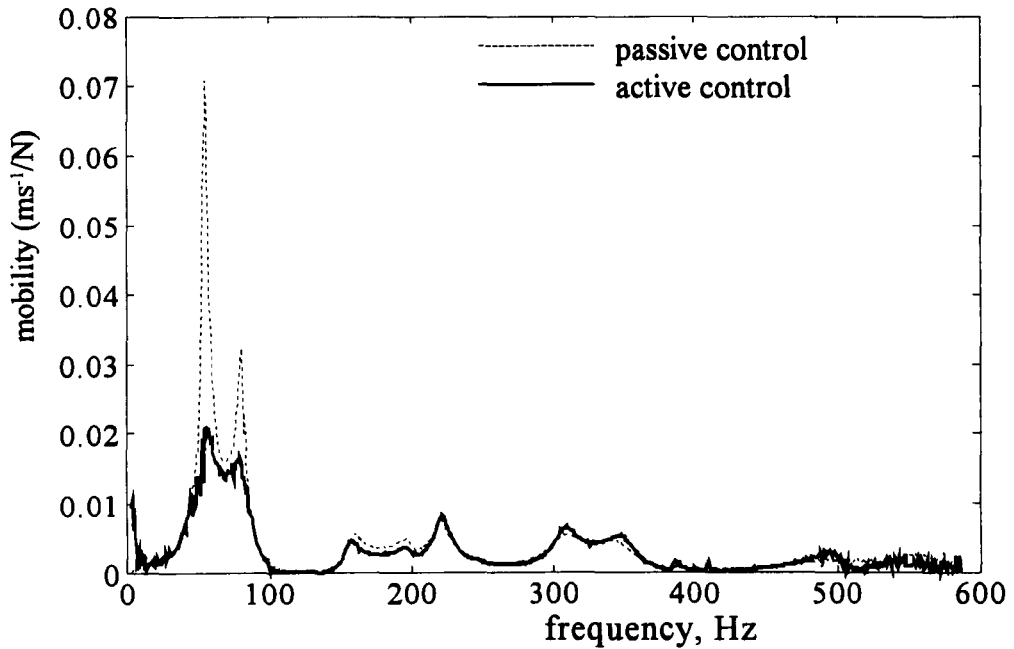


**Figure 19.** Measured FRFs (FRF7\_23) of three-layer plate with and without active control using PZT1 and ACC1 (Figure 11)

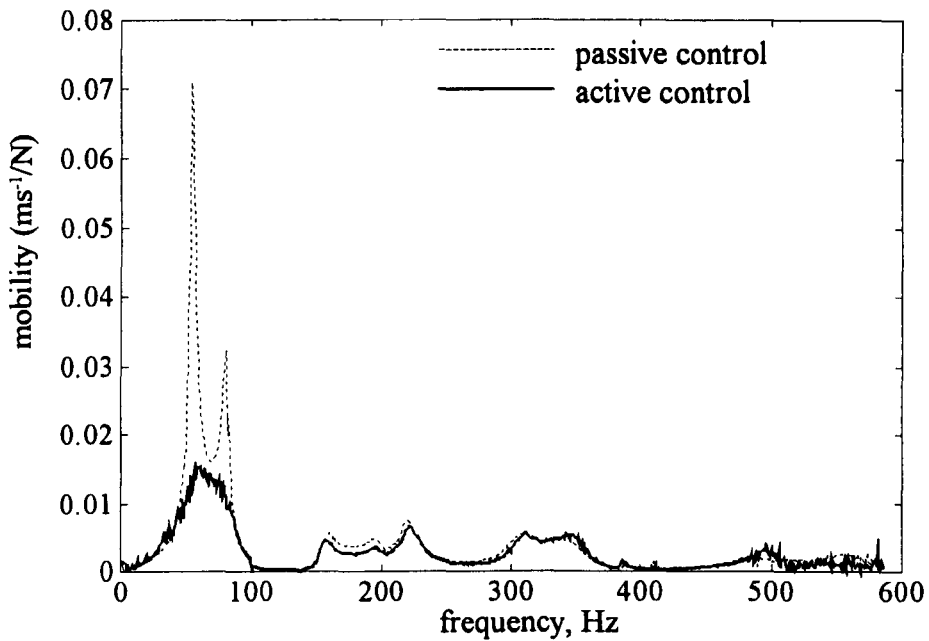


**Figure 20.** Measured FRFs (FRF7\_23) of three-layer plate with and without active control using PZT1 and ACC1 (Figure 11) with an amplified gain factor = 2.4

### **4.3 Experimental results using *Configuration 3***

The corresponding experimental results of simulations in Figures 14 and 15 are shown in Figures 21 and 22, respectively. Figure 21 shows that the amplitude of the first mode is well-suppressed but this does not occur for the second mode, especially when the control gains increase. For the case of redesigning estimator gains (Figure 22), the plots show that the magnitudes of the first two vibration modes are reduced significantly as the control gains are increased.

### **4.4 Experimental results using *Configuration 4***

Figure 23 shows experimental results corresponding to the simulations in Figure 16. As expected, the resulting maximum amplitudes of first two modes do not exceed  $0.01 \text{ ms}^{-1}/N$  (Figure 23(b)). However, the increase in amplitude of mode 5 as the control gains increase does not occur in the experimental results, instead mode 6 just above 300 Hz shows an increase in amplitude. The most effective vibration suppression of the first two controlled modes is obtained using this configuration, two PZT actuators, two sensors and a two-channel amplifier.

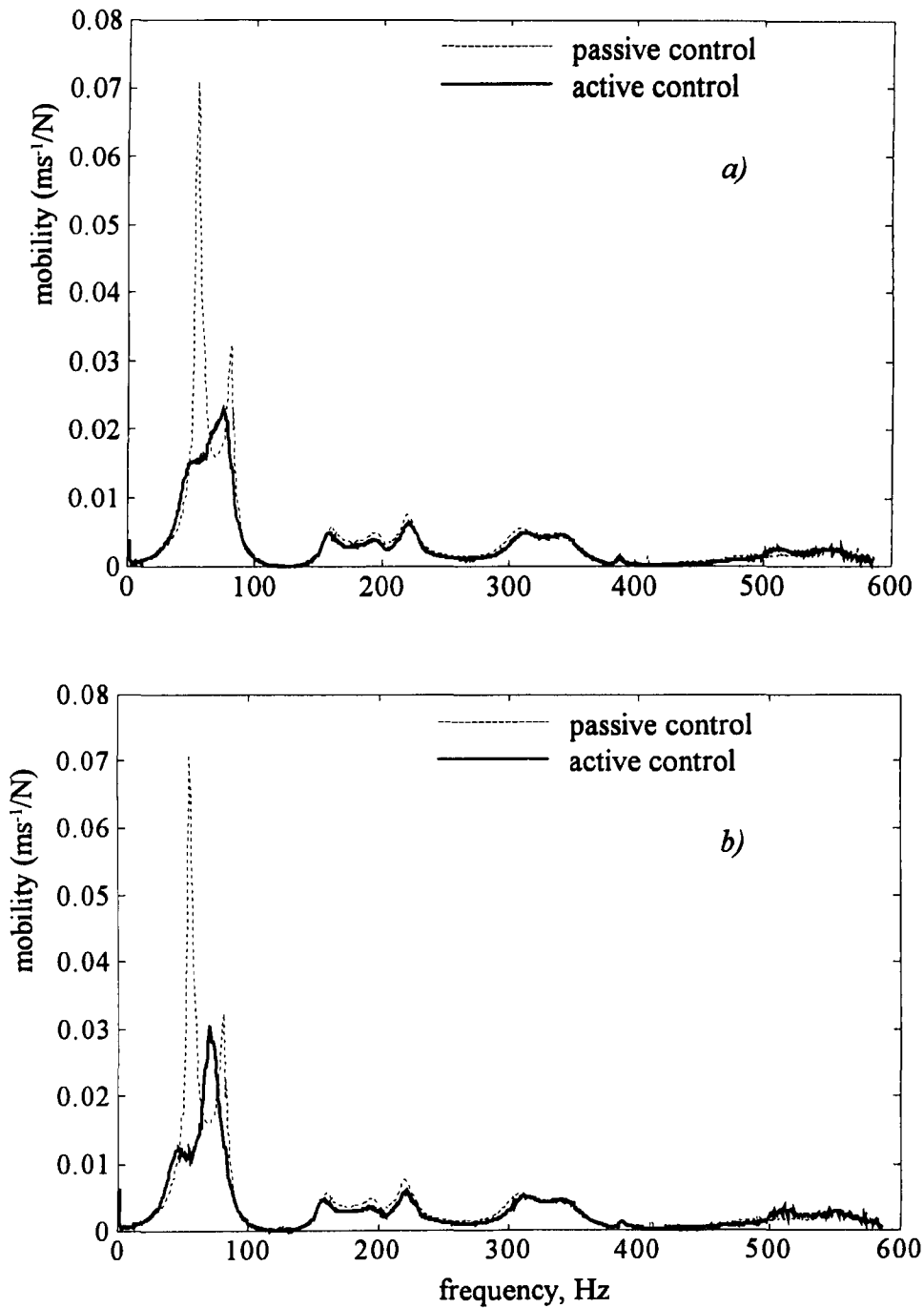


**Figure 21.** Measured FRFs (FRF7\_23) of three-layer plate with and without control using PZT1 and 2 with a 2-channel amplifier and ACC1 (Figure 13)  
 a) gain as designed  
 b) with an amplified gain factor = 1.4

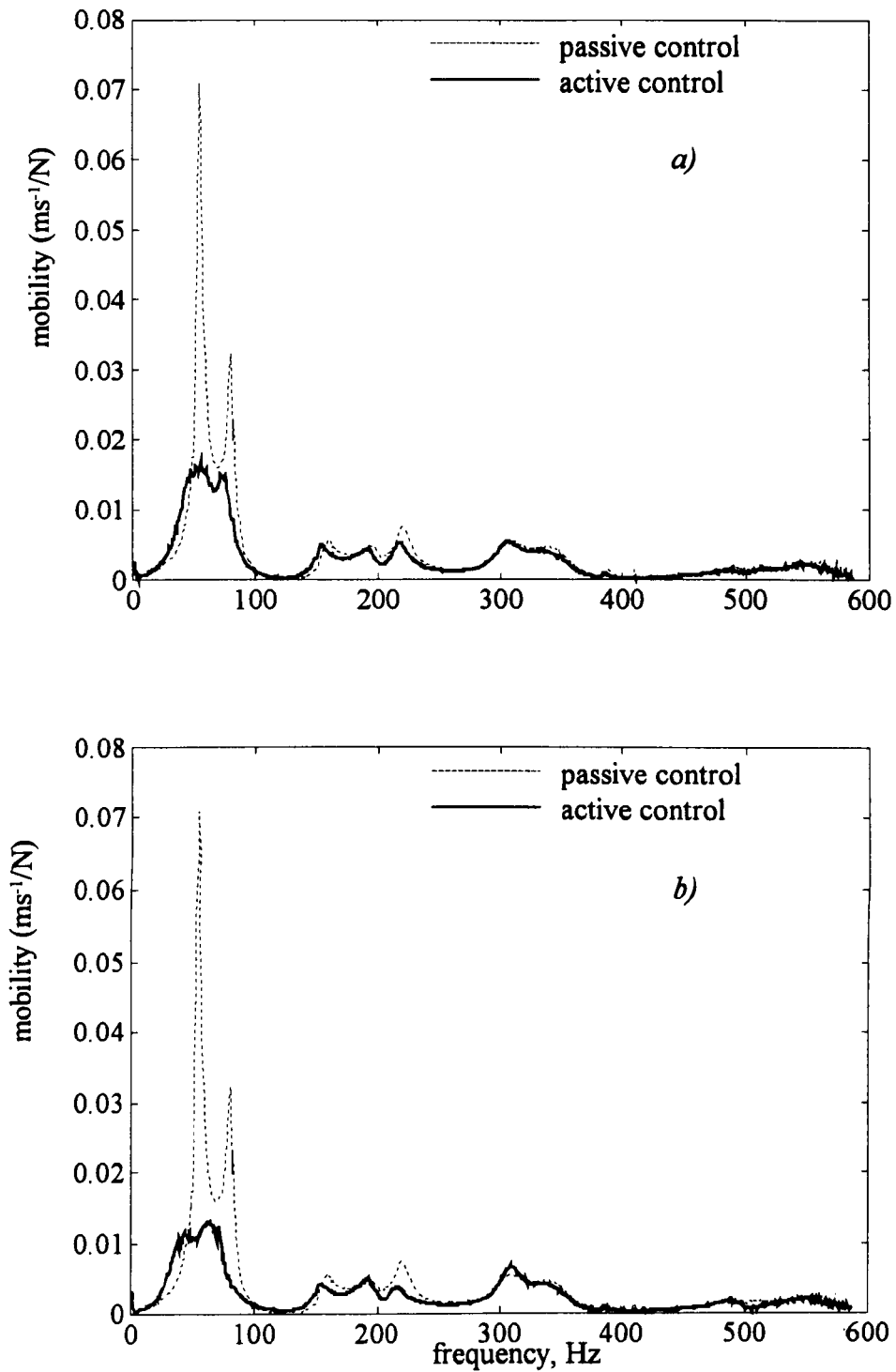


**Figure 22.** Measured FRFs (FRF7\_23) of three-layer plate with and without active control using PZT1 and 2 with a 2-channel amplifier and ACC2 (Figure 13)

a) gain as designed

b) with an amplified gain factor = 2.0

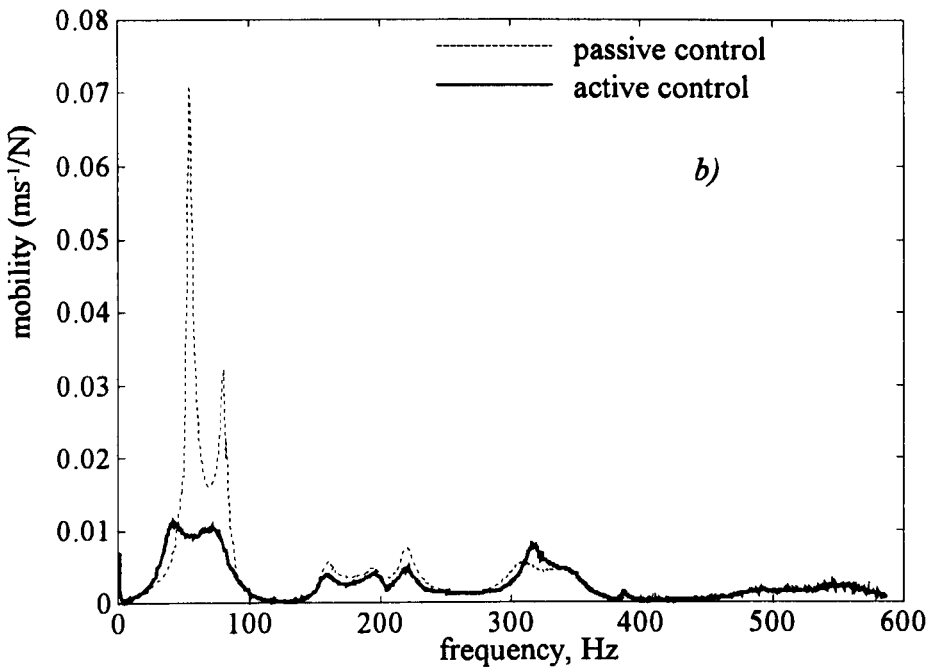
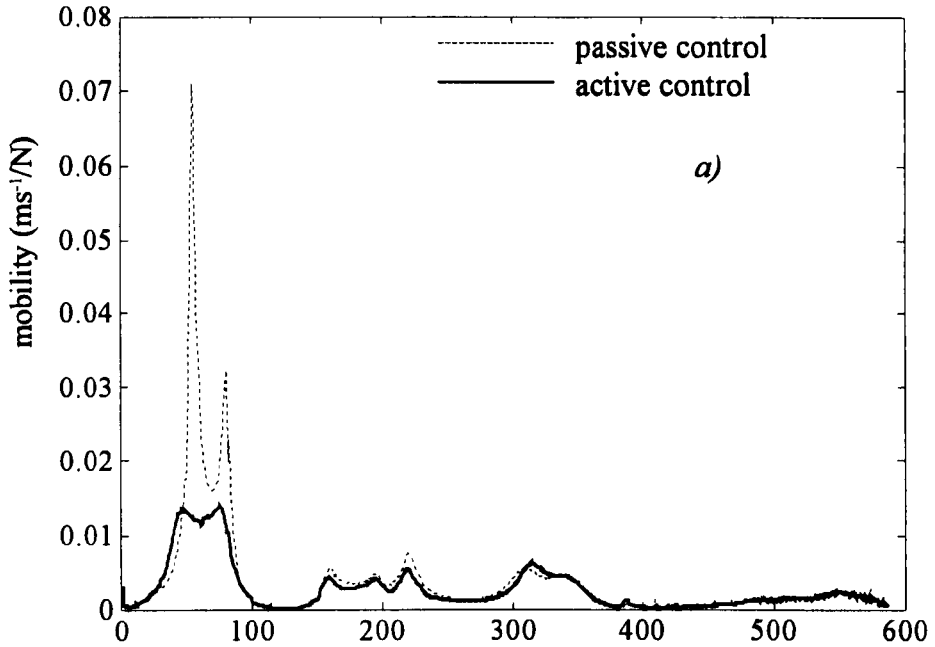


**Figure 23.** Measured FRFs (FRF7\_23) of three-layer plate with and without active control using PZT1 and 2 with a 2-channel amplifier and ACC1 and 2 (Figure 13)

a) gain as designed

b) with an amplified gain factor = 1.6

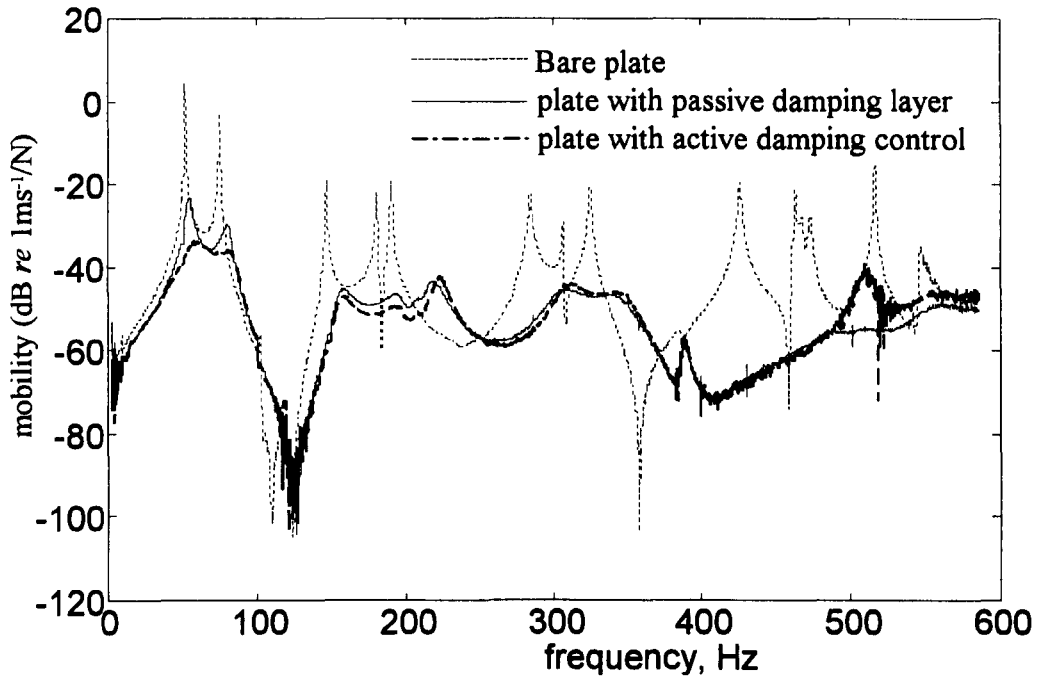


**Figure 24.** FRF7\_23: A comparison of passive and active schemes in relation to untreated plate: the worst case of using a single PZT (a square element) with a single-channel amplifier and a single accelerometer

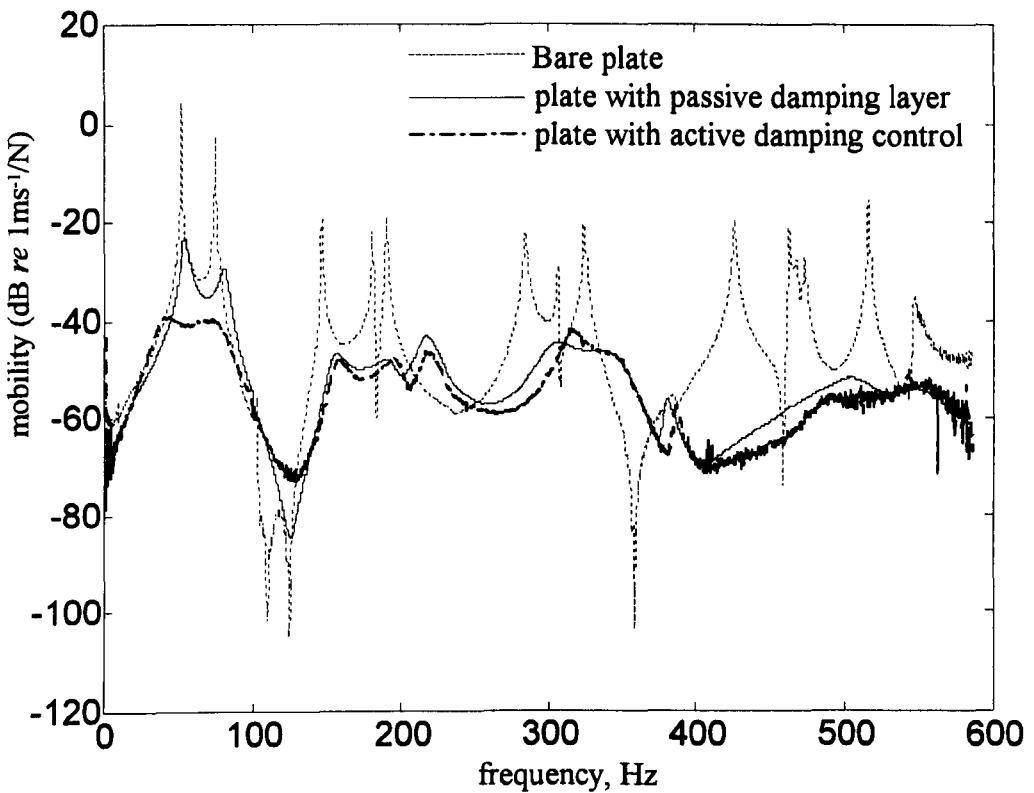


**Figure 25.** FRF7\_23: A comparison of passive and active schemes in relation to untreated plate: the best case of using 2 PZTs with a 2-channel amplifier and 2 ACCs

In Figure 23, it is worthy of note that the level of mode 6 slightly increases as the control gains increase. This arises because mode 6 is the third bending mode where maximum curvature occurs in the middle of the plate, the same as for mode 1. However, this problem could be solved by including mode 6 as a controlled mode. In summary, Figures 24 and 25 show comparisons of FRFs from the actively controlled, passively controlled schemes and the result from the bare plate for the worst and the best cases of the control configuration performed in this study. The worst case of the control configurations is the use of a single square element PZT actuator with a single-channel amplifier and a single accelerometer (results from Figure 18). The attenuation of the first two modes compared to the passive control is about 10 dB and 5 dB, respectively (Figure 24). The active control results provide the best performance using two PZT actuators along with a two-channel amplifier and two accelerometers (Figure 23(b)). Compared with passive control, the attenuation of the first two modes through the active control is increased by 15 dB and 10 dB, respectively (Figure 25).

## **5 CONCLUSIONS**

In this paper, a study of the active constrained layer damping treatment of a clamped-clamped plate has been described. This study has involved both numerical and experimental investigations. The strategy adopted was based upon the development of a model-based approach to control system design. The aim has been to minimise the amount of control hardware required whilst avoiding spillover problems which are liable to degrade performance. The combination of passive and active schemes in the active damping treatment has advantages where inherent damping in the passive damping layer improves the robustness of the actively controlled system and the active function is to

enhanced vibration suppression of the lower frequency modes which are characterised by long wavelengths.

Initially, finite element analysis was used to form the dynamic model of plate treated with the constrained damping layer so that design and performance of both passive and active control could be examined before the implementation stage. An updating algorithm involving pole placement was applied to match the formulated finite element model with the observed behaviour of the treated plate so that the refined model could be used in active control system design.

The development of the active control system involved the transformation of the original finite element model of the plate into a modal state-space description to be implemented in discrete time. The end result of the various computations was a fourth-order estimator/controller. Numerical experiments indicated that such an arrangement was capable of attenuating modes 1 and 2 (in conjunction with a 72 nd order model of the plate) without incurring significant problems due to spillover. This was achieved using only a single sensor and single actuator channel.

The experimental study confirmed the results of the numerical simulations. Various configurations of the control strategies were investigated - a single PZT actuator and single accelerometer - a single PZT actuator activating in  $x$  direction only - two PZT actuators associated with single- or two-channel amplifiers and one or two accelerometers. In the simplest configuration - a single PZT patch and single accelerometer, further reduction of vibration levels in the passively damped plate through the active control is about 10 dB and 5 dB for the first and second modes, respectively. The best performance of vibration suppression was found in the case of using two PZT actuators incorporating with a two-channel amplifier and two accelerometers such that high attenuation of

vibration levels was achieved, 15 dB and 10 dB in the first and second modes, respectively. The influence of sensor locations on the performance of the controlled system has been investigated. Lower estimator gains can be obtained by changing the sensor locations so as to minimise spillover effects and to provide better vibration suppression. Also two configurations of PZT actuator were investigated. A single PZT patch arranged to provide actuation in mutually perpendicular directions, and an arrangement of four PZT patches driven by a single amplifier but designed to activate the plate in a single direction only. Both configurations were effective at controlling modes 1 and 2 but the single PZT patch produced significant excitation of a mode above 500 Hz.

#### **ACKNOWLEDGEMENT**

The authors would like to thank the European Research Office of the US Army for partial funding of the control equipment under contract number N68171-98-M-5388.

#### **REFERENCES**

- Azvine B, Tomlinson G R, Wynne R J and Sensburg O 1994 Vibration suppression of flexible structures using active damping 1994 *4th International Conference on Adaptive Structures*, Cologne.
- Balas M J 1978 Feedback control of flexible systems. *IEEE Transactions on Automatic and Control* **AC-23**, 673-679.
- Baz A and Ro J 1993 Partial treatment of flexible beams with active constrained layer damping. *Conference of Engineering Sciences Society*, Charlottesville, VA.
- Baz A and Ro J 1996 Vibration control of plates with active constrained layer damping. *Smart Materials and Structures* **5**, 272-280.
- Burl J B 1999 *Linear Optimal Control*. California, USA.: Addison Wesley Longman, Inc.

- Chantalakhana C and Stanway R 1998 Control of plate vibrations using smart technology. *Proceedings of the 4th European and 2nd MIMR Conference, Harrogate, UK*, 195-204.
- Chantalakhana C. and Stanway R 2000 Active constrained layer damping of clamped-clamped plate vibrations *Journal of Sound and Vibration*, submitted.
- Dabney J B and Harman T L 1996 *The Student Edition of SIMULINK*. New Jersey: Prentice Hall.
- Franklin G F, Powell J D and Workman M 1998 *Digital Control of Dynamic Systems (3rd edition)*. California, USA.: Addison Wesley Longman, Inc.
- Guyan R J 1965 Reduction of stiffness and mass matrices. *AIAA Journal* **3**, 380.
- Inman D J and Minas C 1990 Matching analytical models with experimental modal data in mechanical systems. *Control and Dynamic Systems* **37**, 327-363.
- LMS 1993 *LMS CADA-PC User Manual*.
- Morgan Matroc 1999 Piezoceramics: manufacturer's data sheets.
- Minas C and Inman D J 1989 Identification of a nonproportional damping matrix from incomplete modal information. *Transactions of the American Society of Mechanical Engineers, Journal of Vibration and Acoustics* **113**, 219-224.
- Ogata K 1987 *Discrete-time Control Systems*. London: Englewood Cliffs, Prentice-Hall.
- Physik Instrumente (PI) Tutorial Manual. 1999 *Web page: <http://www.physikinstrumente.com/tutorial>*.
- Porter B and Crossley R 1972 *Modal Control Theory and Applications*. London: Taylor and Francis.
- Veley D E and Rao S S 1996 A comparison of active, passive and hybrid damping in structural design. *Smart Materials and Structures* **5**, 660-671.

## REFERENCES

- O. J. ALDRAIHEM and R. C. WETHERHOLD, 1997, "Mechanics and control of coupled bending and twisting vibration of laminated beams.", Smart Materials and Structures, Vol. 6, 123-133.
- P. AVITABILE, J. O'CALLAHAN and J. MILANI 1989, "Comparison of system characteristics using various model reduction techniques.", Proceedings of the 7<sup>th</sup> International Modal Analysis Conference, 1109-1115.
- B. AZVINE, 1993, "Vibration control via active damping.", Internal Report-Dynamics & Control Research Group, Department of Engineering, University of Manchester.
- B. AZVINE, G. R. TOMLINSON, R. J. WYNNE and O. SENSBURG, 1994, "Vibration suppression of flexible structures using active damping.", 4th International Conference on Adaptive Structures, Cologne
- B. AZVINE, G. R. TOMLINSON and R. J. WYNNE, 1995, "Use of active constrained-layer damping for controlling resonant vibration.", Smart Materials and Structures, Vol. 4, No. 1, 1-6.
- R. L. BAGLEY and P. J. TORVIK 1983, "Fractional calculus-a different approach to analysis of viscoelastically damped structures.", AIAA Journal, Vol. 21, 741-748.
- T. BAILEY and J. E. HUBBARD Jr., 1985, "Distributed piezoelectric-polymer active vibration control of a cantilever beam.", Journal of Guidance and Control, Vol. 8, No. 5, 605-611.
- M. J. BALAS, 1978, "Active control of flexible systems.", Journal of Optimization Theory and Applications, Vol. 25, No. 3, 415-436.
- M. J. BALAS, 1979, "Direct velocity feedback control of large space structures.", Journal of Guidance and control, Vol. 2, No. 1, 252-253.
- H. BARUH and K. CHOE, 1990, "Sensor placement in structural control.", Journal of Guidance and Control, Vol. 13, 524-533.

- A. BAZ, 1997a, "Boundary control of beams using active constrained layer damping.", ASME Journal of Vibration and Acoustics, Vol. 119, 166-172.
- A. BAZ, 1997b, "Optimization of energy dissipation characteristics of active constrained layer damping.", Smart Materials and Structures, Vol. 6, 360-368.
- A. BAZ, K. IMAM and J. MCCOY, 1990, "Active vibration control of flexible beams using shape memory actuators.", Journal of Sound and Vibration, Vol. 140, No. 3, 437-456.
- A. BAZ, S. POH and J. FEDOR, 1992, "Independent modal space control with positive position feedback.", ASME Journal of Vibration and Acoustics, Vol. 114, 96-103.
- A. BAZ and J. RO, 1993, "Partial treatment of flexible beams with active constrained layer damping.", Conference of Engineering Sciences Society, ASME-AMD-Vol. 167, 61-80.
- A. BAZ and J. RO, 1995, "Optimum design and control of active constrained layer damping.", ASME Journal of Vibration and Acoustics: Special 50<sup>th</sup> Anniversary Design Issue, Vol. 117, June, 135-144.
- A. BAZ and J. RO, 1996, "Vibration control of plates with active constrained layer damping.", Smart Materials and Structures, Vol. 5, No. 3, 272-280.
- J. B. BURL, 1999, "Linear Optimal Control", Addison Wesley Longman, Inc., California, USA.
- K. CHOE and H. BARUH, 1992, "Actuator placement in structural control.", Journal of Guidance and Control, Vol. 15, 40-48.
- E. F. CRAWLEY and J. LUIS, 1987, "Use of piezoelectric actuators as elements of intelligent structures.", AIAA Journal, Vol. 25, No. 10, 1373-1385.
- C. E. CREDE, 1965, "Shock and Vibration Concepts in Engineering Design", Prentice Hall, London.
- B. CULSHAW, 1996, "Smart Structures and Materials", Artech House, Inc., Boston.
- J. B. DABNEY and T. L. HARMAN, 1996, "The Student Edition of SIMULINK", Prentice Hall, New Jersey.

- D. J. DAWE, 1984, "Matrix and finite element displacement analysis of structures.", Oxford University Press, New York.
- J. P. DEN HARTOG, 1934, "Mechanical vibrations.", McGraw-Hill, New York.
- D. J. EWINS, 1984, "Modal testing :theory and practice.", Research Studies Press Ltd., Herts.
- J. L. FANSON and T. K. CAUGHEY, 1990, "Positive position feedback control for large space structures.", AIAA Journal, Vol. 28, 717-724.
- R. FIROOZIAN and R. STANWAY, 1988, "Active vibration control of turbomachinery: a numerical investigation of modal controllers.", Mechanical Systems and Signal Processing, Vol. 2, No. 3, 243-264.
- R. L. FORWARD, 1979, "Electronic damping of vibrations in optical structures.", Journal of Applied Optics, Vol. 18, No. 5, 690-697.
- G. F. FRANKLIN, J. D. POWELL and M. WORKMAN, 1998, "Digital Control of Dynamic Systems (3rd edition).", Addison Wesley Longman, Inc., California, USA.
- M. I. FRISWELL and J. E. MOTTERSHEAD, 1995, "Finite element model updating in structural dynamics.", Kluwer Academic Publishers, The Netherlands.
- D. F. GOLLA and P. C. HUGHES, 1985, "Dynamics of viscoelastic structures-a time-domain, finite element formulation.", ASME Journal of Applied Mechanics, Vol. 52, 897-906.
- L. E. GOODMAN, 1995, "Shock and Vibration Handbook", *Chapter 36*, Editor: C. M. Harris, McGraw-Hill, New York.
- R. J. GUYAN, 1965, "Reduction of stiffness and mass matrices.", AIAA Journal, Vol. 3, 380.
- N. W. HAGOOD and A. von FLOTOW, 1991, "Damping of structural vibrations with piezoelectric materials and passive electrical networks.", Journal of Sound and Vibration, Vol. 146, No. 2, 243-268.
- C. H. HANSEN and S. D. SNYDER, 1997, "Active control of noise and vibration.", E & FN Spon, London.
- S. C. HUANG, D. J. INMAN and E. M. AUSTIN, 1996, "Some design considerations for active and passive constrained layer damping treatments.", Smart Materials and Structures, Vol. 5, 301-313.

- S. R. IBRAHIM and A. A. SAAFAN, 1987, "Correction of analysis and test in modeling of structures: assessment and review.", Proceedings of the 5<sup>th</sup> International Modal Analysis Conference, Vol II, 1651-1660.
- D. J. INMAN and C. MINAS, 1990, "Matching analytical models with experimental modal data in mechanical systems.", Control and Dynamic Systems, Vol. 37, 327-363.
- M. D. JENKINS, P. A. NELSON, R. J. PINNINGTON and S. J. ELLIOTT, 1993, "Active isolation of periodic machinery vibrations.", Journal of Sound and Vibration, Vol. 166, No. 1, 117-140.
- C. D. JOHNSON, 1995, "Design of passive damping systems.", ASME Journal of Vibration and Acoustics: Special 50<sup>th</sup> Anniversary Design Issue, Vol. 117, June, 135-144.
- C. D. JOHNSON and D. A. KIENHOLZ, 1982, "Finite element prediction of damping in structures with constrained viscoelastic layers.", AIAA Journal, Vol. 20, No. 9, 1284-1290.
- D. I. G. JONES, 1979, "Two decades of progress in damping technology.", Aircraft Engineering, Vol. 51, 9-14.
- D. I. G. JONES, 1995, "Shock and Vibration Handbook", *Chapter 37*, Editor: C. M. Harris, McGraw-Hill, New York.
- T. P. KHATUA and Y. K. CHEUNG, 1973, "Bending and vibration of multilayer sandwich beams and plates.", International Journal for Numerical Methods in Engineering, Vol. 6, 11-24.
- M. J. LAM, D. J. INMAN and W. R. SAUNDERS, 1997, "Vibration control through passive constrained layer damping and active control.", Journal of Intelligent Material Systems and Structures, Vol. 8, August, 663-677.
- B. J. LAZAN, 1968, "Damping of materials and members in structural mechanics.", Pergamon, London.
- G. A. LESIEUTRE and U. LEE, 1996, "A finite element for beams having segmented active constrained layers with frequency-dependent viscoelastics.", Smart Materials and Structures, Vol. 5, 615-627.
- W. H. LIAO and K. W. WANG, 1996, "A new active constrained layer configuration with enhanced boundary actions.", Smart Materials and Structures, Vol. 5, 638-648.

- W. H. LIAO and K. W. WANG, 1997, "On the active-passive hybrid control actions of structures with active constrained layer treatments.", ASME Journal of Vibration and Acoustics, Vol. 119, 563-572.
- LMS, 1993, "User Manual.", LMS CADA-PC.
- L. MEIROVITCH and H. BARUH, 1982, "Control of self-adjoint distributed-parameter systems.", Journal of Guidance and Control, Vol. 5, 60-66.
- L. MEIROVITCH and H. BARUH, 1985, "The implementation of modal filter for control of structures.", Journal of Guidance and Control, Vol. 8, No. 6, 707-716.
- L. MEIROVITCH, H. BARUH and H. OZ, 1983, "A comparison of control techniques for large flexible systems.", Journal of Guidance and Control, Vol. 6, 302-310.
- C. MINAS and D. J. INMAN, 1991, "Identification of a nonproportional damping matrix from incomplete modal information.", ASME Journal of Vibration and Acoustics, Vol. 113, 219-224.
- MORGAN MATROC 1999, "Piezoceramics: manufacturer's data sheets."
- J. E. MOTTERSHEAD and M. I. FRISWELL, 1993, "Model updating in structural dynamics: a survey.", Journal of Sound and Vibration, Vol. 167, 347-375.
- A. D. NASHIF, D. I. G. JONES and J. P. HENDERSON, 1985, "Vibration damping", John Wiley and Sons, Inc., New York.
- K. OGATA, 1987, "Discrete-time Control Systems", Englewood Cliffs, Prentice-Hall, London.
- J. ORMONDROYD and J. P. DEN HARTOG, 1928, "The theory of the dynamic vibrations absorber.", Transaction ASME, Vol. 50, A9.
- PHYSIK INSTRUMENTE (PI), 1999, "Tutorial Manual", *Web page: <http://www.physikinstrumente.com/tutorial>*
- R. PLUNKETT and C. T. LEE, 1970, "Length optimization for constrained viscoelastic layer damping.", The Journal of the Acoustical Society of America, Vol. 48, No. 1(part 2), 150-161.

- B. PORTER and R. CROSSLEY, 1972, "Modal control: theory and applications.", Taylor & Francis Ltd., London.
- R. H. RECCA, 1995, "Shock and Vibration Handbook", *Chapter 33*, Editor: C. M. Harris, McGraw-Hill, New York.
- F. E. REED, 1995, "Shock and Vibration Handbook", *Chapter 6*, Editor: C. M. Harris, McGraw-Hill, New York.
- J. A. RONGONG, J. R. WRIGHT, R. J. WYNNE and G. R. TOMLINSON, 1997, "Modelling of a hybrid constrained layer/piezoceramic approach to active damping.", ASME Journal of Vibration and Acoustics, Vol. 119, 120-130.
- D. ROSS, E. E. UNGAR and E. M. KERWIN, Jr., 1959, "Structural Damping", *Sec. 3*, The American Society of Mechanical Engineers.
- A. M. SADRI, R. J. WYNNE and J. R. WRIGHT, 1999, "Robust strategies for active vibration control of plate-like structures: theory and experiment.", Proceeding of the Institution of Mechanical Engineers, Vol. 213, 489-504.
- V. N. SHAH and M. RAYMUND, 1982, "Analytical selection of masters for the reduced eigenvalue problem.", International Journal for Numerical Methods in Engineering, Vol. 18, 89-98.
- I. Y. SHEN, 1994, "Hybrid damping through intelligent constrained layer treatments.", ASME Journal of Vibration and Acoustics, Vol. 116, 341-349.
- I. Y. SHEN, 1995, "Bending and torsional vibration control of composite beams through intelligent constrained-layer damping treatments.", Smart Materials and Structures, Vol. 4, 340-355.
- J. D. SIMON and S. K. MITTER, 1968, "A theory of modal control.", Information and Control, Vol. 13, 316-353.
- R. STANWAY, J. L. SPROSTON and A. K. EL-WAHED, 1996, "Application of electro-rheological fluids in vibration control : a survey.", Smart Materials and Structures, Vol. 5, 464-482.
- E. E. UNGAR, 1971, "Noise and Vibration Control.", *Chap. 14*, New York: McGraw-Hill.

- D. E. VELEY and S. S. RAO, 1996, "A comparison of active, passive and hybrid damping in structural design.", Smart Materials and Structures, Vol. 5, 660-671.
- G. B. WARBURTON, 1954, "The vibration of rectangular plates.", Proceeding of the Institution of Mechanical Engineers, Vol. 168, 371-384.